# Hare-and-hound exercises of the Data Analysis Team of the Seismology Working Group

## by

## Appourchaux and Berthomieu

## May 2005

**HH#1**

# Report of the hare-and-hound exercise of the Data Analysis Team

T.Appourchaux

*Space Science Department of ESA, P.O. Box 299, 2200AG, Noordwijk, The Netherlands*

T.Toutain

*Observatoire de la Côte d'Azur, Département Cassini, UMR CNRS 6529, F-06304 Nice, France*

C.Barban

*Observatoire de Paris, DASGAL, CNRS UMR 8633, F-92195 Meudon, France*

**ABSTRACT**

Here we report on the results of a hare-and-hound exercise performed by the Data Reduction Group. Spectra of 6 different stars have been simulated and fitted for extracting the small and large separation of the stars. Rotational splittings were also fitted. The ability of the group for detecting low-degree stellar p modes is at least proven on high signal-to-noise ratio spectra. Further work will be needed for making the simulation more real and less easy. A new hare-and-hound exercise is already planned.

## 1. Introduction

Hare-and-hounds (H-H) exercises are commonly performed in helioseismology. These kinds of blind tests are heavily linked towards testing inversions. In the recent years, the emphasis has slowly shifted to testing any alleged technique thought to detect g modes. A similar approach for detecting stellar p modes is now envisaged since the strongest modes might be at the limit of detection.

Hereafter, we describe first how the stellar time series are simulated, second how the synthetic spectra are fitted and/or the stellar p-mode parameter extracted. Then, we discuss the different techniques of detecting stellar p modes. We close the report by looking how the simulation can be improved, and set the scene for the next round of H-H.

## 2. Spectrum simulation

In helioseismology, the solar p modes are stochastically excited by convection. It results that the statistics of the spectra is well known: it is a $\chi^2$ with 2 degrees of freedom (Woodard, 1984; Anderson et al., 1990; Appourchaux et al., 1998). For stellar p modes, we have taken the same assumption. As soon as the Fourier spectra can be calculated, the inverse Fourier transform provides the time series. It is not necessary to excite the p modes in the time domain as performed by Barban et al. (1999). The former is more efficient than the latter.
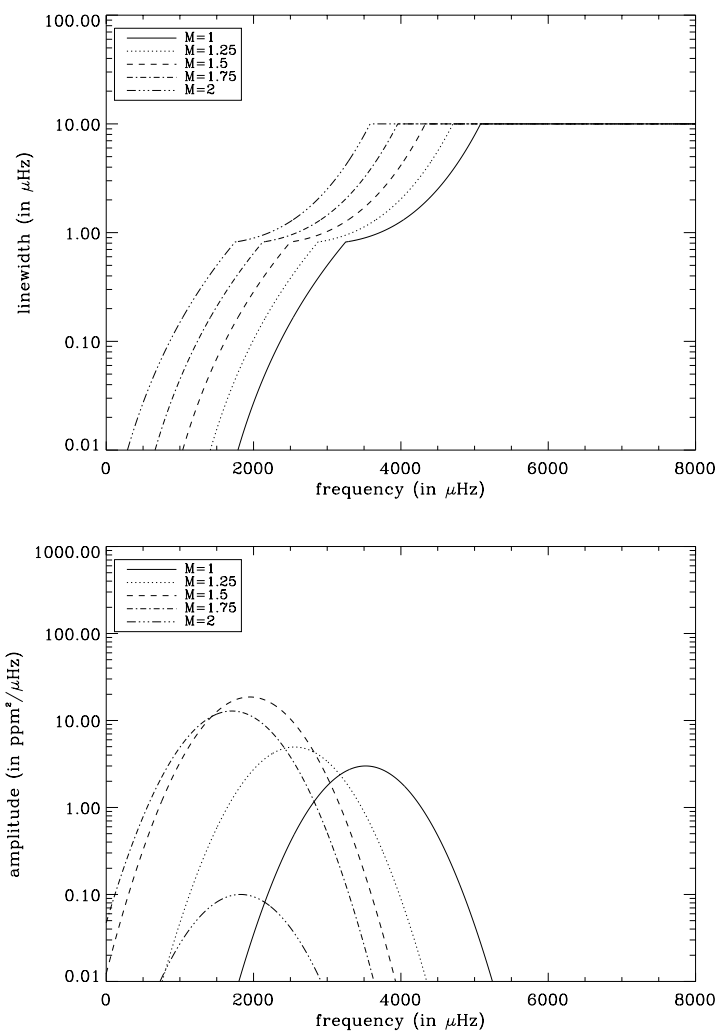
Fig. 1.— Linewidth and amplitude of the modeled stellar p modes as a function of frequency for different stars. They are here independent of age.
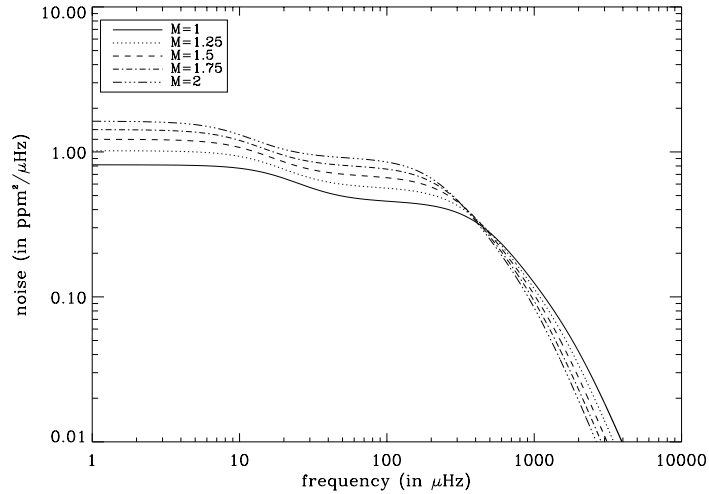
Fig. 2.— Modeled background stellar noise as a function of frequency for different stars. The time scales are a linear function of mass. The amplitude of the 3 different noise are independent of age and mass.

In both cases, we need to know how one can simulate properly the characteristics of the stellar spectrum, namely: Mass, Age, Temperature, Fine internal structure, Internal dynamics, Mode excitation and damping, Stellar and Instrumental noise.

The first three items determine the central frequency ($\nu_0$), the large ($\Delta\nu_0$), the small separation ($D_0$) and the smaller separation ($d_0$) (Christensen-Dalsgaard, 1984). The essential data were taken from Audard & Provost (1994) and were interpolated from 1 $M_\odot$ to 2 $M_\odot$, and from a grid of hydrogen content $X$ ranging roughly from 0. to 0.7. For mass lower than 1 $M_\odot$ we extrapolated the interpolation down to 0.8 $M_\odot$. The formula was used for getting the frequencies of modes $l = 0$ to 3; modes of higher degree were not included in the simulation.

The mode excitation and damping was derived from the work of Houdek (1996) and of Houdek et al. (1999). The amplitudes and linewidths were often extremely simplified. Figure 1 gives an example of the variation of the linewidth with frequency for various stellar masses. Since the model was done very quickly, it is quite likely that these figures do not exemplify fine details as reported by Houdek (1996); it should be taken only as a starting point for a finer modeling.

For simulating the internal dynamics of the stars, we assumed that the stars rotate rigidly with their rotation axis perpendicular to the line of sight. As for the distribution of amplitude with the degrees, we assume that the relative amplitudes follow the geometrical visibilities usually used for the VIRGO data and IPHIR data (Toutain & Fröhlich, 1992).

The noise was derived from that of the solar noise. For the stellar noise, we arbitrary decided that the time scales defining the various super-, meso- and granulation noise be scaled like the stellar mass (i.e. the

heavier the star the longer the time scales) like shown on Fig. 2. Of course, a better work needs to be done for the noise if we want to make the simulations more real.

The simulated time series are 1 month long with a 30-s sampling time. Six time series were simulated for six different stars which main characteristics are given in Table 1. The data were blindly generated so that even the hare could play the role of the hounds.

| Star | Mass (in $M_\odot$) | $X_c$ | $\Delta\nu_0$ | $\Omega_r$ (in $\mu$ Hz) |
|------|------|------|------|------|
| 1 | 1.33 | 0.23 | 84.90 | 1.00 |
| 2 | 1.23 | 0.39 | 106.80 | 0.56 |
| 3 | 1.86 | 0.69 | 81.20 | 1.50 |
| 4 | 1.26 | 0.13 | 87.50 | 1.50 |
| 5 | 1.21 | 0.58 | 120.10 | 0.25 |
| 6 | 0.85 | 0.17 | 151.40 | 0.69 |

Table 1: Main characteristics of the simulated stars. $X_c$ is the hydogen content, and $\Omega_r$ is the rotation rate of the star as a rigid body.

### 3.  Data analysis

#### *3.1.  Echelle diagram*

One of the simplest, quickest and dirtiest method to detect the large separation and other details of the stellar p-mode spectra is to produce an Echelle diagramme. The original idea was from Grec (1981) who used the asymptotic property of the solar p modes for showing how each degree would line up in such a diagramme. The Echelle diagramme consists in cutting in pieces of $\Delta\nu_0$ the spectra of the star, and then to pile up these pieces on top of each other. If modes are indeed detected vertical lines should appear clearly in the diagramme. The trick is really to find the $\Delta\nu_0$ that would produce such 'vertical' lines. With some experience, and with simulated data with high signal-to-noise ratio, it takes just a few tens of minutes to get the proper separation. Trial and error will do especially on a Friday afternoon before the week-end.

Figure 4 shows the results of this procedure, and Table 2 gives the large separation obtained accordingly.

#### *3.2.  Histogram*

This technique was developed by Barban et al. (1999). Figure 5 shows the result of this procedure. Table 2 gives the large separation obtained with this technique.
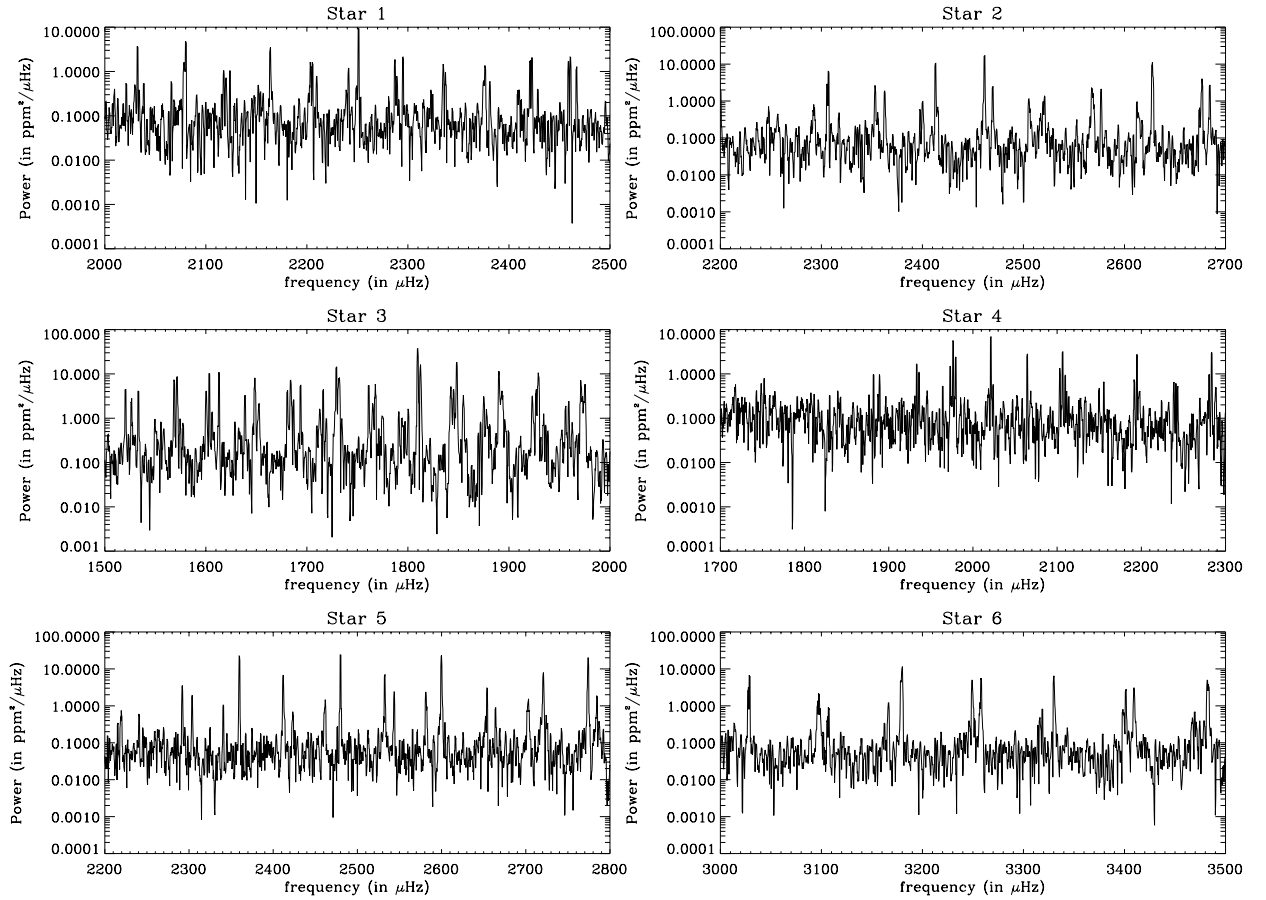
Fig. 3.— Power spectra (smoothed to 1 $\mu$Hz) for the 6 synthetic time series. The signal-to-noise ratio is at best about 100.

### 3.3. *Maximum likelihood fitting*

The technique used for fitting stellar spectra is the same as for full-disk solar spectra Toutain & Fröhlich (1992). We use Maximum Likelihood Estimators known as MLE, for a review see Appourchaux et al. (1998). Table 2 shows the result obtained; all the mode frequencies are available upon request (ask ThierryA or Toutain for details).

## 4. Discussion

It is quite clear that the helioseismologists were at an advantage mainly because they were at the end of the processes: synthetic data production (ThierryA) and MLE (Toutain). As a matter of fact, the analysis and simulation performed are too closely related to solar-type stars. Nevertheless, this bias created an interesting
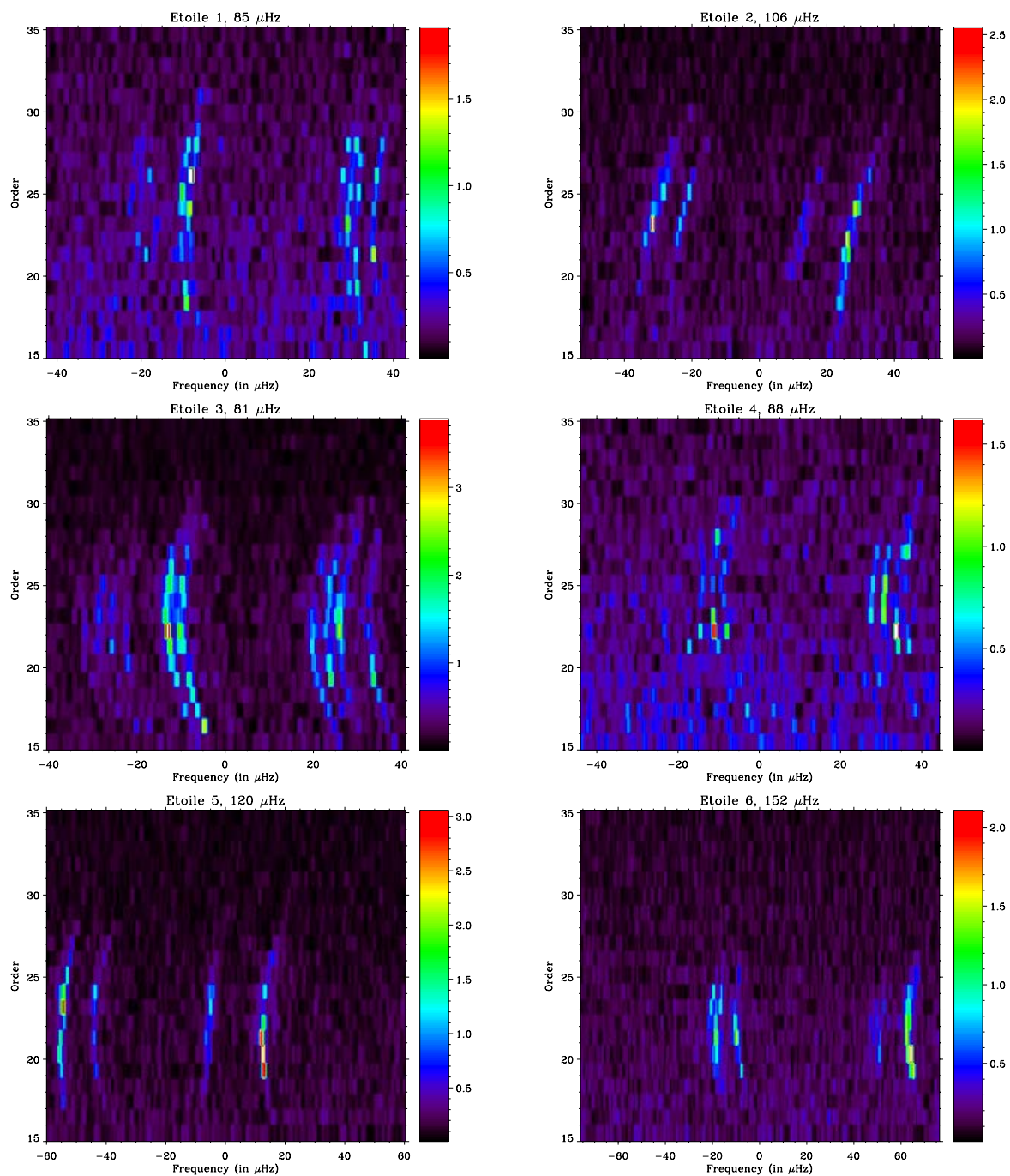
Fig. 4.— Echelle diagrammes for the 6 synthetic stellar spectra. The modes can be identified according to the way the ridges are split. For instance, the top left diagramme shows clearly from left to right, the $l$=3, 1, 2, 0 ridges. The parabolic curvature of the ridges is due to the asymptotic formula used.
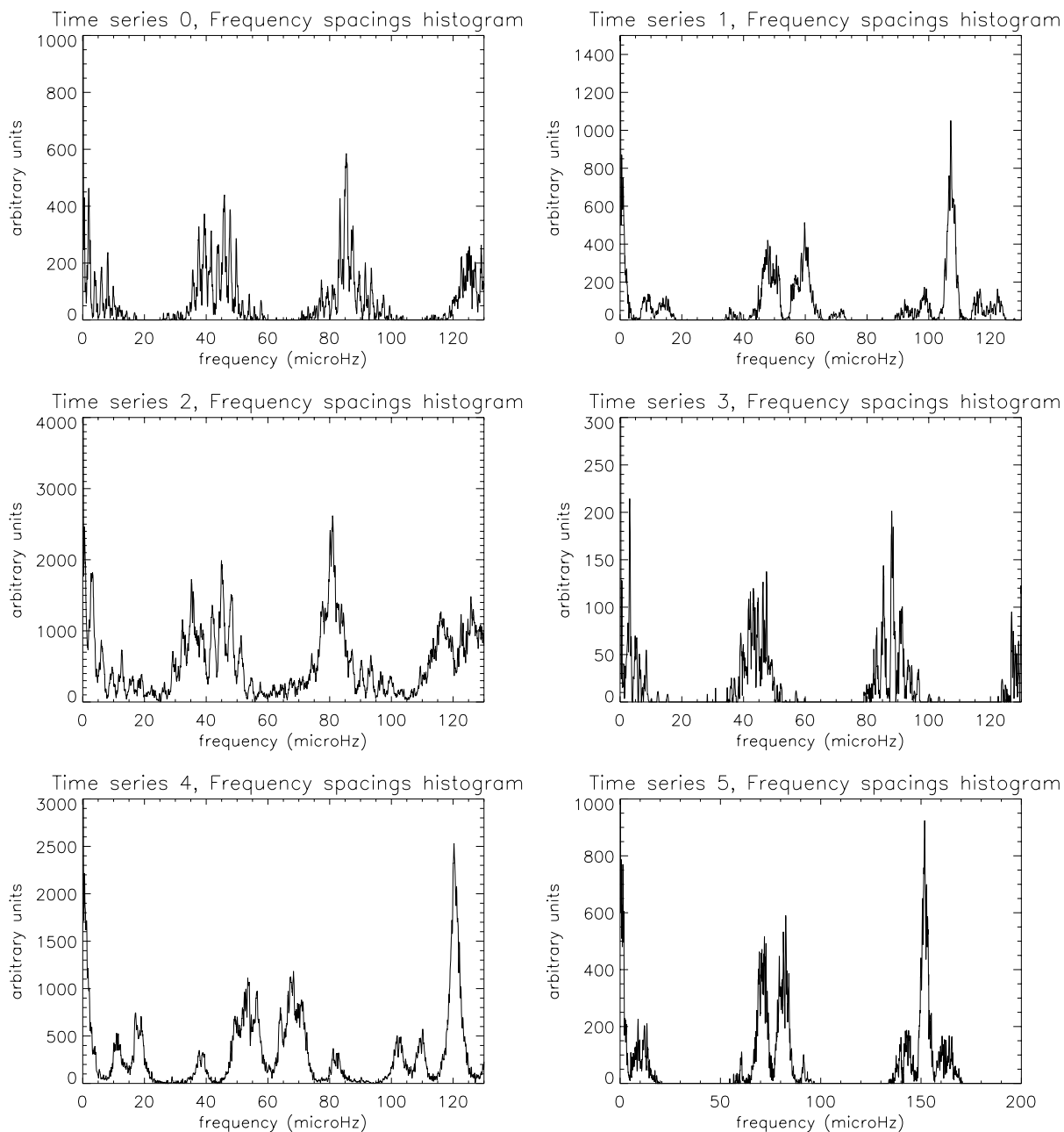
Fig. 5.— Histogrammes of the stellar spectra as computed by Barban et al. (1999). The largest peak indicates the location of the large separation. The second two largest peaks display the mean structure of the mode located at $|\Delta l| = 1$. The sub-structure of within the largest peak is a manifestation of the splitting (See time series 0 and 3, i.e. stars 1 and 4)

.

| Star | Mass (in $M_\odot$) | $\Delta\nu_0$ (in $\mu$ Hz) | | | $\Omega_r$ (in $\mu$ Hz) | | |
|------|------|---------|------|--------|---------|---------------------|--------|
| | | Echelle | MLE | Histo. | Echelle | MLE | Histo. |
| 1 | 1.33 | 85.0 | 85.4 | 90.0 | - | $0.963 \pm 0.034$ | - |
| 2 | 1.23 | 106.0 | 107.0 | 108.0 | - | $0.507 \pm 0.016$ | - |
| 3 | 1.86 | 81.0 | 81.5 | 80.0 | - | $1.502 \pm 0.013$ | - |
| 4 | 1.26 | 88.0 | 88.5 | 87.0 | - | $1.520 \pm 0.012$ | - |
| 5 | 1.21 | 120.0 | 120.0 | 120.0 | - | $0.196 \pm 0.022$ | - |
| 6 | 0.85 | 152.0 | 152.0 | 151.0 | - | $0.659 \pm 0.019$ | - |

Table 2: Main characteristics of parameters derived from the 3 main analysis techniques.

'bug': the psychological approach used by one of the fitter made him thought that the data producer may have forgotten to produce synthetic data for a star with an inclined rotation axis. The simulated data were a bit too easy to play with: a more realistic and a more noisy spectrum should be simulated in the future.

As far as the simulation is concerned, several improvements should be included such as:

- Inclined rotation axis

- Differential rotation

- Better linewidths and amplitudes

- More realistic stellar noise

- Lower signal-to-noise ratio

As far as the H-H exercise is concerned, we will likely make a full H-H involving 2 complete teams of Modelers-Observers doing a double blind H-H using simulated data from the other team. This activity has been started and will be reported during the next team meeting.

### *Acknowledgments*

Many thanks to our beloved PI, Annie Baglin, for keeping alive the flame of the COROT project, and for keeping on fighting: 'You'll never walk alone'. For anyone reading who is that quote from? Send your answer to thierrya@so.estec.esa.nl.

### **References**

Anderson E.R., Duvall J. T. L., Jefferies S.M., 1990, ApJ, **364**, 699

Appourchaux T., Gizon L., Rabello-Soares M.C., 1998, A&AS, **132**, 107

Audard N., Provost J., 1994, A&A, **282**, 73

Barban C., Michel E., Martic M., et al., 1999, A&A, **350**, 617

Christensen-Dalsgaard J., 1984, In: A.Mangeney, F.Praderie (eds.) Space Research in Stellar Activity and Variability, 11, Observatoire de Meudon

Grec G., 1981, Ph.D. thesis, Université de Nice

Houdek G., 1996, 'Pulsation of solar-type stars', Ph.D. thesis, Univeristät Wien

Houdek G., Balmforth N.J., Christensen-Dalsgaard J., Gough D.O., 1999, A&A, **351**, 582

Toutain T., Fröhlich C., 1992, A&A, **257**, 287

Woodard M., 1984, 'Short-period oscillations in the total solar irradiance', Ph.D. thesis, University of California, San Diego

# Seismology of $\delta$ Scuti stars with COROT: prospects for mode identification

C. Barban, M.-J. Goupil, C. Van't Veer

*Observatoire de Paris, DASGAL, UMR 8633, 92195 Meudon, France*

R. Garrido

*Instituto de Astrofisica de Andalucia, C.S.I.C., Apdo. 3004, 18080, Granada , Spain*

## ABSTRACT

$\delta$ Scuti stars are high amplitude, nonradial multiperiodic oscillators. The major problem is the identification of the observed frequencies as specific oscillation modes, however this step is important to provide constraints upon the internal structure of the star.

We show here that despite the complicated frequency distributions which can be expected from COROT space mission for a typical $\delta$ Scuti star, it will be possible to identify at least some modes or at least the degree for low-$\ell$ modes from space data.

## 1.   Introduction

The $\delta$ Scuti stars are pulsating variables located in the lower part of the classical instability strip with spectral type from A2 to F0. They are multiperiodic pulsators oscillating with large amplitude compared to solar-like oscillations (amplitudes from ground-based observations range between a few mmag to 1/10 mag) and periods less than 0.3 days. Only a few 5 to 10 frequencies in general and in some cases up to 30 frequencies in the case of FG Vir (Breger et al. 1998) have been detected from the ground. The observed frequencies span an interval in which models predict much more frequencies than observed. Either the corresponding modes are not excited or they are excited up to much smaller amplitudes that can be detected from ground-based observations. We do not yet understand how modal selection operates, this prevents to identify firmly modes associated with individual frequencies (e.g. to determine the degree, azimuthal order and radial order of each mode) and therefore to take full advantage of the available seismological tools. A better knowledge of the global structure of the frequency spectrum would provide precious indications about modal selection processes. This requires to detect oscillations with much smaller amplitudes and therefore to increase significantly the signal-to-noise ratio.

Observations from space will be characterized by a much higher signal-to-noise ratio than from the ground. This will result in the detection of a much larger set of modes for each $\delta$ Scuti star, by detecting new small amplitude modes and high degree modes. Indeed, high $\ell$ modes are expected to be excited but visibility effects i.e. averaging geometrical effects when observing in integrated light, decrease the observed amplitudes to much smaller values than can be observed from the ground. But the detection of a much larger number of frequencies will yield frequency spectra very much complicated and then it is legitimate to wonder whether mode identification will not be even more difficult to obtain (Dziembowski et al. 1998)? The purpose

of this work is to show how, in space data, it is possible to identify at least some modes or at least the degree of the low-$\ell$ modes, and this despite the complications due to the presence of high $\ell$ modes.

Spectroscopic or photometric techniques have been deviced to identify modes (Garrido et al. 2000). This work is a progress report on our effort to develop an alternative method which does not involve any knowledge of a model and using very precise data, i.e. frequencies, rather than amplitude and phase. An ideal case was presented in Baglin et al. (2000). In this paper, modes up to $\ell = 10$ were assumed to be detected with the low detection threshold of space data. The detected range of frequencies was assumed to be broad enough toward high frequencies and then it included lower frequency part of the asymptotic p-mode regime. It was shown there that although the frequency spectrum is more complex than the one from ground-based observations, it is still possible to obtain the mean value of the large separation and to proceed further in attempting to determine the degree of at least some modes which will constitute the cornerstone of a mode identification.

However from ground-based observations the detected frequencies do not include part of the asymptotic regime. We do not know whether space data will provide frequencies in the asymptotic regime. In the present paper, we therefore discuss the case where these frequencies are not detected. Section 2 describes how the frequency spectrum is built. In Section 3, patterns are searched using frequency spacing histograms. Then echelle diagrams are computed. Discussion and perspectives are given in Section 4.

## 2. Amplitude distribution: visibility effect

We consider a 1.85 $M_\odot$ model (see Baglin et al. 2000 for more details) and retain modes with degree from 0 to 10 with frequencies in the theoretical unstable range [80-410]$\mu$Hz given by the oscillation code written by W. A. Dziembowski (1982). High frequencies which falls in the asymptotic regime are not included. The oscillation amplitudes are computed in the COROT photometric system (370-950 nm), according to Watson (1988) for the flux change for a nonradial pulsation. Stellar model atmospheres are built for that specific purpose with ATLAS9 (Heiter et al. 2001 in prep.) and consistent limb darkening coefficients computed (Barban et al. 2001, in prep.). For the non adiabatic phase lag between temperature and pressure variations, we use the values given by Dziembowski's oscillation code. The intrinsic amplitude is assumed to be the same for all the modes and is chosen so that $\ell = 0$ modes have an amplitude of 1 mmag as typically observed from the ground. For the amplitudes of modes with higher degrees, we used the amplitude ratio with $\ell = 0$. The amplitude ratio depends on the inclination to the line of sight. We averaged the amplitudes obtained for values of the inclination to the line of sight of 0, 20, 40, 60, and 80 degrees.

Figure 1 with a typical result illustrates the visibility effect. In the case of Fig. 1, from the ground with a maximum amplitude of $10^{-3}$ in relative flux, we are able to detect some $\ell = 0$, 1 and 2 modes and from space with COROT, we will see some $\ell = 0,1,2,3,4,6,8$ and 10 modes. So depending on the threshold, we must expect to detect more or less modes with different $\ell$. Whether odd highest $\ell$ modes (5,7,9) will be detected depend on intrinsic amplitude and detection threshold. The different feature for even and odd modes from $\ell = 4$ is attributed to geometric and limb-darkening terms of the expression of flux change. Similar results have
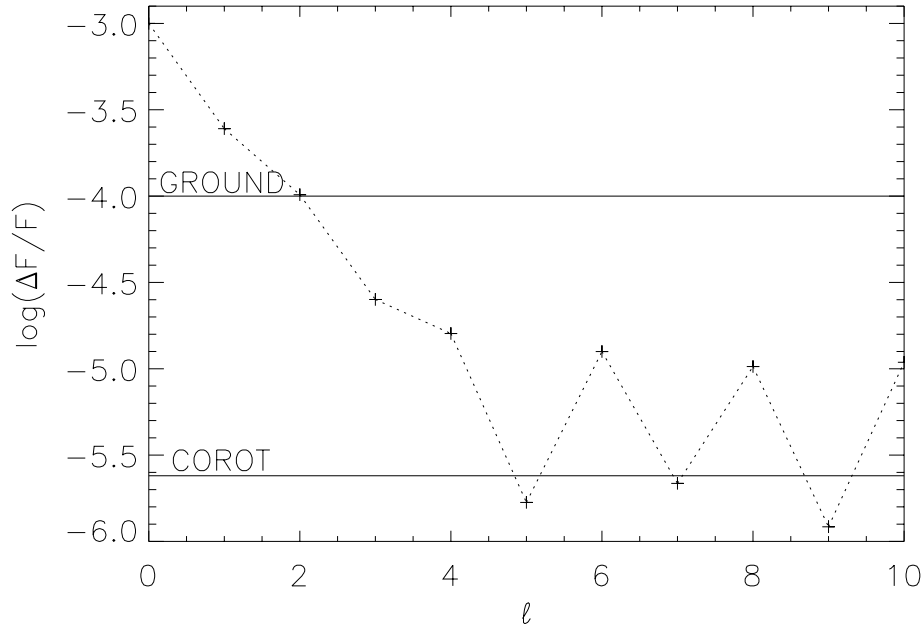
Fig. 1.— Oscillation amplitudes in intensity as a function of $\ell$. This graph is obtained for a frequency 210 $\mu$Hz. The line marked "GROUND" corresponds to a typical detection threshold obtained from the ground: $10^{-4}$. The line marked "COROT" corresponds to the expected space detection threshold of $2 \ 10^{-6}$.

been obtained by Balona & Dziembowski (1999) and by I. Roxburgh (private communication).

To be more realistic, we have adopted an amplitude distribution which looks like FG Vir data (Breger et al. 1998). We arbitrarily defined an amplitude distribution with gaps which yields a frequency spectrum looking like the one of FG Vir. (Barban et al. 2000).

## 3.  Search for patterns in the frequency spectrum

Although the considered oscillation modes are not in the asymptotic regime, We nevertheless search in the frequency spectrum built in Section 2 for some frequency equidistances. Differencies between two frequencies are computed to build a histogram of these differencies which we call a *frequency spacing histogram* (e.g. Breger et al. 1999).

When all the unstable mode frequencies are included, no specific structure can be detected. The histogram is perturbed by high $\ell$ modes which do not respect the equidistance and by mixed and g modes (Barban et al. 2000).

If now we turn to the COROT case, no significant improvement is obtained when we keep the unstable modes with amplitude above $2\ 10^{-6}$. The histogram is still perturbed by nonequidistant modes as in the precedent case. The same is true when we remove high $\ell$ modes which perturb the histogram by increasing the amplitude threshold. That means that now we keep modes with amplitude higher to $10^{-5}$ (Fig. 2)

Because mixed modes of low degree contaminate low frequency regime, we keep the same amplitude threshold of $10^{-5}$ and remove the low frequency modes which are mostly mixed modes and perturb the histogram. Figure 3 shows:

- an excess of signal between approximately 40 and 50 $\mu$Hz with a strong peak at 40 $\mu$Hz. This peak is interpreted as a mean value of the large separation ($\overline{\Delta\nu}$, $\Delta\nu = \nu_{n,\ell} - \nu_{n-1,\ell}$), which differs from the asymptotic value, i.e. 47 $\mu$Hz.

- a low frequency decrease. The decrease at low frequencies is attributed to the remaining mixed modes.

From the ground with a detection threshold of $10^{-4}$, we would obtain Fig. 4.

We have shown here that from space data it is possible, at least, to recover a mean value of the large separation which is not the asymptotic one but which can help to identify modes as we will see in the next Section. Ground based observations can serve to confirm space observations and vice-versa.

### *3.1.   Towards mode identification*

Once $\overline{\Delta\nu}$ is known either as described above (or with another method), it is possible to built an echelle diagram (Unno et al. 1989). This diagram emphasizes the signature of the small separation predicted by the asymptotic theory in function of the degree $l$ of the modes:

$$\nu_{n,\ell+2} - \nu_{n+1,\ell} \sim 2(2\ell + 3)D_\ell(\nu) \tag{1}$$

where $D_\ell(\nu)$ is a quantity which depends on the derivative of the sound speed, and is particularly sensitive to the stellar core (Unno et al. 1989). This can be used as a first step towards identifying the detected modes as $\ell$ place themselves in different patterns. In the case where we are not in the asymptotic regime, we know here that remains such trend at lower frequencies. Then this method can also be used where we are not in the asymptotic regime using the mean value of the large separation corresponding to the considered region.

From simulated ground-based data, it is difficult to say something very precise because of the too small number of modes (Fig. 5). Without models it is difficult to know if the pattern in the echelle diagram is due to $\ell= 0$ or $\ell= 1$.

With the set of modes corresponding to modes with frequencies greater than 200 $\mu$Hz and with modes with amplitude greater than $10^{-5}$, we saw in the last Section that we can determine a mean value of the large separation. This set of modes is now used to build an echelle diagram (Fig. 6) corresponding to the mean
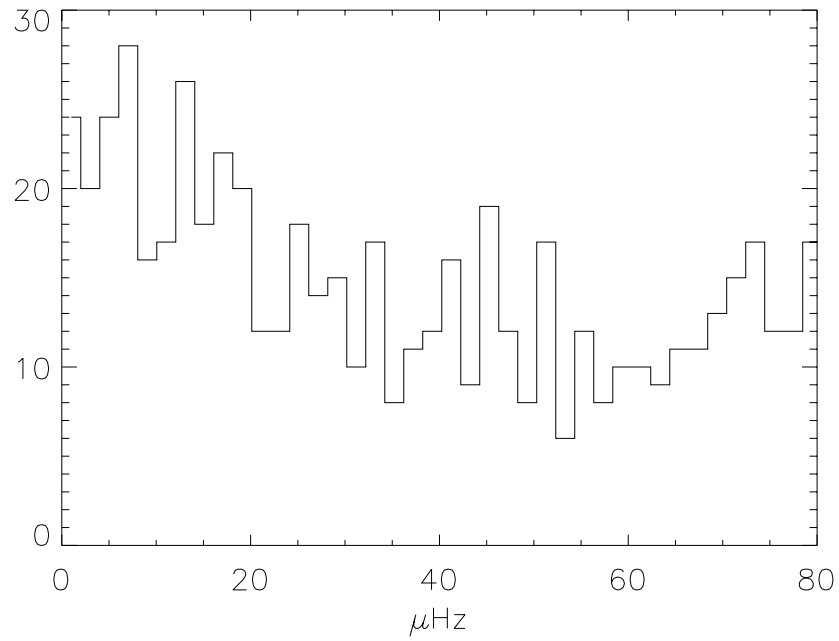
Fig. 2.— Frequency spacing histogram computed in the frequency unstable domain for modes with amplitude greater than or equal to $10^{-5}$
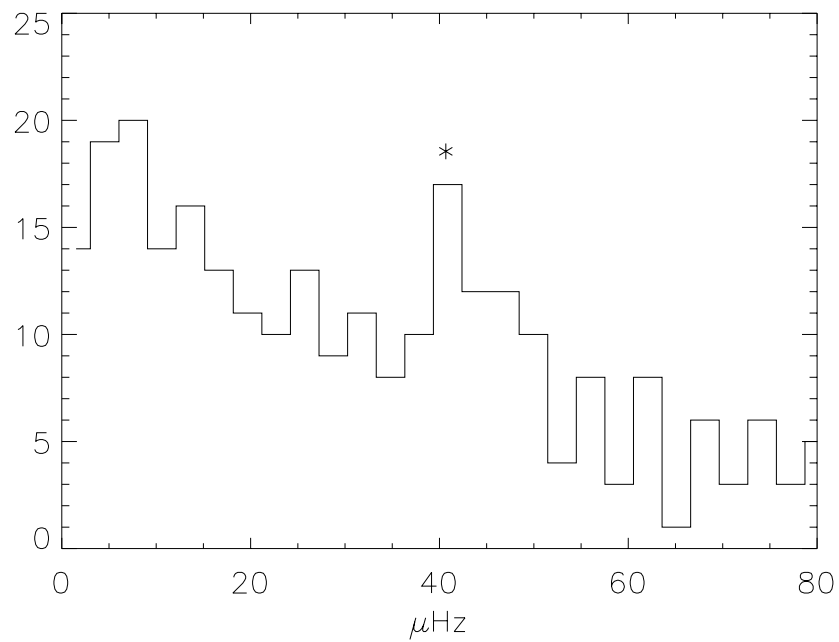


Fig. 3.— Frequency spacing histogram computed from the modes frequencies in [200-409]$\mu$Hz and for modes with amplitude greater or equal than $10^{-5}$.
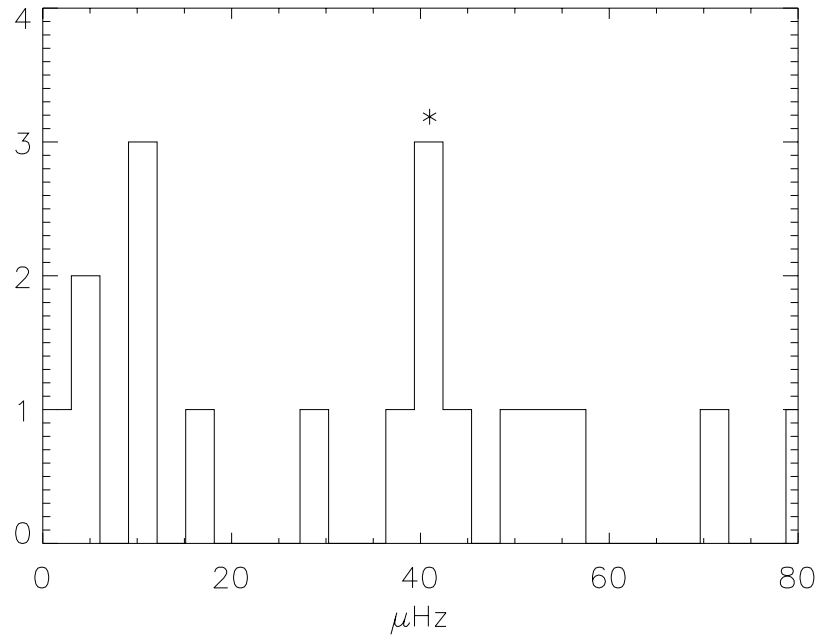
Fig. 4.— Frequency spacing histogram computed from the modes frequencies in [200-409] $\mu$Hz and for modes with amplitude greater or equal than $10^{-4}$.
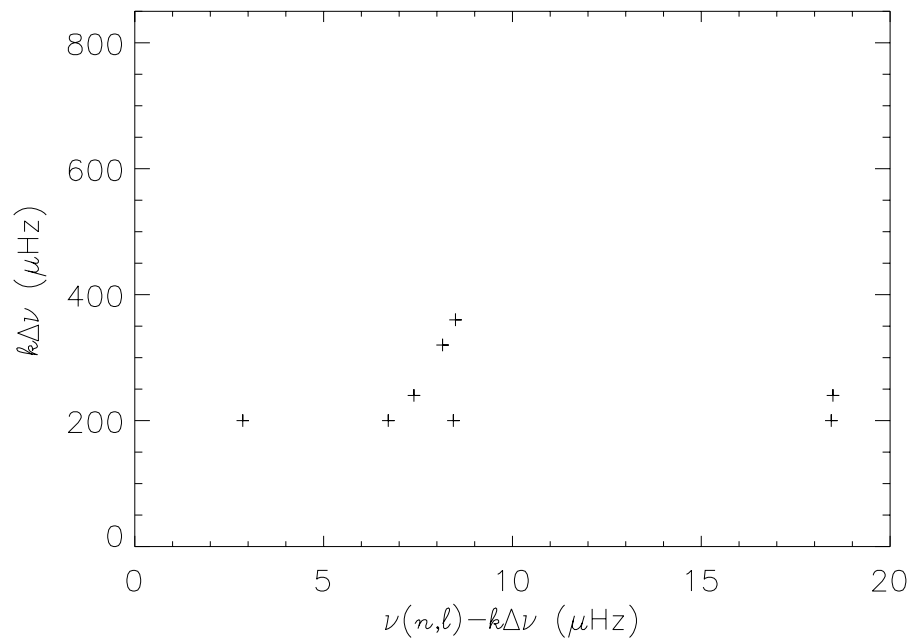


Fig. 5.— Echelle diagram with $k$ as an integer with $\Delta\nu ==40$ $\mu$Hz for $\ell==0$ to $\ell==10$ modes between 200 and 409 $\mu$Hz and amplitudes greater than $10^{-4}$.

value of the large separation found (i.e. 40 $\mu$Hz).
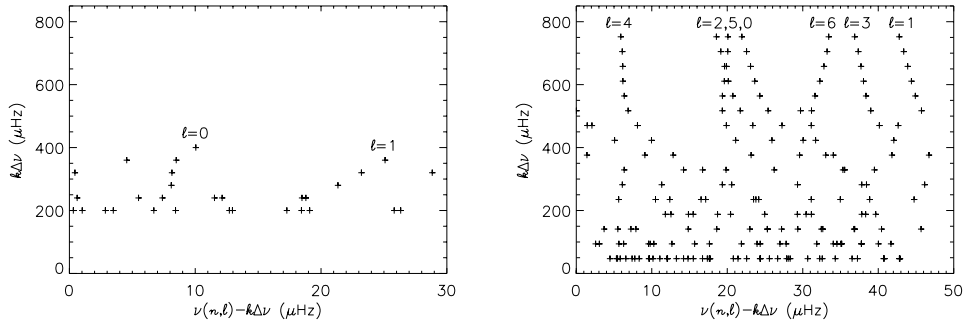


Fig. 6.— Echelle diagram with $k$ as an integer. Left: with $\Delta\nu = 40$ $\mu$Hz for modes between 200 and 409 $\mu$Hz and amplitudes greater than $10^{-5}$. Right: with $\Delta\nu ==47$ $\mu$Hz for modes between 50 and 800 $\mu$Hz.

The unstable modes we consider in this present case have frequencies in the range where everything is mixed up in the echelle diagram of the "ideal case" (Fig. 6, Right). However selecting higher frequencies in the unstable domain and using the value of the large separation given by the histogram (Fig. 6, Left), we can recover nice structures associated to $\ell==0,1$ and 2. We are not far from mode identification.

## 4. Conclusion and perspectives

We have built a frequency data set as can be expected from space data and have shown that it is still possible to recover patterns in the complicated simulated space data frequency spectrum and then to be not far from modes identification. Although dependent on the amplitude pattern chosen here, it is still reasonable to conclude that there exists a regime in frequency and amplitude which is not reacheable from the ground and which remains simple enough to determine $\ell=0$, 1, 2 modes. Once these modes are determined, the other modes can be easily identified.

The frequency data does not include rotational splittings. The study of the effect of rotation is a work in progress. Another next issue will be extracting structure associated to high degree modes and mixed modes.

## Acknowledgements

# REFERENCES

Baglin A., Barban C., Goupil M.J., Michel E., Auvergne M., "Delta Scuti and Related Stars", ASP Conference Series, Vol. 210, 2000, M. Breger & M.H. Montgomery, eds., p. 359

Balona L.A., Dziembowski W.A., 1999, MNRAS 309, 221

Barban,C., Goupil, M.J., Van'tVeer C., Garrido, R. , 2000, Soho/Gong workshop, Spain

Breger M., Pamyatnykh A.A, Pikall H., Garrido R., 1999, A&A 341, 151

Breger M. Zima W., Handler G., Poretti E., Shobbrook R.R., Nitta A., Prouton O.R., Garrido R., Rodriguez E., Thomassen T., 1998, A&A 331, 271

Dziembowski W.A., Balona L.A., Goupil M.-J., Pamyatnykh A.A., 1998, in: Proc. The First MONS Workshop: Science with a Small Space Telescope, eds.: H. Kjeldsen, T.R. Bedding, Aarhus Universitet, p. 127

Dziembowski W.A., 1982, Acta astron. 32, 147

Garrido R., "Delta Scuti and Related Stars", ASP Conference Series, Vol. 210, 2000, M. Breger & M.H. Montgomery, eds., p.67

Unno W., Osaki Y., Ando H. Saio H. Shibahashi H., 1989, Nonradial Oscillations of Stars, University of Tokyo Press, 2nd ed.

Watson R.D., 1988, Ap&SS 140, 225

**HH#2**

# Results

# Peak bagging for solar-like stars

Thierry Appourchaux
*Research and Science Support Department, European Space Agency, Keplerlaan 1,
2200AG, Noordwijk, The Netherlands*

30 September 2002

**Abstract.** The identification of the low-degree p modes in other stars is the challenge of future asteroseismology space missions such as COROT, MONS, Most or Eddington. The identification is based on a priori knowledge of the characteristics of the modes. We shall review the most common assumptions needed for the identification such as basic stellar structure, visibilities, rotational splittings or linewidths. We shall describe a few tools needed for facilitating the identification. As soon as modes are properly identified, the peakbagging of the mode characteristics can begin using Maximum Likelihood Estimation. We give examples of the whole process using solar data and hare-and-hound exercises performed in the frame work of the COROT project.

**Keywords:** Sun, stars, seismology

## 1. Introduction

In the very near future, there shall be a fleet of space missions aiming at understanding the internal structure of the stars: Most[1], COROT[2], MONS[3] and Eddington[4]. All these missions will observe global oscillations of the stars by measuring tiny light fluctuations; they are due to the perturbation of the star surface by the oscillations. The detection and identification of these modes of oscillation is the challenge of all these missions. This challenge is for most stars extremely difficult (e.g. Cepheids) but easier for solar-like stars. For these latter, the Sun has been and is a great aid and example.

Hereafter after having defined what is meant by solar-like stars, I explain how the current identification can be based on that of the

---

[1] Microvariability and Oscillations of Stars, a Canadian mission to be launched in April 2003 (Matthews et al., 2000)

[2] COnvection and ROTation, a CNES mission to be launched in Nov 2005 (Baglin and The COROT Team, 1998)

[3] Measuring Oscillations in Nearby Stars, a Danish mission under study to be launched in 2005 (Kjeldsen et al., 2000)

[4] A mission part of the 'Cosmic Vision' programme of ESA, to be launched in 2008 (Favata et al., 2000)

Sun case. When the identification is achieved, peak bagging[5] can be started; the theory of which is explained here. The practice of mode identification and peak bagging is developed through the use of hare-and-hound exercise. The results of such exercises carried out by the COROT Data Reduction Group are presented here.

## 2.   What is a solar-like star?

The definition of a solar-like star depends on whom you talk to. There are basically 3 'definitions' driven by:

1. *the stellar structure*: the solar-like star is similar to the Sun, i.e. with an outer convection zone and a radiative zone. Stars with a mass smaller than 1.2 $M_\odot$ satisfy the criterion as they do not have a convective core yet (Iben and Ehrman, 1962; Cox and Giuli, 1968).

2. *the excitation process of the oscillations*: the process is similar to that of the Sun, i.e. due to turbulent convection (Houdek et al., 1999). It occurs in stars with mass smaller than 2 $M_\odot$ with an outer convection zone even if it is very shallow (Houdek et al., 1999); the efficiency of the process is driven by the turbulent Mach number $M_t$ (Houdek et al., 1999) that is maximum for 1.6 $M_\odot$. Above roughly 1.5 $M_\odot$ the stars have overstable modes; they enter the Cepheids instability strip (Houdek et al., 1999).

3. *the structure of the oscillation spectrum*: a regular spacing of the modes must be observed as predicted by asymptotic frequencies (Tassoul, 1980). The regular spacing provides the basis for a diagnostic tool: the *echelle diagramme* devised by Grec (1981) for the Sun.

The latter definition is the most relevant. The reason for this choice is the power of the echelle diagramme as a diagnostic tool. The structure of the ridges in the echelle diagramme of a solar-like star looks like those of the Sun. The experience gained in helioseismology will be a considerable help in this respect, especially for mode identification.

---

[5] peak bagging is a term coined by Jesper Schou who is a keen moutain climber. Such individuals use to record climbed peaks in a book and referred to it as the peak bagging list. . .

## 3.  Past and present mode-identification methodology

### 3.1.  IN THE EARLY AGE OF HELIOSEISMOLOGY

The first identification and identification of the solar oscillations as global modes (low degree) is attributed to Claverie et al. (1979). They identified the regular spacing based on the prediction made for low degree, low order mode frequencies by Iben and Mahaffy (1976). They had enough foresight for finding that the detected modes were higher order modes of about $n > 20$. Unfortunately, they could not identify the degree of the modes because the length of the time series did not allow for separating the odd degrees ($l = 1 - 3$) from the even degree ($l = 0 - 2$)[6]. Such an identification was performed by Grec et al. (1980) using the echelle diagramme and the difference of the small frequency separation. The length of the time series was such that they had to collapse the power along the ridges in order to increase the signal-to-noise ratio (Fossat et al., 1981). At this stage, such a technique allowed to resolve the rotational splitting (Grec et al., 1983). The identification of the order $n$ was only made possible by identifying the f-mode ridge in the $(l, \nu)$ obtained by making images of the Sun (Deubner, 1975).

### 3.2.  IN THE XXIST CENTURY AND BEYOND

From helioseismology, we can identify three steps in the mode identification, all using the echelle diagramme:

1. determination of the large frequency separation (i.e. $\Delta\nu_0$)

2. degree identification and determination of the small frequency separation (i.e. $\delta_{02}, \delta_{13}$)

3. rotational splitting and star inclination estimation

These steps are intimately linked to the length of the time series and the signal-to-noise ratio. A typical large frequency separation for a solar-like star ranges from 40 $\mu$Hz to 170 $\mu$Hz which is easily resolved by observing a star over a few hours (Audard and Provost, 1994). The small frequency separation is more difficult to retrieve as it ranges typically from 3 to 13 $\mu$Hz (Audard and Provost, 1994), and requires a few days before resolving it. The visibility of the various degrees can also be used for identifying the modes in the second step. For instance the $l = 3$ modes are significantly damped by the integration over the

---

[6]  each pair presents a different small frequency separation of 10 $\mu$Hz for $l = 0 - 2$ and 13 $\mu$Hz for $l = 1 - 3$
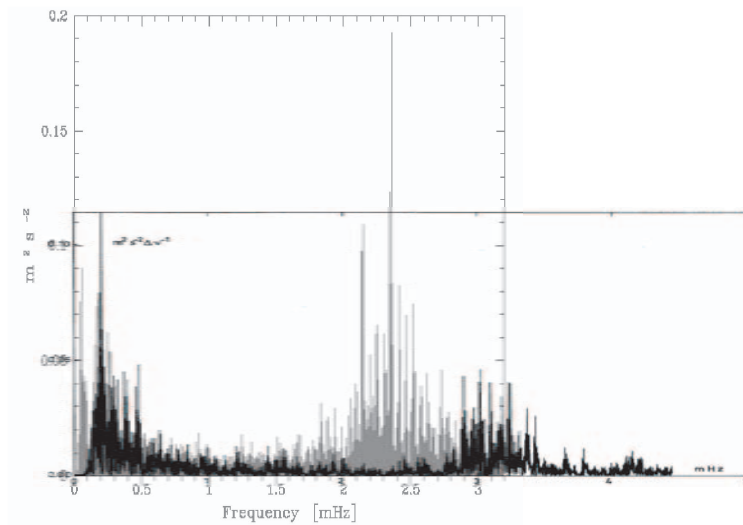
*Figure 1.* The power spectra of the Sun observed by Grec and Fossat (1977) (Black) and of $\alpha$ Cen observed by Bouchy and Carrier (2002) (Grey). Thanks to modern technology, they were put to the same scale showing that the stellar observations of today match the solar observations of the 70's. Both spectra show what can be obtained for a few days of observation stellar radial velocities. The frequency at which the modes are maximum depends upon the

stellar disk (Christensen-Dalsgaard and Gough, 1982 for velocity and Toutain and Gouttebroze, 1993 for intensity); it renders the $(l = 0 - 2)$ ridge significantly different from that of the $(l = 1 - 3)$ ridge in the solar case. The rotational splitting is even more challenging: it does require a few months of observation in the case of the Sun, as its rotation period is of the order of a month.

The order identification requires more technological developments. In the not too distant future space based interferometers may provide the first low-resolution images of the stars. If it were possible to make higher-resolution images of the stars, the f-mode identification would certainly be achieved for stars; this is likely to a be dream for the XX1st century and beyond.

At the time of writing, only two stars have been observed showing unambiguously solar-like p modes: the Sun and $\alpha$ Cen. These two stars are the test bed of the identification process described above. Figure 1 shows what can be obtained by observing the Sun (Grec and Fossat, 1977) and $\alpha$ Cen (Bouchy and Carrier, 2002) over a few days. The large separation is easily identified for both stars. For $\alpha$ Cen, the echelle diagramme does reveal the small separation in a more obvious manner (Bouchy and Carrier, 2002). As for the splitting, the time series are still

too short for $\alpha$ Cen for revealing the splitting. Careful attempts have been made by (Bouchy and Carrier, 2002) for deriving the rotational splitting of the modes of $\alpha$ Cen but more observing time is required. The measurements of the rotational splitting for low-degree modes is rather difficult. That is only in the mid-90's, that reliable splittings could be obtained for the Sun using the theory of power spectrum fitting. It is likely that such measurements for the stellar case will require extreme care before getting some confidence in the results, but as we show hereafter the theory of power spectrum fitting is now well mastered.

## 4. Theory of peak bagging

Before we can proceed with the peak bagging, it is necessary to have been able to properly identify the modes as described in the previous section. This is a very important step allowing to tag each ridge in the echelle diagramme with a degree $l$. Peak bagging means derivation of the mode parameters through power spectrum fitting. The theory of power spectrum fitting for the Sun as a star is now well developed. It has been described in numerous articles and is now well understood; it is based on the use of Maximum Likelihood Estimators (MLE) (See Duvall and Harvey, 1986 and Appourchaux et al., 1998 for a review). Here I briefly summarize the technique. The power spectrum is fitted using MLE assuming:

- a statistics for the spectrum

- a model for the modes

The statistics of the spectrum for uninterrupted time series is a $\chi^2$ with 2 degree of freedom (Gabriel, 1994). The model of the modes includes the mode frequency, the mode linewidth, the mode amplitude, the mode profile and the background noise. In some case, modes of different degrees overlaps ($l = 0 - 2$, $l = 1 - 3$), they are usually fitted together. The simultaneous fitting these modes require to know the visibility of the modes. For intensity this is given by Toutain and Gouttebroze (1993) while for velocity this is given by Christensen-Dalsgaard and Gough (1982). The rotational mode splitting and the inclination of the star have to be taken into account. There are up to $2l + 1$ components depending on the inclination of the star. The star inclination is taken into account depending on the way the modes are observed (velocity or intensity). The spherical harmonics eigenfunctions has to be weighted by the projection onto the line of sight or by the limb darkening. For intensity, the visibilities of the modes can simply

be approximated using the decomposition given by quantum mechanics rotation matrices (Toutain and Gouttebroze, 1993).

Error bars on the parameters are derived using the inverse of the Hessian (or curvature matrix) (Appourchaux et al., 1998; Toutain and Appourchaux, 1994). The error bars derived give a good estimate of the true error bars (Appourchaux et al., 1998). The validity of such error bars can be tested using the $z$ test as described by Chaplin et al. (1998); this is a test comparing internal and external error bars.

Finally, the significance of parameters (under the $H_0$ hypothesis) can be checked using the likelihood ratio test as described by Appourchaux et al. (1998). This test is rather useful for assessing the adequacy of the model fitted to the data.

## 5. Mode identification and peak bagging in practice: hare-and-hound exercise

As coined by an anonymous scientist:'In theory there is no difference between theory and practice; in practice there is'. The theoretical approach described above needs to be tested with *real* data. In the history of helioseismology, the *real* data have been sometimes fabricated in a such a way that it looked like a road runner chase. The term hare and hound[7] appeared in the GONG[8] Newsletter #9 of 1988 when the GONG Inversion team performed simulated inversion on data fabricated by a hare (Douglas Gough).

Within the COROT team, we found that it would be useful to have such a hare-and-hound exercise that would simulate (as well as stimulate) the mode identification and the peak bagging. The steps for this exercise are the following:

— a Team A generates theoretical mode frequencies and synthetic time series

— a Team B analyzes the time series, performs mode identification, peak fitting and structure inversion

The two teams have no access to any other information but the time series and the known characteristics of the star. Nothing else is allowed.

### 5.1. TEAM A: THE MAKING OF SYNTHETIC TIME SERIES

The steps for making the artificial time series are very similar to those needed for using MLE. You need to assume:

---

[7] In French we would rather call it: *le jeu du chat et de la souris*
[8] Global Oscillation Network Group

— a statistics for the (Fourier) spectrum

— a model for the modes

The statistics of each component of the Fourier spectrum is assumed to be normally distributed with a zero mean and an rms value described by the model for the modes. For the model of the modes, the following data are needed:

— the characteristics of the solar-like star

— the theoretical or asymptotic mode frequencies (à la Tassoul)

— the mode visibility (Christensen-Dalsgaard and Gough, 1982; Toutain and Gouttebroze, 1993)

— the excitation profile and linewidth (Houdek et al., 1999; Samadi and Goupil, 2001; Samadi et al., 2001)

— the rotational splitting and stellar inclination

— the background stellar noise derived from that of Trampedach et al. (1998) or of the Sun as in Harvey (1993)

— any other parameter not mentioned above (asymmetry, trick, mind twister or anything else to make it more *real*)

As soon as each Fourier component is properly modeled, an inverse Fourier transform provides the necessary time series that will be passed to the next team.

## 5.2. Team B: Power spectrum analysis

The power spectrum analysis can be done in various ways. Here I recommend to perform the steps as described in Section 3 and 4, i.e. to make an echelle diagramme of the power spectrum, perform mode identification and then to fit the modes according to a model. When the p-mode parameters are obtained the last task of this team is to invert the mode frequencies in order to derive the stellar structure. This is beyond the scope of this talk but this is discussed by Berthomieu in these proceedings in the frame work of the COROT HH exercise described hereafter.

## 5.3. The COROT HH exercises

The Asteroseismology and Exoplanet-search mission of the French space agency (CNES) is going to be launched at the end of 2005. There

are several scientific groups being involved in the preparation of the mission. The Seismology Working Group (SWG) prepares the data analysis and scientific interpretation of the seismology data. The Data reduction group of the SWG is more precisely in charge of the data analysis aspects. This group has set up three different hare-and-hound exercises[9]:

- HH#1 Validation of power spectrum fitting technique (no inversion, asymptotic frequencies)

- HH#2 Recovery of the initial stellar model for synthetic stars (full cycle as described above)

- HH#3 Choice of targets

The first exercise is over and lead to the validation of power spectrum fitting performed by different groups (Institut d'Astrophysique Spatiale, Orsay: Boumier; Observatoire de Nice: Toutain; European Space Agency: Appourchaux. The last exercise is on going. The second HH exercise is also over and I report on the results obtained.

### 5.3.1. *The teams*
There were three teams involved in the process:

- *Meudon*: Observatoire de Meudon (stellar model and inversion) + Appourchaux (time series and power spectrum fitting)

- *Nice*: Observatoire de Nice (stellar model and inversion) + Toutain (time series and power spectrum fitting)

- *Queen Mary*: Queen Mary stellar (model and inversion) + Barban (time series and power spectrum fitting)

Each team produced synthetic time series and passed it on to the 2 other groups for power spectrum fitting and structure inversion.

### 5.3.2. *A piece-of-cake case: Nice synthetic data*
Figure 2 shows the echelle diagramme obtained for the *Nice* synthetic data. The time series are 150-day long and sampled at 60 sec. The frequencies fitted are obtained within about 0.1 to 0.2 $\mu$Hz of the theoretical frequencies. SImilar results were obtained with an other piece-of-cake time series that of the *Meudon* team. The frequency comparisons and inversion associated with this time series are presented elsewhere in these proceedings by Berthomieu et al.

---

[9] The activity related to these HH exercise can be found in http://virgo.so.estec.esa.nl/html/corot/datagroup/hh.html
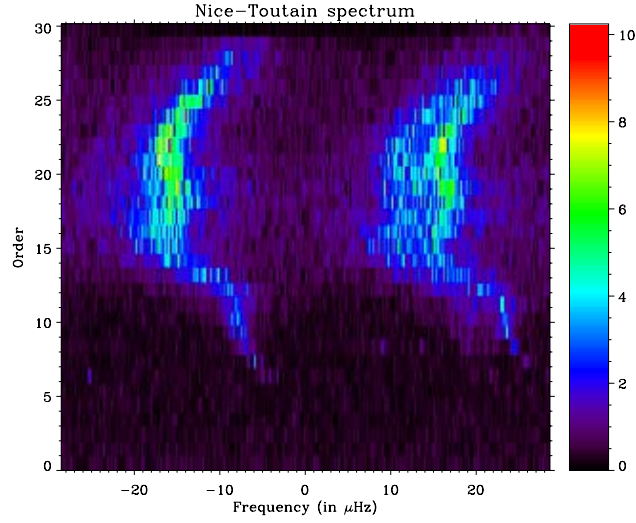
*Figure 2.* Echelle diagram of the *Nice* time series. The large separation is about 58 $\mu$Hz. The ridge at the left hand side is due to the $l = 1$ modes. The identification is rather easy because the ridge at the right hand side show a more complex structure related to the splitting of the $l = 2$ modes interfering with the $l = 0$ mode ridge. The order labeling the $y$ axis have no absolute meaning.
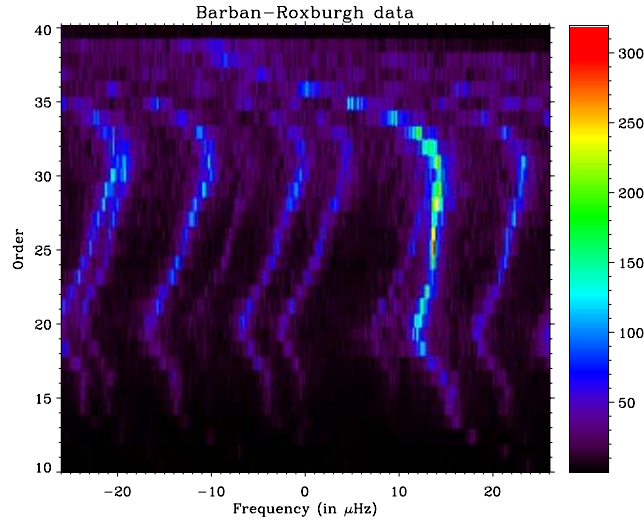


*Figure 3.* Echelle diagramme of the *Queen-Mary* time series. The bright ridge at $+12$ $\mu$Hz is identified as due to the $l = 0$ modes; it is the only one ridge with this shape. The 3 parallel ridges at $-23\mu$Hz, $-13\mu$Hz and $-3\mu$Hz are attributed to the $m = -1$, $m = 0$ and $m = +1$ modes of $l = 1$; the splitting is about $10\mu$Hz. The ridges left over (5 of them) were attributed to the $l = 2$ modes; the $m = 0$ mode ridge crosses the $l = 0$ mode ridge. The $m = -2$ and $m = -1$ mode ridges seemed to be on either side of the $l = 1$, $m = +1$ mode ridge, while the $m = +1$ and $m = +2$ mode ridge are on either side of the $l = 1$, $m = -1$ ridge.
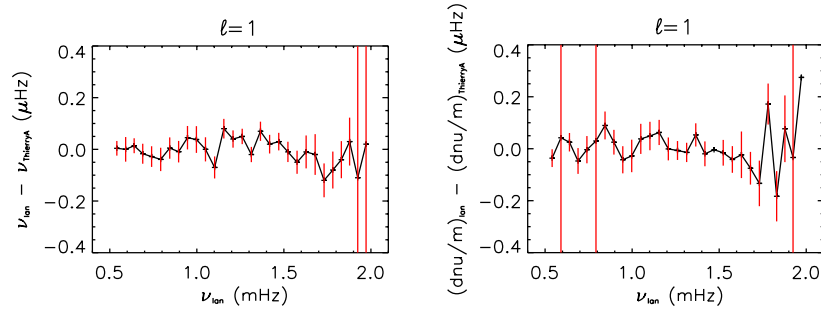
Figure 4. Comparison between the parameters fitted by the *Meudon* team with the theoretical parameters of the *Queen Mary* team; (left) for the $l = 1$ mode frequencies, (right) for the $l = 1$ mode splitting. The agreement between the input and the fit is excellent for $l = 1$; a similar agreement was obtained for $l = 0$.
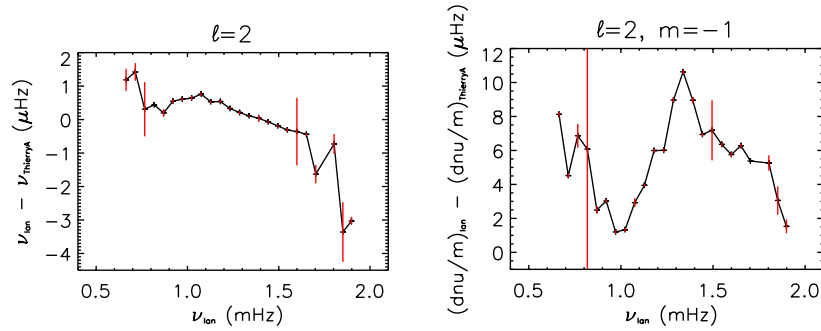


Figure 5. Comparison between the parameters fitted by the *Meudon* team with the theoretical parameters of the *Queen Mary* team; (left) for the $l = 2$ mode frequencies, (right) for the $l = 2, m = 1$ mode splitting. The agreement between the input and the fit is extremely poor. The misidentification of the $l = 2$ is obvious; the ridge identified as an $l = 2, m = 0$ was as a matter of fact a $l = 3, m = -2$.

### 5.3.3. A difficult case: Queen Mary synthetic data

Figure 3 shows the echelle diagramme for the *Queen Mary* synthetic data. The identification as explained in the caption is somewhat more difficult, to say the least. The main problem is that it seemed that the mode visibility was not according to what is usually expected, in addition the large 'apparent' rotational splitting confused even more the data fitters. The $l = 0$ and $l = 1$ modes were identified with some confidence. De facto we did not assume a common amplitude for the $l = 2$ modes constrained by the visibility of the multiplet as given by Toutain and Gouttebroze (1993). Instead we assumed that the $l = 2$ multiplet had 5 different amplitudes not constrained by geometrical visibility. This was as matter of fact a correct assumption verified *a posteriori*, but not sufficiently correct as it turned out that the $l = 3$ mode ridge was improperly labeled as being $l = 2$.

Figures 4 and 5 shows the results obtained when comparing the output fitted parameters with those of the input theoretical parameters. The results obtained for Figure 4 are typical of what we obtained for other time series (See Berthomieu et al in these proceedings), or for the $l = 0$ of the *Queen-Mary* time series. Figure 5 is an example of what happens when modes are misidentified. This exemplifies again the usefulness of the *echelle diagramme* as a diagnostic tool.

## 6. Conclusion

I have shown that mode identification and power spectrum fitting for solar-like stars benefit from 20 years of helioseismic experience. The methodology explained here can be easily applied when the signal-to-noise ratio is rather high. When this is not the case other techniques have to be used that are beyond the scope of this review. Hands-on experience for solar-like stars awaits the avaibility of space-based measurements (COROT, MOST). Within the Corot team, the waiting has been replaced by the use of hare-and-hound exercises. Examples of the results obtained within the COROT team show what can happen when one encounters the expected and the unexpected. This is the latter that is most interesting.

## Acknowledgements

## References

Appourchaux, T., L. Gizon, and M. C. Rabello-Soares: 1998. *A&A Sup. Series* **132**, 107.

Audard, N. and J. Provost: 1994. *A&A* **282**, 73.

Baglin, A. and The COROT Team: 1998. In: F.-L. Deubner, J.Christensen-Dalsgaard, and D.Kurtz (eds.): *IAU Symp. 185: New Eyes to See Inside the Sun and Stars*, Vol. 185. p. 301, Kluwer Academic Publishers, Dordrecht, The Netherlands.

Bouchy, F. and F. Carrier: 2002. *A&A* **390**, 205.

Chaplin, W. J., Y. Elsworth, G. R. Isaak, R. Lines, C. P. McLeod, B. A. Miller, and R. New: 1998. *MNRAS* **300**, 1077.

Christensen-Dalsgaard, J. and D. O. Gough: 1982. *MNRAS* **198**, 141.

Claverie, A., G. Isaak, C. McLeod, H. van der Raay, and T. Roca Cortés: 1979. *Nature* **282**, 591.

Cox, J. P. and R. T. Giuli: 1968, *Principles of stellar structure*. New York, Gordon and Breach.

Deubner, F.-L.: 1975. *A&A* **44**, 371.

Duvall, T. L., J. and J. W. Harvey: 1986. In: *Seismology of the Sun and the Distant Stars*. p. 105.

Favata, F., I. Roxburgh, and J. Christensen-Dalsgaard: 2000. In: T.C.Teixeira and T.R.Bedding (eds.): *The Third MONS Workshop: Science Preparation and Target Selection*. p. 49, Aarhus Universitet.

Fossat, E., G. Grec, and M. Pomerantz: 1981. *Solar Physics* **74**, 59.

Gabriel, M.: 1994. *A&A* **287**, 685.

Grec, G.: 1981, 'Thèse de doctorat'. Ph.D. thesis, Université de Nice.

Grec, G. and E. Fossat: 1977. *A&A* **55**, 411.

Grec, G., E. Fossat, and M. Pomerantz: 1980. *Nature* **288**, 541.

Grec, G., E. Fossat, and M. A. Pomerantz: 1983. *Solar Physics* **82**, 55.

Harvey, J.: 1993. *ASP Conference Series* **42**, 111.

Houdek, G., N. J. Balmforth, J. Christensen-Dalsgaard, and D. O. Gough: 1999. *A&A* **351**, 582.

Iben, I. and J. Mahaffy: 1976. *ApJ Letters* **209**, L39.

Iben, I. J. and J. R. Ehrman: 1962. *ApJ* **135**, 770.

Kjeldsen, H., T. R. Bedding, and J. Christensen-Dalsgaard: 2000. In: L.Szabados and D.Kurtz (eds.): *ASP Conf. Ser. 203*. p. 73.

Matthews, J. M., R. Kuschnig, G. A. H. Walker, J. Pazder, R. Johnson, K. Skaret, E. Shkolnik, T. Lanting, J. P. Morgan, and S. Sidhu: 2000. In: L.Szabados and D.Kurtz (eds.): *ASP Conf. Ser. 203*. p. 74.

Samadi, R. and M.-J. Goupil: 2001. *A&A* **370**, 136.

Samadi, R., M.-J. Goupil, and Y. Lebreton: 2001. *A&A* **370**, 147.

Tassoul, M.: 1980. *ApJ Sup. Series* **43**, 469.

Toutain, T. and T. Appourchaux: 1994. *A&A* **289**, 649.

Toutain, T. and P. Gouttebroze: 1993. *A&A* **268**, 309.

Trampedach, R., J. Christensen-Dalsgaard, A. Nordlund, and R. F. Stein: 1998. In: H. Kjeldsen and T. Bedding (eds.): *The First MONS Workshop: Science with a Small Space Telescope*. p. 59, Aarhus Universitet.

# Hare & Hound exercise with simulated COROT data

G. Berthomieu [1], T. Appourchaux[2] on behalf of the COROT
Seismology Working Group[†]

[1] *Département Cassini, UMR CNRS 6529, Observatoire de la Côte d'Azur, BP
4229, 06304 Nice Cedex4, France.*
[2] *Research and Science Support Department of ESA, ESTEC, P.O.Box 299,
NL-2200AG Noordwijk, The Netherlands.*

**Abstract.** With the aim of preparing the interpretation of future COROT observations, a Hare-and-Hound exercise has been performed on a solar-like oscillating star. The methods used to construct simulated time series and to recover the properties of the star using the frequencies extracted from these time series are described and the comparison between the results and the theoretical inputs are presented.

## 1. Construction of simulated time series

Two hare-and-hound exercises (H&H) have been performed, by the teams of the COROT sismogroup. The different steps of the H&H exercise are the following:

- Construct a stellar model $M$ (mass), $Y$ (helium), $Z/X$ (metallicity), $\zeta_{ov}$ (overshoot) with constraints[1] on luminosity ($L/L_\odot$), effective temperature ($T_{eff}$) and metallicity ($Fe/H$). Compute the frequencies of the models $\nu_{n,\ell}$. Construct a simulated time series which represents what the observation of the pulsating model by COROT would give.

- Extract the frequencies: hereafter referenced as "observed frequencies" $\tilde{\nu}_{n,\ell}$ and rotational splittings (not yet exploited).

- Interpret them in terms of internal structure and rotation of the star. Hereafter results concern the direct approach that is the search for the closest model to the "observations". No inversions are presented.

Two input models (respectively Ex1 and Ex2), satisfying the constraints, have been constructed by the Nice and Meudon groups using the CESAM code; their frequencies computed and provided to the teams in charge of constructing the time series (referenced hereafter by Appourchaux, Toutain, IAS). Simulated time series are constructed assuming amplitudes and damping rates according to Houdek et al. (1999 *A&A*, 351, 582), stellar noise according to solar noise (or even flat) + COROT noise and a given inclination of the stellar rotation axis.

---

[†] *T. Appourchaux, C. Barban, F. Baudin, G. Berthomieu, M. Bossi, P. Boumier, M.J. Goupil, Y. Lebreton, P. Morel, B.L. Popielski, J. Provost, T. Toutain, I. Roxburgh*

[1] The constraints on the models are: $0.86 < log(L/L_\odot) < 0.89$ ; $3.8062 < log(T_{eff}) < 3.8195$ ; $0.019 < Z/X < 0.03$
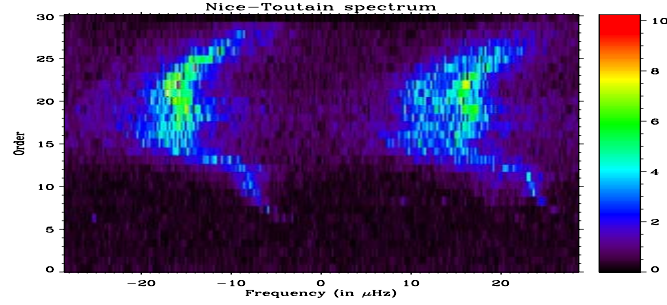
*Figure 1.* The echelle diagram for Ex1
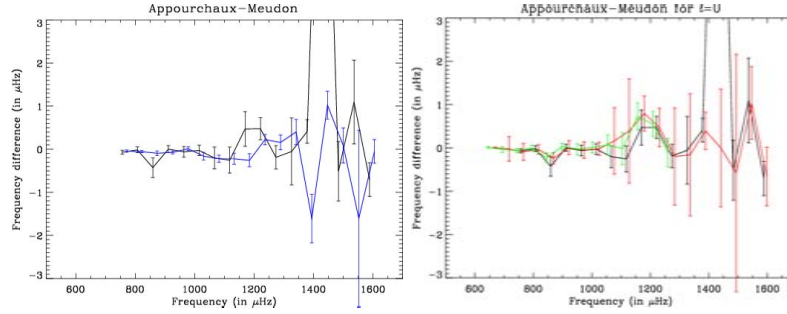


*Figure 2.* a)Difference between extracted frequencies and theoretical input frequencies for Ex2 ($\ell = 0$ in black,$\ell = 2$ in blue) relatively to the frequency.b) Difference between extracted frequencies by three independent groups and theoretical input frequencies for Ex2, $\ell = 0$ relatively to the frequency.

The identification of the modes ( degree $l$ and azimuthal order $m$) is made with the help of the echelle diagram. The degrees are identified according to the splitting structure of the $(l = 0, l = 2)$ pair versus that of the $(l = 1, l = 3)$ pair.

The determination of the mode parameters (here principally frequencies) is made using Maximum likelihood estimators. The model used for fitting assumes a Lorentzian profile of the mode, a degree-dependent visibility, a rotational splitting, a star inclination and a flat background noise. The statistics of the power spectra is a $\chi^2$ with 2 d.o.f. The modes are fitted by pairs over a 40-$\mu$ Hz (or so) window. Figure 2 give the differences between the extracted frequencies and theoretical input frequencies.

## 2. Interpretation of the "Observed frequencies"

In Ex2, according to Berthomieu et al 2002, Provost et al. 2001, the aim is to select the models which fit the "observed" large spacing
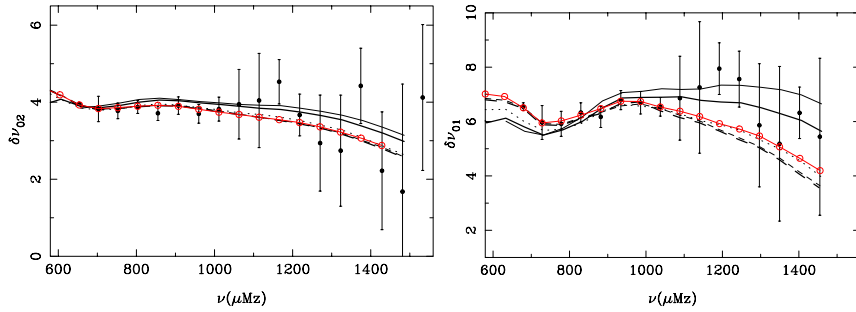
*Figure 3.* Small frequency spacings $\delta\nu_{02}$ and $\delta\nu_{01}$ for different models satisfying "observed" large spacing, "observations" (full dots) and input model (open circle) with $M_1$ (heavy line), $M_2$ (dashed line).
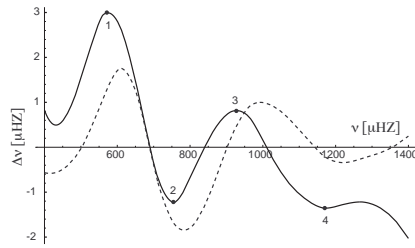


*Figure 4.* Reduced echelle diagram for degree $l = 0$ for a model (solid curve) and observations (dashed).

$\Delta_{n,\ell} = \nu_{n,\ell} - \nu_{n-1,\ell}$ and the small "observed" spacings defined by: $\delta\nu_{\mathbf{02}} = \nu_{\mathbf{n},\ell=\mathbf{0}} - \nu_{\mathbf{n-1},\ell=\mathbf{2}}$ ; $\delta\nu_{\mathbf{01}} = \mathbf{2}\nu_{\mathbf{n},\ell=\mathbf{0}} - (\nu_{\mathbf{n},\ell=\mathbf{1}} + \nu_{\mathbf{n-1},\ell=\mathbf{1}})$. Small spacings are sensitive to the core overshoot parameters, with a highest sensitivity at high frequency.

Among all the models which fit the large spacing, the fit with "observed small frequency spacings" in large frequency range favours models with low core overshoot M1 (considered as first choice: output1 in table 1), while the fit in the low frequency range where the error bars are smaller favour models M2 (output2 in table 1).

In Ex1, the frequencies for $l = 0$ are developped according to: $\nu_{n,0} = \nu_{cut}^0 + k < D_0 > + \nu_{offset}^0$, where $< D_0 >$ is a mean large spacing, $\tilde{\nu}_{offset}^0$ is a third order polynomial fit of "observed" $\nu_{offset}^0$ The reduced echelle diagram ( figure 4) is defined by the difference $\nu_{offset}^0 - \tilde{\nu}_{offset}^0$. Four extreme points are chosen to characterize the spectrum. These points and the mean large spacing are used to constrain the five parameters involved in the model computations (see Popielski et al 2001). Several models can fit well the constraints. The "best fit" model is choosen as that which reproduces the most of frequencies.

Table I. Comparison between "input" and "output" models for the two exercises.

|  | Ex1 | Input Nice | Output Meudon | Ex2 | Input Meudon | Output1 Nice M1 | Output2 Nice M2 |
|---|---|---|---|---|---|---|---|
| $M/M_\odot$ |  | 1.54 | 1.52 |  | 1.48 | 1.50 | 1.50 |
| X |  | 0.712 | 0.722 |  | 0.715 | 0.70 | 0.715 |
| Z/X |  | 0.025 | 0.024 |  | 0.0210 | 0.0214 | 0.0210 |
| $\zeta_{ov}$ |  | 0.0 | 0.04 |  | 0.15 | 0.05 | 0.15 |
| $log(L/L_\odot)$ |  | 0.840 | 0.828 |  | 0.86 | 0.88 | 0.870 |
| $log(T_{eff})$ |  | 3.817 | 3.814 |  | 3.809 | 3.81 | 3.811 |
| Age (My) |  | 1699 | 1908 |  | 2200 | 1810 | 2050 |
| $X_c$ |  | 0.159 | 0.190 |  | 0.17 | 0.09 | 0.19 |
| $r_{core}/R_\star$ |  | $5.82\ 10^{-2}$ | $6.12\ 10^{-2}$ |  | $5.9\ 10^{-2}$ | $5.2\ 10^{-2}$ | $6.2\ 10^{-2}$ |
| $r_{ZC}/R_\star$ |  | 0.915 |  |  | 0.922 | 0.917 | 0.926 |

## 3. Conclusion

The data analysis of the simulated time series has produced "observed frequencies" in good agreement with the input theoretical frequencies except in low and moderate frequency range. The errors are of the order of 0.1 to $0.5\mu$Hz except in the large frequency domain. Using these "observed" frequencies we are able to find models close to the input models but the solution is not unique. In Ex2, the results stress the importance of the small spacing $\delta\nu_{01}$, very sensitive to the core overshooting, for discriminating the models. However the "observed $\delta\nu_{01}$" have large errors in the high frequency domain. This may alter the choice of best fit. In Ex1, despite the use of different stellar evolution codes and oscillation codes the input and output models are rather close. For future works, we need to improve the criteria of model selection and to study the sensitivity of the models to stellar parameters, to numerical codes and to the physics. The next step will be to perform the inverse problem with the best models as reference model.

## References

Berthomieu G., Toutain T., Gonczi G., Corbard T., Provost J., Morel P.: 2001, Proceedings of SOHO10/GONG2000, ESA SP-464, 411

Popielski B., Goupil M.J.: 2001, Proceedings of the COROT Week 1 Vienna http://www.astrsp-mrs.fr/projets/corot/meeting/CW1.html

Provost J., Berthomieu G., Morel P.: 2001, COROT H&H2 results and conclusions, http://www.astrsp-mrs.fr/projets/corot/meeting/CW1.html

# Fitting and interpretation

# Results on the HH exercise: how did I fit the data?

T.Appourchaux

September 14, 2001

## 1   Goal

The goal of this document is to report on what one of the data fitter of the team B (Meudon-Appourchaux-Nice and consort) have done.

## 2   The approach

There are few simple steps that are used to reduce the data such as:

- timeseries plot

- histogram of the time series (gap detection)

- interpolation of the gaps (if possible)

- compute the fft of the timeseries

- echelle diagramme of the power spectra (looking for a credible $\Delta\nu$)

- identifying degrees in the echelle diagramme

- run a statistical test to check for peaks to be fitted

- fit the power spectra

For this latter step, we usually assume the following:

- the mode of a multiplet are excited with the same amplitude modulated by the visibility for each $(l, m)$

- the visibility for each $(l, m)$ is a function of the angle of inclination of the star onto the line of sight ($i$ ?)

- the visibilities are computed neglecting the limb darkening

1

- the mode splitting for a multiplet is fitted using $a_i$ using Clebsh-Gordan coefficients (see associated report), the maximum $i$ depends on the number of multiplet in a mode ($2l+1$ components)

- the statistics of the spectra is assumed to be a $\chi^2$ with 2 d.o.f

- spectra are fitted using Maximum Likelihood Estimators

- other details depend on the spectrum analysed

# 3 Results

## 3.1 Nice-Toutain spectrum

The timeseries seems to have no peculiar problem. Figure 1 shows the power spectrum. The modes are clearly visible from 250 $\mu$Hz to 1800 $\mu$Hz. Figure 2 shows the echelle diagramme with a spacing adjusted by hand of 57 $\mu$Hz. The ridges are easily identified and we can proceed to fitting the data.

The $l = 0$ and $l = 2$ modes are fitted in pair assuming a common linewidth, 2 different amplitudes (one for $l = 0$, a common one for the $l = 2$ multiplet), an angle of star inclination, a common flat noise and a single splitting $a_1$.

The $l = 1$ and $l = 3$ are fitted in the same manner, except that a test for the presence of $l = 3$ check whether the spectrum should be fitted for a pair $l = 1 - 3$ or simply just for $l = 1$. Although, most of the time the test did not detect the presence of the $l = 3$, it happens that the $l = 3$ could be seen by eye, at least one component of the multiplet. Unfortunately, this may not be enough to properly derive the characteristics of the $l = 3$ modes.

Given the fact, that the $l = 1$ gave a rather consistent splitting, the $l = 0 - 2$ was fitted again by giving as a starting parameter a value close to that of $l = 1$, but free nevertheless. Likely the same approach may be used to refit $l = 3$.

## 3.2 Roxburgh-Barban spectrum

Figure 3 shows a subsection of the timeseries and its associated histtogram. Some zeros put at regular places (and a large one somewhere else) give obviously problems. Figure 4 shows the effect of the 20-min periodic gap as a 833-$\mu$Hz modulation. After finding the gaps, those are corrected by simply interpolating with data before and after the gap. Figure 5 shows the same chunk of the timeseries after the correction. Figure 6 shows the power spectrum after correction. The modulation has dropped by more than a factor 100. A small peak appear at around 164.12 $\mu$Hz, still pondering about whether it is an artifact or a g mode... Finally Figure 7 shows the echelle diagramme with a spacing of 52 $\mu$Hz. This echelle diagramme is not easy to read at all. It required lots of thinking before we could do somthing about it. Finally, we come to a solution where the brightest ridge is due to the $l = 0$, and the other ridge are due to

2

## Nice−Toutain spectrum
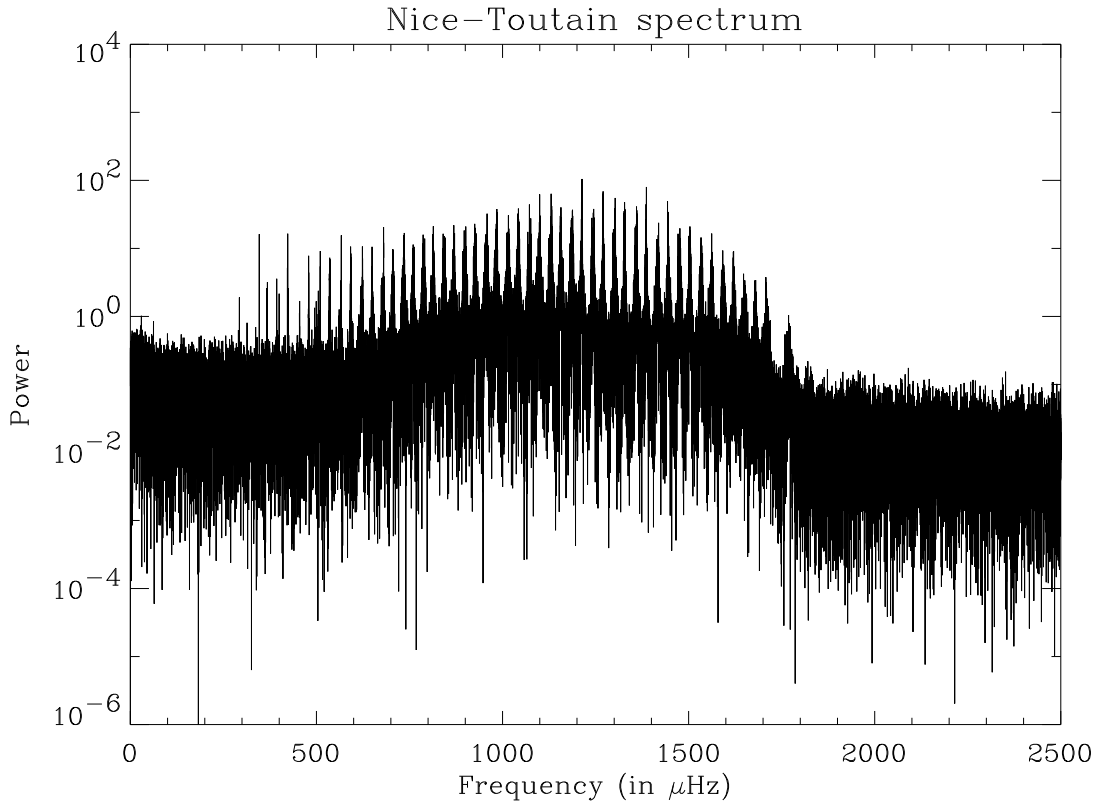


Figure 1: Power spectrum as a function of frequency

$l = 2$ and $l = 1$ split by 10 $\mu$Hz, giving in total 1+3+5=9 ridges. The trouble is that some ridges appear to be fainter for $m$=-2 than for $m = +2$. For regular stars, this is unlikely but given the fact that the star rotates about 25 times faster than the Sun, we can expect other peculiarities. In addition, it seemed that the ridges of a given $l$ were not equally spaced, which is not unlikely because the star is squashed and the spherically symmetric structure of the star does not exist anymore. But if it were the only problem that woudl have been simple. Unfortunately, the ridges for $l = 2, m = +2$ alias into the ridge for $l = 1, m = -1$, and vice-versa. The solution I chose for fitting the data was the following:

- fit spectrum over 70 $\mu$Hz or so
- assume a common linewidth for all degree
- fit simultaneously $l = 0, 1, 2$

3
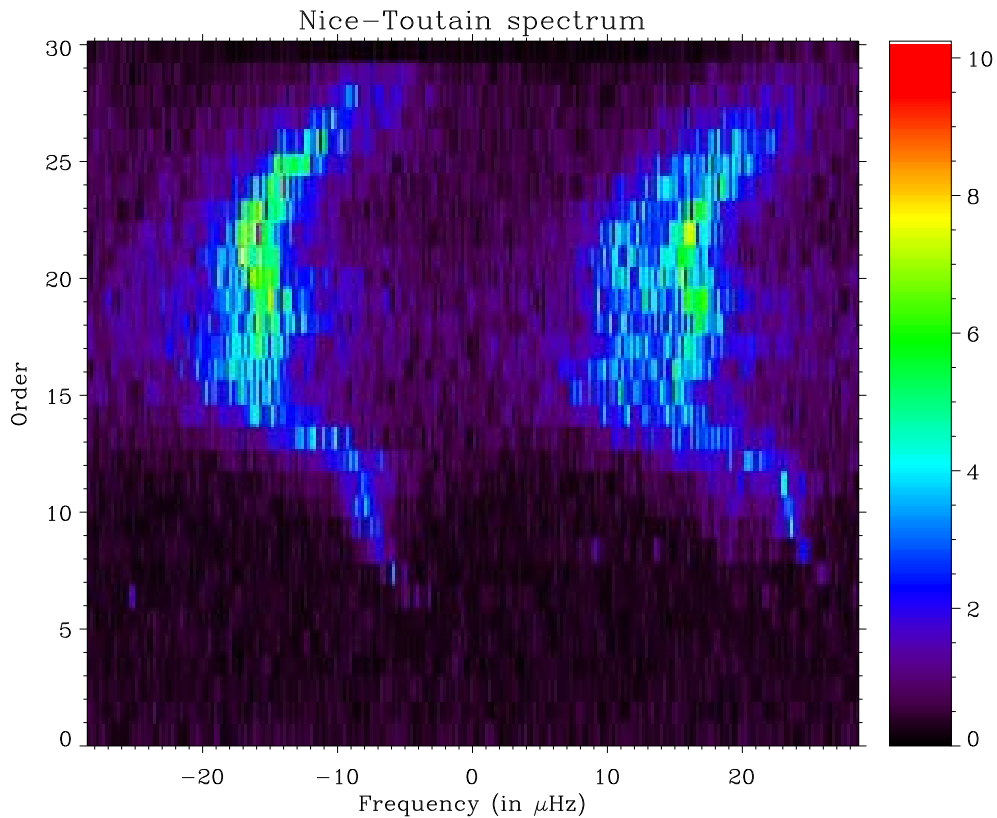
Figure 2: Echelle diagramme with a spacing of 57 $\mu$Hz. Given the structure of the ridges, we assumed that the left-hand side ridge is due to the $l = 1$ and $l = 3$ modes, and the right-hand side ridge to the $l = 0$ and $l = 2$ modes.

- fit with a fixed frequency the two spurious peak (alias of $l = 2, m = 2$ and alias of $l = 1, m - 1$

- assume a splitting of 10 $\mu$Hz

- fit $l=1$ and $l=2$ with $a_i$ coefficient up to $i=2$, $i=4$ respectively

- and a flat noise

The fit works properly and return good results, whether they reflect what was out inside is an other story (comme dirait Kipling...).

Please forgive me for misspelling, lack of accuracy and details..., time is running out...

4
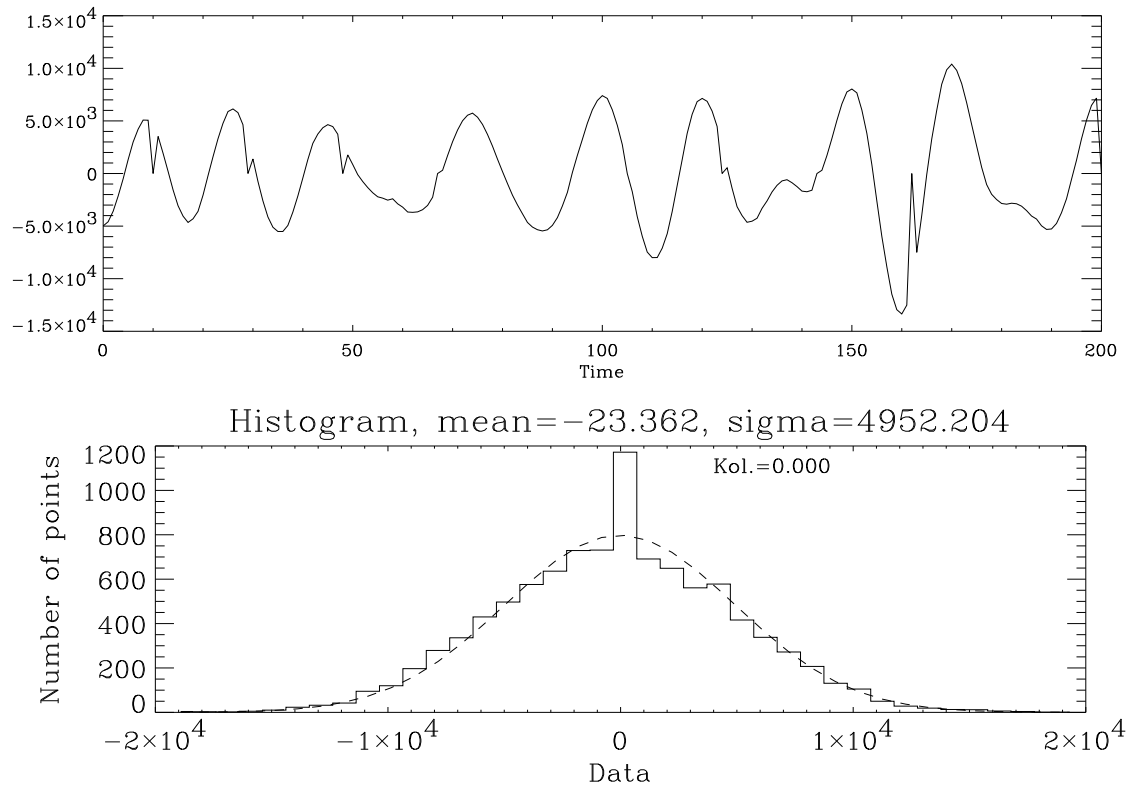
Figure 3: Timeseries showing the 20-min gaps and the histogram.
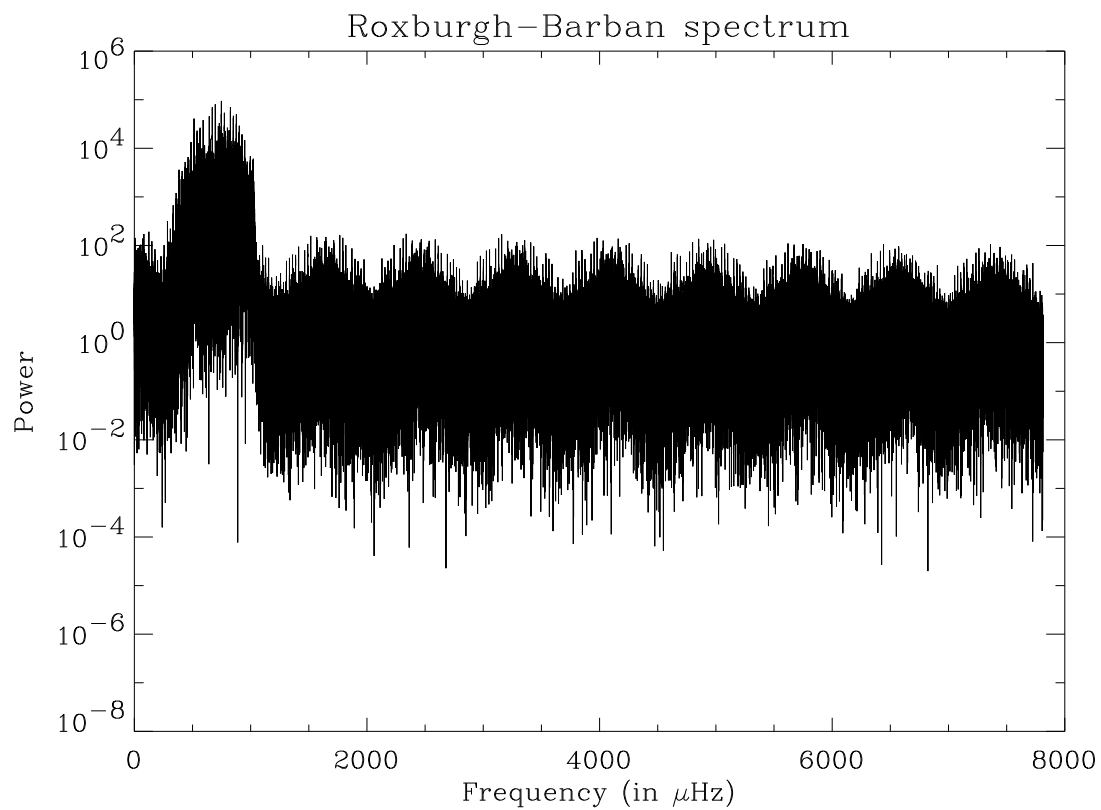
Figure 4: Power spectra of the raw data. The 833-$\mu$Hz modulation due to the gap is easily visible, so are the modes.
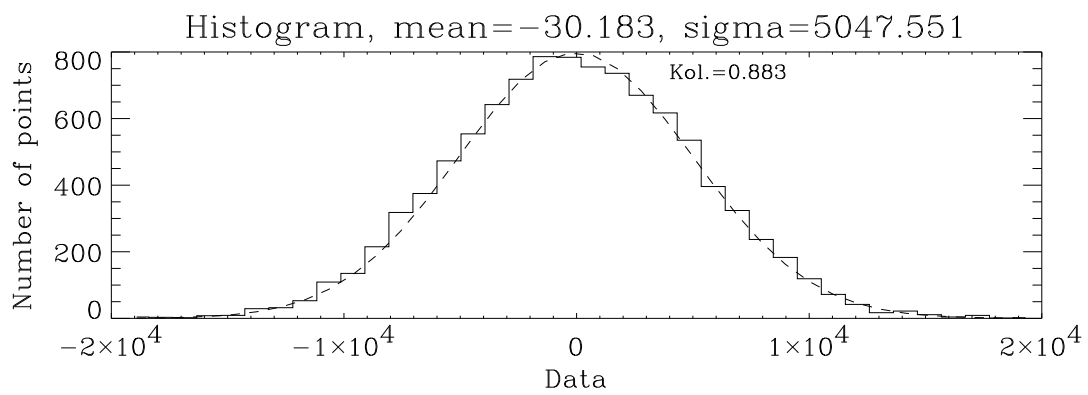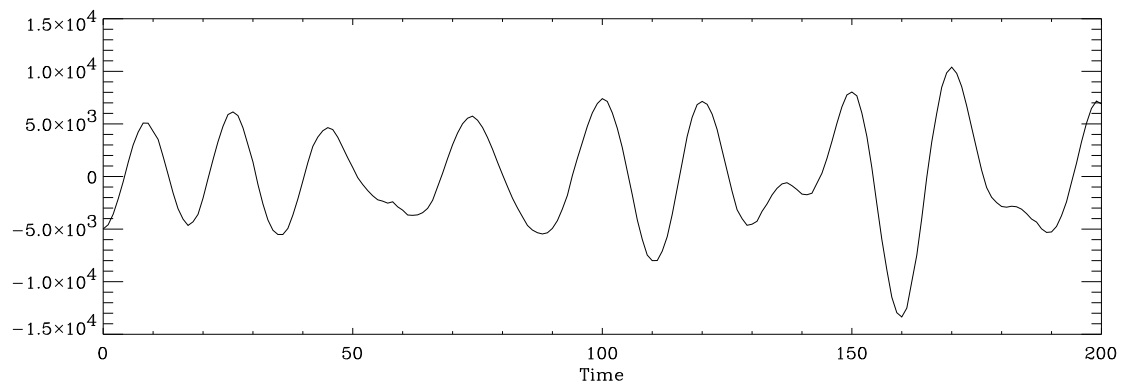
Figure 5: Timeseries showing the 20-min gaps and the histogram after filling the gaps.

7
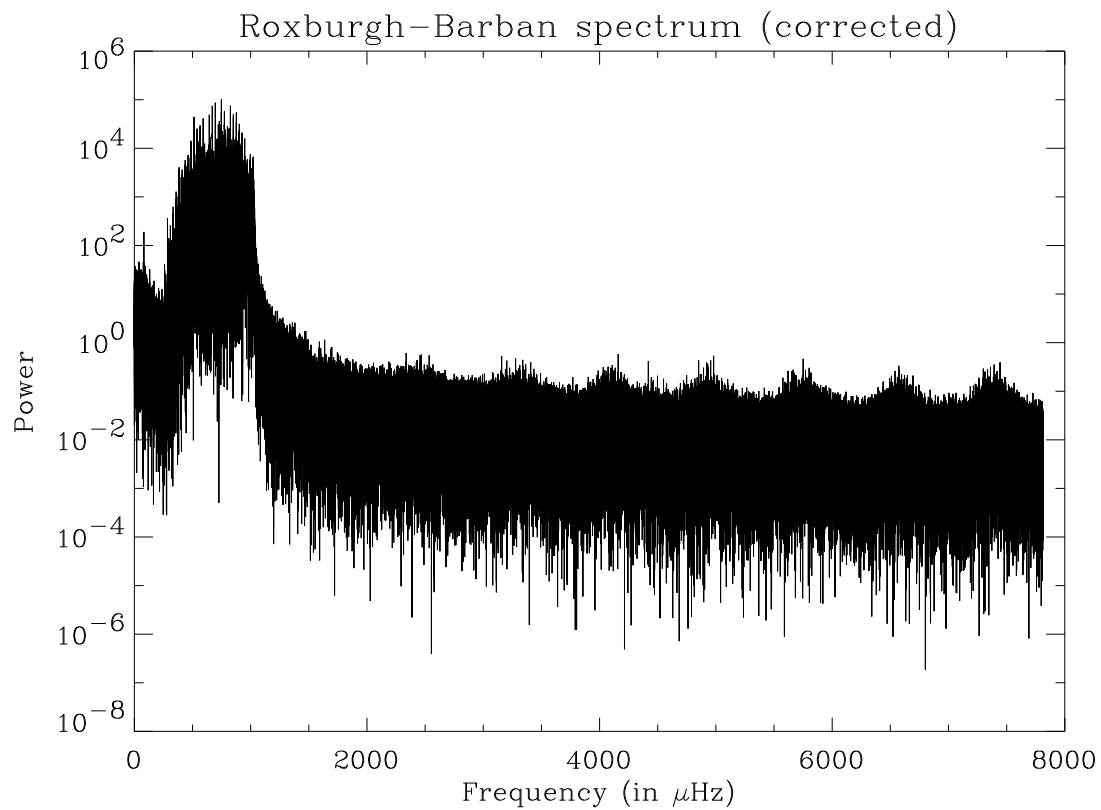
Figure 6: Power spectra of the corrected data. The 833-$\mu$Hz modulation due to the gap reduced by a factor 100.

Roxburgh–Barban spectrum
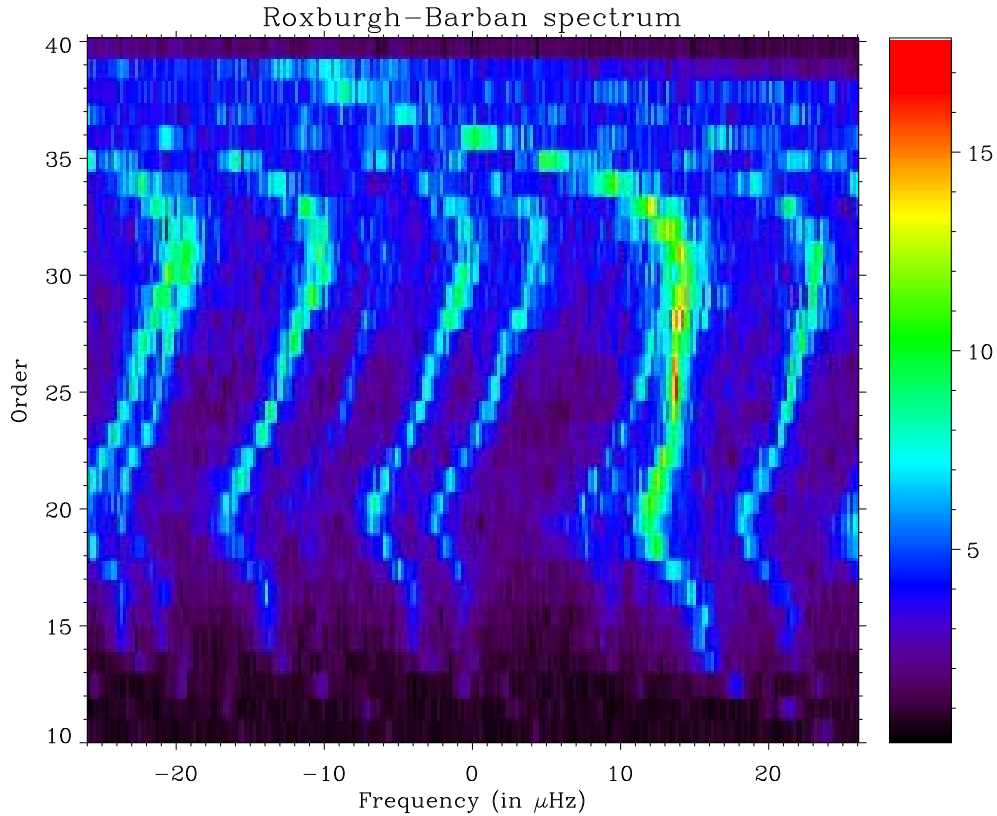
Figure 7: Echelle diagramme with a spacing of 52 $\mu$Hz. Given the structure of the ridges, we assumed that the strongest ridge is the $l = 0$ modes. We assumed that the splitting was 10 $\mu$Hz. The tiny ridge crossing the $l = 0$ mode was believed to be due to the $l = 2, m = 0$ modes; the ridge corresponding to $l = 2, m = 1$ is at the rightest while the $l = 2, m = 2$ wraps around and appear at the left hand side; the $l = 2, m = -1$ is close to the zero frequency while the $l = 2, m = -2$ appears to be the faintest of all; the $l = 1, m = 0$ ridge is roughly at -15 $\mu$Hz while the $l = 1, |m| = 1$ ridges are on either side.

# Hare-hound exercise: Report on preliminary work on the interpretation of frequencies extracted from simulated time series

*Provost J., Berthomieu G., Morel P.*

We have considered the set of frequencies extracted by T. Toutain from the simulated time series "Meudon-Appourchaux", hereafter refered as "observed" frequencies. The degrees are given but the radial order have not been identified. This can be done in principle by comparison with the frequencies of a stellar model close to the star. Our first step is to select such a model among the set of models in the HR diagram box.

## I. Large and Small differences analysis

As a first step, we have used the asymptotic properties of the acoustic frequencies and considered the large and small differences defined by:

$$\Delta\nu_\ell = \nu_{\mathbf{n},\ell} - \nu_{\mathbf{n-1},\ell} \tag{1}$$

$$\delta\nu_{\mathbf{02}} = \nu_{\mathbf{n},\ell=\mathbf{0}} - \nu_{\mathbf{n-1},\ell=\mathbf{2}} \tag{2}$$

The large differences are plotted relatively to the frequency for degrees $l = 0, 1, 2$ in the upper pannel of the first figure, $\delta\nu_{\mathbf{02}}$ is plotted in the lower pannel.
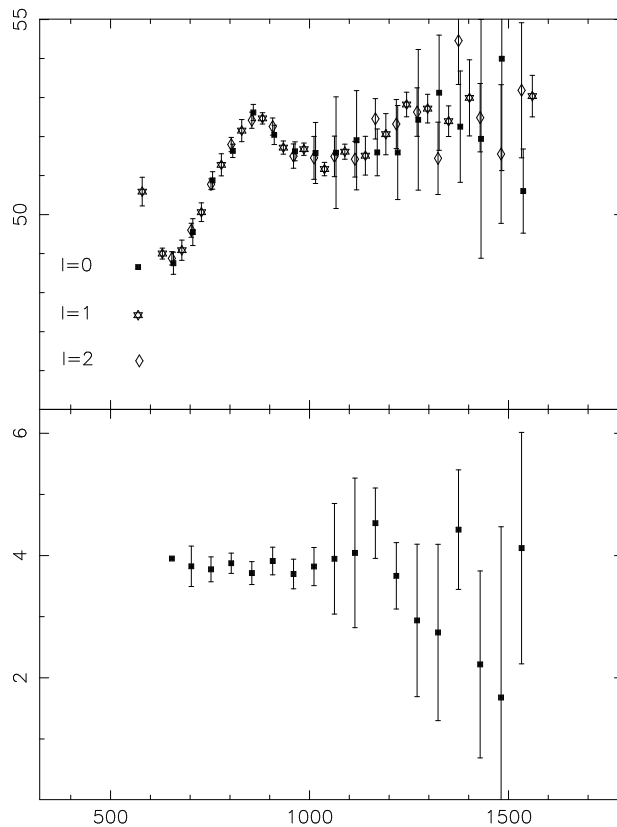
It is seen that the large spacing is not constant. A very crude mean value of large frequencies $\overline{\Delta\nu_0}$ can be defined with some uncertainty: $\overline{\Delta\nu_0} \sim 52. \pm 0.5\mu$Hz. We compute a set of stellar models which satisfy the constraints on luminosity $L$, effective temperature $T_{eff}$ and chemical composition Z/X defined by the hare hound exercise

$$0.83 < log(L/L_{Sun}) < 0.89; \quad 3.8062 < log(T_{eff}) < 3.8195; \quad 0.019 < Z/X < 0.03$$

Then we select among these models those which frequencies have a large spacing within the "observed" domain. This corresponds to selecting models with given mean density. The same is done for the small spacing. We estimate: $\overline{\delta\nu_{02}} \sim 3.92 \pm 0.15\mu$Hz.

For comparison, the large and small differences for a theoretical model $M/M_\odot = 1.45, \quad Z = 0.015, \quad \zeta = 0.3$ is given in Figure 2.
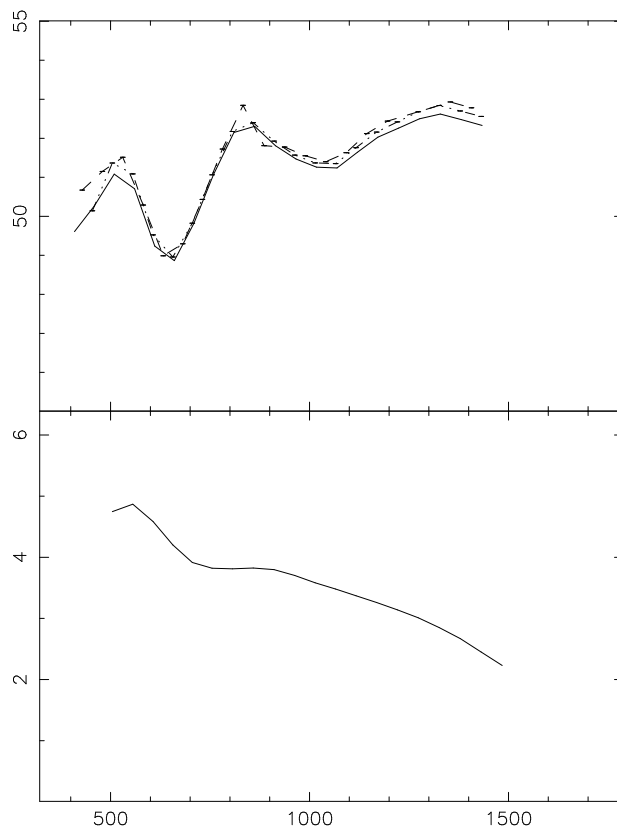
## Mean values of Large and Small frequency differences
## for a set of models

A set of models has been computed with different values of the core overshoot parameter $\zeta$, the mass $M/M_\odot$ and the heavy element abundances Z. The figure represents the mean values of the small difference $\delta\nu_{02}$ relatively to the mean large difference $\Delta\nu_0$ for these models with the following characteristics:

$\zeta = 0.$   $(M/M_\odot, Z)$: (1.5, 0.015), (1.59, 0.02) (full triangle)

$\zeta = 0.1$                 : (1.45-1.47, 0.015), (1.53, 0.0175), (1.54, 0.02) (full circle)

$\zeta = 0.2$                 : (1.45-1.47, 0.015), (1.525, 0.02) (full star)

$\zeta = 0.3$                 : (1.45-1.47, 0.015), (1.47, 0.0175) (open star)
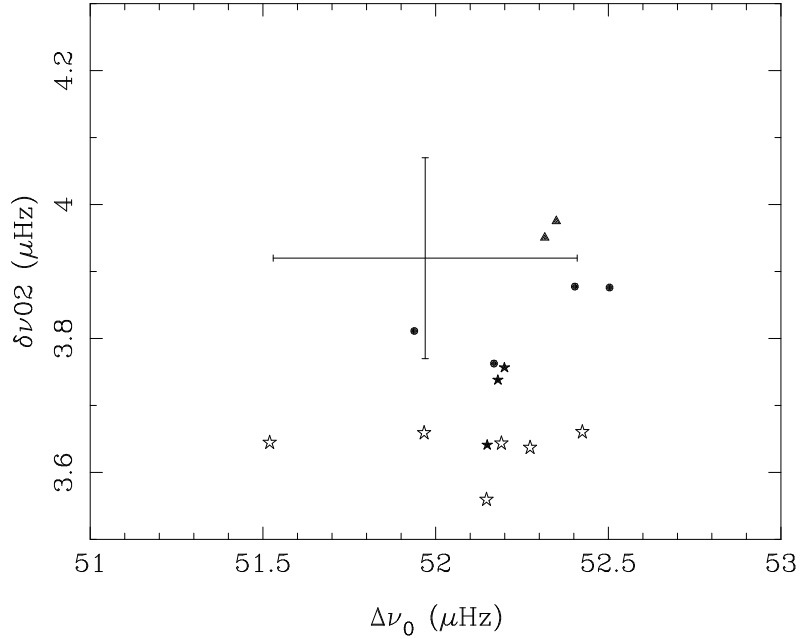


The cross in the figure represents the domain in $\delta\nu_{02}$ and $\Delta\nu_0$ estimated from the "observed" frequencies.

# Small frequency differences $\delta\nu_{0,1}$ for TT-TA-Meudon and models

$$\delta\nu_{0,1} = 2\nu_{n,\ell=0} - (\nu_{n,\ell=1} + \nu_{n-1,\ell=1})$$
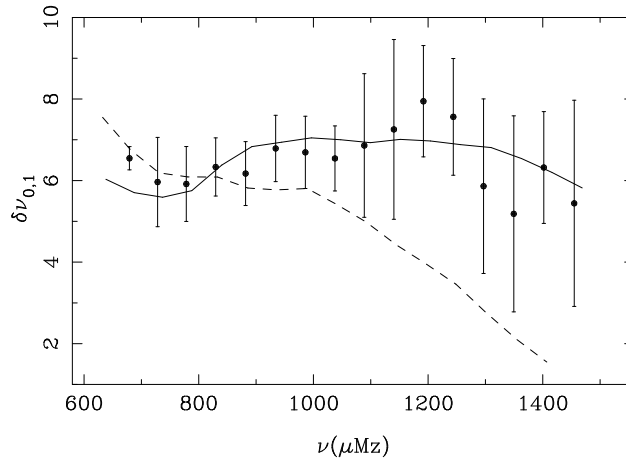


The full line corresponds to a model with $M/M_\odot = 1.5$, $Z = 0.015$, $\zeta = 0.05$, the dashed line corresponds to the model of figure 2.

# Mean small frequency differences $\delta\nu_{0,1}$ and $\delta\nu_{0,2}$ for a set of models
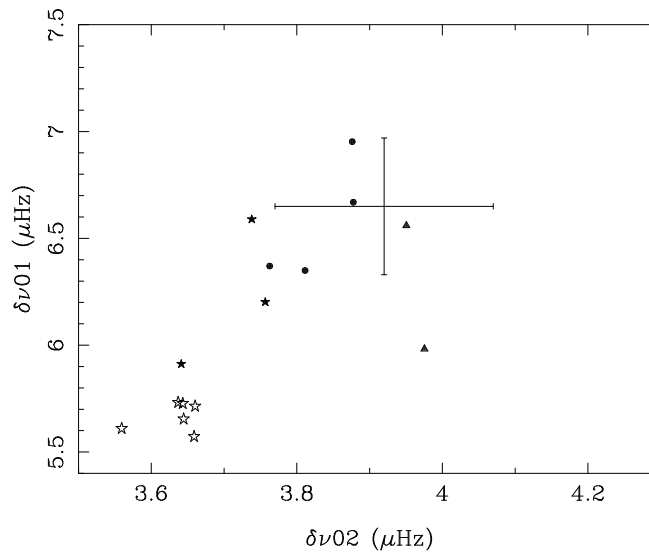


In conclusion:
On the basis of the considered criteria, the models with low core overshoot parameter better fit the "observed" data.
This analysis allows to select some models to carry on some inversions.
Others global characteristics of the frequencies are needed to infer properties of the unknown model.

# First results of asteroseismic exercise from Meudon

Błażej L. Popielski, Marie-Jo Goupil

**Abstract**

We present an application of the classic seismological forward problem in the context of solar-like oscillations. The range and quality of input frequency data are similar to those anticipated for observations from future space missions. The project is part of *hare and hound* exercise of the COROT SWG[1]. We focus on the possibility of reproducing p-mode spectra. However, we emphasize also the importance of mixed modes for sounding the deep interior.

## 1   Introduction

There is a strong need to reproduce the pulsational behavior of distant stars after the success of helioseismology. High quality spectra are being obtained as a result of months of dedicated satellite observations (Baglin, 1998). Investigating the solar-like oscillations is the first step for asteroseismology. While the number of detected frequencies is expected to be significantly lower than for the sun, blind experiments *(hare and hound* exercise) between independent groups have been undertaken. This work is the result of one of the groups working with two sets of frequencies.

In Section 2, we present the rules of the exercise concerning building a model and its oscillation frequencies. Next, we concentrate on accompanying the reader through the whole data analysis process. In Section 3 we focus on a simulated spectrum to reduce the number of important parameters. We describe then our forward method and present the resulting models which are believed to represent best the investigated observed frequency data (Section 4.).

## 2   Exercise rules

A set of artificial "observed" noise-free frequencies gives us opportunity to check our ability to find a solar-type model reproducing frequencies. The rules are based on what realistic conditions we hope to obtain for each target star of specific mission (see Provost, 2001). The assumptions of the *hare and hound* exercise concerning model (called observations starting from this point) refer to

---

[1]Latest news available at http://dasgal1.obspm.fr/~michel/COROT-SISMO.html.

ranges in metal abundance $(Z/X)$ and HR-diagram parameters $(T_{eff}, L/L_\odot)$. The ranges are as follows:

$$Z/X \in [0.019, 0.03],$$
$$\log T_{eff} \in [3.806, 3.82],$$
$$\log L/L_\odot \in [0.83, 0.89].$$

The frequency set includes low degree $(\ell \leq 3)$ modes, and contain rotationally split components $(m \neq 0)$. There are 5 modeling parameters in game: mass, $M$, hydrogen abundance, $X$, metal abundance, $Z$, mixing length parameter, $\alpha$, and overshoot parameter, $d_{ov}$. The mean spectral accuracy predicted for COROT mission is $\sim 0.1$ $\mu$Hz, however it may vary from one mode to other (Baglin, 1998). We try to reproduce the spectra with predicted frequency accuracy.

In this work, we deal with two sets of artificial data.

# 3 Spectral analysis

## 3.1 Echelle diagram

One-to-one frequency separation histogram (Figure 1.) reveals main regular spacings in the spectrum. The main sinusoidal shape (with period of $\sim 50$ $\mu$Hz) is due to the mean separation of two consecutive multiplets of equal spherical degree, $\ell$. We find frequencies of $\ell = 0, 1, 2, 3$ modes on a spectral distance of this size. This distance is approximately equal to the mean large separation[2], $\langle D \rangle = \frac{1}{N} \sum_{n,\ell} D_{n\ell}$, where $D_{n\ell} = \nu_{n\ell 0} - \nu_{n-1\ell 0}$. It is basis of so-called echelle diagram (Grec, 1981). Echelle diagram is result of cutting the spectrum into such pieces and arranging them one above another. The frequency, $\nu$, and the echelle-diagram coordinates, $\nu_{offset}$ and $\nu_{cut}$, are related by following formulas,

$$\nu_{offset} = \nu - \nu_{cut},$$
$$\nu_{cut} = \nu_{cut}^0 + k \langle D \rangle,$$

where two constants, $\langle D \rangle$ and $\nu_{cut}^0$, need to be specified and $k$ is an integer. While $\langle D \rangle$ is the signature of the mean density (thus the age), $\nu_{cut}^0$ has no physical meaning. It is fixed *a priori* for visualization purposes.

However, there are also fine structure peaks in the frequency separation histogram. They are due to the rotational splitting of the modes. The frequencies of $m = 0$ modes, i.e. centroids, may be distinguished in Figure 2. In order to focus on those frequencies we have to reduce equidistant frequencies of same radial order for all spherical degrees (Figure 3.). Figure 3. is an echelle diagram of observations and a model, as well. Each of the two sets consists of 4 branches of adiabatic frequencies of different spherical degree. The branches are similar curves. Model frequencies are present in adiabatic and non-adiabatic versions.

---

[2]Several groups use geometric mean instead of the arithmetic one. We quote here the one we used.
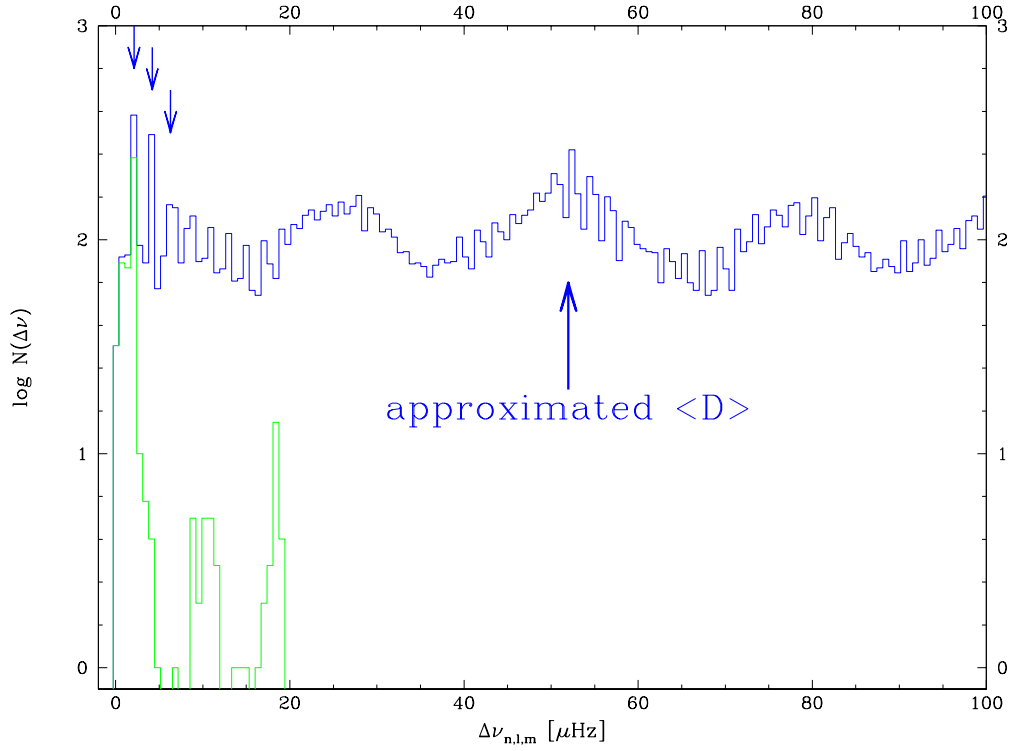
Figure 1: Frequency separation histograms for `set1`. Two curves relate to two separation sets, one-to-one separations (blue) and separations between two consecutive frequencies (green). The last-mentioned reveals two main peaks: one for rotational splitting ($\sim 2.1$ $\mu$Hz) almost uniform for all modes and the multiplet frequency separation ($\sim 18.3$ $\mu$Hz).
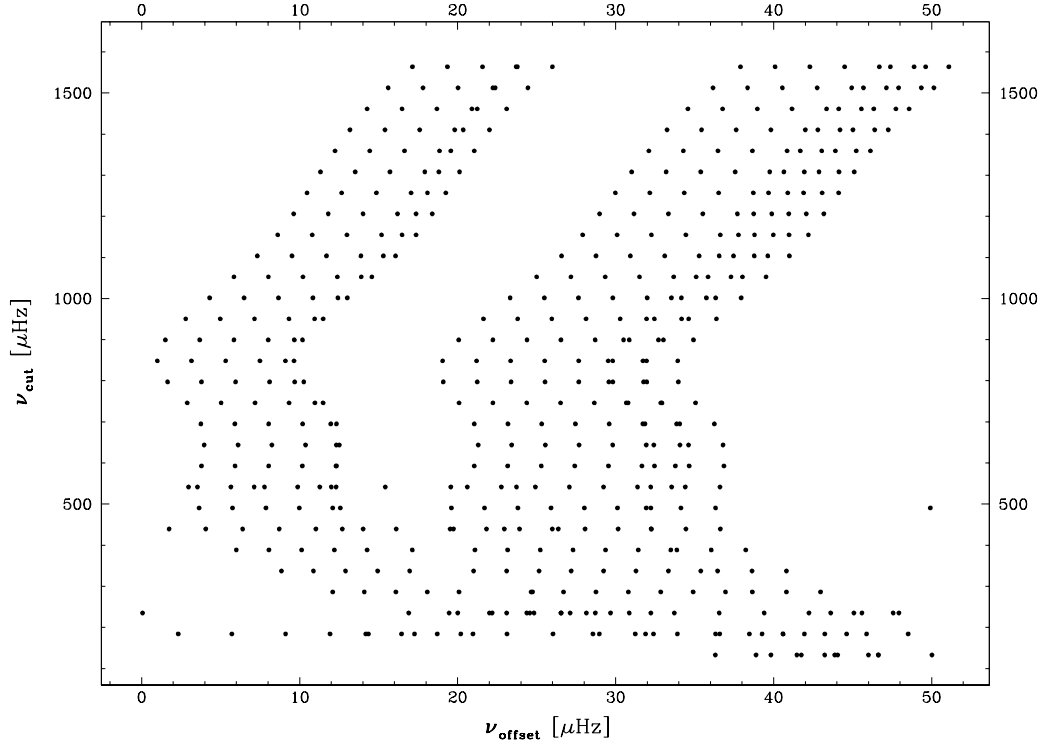
Figure 2: Echelle diagram for observed frequencies (`set1`). Most of horizontal frequency counts give 16. It is the sum of four multiplets of low spherical degree. Equidistant frequencies let us find appropriate $\ell$. Lower part of the diagram is dominated by the mixed-modes. Their interpretation is much harder, while the don't obey asymptotic relations. Originate could be easily rescaled to fit radial degree.
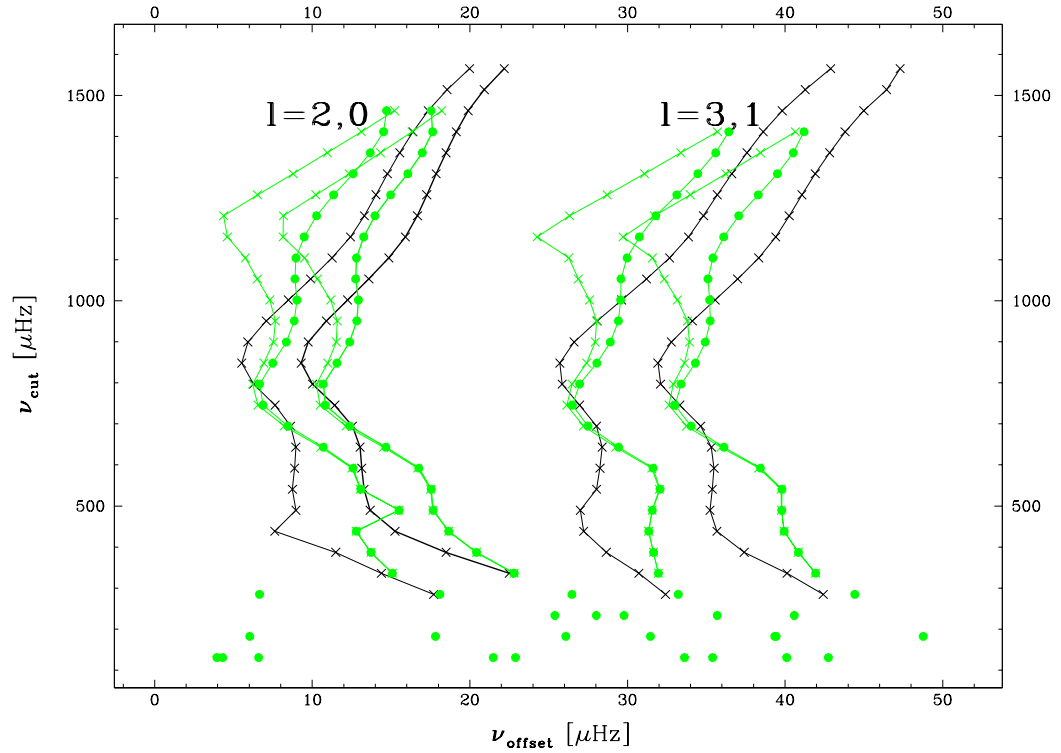
Figure 3: Same as in Figure 3. stripped of the rotational splitting. Observational frequencies are shown (black x), as well as adiabatic and non-adiabatic frequencies of a model (green dots and crosses, respectively). Observed radial mode branch is bold.

In the high frequency domain non-adiabatic corrections perturb the model spectra in an important way. We expect to reproduce real observational data, once available. However, there are certain important spectral signatures in this frequency region reveals. For this reason, we focus on $[400, 1400]$ $\mu$Hz frequency domain. Lower frequency limit omits g-mode domain, where the asymptotic behavior is hard to encounter. On the other hand the acoustical cutoff frequency gives the upper limit ($\sim 1500$ $\mu$Hz). We keep in mind however that some of high frequencies from that domain may be also polluted.

## 3.2   Spectral parameters

The mean large frequency separation ,$\langle D \rangle$, is the crucial spectral parameter. It is sensitive to the mean stellar density However, it is one of many (see Figure 3.). It is a convenient diagnostic parameter, but in this work, we use mean offset frequency (echelle abscissa) for centroids of radial modes, $\left\langle \nu_{offset}^0 \right\rangle$, where

$$\nu_{n0} = \nu_{cut}^0 + k \langle D_0 \rangle + \nu_{offset}^0(\nu_{n0}).$$

This quantity is more practical for the purpose of frequency reproduction, while the mean large separation corresponds to its derivative and in fact some of frequency information is lost.

In this work we define and make use of 9 spectral parameters in total:

- $\left\langle \nu_{offset}^0 \right\rangle$, mean offset frequency for radial mode branch at fixed $\nu_{cut}^0$,

- $(\nu_1, \Delta\nu_1)$, $(\nu_2, \Delta\nu_2)$, $(\nu_3, \Delta\nu_3)$, $(\nu_4, \Delta\nu_4)$, extreme points of reduced echelle diagram for $\ell = 0$ branch, see Figure 4.

The echelle diagram reduction, we use, is done by subtracting low, i.e. 3rd, order polynomial fitted to the observations, $\tilde{\nu}_{offset}^0(\nu)$, from the standard echelle data, $\nu_{offset}^0(\nu)$,

$$\Delta\nu_{offset}^0 = \nu_{offset}^0(\nu) - \tilde{\nu}_{offset}^0(\nu).$$

This procedure brings to light small changes in the echelle diagram. These are subtle but the most significant changes and still surpass the error magnitude. We emphasize that you need to reproduce the 9 spectral parameters with an appropriate model.

# 4   Model search

The mean large separation diminishes with age of a star on the main sequence. The change of the mean offset frequency at constant $\nu_{cut}^0$ is quite more complicated. However it is only the matter of modeling ability, to reproduce $\left\langle \nu_{offset}^0 \right\rangle$ with certain accuracy for a model of chosen ZAMS parameters. The impact

6
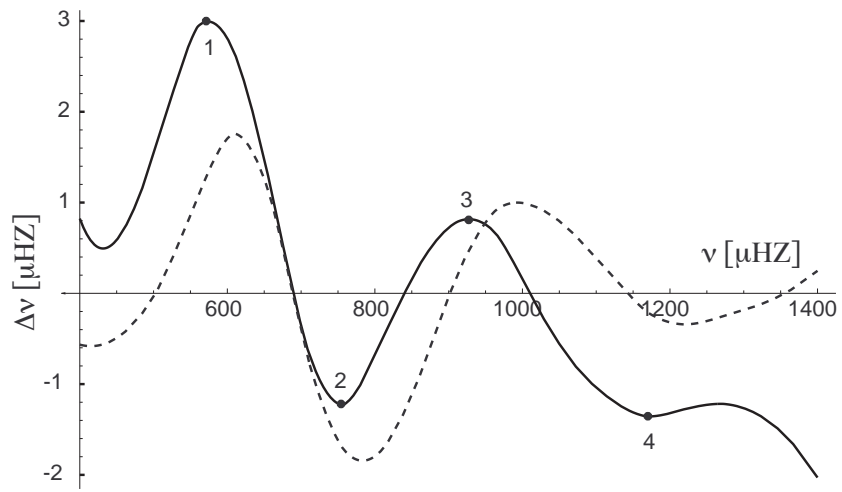
Figure 4: Reduced echelle diagram (see text) for a model (solid) and observations (dashed). The four extreme points serve their coordinates to characterize spectra.

of 5 such parameters on a model constructed in this manner is shown in Figure 5. Although large separation is used, 5 model parameters may be divided into those shifting spectral features (bumps) to higher $(M/M_\odot, d_{ov})$ and lower frequencies $(X, Z, \alpha)$. This behavior of each of the parameters change when models quit MS.

Note that we expect to find appropriate model on the cooling part of the track, because the ratio of the lifetime on the heating to that on the cooling part is about 0.5.

If we consider series of $n$ models representing vicinity of a departure model, we result in series of spectral characteristics:

$$\{\nu_1^{(1)}, \nu_2^{(1)}, \nu_3^{(1)}, \nu_4^{(1)}, \Delta\nu_1^{(1)}, \Delta\nu_2^{(1)}, \Delta\nu_3^{(1)}, \Delta\nu_4^{(1)}\},$$

$$...$$

$$\{\nu_1^{(n)}, \nu_2^{(n)}, \nu_3^{(n)}, \nu_4^{(n)}, \Delta\nu_1^{(n)}, \Delta\nu_2^{(n)}, \Delta\nu_3^{(n)}, \Delta\nu_4^{(n)}\}.$$

If the range of those parameters encompasses corresponding observational values, $\{\nu_1^{(o)}, \nu_2^{(o)}, \nu_3^{(o)}, \nu_4^{(o)}, \Delta\nu_1^{(o)}, \Delta\nu_2^{(o)}, \Delta\nu_3^{(o)}, \Delta\nu_4^{(o)}\}$, we interpolate to find out model parameters. We are able to approach the observations using this method repeated in an iterative way. This method is quite demanding from numerical point of view. It is however clear that quality of interpolation reduces number of necessary iterations.

We carried all stellar modeling with Warsaw evolutionary code with high quality equation of state (Rogers, Swenson & Iglesias, 1996) and opacity tables (Rogers & Iglesias, 1996). Grain and molecular opacities were adopted as well as conductive ones. The burning rates were based on Bahcall (1995).

In our search we used 5 parameter interpolation. Thus, we had to choose 5 spectral parameters to solve the set of 5 equations, in order to reproduce the observed ones. We find it useful to deal with $\nu_1$, $\nu_2$, $\nu_3$, $(\Delta\nu_1 - \Delta\nu_4)$ and $(\Delta\nu_3 - \Delta\nu_2)$. The effect of 3rd order in each modeling parameter was taken into account. We benefited the Mathematica(TM) 3.0 calculating engine to provide interpolation and the solution as well.

It should be stressed that this method is constraint independent. There is uniqely the shape of the radial mode $(\ell = 0)$ branch of echelle diagram which is reproduced. It is obvious however that the resulting models (or their lack) depend on the departure model. It is recommended to start iterations from several departure models.

## 4.1  Model choice criteria

Once several iterative searches are done we may obtain several models that fit well. We have to choose one model spectra that fits best. We consider this is the one reproducing the most of frequencies. To be precise, for each frequency of a model we calculate its distance to the closest observed one, $\left|\nu_{n\ell}^{model} - \nu_{n\ell}^{obs}\right|$.
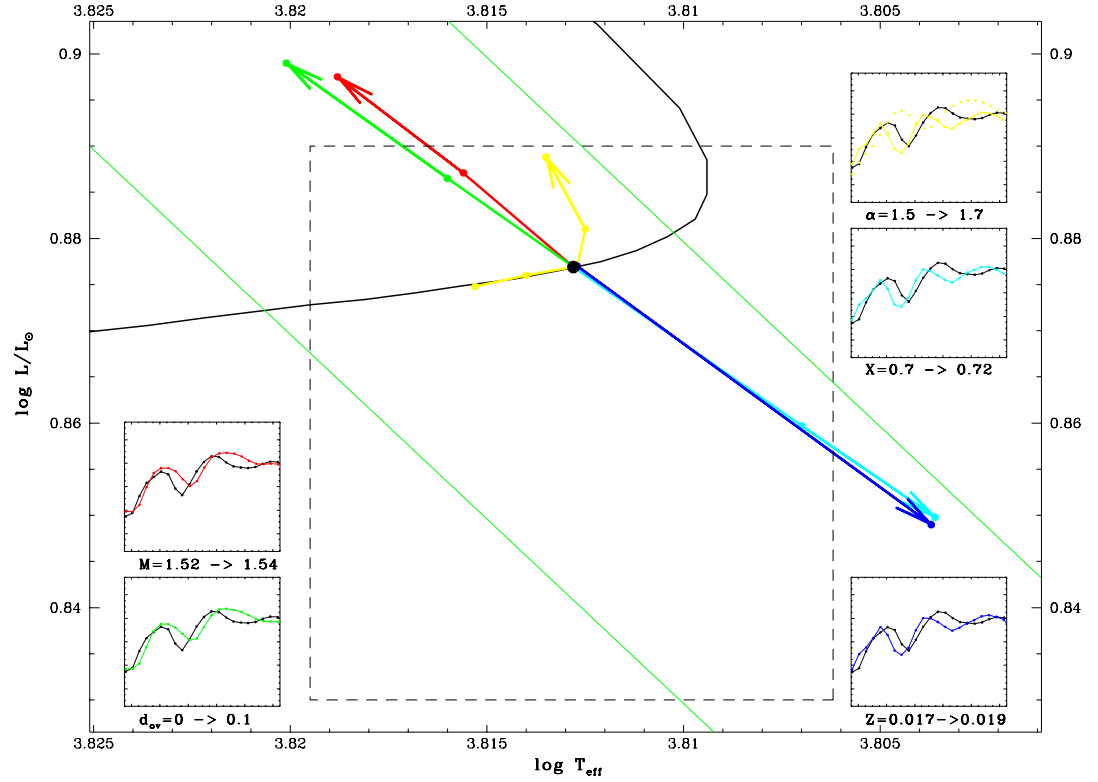
Figure 5: HR diagram showing the effects of ZAMS parameters. The arrows connect models with only one parameter changed. All the models have the observational $\left\langle \nu_{offset}^{0} \right\rangle$. The dashed box indicates the HR diagram *hare and hound* domain. The insets, $D_0(\nu)$, show the parameter influence on the $\ell = 0$ spectrum. Green lines are constant radius lines. The evolutionary track is also drawn (black line).
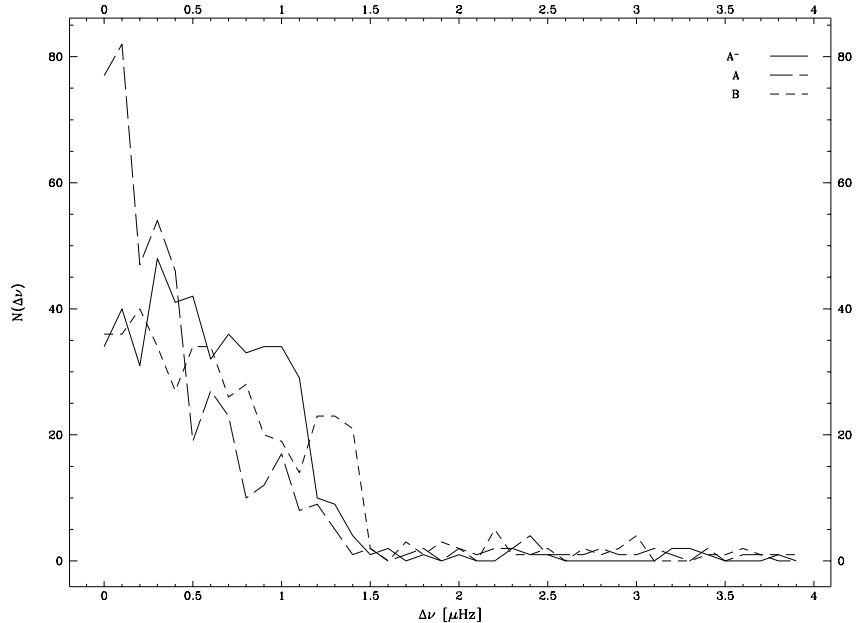
Figure 6: Histograms of differences between two spectra. 3 model spectra are compared with the observed one. $A^-$ and $A$ are following evolutionary models spectra. $A$ model is the one with correct $\left\langle \nu_{offset}^0 \right\rangle$ and also the one shown in Figure 3. $B$ is a 1.5 $M_\odot$ model.

Histogram of such distances $N(k\delta\nu, (k+1)\delta\nu)$, for $k \geq 0$ and $\delta\nu \ll \nu^{obs}$, contains an unbiased and frequency-free information on the spectral fit. Next, we fit

$$f(\Delta\nu) = a_1 \exp(-a_2 \Delta\nu)$$

function to the histogram. Figure 6. presents 3 histograms data for models. Comparison of well-fitted spectra is in that way reduced to comparing $a_1$ and $a_2$ values for different models. While the number of compared frequencies is the same, it is $a_1$ or $a_2$, that let us choose: the greater − the better fit.

The table below together with the Figure 6. let us distinguish the difference between "$\chi^2$ minimum" and "histogram" criteria.

| model | $\chi^2$ | $a_1$ | $a_2$ |
|-------|----------|-------|-------|
| A-    | 8.160    | 50.7  | 1.02  |
| A     | 8.525    | 100   | 81.94 |
| B     | 2.709    | 44.6  | 0.96  |

10

| model | $M/M_\odot$ | $X$ | $Z$ | $\alpha$ | $d_{ov}$ | $a_1$ |
|-------|-------------|-----|-----|----------|----------|-------|
| C | 1.52 | 0.722 | 0.0175 | 1.7 | 0.04 | 10.17 |
| D | 1.525 | 0.71 | 0.019 | 1.67 | 0.02 | 8.78 |
| E | 1.363 | 0.703 | 0.0122 | 1.728 | 0.2 | 6.93 |

| model | t $[10^9\mathrm{yr}]$ | $X_c$ | $\log L/L_\odot$ | $\log T_{eff}$ | $r_c/R$ |
|-------|------------------------|-------|------------------|----------------|---------|
| C | 1.908 | 0.172 | 0.828 | 3.8142 | 0.058 |
| D | 1.770 | 0.170 | 0.830 | 3.8148 | 0.058 |
| E | 2.333 | 0.246 | 0.823 | 3.8216 | 0.062 |

Table 1: Model parameters from spectral fit to `set1`.

## 4.2 Search results

The goal was to find parameters of a model reproducing observed frequencies. As mentioned earlier, for our analysis we used two sets of artificial observations. The first one (`set1`) is an intergroup data. Its true parameters are unknown for us. The second one (`set2`) is an auxiliary one. It was generated by one of us and analysed by the other one. Its parameters were kept hidden until the end of analysis. In Table 1. we quote three models being results of three independent iterations for `set1`. There is visibly no perfect model found. For those 3 models, parameters span widely. However using our $a_1$-criteria we can choose the best (C).

The `set1` data was provided with frequency errors. Thus, we are allowed to compare the errors with spectral differences for models C, D, E and `set1` (Figure 7.).

Tabularized models lay outside the HR box of the *hare and hound* exercise. It could be the effect of modeling physics (equation of state, burning rates etc.) but certain general ease of reproducing radial branch could be the cause, as well. We incline to the second scenario, thus we suggest the need of reproducing also other quantities, apart from those of radial mode branch. Small separations and $f_n = \nu_{n1} - \nu_{n0}$ separations should do. In Figure 8. we present large, small and $f_n$ separations for `set1` and a model.

There is however another set of constraints for the models. This is the set of frequencies of mixed-modes. In case of `set2` we had an opportunity to verify its applicability, while two mixed-modes are present in the set. They are modes captured during their avoided crossing event. They propagate in the envelope and in the convective core as well, thus their frequencies are important to be reproduced, as far as deep interior is concerned. Frequencies of those modes rise with age because of rising Brunt-Väisälä frequency at the edge of shrinking hydrogen core.

In our analysis those additional observables were simply frequencies of two mixed-modes. They were incorporated among 5 parameters of the interpolation procedure, described in Section 4. The iteration was carried as described earlier, except several steps that were enriched in the "mixed" parameters. Result of
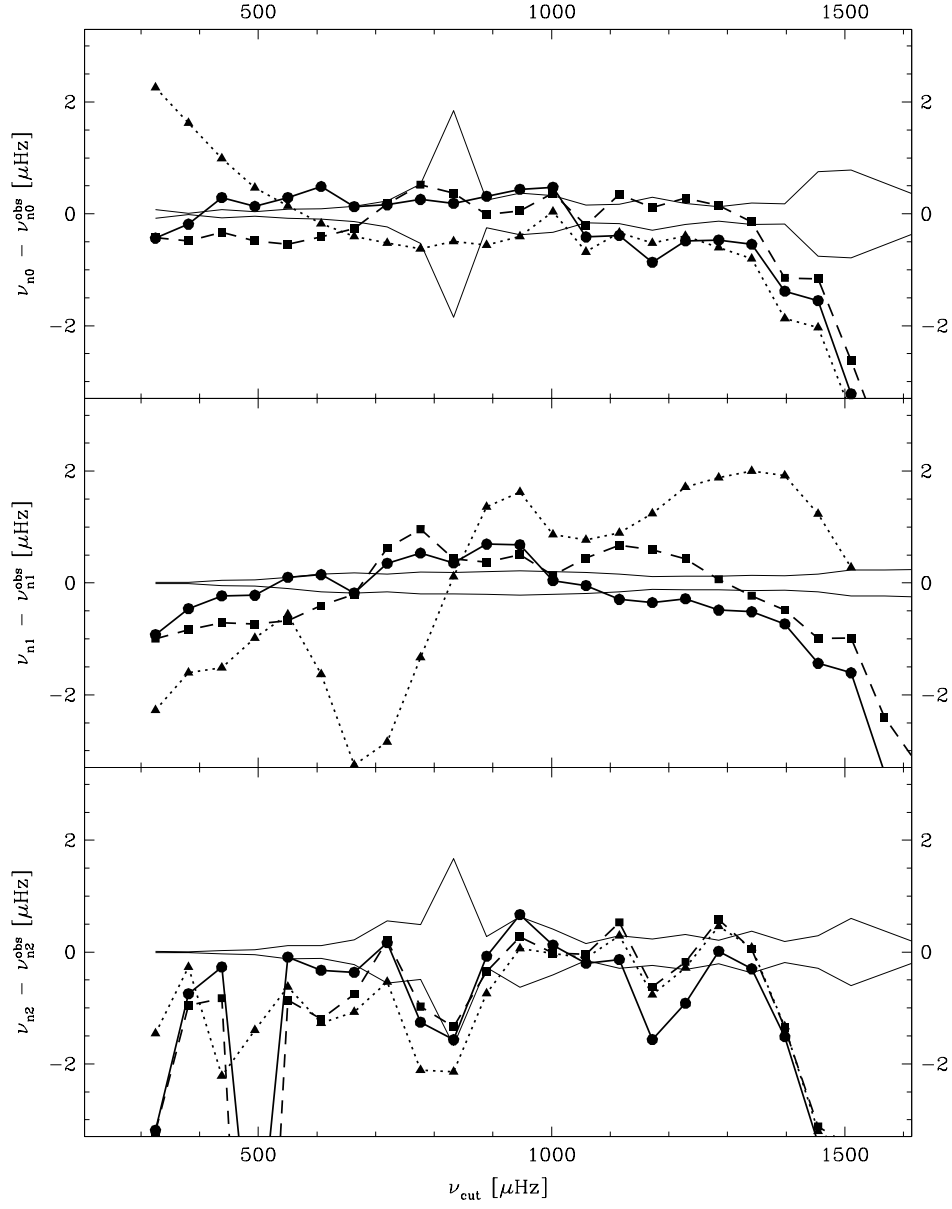
Figure 7: Frequencies of 3 fitted models from Table 1. relative to the observed frequencies. Each diagram corresponds to modes of one spherical degree, $\ell$. Each model is shown with different line and pointstyles, C – solid line and circles, D – dashed line and squares, E – short dashed line and triangles. Symmetrical horizontal solid curves relate observed frequency errors.

12
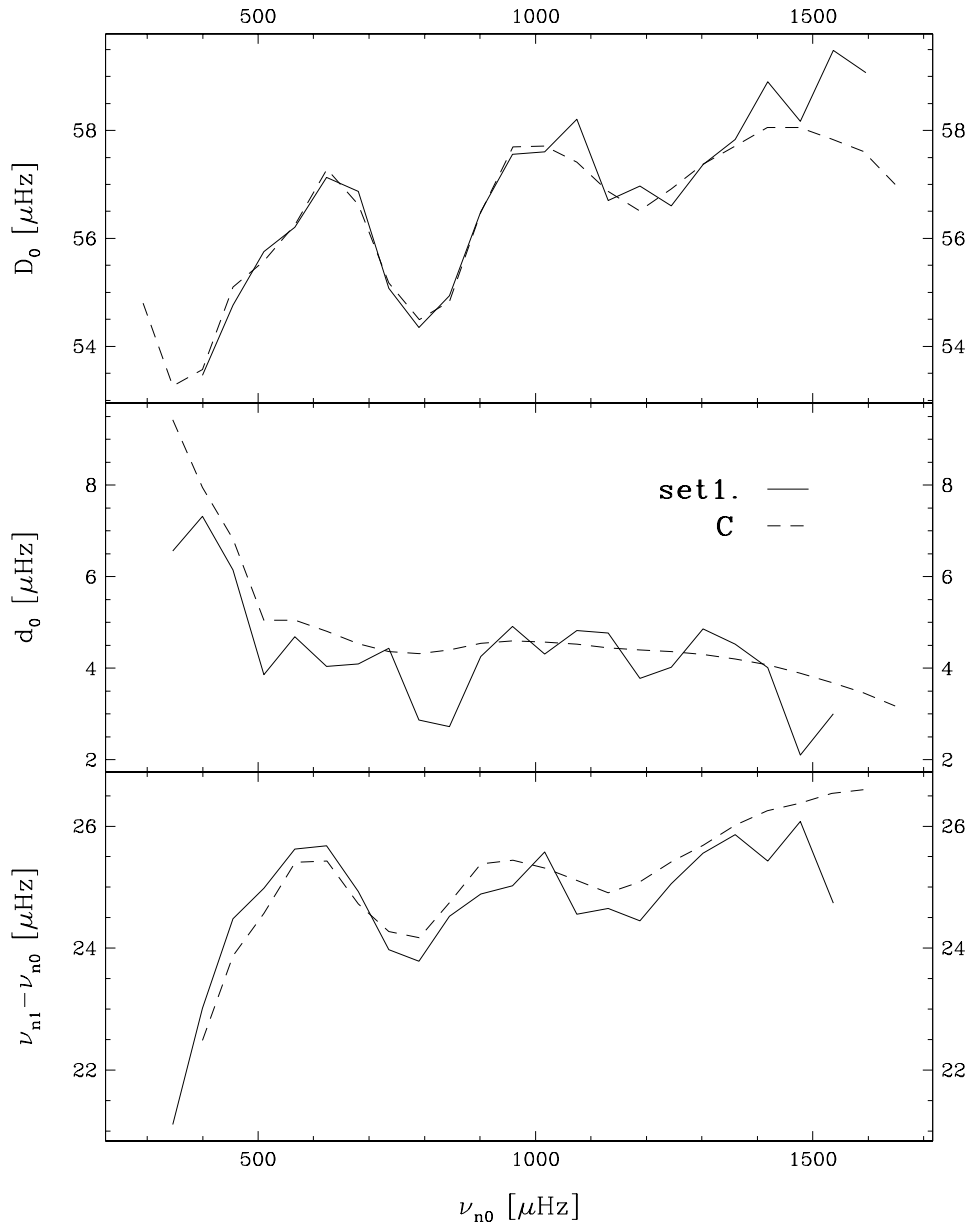
Figure 8: Large separations, small separations and $\nu_{n1} - \nu_{n0}$ for set1 and model C. We are not able to reproduce, for example, the small separation profile observed, so far.

| model | t $[10^9 \text{yr}]$ | $X_c$ | $\log L/L_\odot$ | $\log T_{eff}$ | $r_c/R$ |
|---|---|---|---|---|---|
| $C^1$ | 1.893 | 0.179 | 0.8280 | 3.8150 | 0.0583 |
| $C^1_{CESAM}$ | 2.009 | 0.140 | 0.8182 | 3.8118 | 0.0564 |

Table 2: Evolutionary parameters of two models with close p-mode spectra, according to different codes.

the search (model F), reproduced well both p-mode and mixed-mode spectra. Some of its parameters coincide with true parameters kept secret so far. The mass and chemical composition are found to fit.

## 4.3 Uncertainties

There is also the comparison between two independent evolutionary and pulsational codes among advantages of the *hare and hound exercise*. Equipped with such tools, we are able to evaluate some intrinsic uncertainties in model parameters coming from different modeling algorithms. In our simple analysis we focused on one nonrotating model with imposed ZAMS parameters (same as for model C). Oscillation frequencies of the model coming from code1 ($C^1_{CESAM}$) were then reproduced using code2. Two models ($C^1_{CESAM}$, $C^1$) which p-mode spectra match (Figure 9.) were then compared. Table 2. quotes some evolutionary quantities for the models. We see that the acoustic spectra coincidence is hardly affected by the strong difference in the structure of deep interior. This difference is probably due to the adopted burning rates. The HR diagram uncertainty is illustrated in Figure 10. Similar shift between the models concerned can be reproduced by changing the imposed envelope depth for the evolutionary calculations. We claim, this might be one of important modeling parameters that should be fine-tuned to reduce modeling uncertainty. We found that opacity or equation of state errors, due to interpolation grid, are not so significant.

## 5 Conclusion

We are able to reproduce most of spectral features from both `set1` and `set2` using two completely different evolutionary and oscillatory codes. Our forward method of searching models that fit radial mode frequencies works well in the framework of *hare and hound*. It is obvious that our models still need to be constrained for $\ell = 1, 2$ p-modes. We claim, however, that incorporating few mixed-mode frequencies in the analysis is a useful extension, while their frequencies are very sensitive to age changes. Thus, we emphasize the advantages of choosing evolved solar-like star among targets of an asteroseismology mission.

We stress also the necessity of fine-tuning of the evolutionary parameters (for example, envelope depth). Revision of burning rates adopted is also advised in order to minimize evolutionary uncertainties. Those are sources of additional errors in any method of reproducing spectra.

14
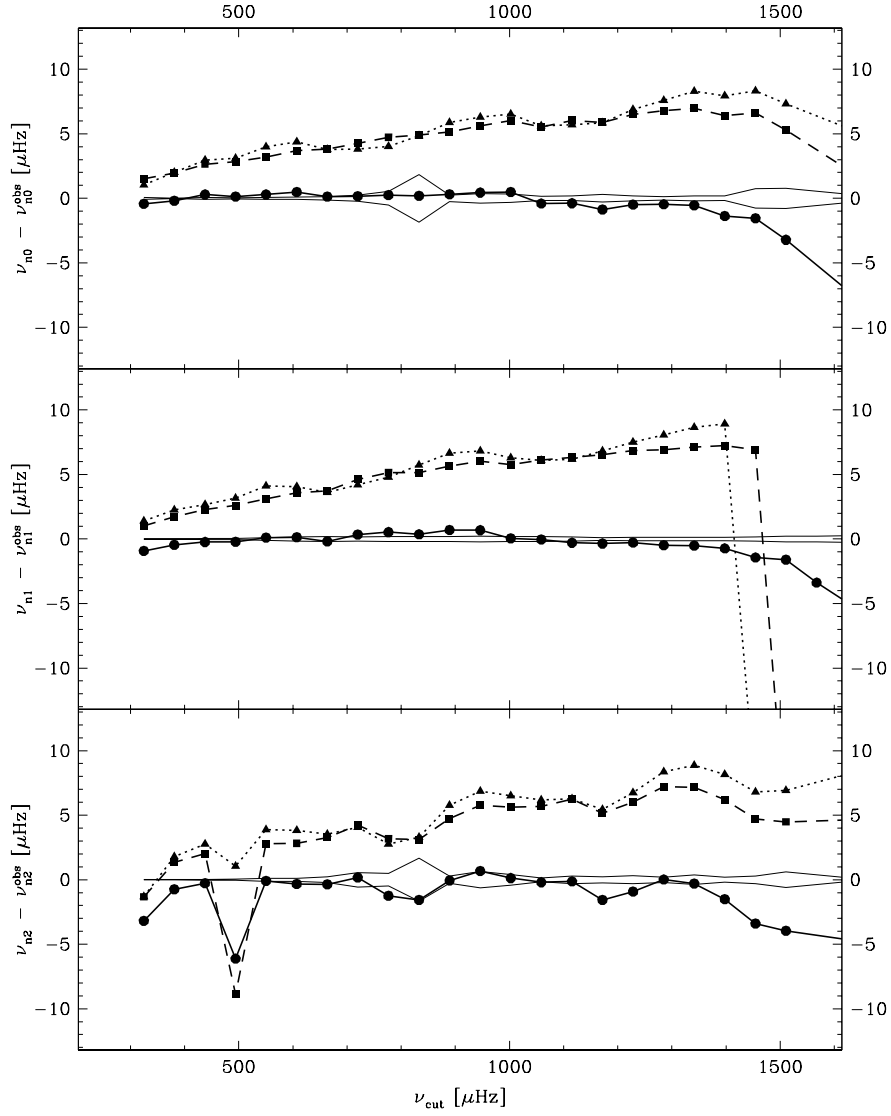
Figure 9: Model frequencies for $\ell = 0, 1, 2$ for C (dots), $C^1$ (squares) and $C^1_{CESAM}$ (triangles). All frequencies are shown relative to those from set1. Differences in the deep interior structure are visible for mixed-modes ($\sim 500$ $\mu$Hz for $\ell = 2$).
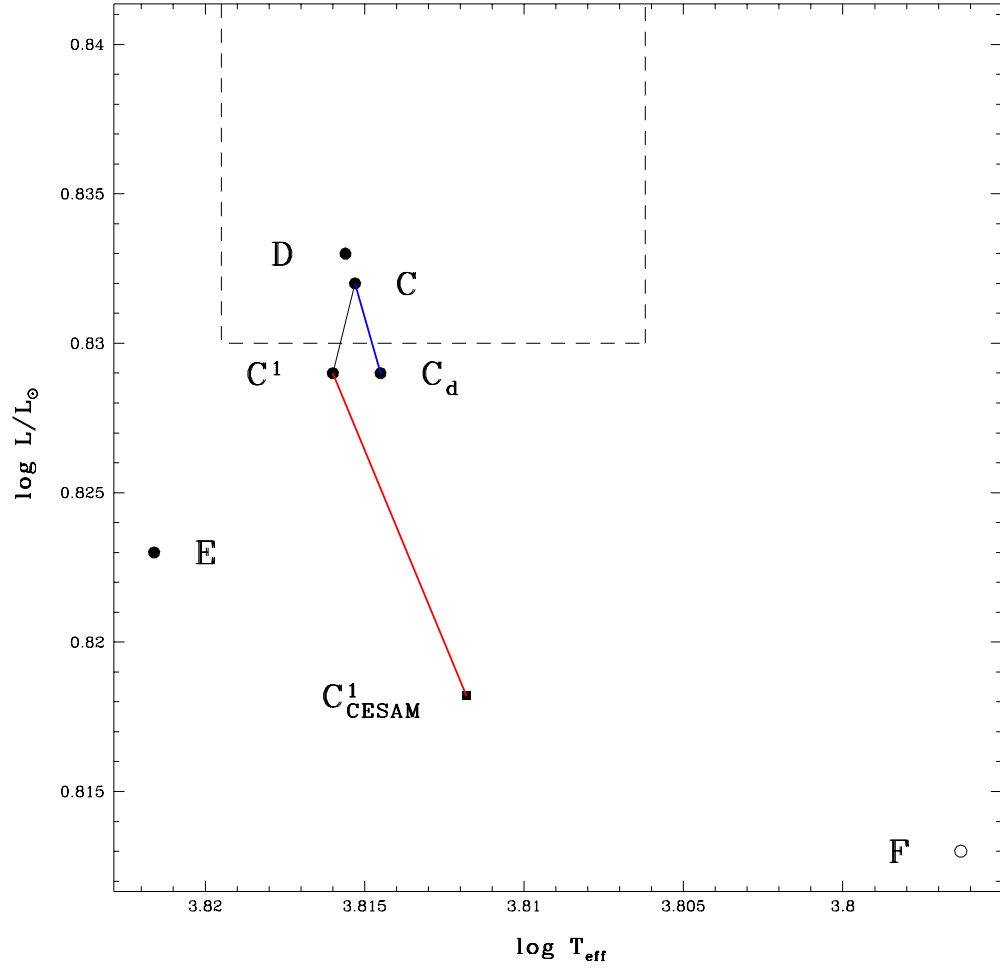
Figure 10: HR diagram positions for some discussed oscillating models. Red line connects two different models with very similar pulsational behavior. Blue line connects two models with different envelope depth (C: $M_{env}/M = 5\%$, $C_d$: 3%). Dashed line encompasses *hare and hound* box.

16

# 6    Acknowledgements

# References

[1] Baglin, A. and The COROT Team, 1998, Asteroseismology from space - The COROT Experiment, *IAU Symp. 185: New Eyes to See Inside the Sun and the Stars*, **185**, 301

[2] Bahcall, J.N. and Pinsonneault, M.H., 1995, *Rev. of Mod. Physics*, **67**, 781

[3] Grec, G., 1981, *Ph. D. thesis*, Université de Nice

[4] Provost, J., 2001, About frequency properties of solar-like stars, *COROT SWG Milestones Proceedings*, `http://dasgal.obspm.fr/~michel/MilestoneProc/SWGproc2000.html`

[5] Rogers, F.J., Swenson, F.J. and Iglesias, C.A., 1996, *Astrophys. J.*, **456**, 902

[6] Iglesias, C.A. and Rogers, F.J., 1996, *Astrophys. J.*, **464**, 943

# Generation

<div align="center">

**Simulation of COROT time series**
**Hare and Hound Exercise**

**C. BARBAN, NSO/DASGAL**

</div>

# 1   Simulated Stellar signal Power Spectrum

I assume that the peak associated to an oscillation mode in the power spectrum has a Lorentzian profile and I follow the recommendation of Anderson et al. 1990 to build the power spectrum.

## 1.1   Oscillation frequencies

Oscillation frequencies are provided by Ian Roxburgh.

## 1.2   Amplitudes

I use the estimates of the maximum oscillations amplitude of Houdek et al. (1999) (data found on MONS web site: http://www.obs.aau.dk/ jcd/MONS/solarlike/mode-param.html).
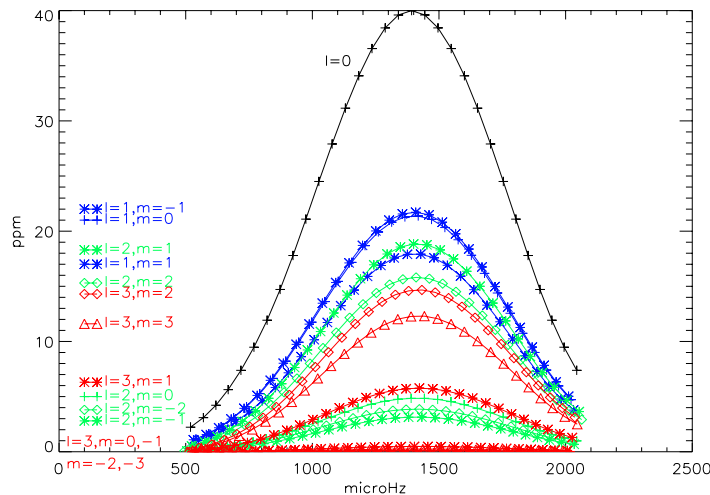


Figure 1: Amplitude as a function of frequency for $\ell=0$, the multiplet $\ell=1$, the multiplet $\ell=1$ and the multiplet $\ell=3$ before correction.

I adopt as the amplitude distribution a bell shape similar to what is observed for the Sun with a maximum of 40 ppm around the predicted maximum amplitude frequency. Then, for $\ell=0$ modes, I mimic this amplitude distribution by a Gaussian shape. I assume

the same amplitude distribution for modes $\ell \neq 0$. To mimic whole disk intensity observations, I apply to $\ell \neq 0$ modes visibility coefficients. These coefficients are calculated for the COROT photometric system using the equation of relative variations of flux of Watson 1988. I made a mistake in the computation of the visibility coefficients, then the first time series sent to the data fitter corresponds to Figure 1, after correction I obtain Figure 2 and this corresponds to the second time series sent.
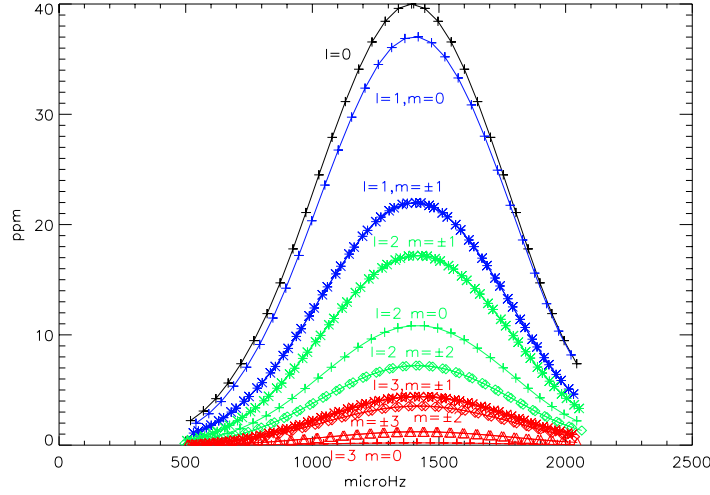


Figure 2: Amplitude as a function of frequency for $\ell$=0, the multiplet $\ell$=1, the multiplet $\ell$=1 and the multiplet $\ell$=3 after correction.

## 1.3   Linewidths
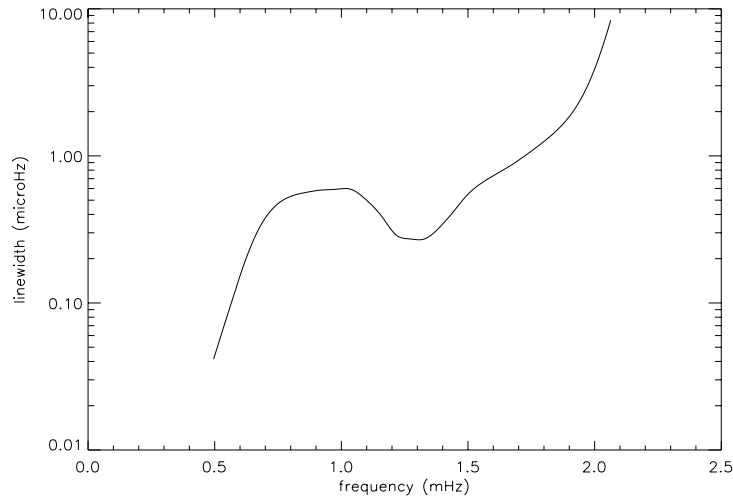


Figure 3: Linewidth as a function of frequency for a stellar model of M=1.5M$_\odot$, L=6.5725L$_\odot$, Teff=6.4053D3 K, Xc=5.0D-2.

The linewidths are taken from Houdek et al. (1999) (data from MONS web site) (Figure 3).

## 1.4 Background stellar noise

I adopt a stellar background noise similar to that observed for the Sun (Figure 4) and based on Appourchaux et al. (2000).
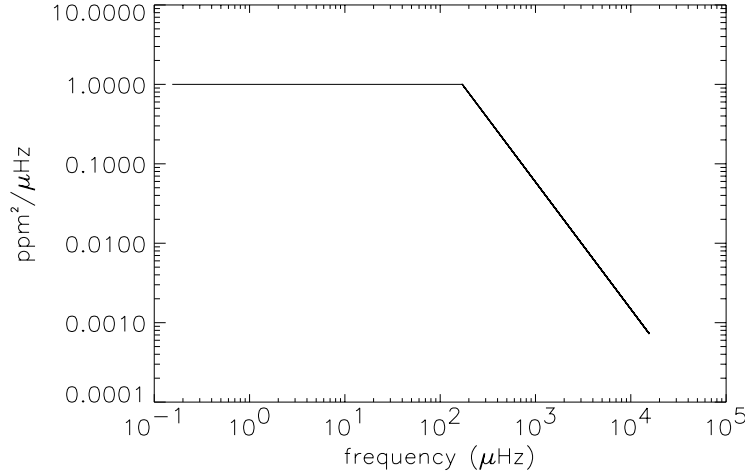


Figure 4: Modeled background stellar noise a a function of frequency (deduced from Fig. 2 of Appourchaux et al. (2000)).

# 2 Simulated Time Series

## 2.1 Stellar signal, $s_s(t)$

The time series data is obtained by computing the inverse Fourier Transform of the built Fourier spectrum.

## 2.2 Instrumental noise Time Series, $s_i(t)$

- A white noise of 0.7 *ppm* for 5 observations days is introduced ($s_{i1}(t)$).

- The orbital noise (f=(1/6092) Hz, amplitude=40 ppm) is also introduced ($s_{i2}(t)$).

Then the final instrumental time series is: $s_i(t) = s_{i1}(t) + s_{i2}(t)$

## 2.3 Final Time Series, $s(t)$

The final time series with a sampling of 32 s and a total length of 150 days is:

$$s(t) = (s_s(t) + s_i(t)) * w(t)$$

where $w(t)$ is function of time: $w(t) = 0$ for some points and $w(t) = 1$ for the other points.

I introduce in $w(t)$:

- the effect of the solar panels rotation (for the first two months of the total 5 months, I remove data each 10 days over a period corresponding to the length of the orbit, the same thing is done for the last 2 months of the total 5 months).

3

- a breakdown: I remove data over 3 days.

- the effect of the activation of the "magneto coupleurs": I remove 4 points in the time series spread out over the first half of the length of the orbit, I did the same thing for the 2nd half of the orbit.

*References:*

Appourchaux et al. 2000, COROT SWG meeting, Sept. 2000
Anderson et al., 1990, A&A 364, 699
Houdek et al., 1999, A&A 351, 582
Watson , 1988, Ap&SS 140, 225

# On the construction of synthetic time series Version 1.3

T.Appourchaux

April 5, 2002

## 1 Goal

The purpose of this document is to set a reference for generating artificial time series simulating stellar power spectrum.

## 2 Background

### 2.1 Methodology

The generation of time series is based upon the formalism developed for digital electronic processing. For instance, it is well known that for reconstructing a given signal in time, the minimum sampling frequency is given by the spectral content that we wish to recover. For example, let's assume that the maximum frequency is $\nu_{max}$, the sampling time corresponding is $1/2/\nu_{max}$, or the inverse of the Nyquist frequency ($=2\nu_{max}$). Other technical considerations such as aliasing, may come into play but we leave that to the digital-reconstruction-signal expert, or to the next version of the document.

When the Nyquist frequency is known, the number of points in the time series will define the frequency resolution from which we can generate the sampled spectrum. So for reconstructing a signal, it is not needed (it is superfluous...), to generate a highly resolved spectrum (corresponding to a long time series) when the time series itself is much shorter. The reconstruction will not be better.

### 2.2 Convention of Parseval's theorem

This is basically a theorem addressing energy conservation. Typically, projecting a function of time into an expansion of orthogonal function of time (sine and cosine) will not modify the energy (or the norm) of this function.

$$\int p d\nu = \sigma^2 \tag{1}$$

1

where $p$ is the spectral density power of the process (in ppm$^2$/$\mu$Hz for example) and $\sigma$ is the root mean square of the process in time.

For instance for white noise, we can write:

$$P_0 \Delta \nu = \sigma^2 \tag{2}$$

where $P_0$ is the power spectra density of the white noise (assumed to be independent of the observation), $\Delta \nu$ is the bandwidth over which this random process is observed and $\sigma$ is the standard deviation of the random process in time.

In the same spirit, for a sine wave we have that the energy of the wave is given by:

$$\frac{A^2}{4} + \frac{A^2}{4} = \frac{A^2}{2} \tag{3}$$

The left hand side of the equation represents the sum of the 2 terms that appear in the positive and negative part of the power spectrum, while the right hand side is just the expression of the energy of the wave (or the square of the rms amplitude of the wave).

Now if we assume a lorentzian profile for a p mode peaking at A ppm$^2$/$\mu$Hz and a FWHM of $\Gamma$ then the integrated power is $P = 2 \times \pi A \Gamma / 2$. The factor 2 in front comes from the fact that we need to take into account the negative and positive side of the spectrum.

## 2.3 Mode amplitude in the literature

The theoretical mode amplitude computed by Houdek (1999) is the rms velocity or intensity amplitude derived from the energy in the mode. Therefore the peak amplitude in the power spectrum can be derived from the rms amplitude using Parseval's theorem and we have:

$$A = V_{rms}^2 / \pi / \Gamma \tag{4}$$

This is assuming that the profile is lorentzian. It should be noted that the $V_{rms}$ is usually derived from just $A \times \Gamma$ and the $\pi$ seems to be forgotten... unless I made a mistake. To be discussed and verified.

# 3 Recipe for time series generation

Here are the steps needed for generating a time series obeying a prescribed power spectrum:

- Assume a Nyquist frequency ($\nu_{max}$) or a sampling time ($\Delta t = 1/\nu_{max}$).

- Assume a length for the time series or the number of points in the power spectrum ($N$)

2

- The power spectrum is derived from whatever is known or assumed about the instrument or the star. The units of choice here are ppm$^2$/$\mu$Hz

- Generate the power spectrum for half the number of points ($N/2$).

- Multiply the spectral density by the size of the frequency bin ($1/N/\Delta t$) expressed in $\mu$Hz if this is the unit of choice. This takes into account the length of the time series.

- Take the square root of the power to get the amplitude

- Multiply the amplitude spectrum by a complex random variable with each component having a normal distribution where the real (or imaginary part) has a mean of 0 and an rms of 0.5. The real and imaginary parts are independent of each other.

- The amplitude spectrum now obtained needs to be symmetrized because the time series is real, i.e. $F(-\nu) = F^*(\nu)$. We get the final Fourier spectrum.

- Invert the Fourier spectrum

- Check that the imaginary part is indeed negligible compared to the real part.

The final check is done by comparing the results given by Parceval's theorem. Let's assume that a noise of 1 ppm$^2$/$\mu$Hz has been generated over a bandwidth of 16666 $\mu$Hz (1 over 60 s). The expected rms value of the corresponding time series should be $\sqrt{1 \times 16666}$=129 ppm. So if $A = \Gamma = 1$, then the rms is $\sqrt{\pi}$=1.77 ppm

## 4    The Corot noise level

It does make sense to relate the 0.6 ppm in 5 days given in the Corot literature to 'real' amplitude in the time series. The reference document is 'Corot: scientific program and specifications, March 1998'.

The reference document mentions a signal-to-noise ratio of 15 as a baseline for reaching a frequency precision close to what would be obtained with a large signal-to-noise ratio (say 100). The signal-to-noise ratio of 15 combined with a typical solar-like amplitude of 2.5 ppm gives a noise level to be reached in 5 days (typical solar-like mode lifetime) of 0.18 ppm$^2$/$\mu$Hz, The typical noise is therefore in a 5-day frequency bin 0.64 ppm (0.18 $\times$ 2.3).

Now what does it mean for a mode? The peak amplitude in the power spectrum is 0.18 $\times$ 15=2.7 ppm$^2$/$\mu$Hz. Then the total power of this mode with a 5-day lifetime is $\pi \times 2.7 \times 2.3 = 19.5$ ppm$^2$, or 4.4 ppm in the time series. This latter number is nothing less but the 'usually quoted amplitude of the mode'

3

time the square root of humble $\pi$ (4.4=2.5 $\times \sqrt{\pi}$). Hope this clarify the situation now.

# 5    A remark...

Please bear with me as this report was written under the influence of a flu, an insomnia, an amnesia and other neurotic behaviours.

# On expressing mode splitting with Clebsh-Gordan coefficients and related issues

T.Appourchaux

September 14, 2001

## 1 Goal

The goal of this document is to express the splittings given in terms of $(\nu_m - \nu_0)/m$ as a function of the $a_i$ expansion based on Clebsh-Gordan coefficients.

## 2 Background

In the antique age of helioseismology (before the 90's or so), mode splittings were usually expressed in term of Legendre polynomials. Unfortunately, these polynomials are orthogonal only on a continuous space (between [-1,1]) not on a discrete set such as (-1,0,+1) for $l=1$, for exanple. Therefore, other expansion are required that can either be computed by hand or derived from quantum mechanics.

## 3 Clebsh-Gordan expansion

Riztwoller and Lavely (1991) derived the following polynomials from quantum mechanics. The splittings are expressed as follows:

$$\nu_{(l,m)} - \nu_{(l,0)} = \sum_{i=1}^{i=n} a_i l \mathcal{P}_l^i(m) \tag{1}$$

where

$$\mathcal{P}_l^1(m) = \frac{m}{l} \tag{2}$$

$$\mathcal{P}_l^2(m) = \frac{6m^2 - 2l(l+1)}{6l^2 - 2l(l+1)} \tag{3}$$

$$\mathcal{P}_l^3(m) = \frac{20m^3 - 4m(3l(l+1) - 1)}{20l^3 - 4l(3l(l+1) - 1)} \tag{4}$$

$$\mathcal{P}_l^4(m) = \frac{70m^4 - 10m^2\left(6l(l+1) - 5\right) + 6l(l+1)\left(l(l+1) - 2\right)}{70l^4 - 10l^2\left(6l(l+1) - 5\right) + 6l(l+1)\left(l(l+1) - 2\right)} \tag{5}$$

Please note that for all $i$ we have $\mathcal{P}_l^i(l) = 1$. The polynomials are derived from Eqs (39) to (44) of Riztwoller and Lavely (1991). The derivation of $(\nu_m - \nu_0)/m$ is then straightforward using Eqs (1) to (5).

Bon courage!

# HH#3

# Seismic interpretation of solar-like targets
## Progress report

*G. Berthomieu & Seismic interpretation group*
*Laboratoire Cassini, OCA, Nice*

Participants: *G. Berthomieu, J Ballot & CEA group, MJ. Goupil, Y. Lebreton, J Lochard, A. Mazumdar, E. Michel, J. Montalban & Liège group, P. Morel, J. Provost, I. Roxburgh*

The aim of the group was to give priorities to 4 stars as COROT targets: HD49933, HD43318, HD45067, HD57006. These stars are solar-like stars with different masses and evolutionnary stages. Their position in the HR diagram is indicated in figure 1 where evolutionnary tracks with (dashed line) and without (full line) core overshoot are also plotted. HD49933 is at the begining of the main sequence phase, HD43318 and HD45067 may be either at the end of the main sequence phase or in a post main sequence phase according to the physics used for stellar modelling, HD57006 is always in a post main sequence phase.
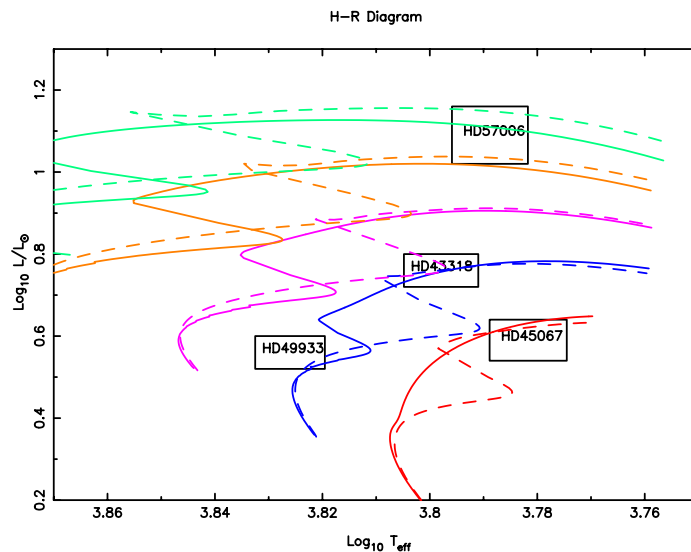


Figure 1: Position of the four solar-like targets in the H-R diagram.

The work has been done in strong collaboration with the data analysis group through a Hare and Hound exercise. (see the report of T. Appourchaux). Our aim was to use the frequencies extracted from the simulated time series to infer the structure of the input model. Following what has been done for the Sun, the method used by all the groups wasa model calibration, that is trying to construct a stellar model which satisfied as closely as possible all the constraints.

Different criteria have been used to achieve this task. For the seismic interpretation, the frequencies are not used directly because we know from the solar case that they include contributions of surface effects, activity,.... Thus linear combinations of the frequencies

where these contributions cancel more or less are prefered. The criteria which have been used are the following:

- Position in the HR diagram and chemical constraints
- Large frequency differences $\implies$ Mean density of the star
- Small frequency spacing $\implies$ core structure $\implies$ age, evolutionary stage
- Second difference of frequencies
  $\implies$ Acoustic depth of the convection zone and the helium ionisation zone

The last criterium gives information on the star independently of the stellar model.

The results and their interpretation have been discussed in a meeting in Paris. The contributions of Lochard et al, Ballot et al, Montalban et al, Mazundar et al., Provost et al., are available at the web address: http://virgo.so.estec.esa.nl/html/corot/datagroup/third_hh.html. This report gives a summary of their work.

## A) Inferences from the position in the HR diagram and metallicity constraints

To construct a stellar model, the unknowns parameters are the mass $M_\star$, the age $t$, initial helium and heavy elements abundances Y, Z/X, and the parameters describing the convection: the mixing length parameter $\Lambda$, and the core overshoot parameter $\zeta_{ov}$.

Three constraints : the bolometric magnitude $M_{bol}$, the effective temperature $T_{eff}$, and the surface metallicity $F_e/H$ are generally derived from astrometric, photometric and spectroscopic observations. They lead to select a range of parameters at given physics which may correspond to different evolutionary stages for the star as is seen in figure 1. for HD43318 and HD45067.

## B) Seismic analysis: Large frequency differences

The large frequency differences are defined by: $\Delta\nu_{l,n} = \nu_{l,n} - \nu_{l,n-1}$ The mean value at high frequencies is related to the mean density of the star.
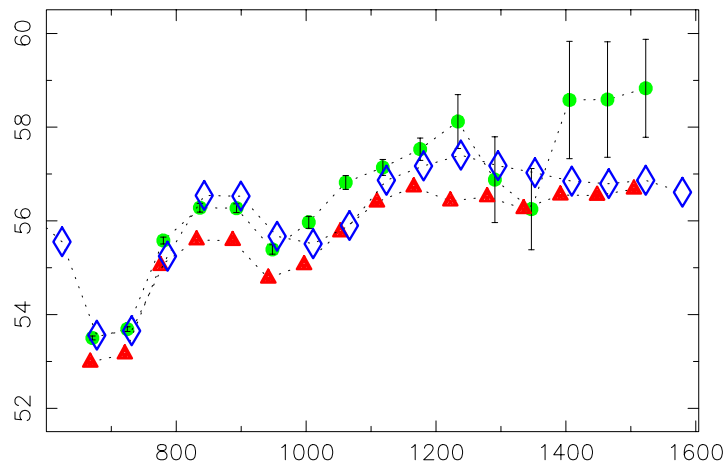


Figure 2: Large frequency differences for the input model (triangles), the closest model (losanges) and data from simulated time series of HD43318 (full dots).

As seen in figure 2, there is a systematic difference between the large frequency differences from the input model and closest model in the case of HD43318. This is due to

the fact that the simulated time series for that star includes "surface and activity effects" which have a quasi linear dependence on the frequency.

## C) Seismic analysis: Small frequency differences

The small frequency differences are sensitive to the properties of the stellar core and thus to the age and evolutionary stage. They are defined by:

$$\delta\nu_{0,2} = \nu_{0,n} - \nu_{2,n-1}$$
$$\delta\nu_{0,1} = \nu_{0,n} - (\nu_{1,n} + \nu_{1,n-1})/2$$
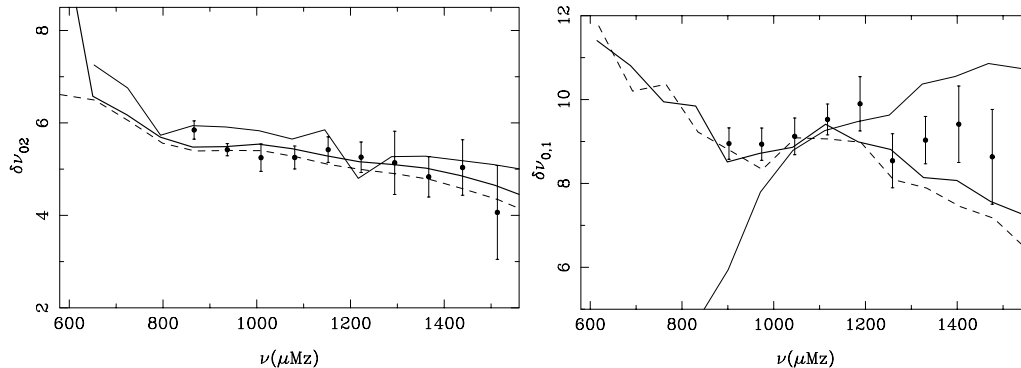


Figure 3: Small frequency spacing $\delta\nu_{0,2}$ and $\delta\nu_{0,1}$ for two main sequence (heavy and dashed line) and one post main sequence model (thin line) of HD45067.

It is seen from figure 3 that $\delta\nu_{0,1}$ is the more sensitive diagnistic of the age i.e. the evolution state of the star. With this indicator we can discriminate between a main sequence and post main sequence model.

## D Second difference of frequencies: Acoustic depth of the convection zone and Helium ionisation zone

Discontinuities in sound speed derivatives introduces oscillations in the frequencies. Such discontinuities occur at the basis of the convection zone where we have an adiabatic gradient in the convection zone and a radiative gradient in the radiative zone just below. There is also a rapid variation of the adiabatic exponent $\Gamma$ in the ionization zone of Helium II which induces a rapid variation of the sound speed. The oscillating terms in the frequencies are visible in the second difference in frequencies. Their periods are related to the acoustic depth of the layer where the discontinuity takes place.

Table 1: Comparison of the acoustic depths of the basis of the convection zone and location of the helium II ionisation zone estimated from the simulated data and their theoretical value from the input model.

| $\star$ | $\tau_{CZ}$ | $\tau_{CZ}$ input | $\tau_{He_{II}}$ | $\tau_{He_{II}}$ input |
|---|---|---|---|---|
| HD43318 | 3763 $\pm$134 | 3877.8 | 1518 $\pm$ 98 | 1614.7 |
| HD49933 | 1445 $\pm$ 68 | 1434 | 663 $\pm$ 49 | 660 |

This determination of the acoustic depths $\tau_{CZ}$ and $\tau_{He_{II}}$ is important because it may be used to select the closest model when some problems arise with the small spacings. This has been the case for HD49933 due to the problems with rotational splitting (see report of T. Appourchaux) and the values derived for $\tau_{CZ}$ and $\tau_{He_{II}}$ have been used to calibrate different global parameters of the model. Figure 4 illustrates the calibration of chemical composition with acoustic depths.
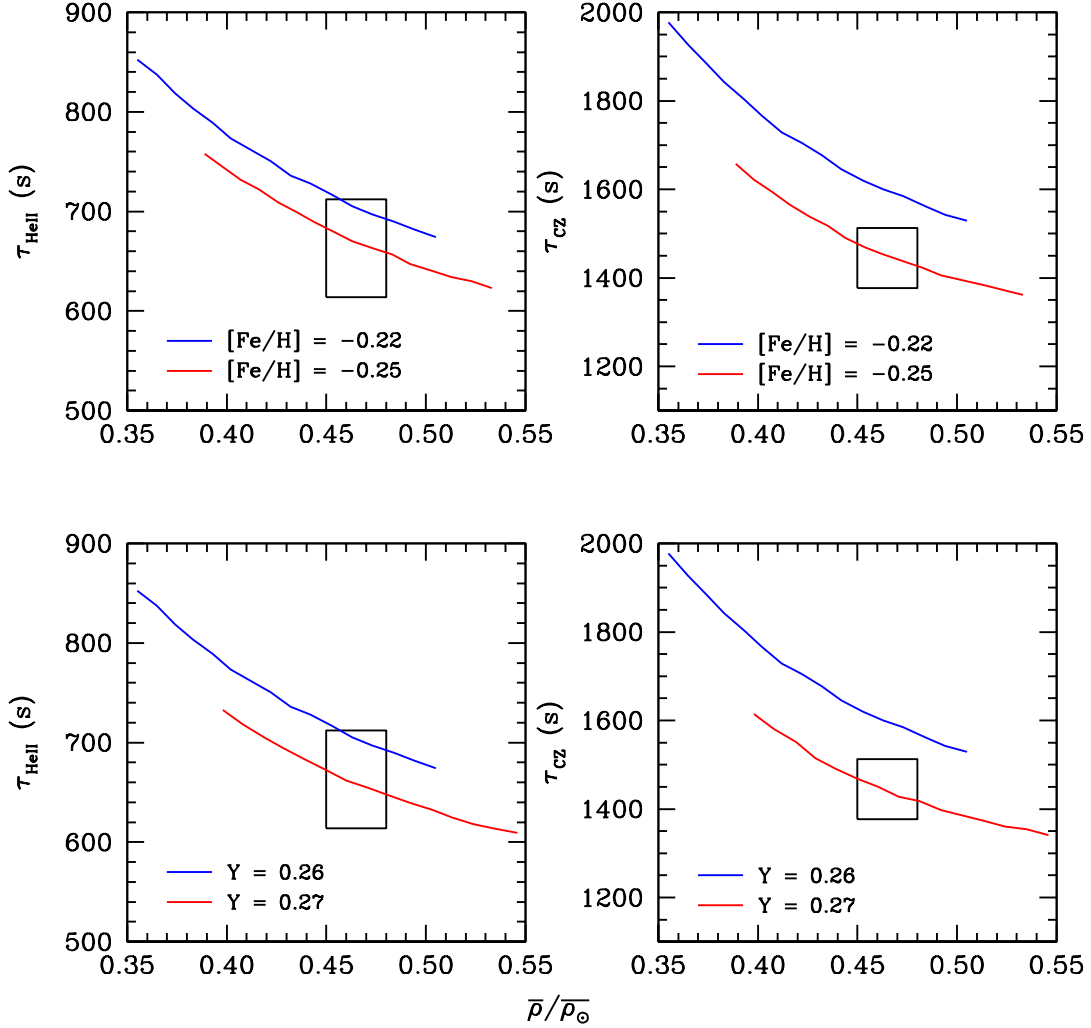


Figure 4: Calibration for HD49933 of helium abundace and metallicity with acoustic depths of convection zone boundary and helium ionisation zone constraints versus mean density constraint derived from the large frequency differences.

## E. Results of H&H3 exercise

Table II illustrates the results of HH3 exercise and the kind of problems encountered. All the results obtained by the different groups and discussed during the Paris meeting are

not reproduced here but can be seen on the web.It must be kept in mind that the results, and thus their interpretation, depend on the assumptions which have been made first on the construction of both theoretical models and simulated time series.

For the first star HD49933, the input and output models agree despite the fact that problems have arised in the identification of modes $l = 0$ and 2 turning the small spacing unusable constraint. (see T. Appourchaux's report). The results for the second star HD43318 are more instructive. The input model was constructed including microscopic diffusion of helium and heavy elements and some additional mixing to prevent surface abundance anomalies. The search for closest model was made without including any diffusion mecanism. This explains the difference in mass, surface abundaces and central hydrogen. However the acoustic depths of convection zone base and heliumII ionisation zone are close and more surprisingly the convective core radius. It seems as if a difference in overshoot parameter compensated the lack of diffusion. This is being studied.

The case of HD45067 is particular because the input model was constructed with a metallicity totally out of the range admitted for that star as it is seen in the table. The luminosity too was derived with an old solar bolometric magnitude. The search of closest model has shown this difficulty to fit with constraints. Nevertheless, the use of frequencies allowed to find acoustic depths of convection zone base and heliumII ionisation zone close to the those of the input model and also the radius of the convective core.

No theoretical interpretation has been carried for the star HD57006.

Table II: Values of the mass (in solar unit) $M/M_\odot$, the surface abundances in helium and heavy elements $Y_s$, $Fe/H_s$, the central hydrogen content $X_c$, the acoustic depth of convection zone $\tau_{CZ}$ and heliumII ionisation zone $\tau_{He_{II}}$, the core radius $r_{core}$ and the core overshoot parameter$\zeta_{ov}$ for the input and output (closest model) models.

| $\star$ | $M/M_\odot$ | $Y_s$ | $Fe/H_s$ | $X_c$ | $\tau_{CZ}$ | $\tau_{He_{II}}$ | $r_{core}$ | $\zeta_{ov}$ |
|---|---|---|---|---|---|---|---|---|
| **HD49933** | | | | | | | | |
| Input | 1.25 | 0.26 | -0.25 | 0.5 | 1434 | 660 | 0.093 | 0.2 |
| Output | 1.25 | 0.27 | -0.22 | 0.505 | 1438 | 667 | 0.097 | 0.2 |
| **HD43318** | | | | | | | | |
| Input | 1.45 | 0.19 | -0.116 | 0.109 | 3878 | 1615 | 0.061 | 0.05 |
| Output | 1.38 | 0.26 | -0.08 | 0.18 | 3763 | 1471 | 0.062 | 0.15 |
| | | | | | $r_{CZ}$ | | | |
| **HD45067** | | | | | | | | |
| Input | 1.31 | 0.29 | +0.17$^\star$ | 0.12 | 0.78 | | 0.059 | 0.09 |
| Output | 1.18 | 0.27 | -0.23 | 0.115 | 0.84 | | 0.0595 | 0.15 |

$^\star$ out of the observational range $Fe/H \sim -0.17 \pm 0.1$

## F. Conclusion

The results of the exercise have shown our ability to recover the evolutionary stage of the star and properties of the structure, particularly the acoustic depth of the basis of the convection zone and of the HeliumII ionisation zone, independently of a model. The radius of the convective core is also in ageement with input one. The introduction in the frequencies of the surface effects induces a shift in the values of the large differences $\Delta\nu_{l,n}$ and thus some uncertainty in the calibrationof the mean density of the star. For small frequency differences this effect can be suppressed by dividing them by $\Delta\nu_{l,n}$.

As far as the COROT targets are concerned, it is suggested to give a good priority to the stars HD49933, HD43318 and HD45067. A lower priority is given to the star HD57006 due to the complexity of its spectrum induced by the fact that it is a rather evolved star.

More work is to be done on the signature of diffusion and core overshoot on the frequencies, on the effect of activity and surface effects, on evolved stars. Moreover, only the direct problem of looking for a stellar model which satisfies all the constraints has been considered. Inversion technics adapted to the COROT data must be developped.

Despite the fact that some rotational splitting has been added in the H&H exercise no work has been done on the rotation. Such a work is planed for next exercise.

# MODE EXTRACTION FROM TIME SERIES: FROM THE CHALLENGES OF COROT TO THOSE OF EDDINGTON

## Paper presented by and with the courtesy of Jesper Schou

**T.Appourchaux[1], O.Moreira[1], G.Berthomieu[2], and T.Toutain[2]**

[1]European Space Agency, P.O.Box 299, 2200AG Noordwijk, The Netherlands
[2]Département Cassini, UMR CNRS 6529, Observatoire de la Côte d'Azur, BP 4229, 06304 Nice Cedex 4, France

### Abstract

With more than 30 years of experience in extraction of eigenmodes from power spectra of solar signals, we are now almost ready to apply this knowledge onto the fore-coming missions: COROT and Eddington. Unfortunately, the fitting task differs by 3 orders of magnitude; COROT will be able to get time series of stellar light for some 30 stars, while Eddington will be able to gather such data for about 50000 stars. While for COROT, our current tools can be applied *by hand*, the case of Eddington is *somewhat* more complex. We are looking forward having automatic fitting procedures that will allow to recover mode parameters for about 90% of the solar-like stars. Unfortunately, about 10% of these stars will require some more delicate attention that will cost time to take care of. We will use the example of the infamous HD57006, known to be quite evolved with a difficult eigenmode spectrum, to explain how a star can evolve from an easy-to-fit target (90% of the solar-like stars) to a difficult-to-fit target (10% of the remaining stars). In the latter case, new techniques for detecting narrow peaks (g-mode like) out of broad peaks (p-mode like) has been devised in the context of the hare-and-hound exercise of COROT. This latter and other techniques will be used to implement the automatic fitting procedure for the remaining 10% of Eddington solar-like stars.

Key words: Stars: structure – Data analysis: time series – Data analysis: spectra fitting

## 1. Introduction

In the very near future, there shall be a fleet of space missions aiming at understanding the internal structure of the stars: MOST[1], COROT[2] and Eddington.

All these missions will observe global oscillations of the stars by measuring their tiny light fluctuations. The detection and identification of these modes of oscillation is the challenge of all these missions. This challenge is for most stars extremely difficult (e.g. Cepheids) but easier for solar-like stars. When the identification is achieved, peak bagging can be performed. The theory of mode identification and peak bagging has been reviewed by Appourchaux (2003); it is now believed to be well understood.

In the context of the COROT mission, the practice of mode identification and peak bagging is developed through the use of hare-and-hound exercise. During this exercise, it appears that a very challenging star (namely HD57006) brought a new dimension to the usual challenge [3]. Here we would like to take this star as an example of the kind of difficulties that the Eddington mission may face. For that purpose, we will follow HD57006 throughout its lifetime from the ZAMS[4] until its nowadays evolutionary state.

## 2. Mode identification and peak bagging

The reader may wish to read the review on the subject by Appourchaux (2003), we summarize that review for the sake of completeness.

The mode identification for solar-like stars is performed using the *Echelle diagram*. It is based on the fact that the low-degree mode frequencies of successive orders ($n$) of a given degree ($l$) are distant from each others by roughly the acoustic diameter of the star ($\Delta\nu_0$). The piling up of section of the power spectrum (of the stellar time series) cut into piece of length $\Delta\nu_0$ produces 'ridges' of power along an ideal vertical line. The location of the ridges with respect to each other provides the means of tagging the ridges with a given $l$.

The next step is the peak bagging operation which theory can be found in Appourchaux et al. (1998) and Appourchaux (2003). It consists in fitting the power spectrum using Maximum Likelihood Estimators (MLE) and a model of the mode profile including parameters such as frequencies, linewidth, splittings, background noise and profile shape. Error bars of parameters can be derived as well as the significance of these parameters (Appourchaux et al., 1998).

---

[1] Microvariability and Oscillations of Stars, a Canadian mission to be launched in June 2003
[2] COnvection and ROTation, a CNES mission to be launched in mid 2006

[3] See papers of the Third COROT week in http://www.astro.ulg.ac.be/orientation/asterosis/week3
[4] Zero Age Main Sequence

---

## 3. THE CHALLENGES IN THEORY

### 3.1. COROT VS EDDINGTON

The COROT mission shall be able to observe up to ten primary seismological targets for which there will be a high signal-to-noise ratio as to perform proper mode identification and peak bagging. The COROT secondary targets can amount to less than a hundred. The Eddington mission shall be able to observe more than 50000 stars.

For COROT, the primary targets can be analyzed by a single scientist. The mode identification and fitting can be carefully analyzed. Modes out of the main stream can be fitted by hand, and each fitted mode can be assessed for its validity. One could imagine that the secondary targets are also analyzed by the same scientists; the task may start to be somewhat difficult to handle.

For Eddington, this hand crafted work is to be abandoned. Automated ridge identification, mode fitting and fit rejection has to be implemented. At the time of writing, the first task is still done by hand using the *Echelle diagram* and adjusting the large separation as to have vertical ridges. We could envisage a step where after computing the power spectrum, one identifies the excess power, filter the excess power and compute the Fourier transform for extracting the large separation (or as a matter of fact $\Delta\nu_0/2$); this technique was used by Gelly et al. (1986) on the $\alpha$-Cen data. The next step is to compute the *Echelle diagram* using the derived large separation. As for the proper ridge identification, one could try to fit[5] 2 pairs of peaks ($l = 0 - 2$ and $l = 1 - 3$) over $\Delta\nu_0$; the amplitude of the fitted peaks and their location would automatically provide the degree tagging. The mode fitting can then be done as *usual*. The last step is the validation of the fit. It is envisaged that each mode be assessed for its significance using the likelihood ratio test (Appourchaux et al., 1998).

### 3.2. THE STELLAR EVOLUTION

But the real challenges of either COROT or Eddington may lie beyond these mundane details. The identification and fitting steps described above can be applied to well-behaved solar-like stars; that is about 90% of the solar-like stars to be observed by Eddington. The remaining 10% are evolved solar-like stars for which the automated techniques fall apart. Here we should outline that we do not really know the proportion of evolved stars to that of *good* stars. Even if we were to have only 0.1% of evolved solar-like stars in the Eddington mission, we would have the same challenging difficulties. As we will outline, this part of the challenge is not to be neglected.

Here we would like to follow the evolution of a star, to scan the many stars of Eddington. We start with a star
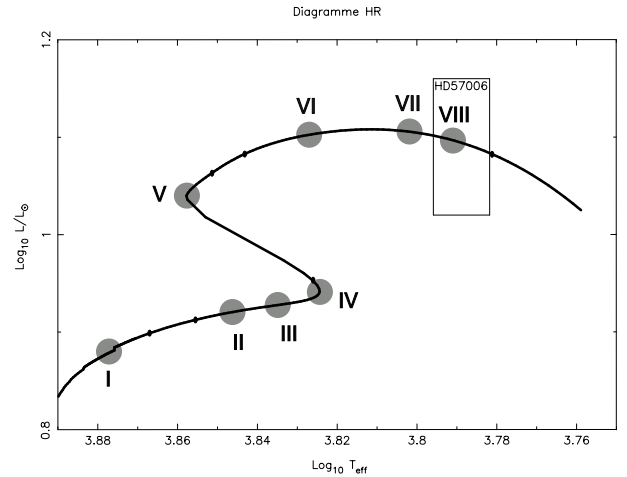


*Figure 1. The Hertzsprung-Russell diagram of HD57006. We computed the mode frequencies of models labeled from I to VIII located at different positions on the evolutionary track of the H-R diagram. The first four locations follow the evolution of the star until the central hydrogen content is about 5%. The last four locations follow the evolution of the star during the burning of hydrogen in shell. The transition from model IV to V is too fast by stellar standard but likely long enough by human standards for being observed.*

at the ZAMS, and study how the *Echelle diagram* evolves with the star, and how the difficulties evolve.

Here we chose the COROT primary target HD57006 which scientific value is being assessed by the Seismology Working Group of the eponymous mission. The assessment is being performed in the frame work of the third hare-and-hound exercise of COROT (Appourchaux, 2003).

The star HD57006 has been represented by a $1.65 M_\odot$ stellar model; that is still a solar-like star, according to the definition of Appourchaux (2003), when not evolved. It is nowadays sufficiently evolved as to have entered the phase of burning hydrogen in shells, i.e. it has an helium core. This produces a large peak in the Brunt-Vaïsala frequency at the core of the star. It leads to the existence of the so-called mixed modes that have a p-mode character in the outer stellar regions, and a g-mode character in the stellar core. The mixed modes, if detected, are powerful tools (like the g modes) for understanding the internal structure of the star. Unfortunately, their mixed character make them difficult to detect for they do not follow the asymptotic relationship given by Tassoul (1980); in other words they do not line up for making ridges.

In order to see how the *Echelle diagram* changes with the evolution of HD57006, we computed frequencies of low-degree modes all along the evolution track of the star as outlined by Fig. 1. The *Echelle diagrams* for each evolution stage in the central hydrogen burning phase are shown in Fig. 2; and for the hydrogen burning phase in shell in Fig. 3.

---

[5] where the peak power is maximum
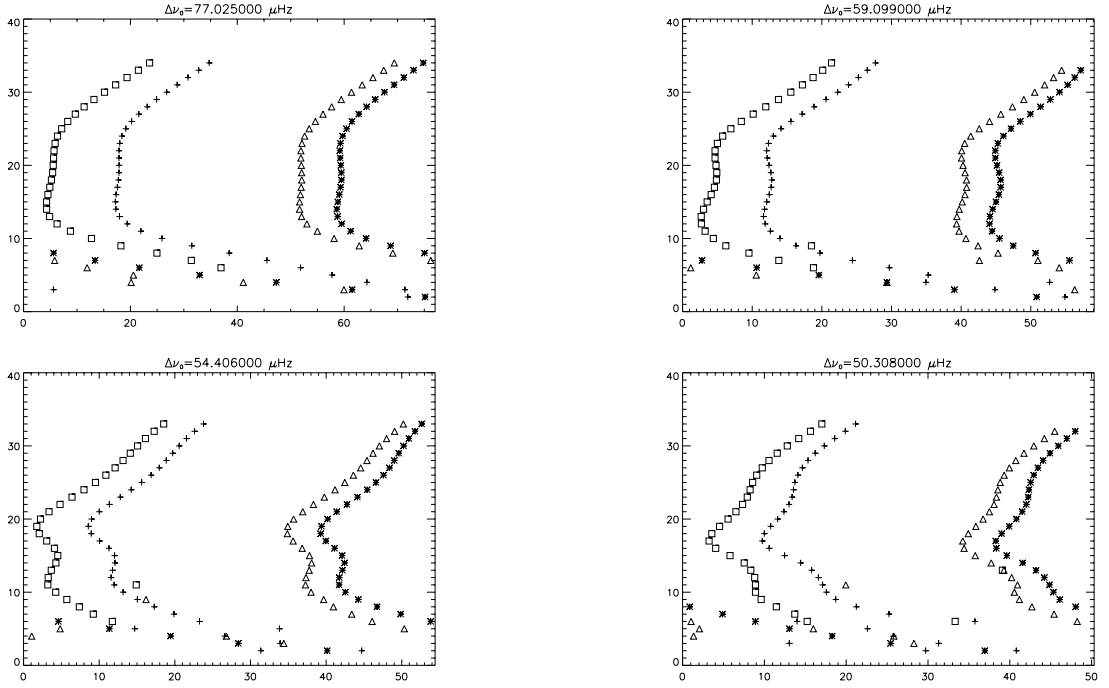
Figure 2. *Echelle diagram for the first four stages of the evolution of HD57006 during the central hydrogen burning phase; I (left, top), II (right, top), III (left, bottom), IV (right, bottom). The echelle diagrams display the order as a function of frequency; the large separation is annotated atop the diagram. The **star** and **triangle** are the l=0 and l=2 modes; the **plus** and **square** are the l = 1 and l = 3 modes.*
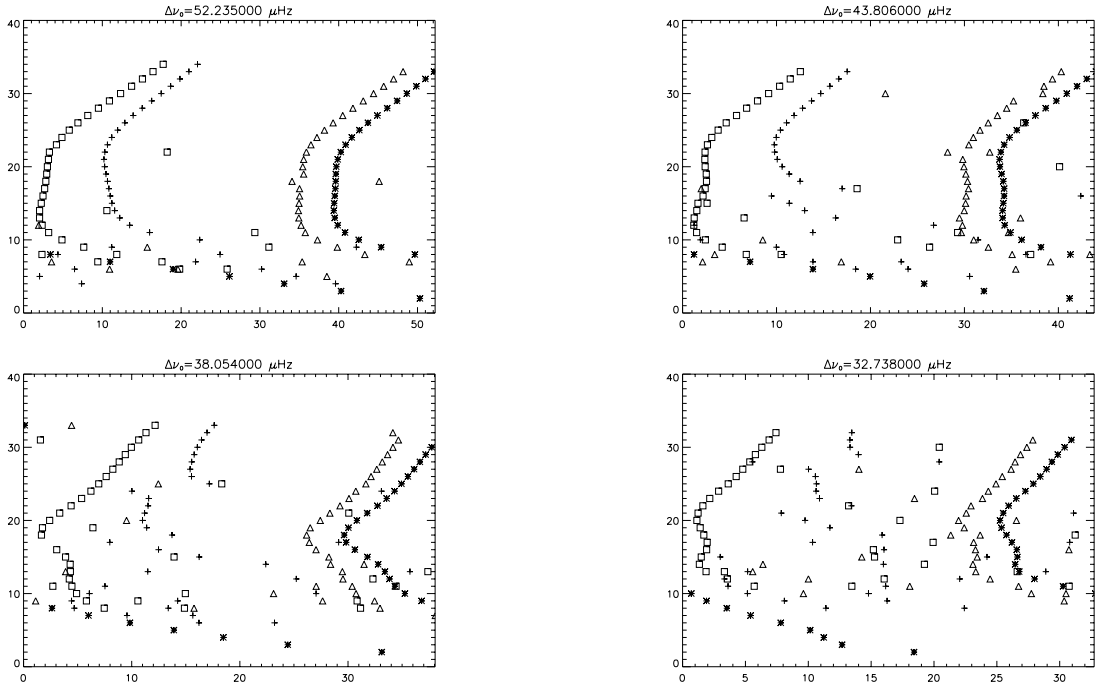


Figure 3. *Echelle diagram for the first four stage of the evolution of HD57006 during the hydrogen burning phase in shells; V (left, top), VI (right, top), VII (left, bottom), VIII (right, bottom). The echelle diagrams displays the order as a function of frequency; the large separation is annotated atop the diagram. The **star** and **triangle** are the l=0 and l=2 modes; the **plus** and **square** are the l = 1 and l = 3 modes.*

In the first evolution stage, the mode identification and fitting would be rather classic. The large separation decreases due to the increase in the stellar radius. The ridges get closer from each other; the $l = 0$ and $l = 2$ mode-ridge separation decreases from 8 $\mu$Hz to 4 $\mu$Hz in this phase. This stage of the evolution is likely to be similar to that of 90% of Eddington's solar-like stars.

In the second evolution stage, the mode identification and fitting gets more difficult and challenging. The separation between the $l = 0$ and $l = 2$ mode ridge decreases even more to a mere 2 $\mu$Hz. The tagging of each ridge could be made extremely difficult if the linewidth mode is about 1 $\mu$Hz. Nevertheless, it is possible to fit the mode pair as a single mode giving very limited information about the internal structure of the star. Mixed modes start to appear especially for $l = 1$. The $l = 1$ mode ridge is progressively destroyed and disappears completely, rendering their tagging almost impossible. The $l = 1$ modes start to appear everywhere and are even sometimes right next to the other regular p modes. Due to their mixed character, the $l = 1$ modes are likely to be long-lived modes. Due to their erratic location in the *Echelle diagram* the mixed $l = 1$ modes are bound to have mode frequencies close to the short-lived modes; in which the identification becomes even more difficult. This stage of the evolution is likely to be similar to that of the remaining solar-like stars of Eddington.

### 3.3. STELLAR ROTATION

An additional difficulty to the mode identification is the influence of the rotation upon the determination of the mode frequencies. When the small separation ($\delta_{02}, \delta_{13}$) is about 2-3 times the rotational splitting, the proper derivation of the frequencies of the $l = 0 - 2$ and $l = 1 - 3$ modes get ambiguous. It leads to small separation being negative. This ambiguity is likely to happen for solar-like stars with a rotational splitting ranging from 1 to 5 $\mu$Hz. In this case, it is required to fit the mode parameters not locally around the $l = 0 - 2$ or $l = 1 - 3$ pair but globally over the spectrum as already implemented by Jiménez et al. (2002) and Gelly et al. (2002) (See Neiner & Appourchaux in these proceedings).

### 4. HD 57006 AS AN EVOLVED STAR

The star HD 57006 is one of the candidate primary target of COROT. In the framework of the third hare-and-hound exercise of COROT Seismology working group, a 150-day long time series was generated by one of the authors (TT) with frequencies provided by another author (GB). The task of the data fitter (the 2 other authors: OM and TA) was to derive the frequencies of the detected modes.

Figure 4 shows the power spectrum of the time series. The distribution of the modes in the *Echelle diagram* in Fig 4 does not permit to take any conclusion about any

$l$ but $l$=0, in addition for higher orders it starts to be scrambled. As a matter of fact we realize *a posteriori* that the single ridge attributed to the $l = 0$ modes was mixed with the $l = 2$ modes (See Fig 3). The detected modes fall in 2 categories:

– short-lived modes ($l$ tagged or unknown $l$)
– long-lived modes (unknown $l$)

A specific strategy for each category is described hereafter.

### 4.1. SHORT-LIVED MODE DETECTION

The $l = 0$ modes were fitted as single modes using MLE. The other detected short-lived modes for which there was no possible $l$ tagging were also fitted in the same manner.

### 4.2. LONG-LIVED MODE DETECTION

As mentioned in the previous section, long-lived modes appear because of the mixed character of the modes. They can be seen in Fig 4 as sharp peaks. There are two main cases to be considered:

– long-lived mode alone
– long-lived mode embedded in short-lived mode

The first case happens at low order (low frequency below 300 $\mu$Hz). The second case happens at higher frequency (typically order 13).

**Narrow peaks alone**: If one considers a pure noise signal with a $\chi^2$ statistical distribution, the probability that the power within one bin is greater than $m$ times the mean of the noise power, $\sigma$, is:

$$\mathcal{P}_N(m) \approx Ne^{-m} \qquad (1)$$

By setting a given value for $\mathcal{P}_N(m)$, for instance 10% (which means 10% probability that a peak due to noise is above $m$), choosing a window range in our spectrum that contains $N$ bins, and estimating $\sigma$, one can derive using the equation (1) the correct value for $m$. This way, we have a statistical test for detecting the peaks that can be considered as having a low probability of being due to noise. This classical test was used by Appourchaux et al. (2000) for detecting long-lived p modes and g modes in the SOHO data.

**Narrow peaks mixed with short-lived modes**: Above 300 $\mu$Hz the peaks that we wanted to analyze are among broad modes (See Fig 4). Therefore, the application of the aforementioned test directly to the power spectrum is not very useful because it detects peaks that are part of a single broad mode. In this case we cannot assume that the detected peaks are all individual modes. Furthermore in some cases the detected peaks are very close to the broad modes; it becomes impossible to assume reliably if they are sharp modes or if they are just part of the broad mode. We
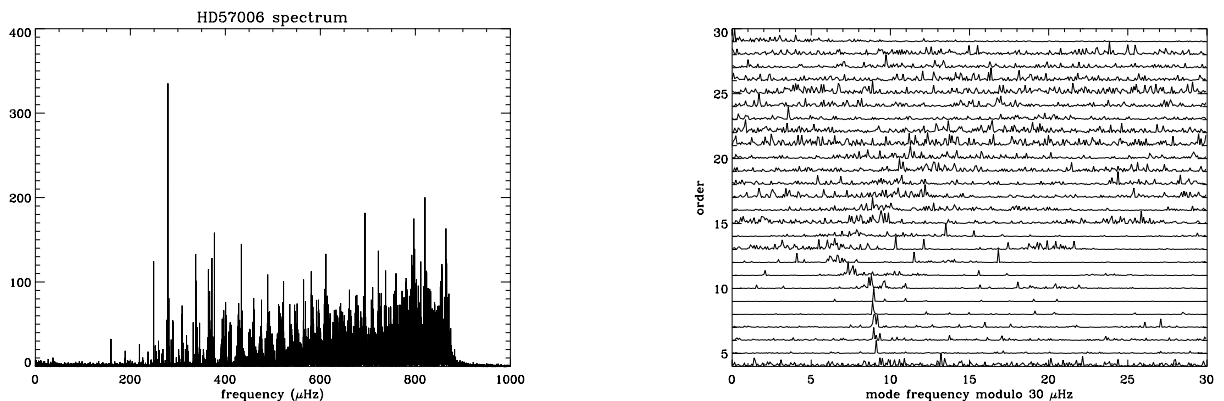
Figure 4. On the left hand side is the spectrum of the star HD57006 for model VIII, and on the right hand side the corresponding Echelle diagram with $\Delta\nu_0 = 30\mu Hz$. The many peaks visible for higher orders are due to the larger linewidth of the modes at higher frequencies.

need to find a test that can distinguish the broad modes from the sharp modes.

In order to solve this problem, we devised a technique that:

1. Fit the short-lived modes using MLE
2. Correct the spectrum for the fitted model
3. Apply the aforementioned test as if we had only narrow peaks

**Step 1**: Assuming that p modes are stochastically excited oscillator, one can derive that the power spectrum of p modes oscillator is distributed around a mean Lorentzian profiles with a $\chi^2$ probability distribution (Anderson et al., 1990; Appourchaux et al., 1998). The power spectrum of the p modes can be described as:

$$P(\nu) = M(\nu)F(\nu), \tag{2}$$

where $F(\nu)$ is a random function with a $\chi^2$ statistical distribution with 2 d.o.f, and $M(\nu)$ is the model of the fitted mode made of a single Lorentzian profile plus noise. One can fit this model to the observed power spectra using the Maximum Likelihood Estimators technique (Anderson et al., 1990; Toutain and Appourchaux, 1994); this is the classic and well-known approach used for short-lived modes.

**Step 2**: After having done the fitting, one can divide the power spectrum by the fitted profile $M'(\nu)$, one obtains:

$$P'(\nu) = \frac{P(\nu)}{M'(\nu)} \sim F(\nu) \tag{3}$$

In a first approximation $P'(\nu)$ has a $\chi^2$ statistical distribution with 2 d.o.f. This is an approximation because $M'(\nu)$ is derived from data and has also a statistical distribution that should be taken into account. We have performed a Monte-Carlo analysis confirming that indeed $P'(\nu)$ has such a statistical distribution. This way we solved the problem of the mixing between the sharp modes and the broad modes.

**Step 3**: Applying the $\chi^2$ test to HD57006 spectrum, we set $\mathcal{P}_N(m) = 10\%$, $\sigma = 1$, and a window size of 30 $\mu$Hz (corresponding to 389 bins). This last step is the same as for the long-lived modes alone.

For each window we use the stepped approach. The result of which can be seen in Fig. 5.

The comparison with the original frequencies[6] gave that only about 1 peak was misidentified over the band $200\mu$Hz-$500\mu$Hz. On average we should statistically have had 1 peak ($\pm$ 1) due to noise. It validates the approach taken for detecting long-lived modes either singled put or embedded in short-lived modes.

### 4.3. $l$ TAGGING OF THE FREQUENCIES

The $l$ tagging of the frequencies of the modes could not be derived from the Echelle diagram apart for the $l = 0$ modes. As a matter of fact, due to the width of these p modes, we may have fitted the mean location of the $l = 0 - 2$ ridge.

The $l$ tagging for the non-$l = 0$ p modes would need to be derived from the splitting. After having derived the frequencies of the modes for the 2 categories, we performed a correlation analysis on the extracted frequencies for getting the signature of a possible splitting. Since we did not find any splitting signature, we could not tag further the identified modes. At least we were able to derive the frequency of the modes for the 2 categories as explained above.

Our inability to properly tag the frequencies of the modes has serious consequences for the usefulness of such a star for understanding its internal structure. We could imagine a scheme where we could search for the stellar model for which mode frequencies would match the fitted mode frequencies. Given the erratic behaviour of the $l = 1$ mode frequencies, this exercise could be 'easily' achieved

---

[6] Comparison performed a posteriori
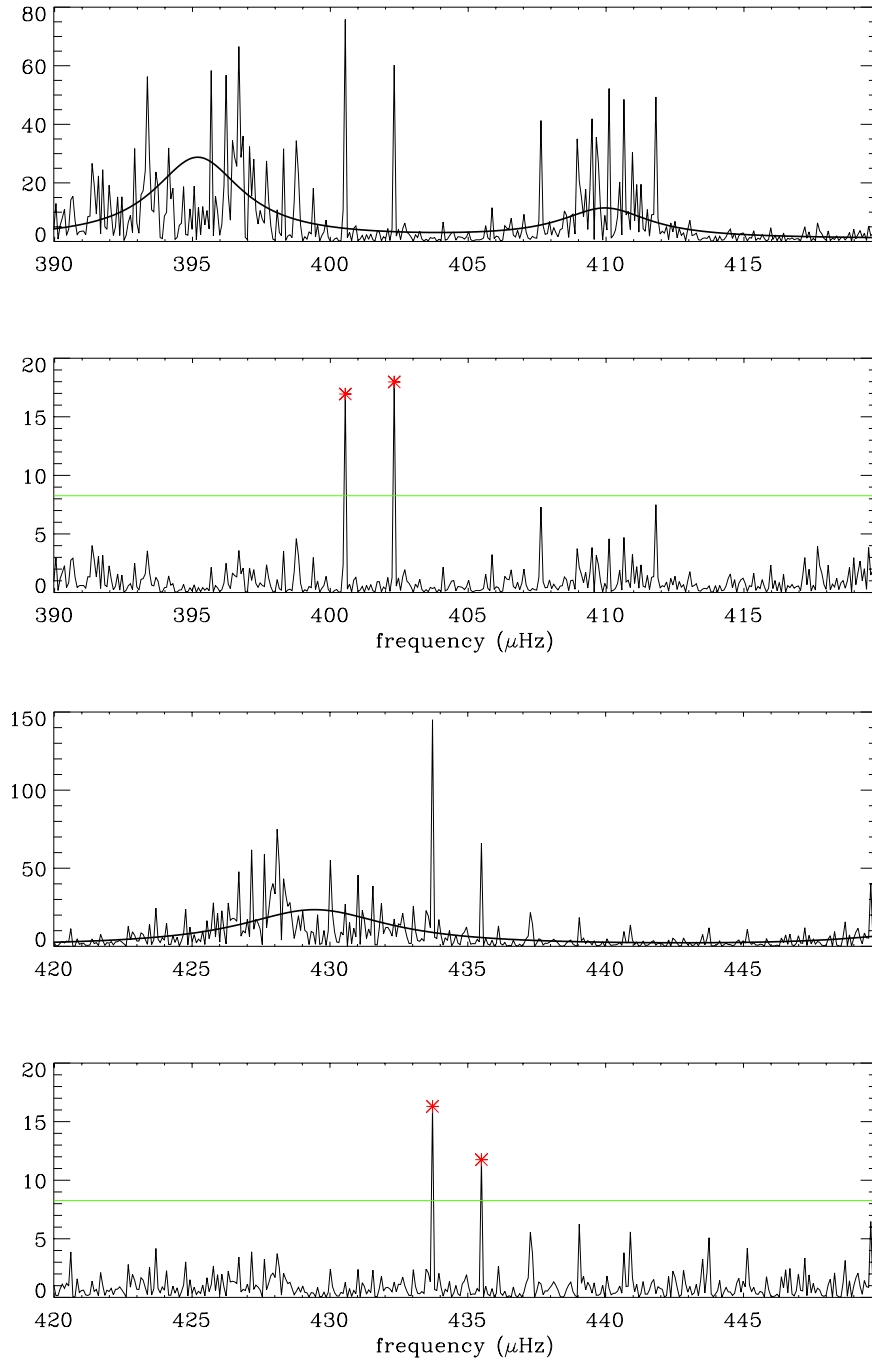
*Figure 5. Result of the test for two different ranges of frequencies. The fitting is presented on the top of the figure, and the power spectrum divided by the fitted model, as well as the bins above the 10% probability level, are presented on the bottom of the figure.*

for comparing input frequencies and output frequencies of a stellar model coming out of a single routine (e.g. the CESAM code). This is only of pure academic interests as the stars do not follow the CESAM code...

The only way out would be to use color information for tagging the frequencies of the modes. This method is not used for solar-like stars but is very useful for say Cepheids. It will involve proper computing of the radiative transfer that is likely not to be easy. Nevertheless, a simple approximation to that problem is well known (Toutain and Gouttebroze, 1993). This additional color information is likely to be useful for COROT, and should become a must for Eddington.

## 5. Conclusion

In this paper, we concentrated mainly on the fitting challenges that the COROT and Eddington missions are going to face. For each stage of the stellar evolution there are two challenges to be solved:

- **Challenge I**: power spectra fitting for solar-like stars in their hydrogen burning phase
- **Challenge II**: power spectra fitting for solar-like stars in their hydrogen-shell burning phase

**Challenge I** provides no major problem for fitting most of star spectra; this can even be automated.

**Challenge II** is mainly related to properly identify the degree of the modes. This challenge is much more difficult and could cost a lot of time as it is only solvable by hand at the time of writing. For this purpose, we devised an automated method for identifying long-lived modes embedded in short-lived modes. So we have been able to solve part of **Challenge II**. The bulk of this challenge may only be solved by covering a given evolutionary track with stars of similar masses; thereby trying to follow with different stars how the mixed modes could appear. Additional information related to color could be brought in for the degree identification. This could make the automation feasible. The automation of the mode identification and fitting for **Challenge II** is still in its infancy but 2 research tracks have been laid out. They shall be tested with COROT and perfected for Eddington.

### References

Anderson, E. R., J. Duvall, T. L., and S. M. Jefferies: 1990. *ApJ* **364**, 699–705.

Appourchaux, T.: 2003. *Ap&SS* **284**, 109–119.

Appourchaux, T., C. Fröhlich, B. Andersen, G. Berthomieu, W. Chaplin, Y. Elsworth, W. Finsterle, D. Gough, J. T. Hoeksema, G. Isaak, A. Kosovichev, J. Provost, P. Scherrer, T. Sekii, and T. Toutain: 2000. *ApJ* **538**, 401.

Appourchaux, T., L. Gizon, and M. C. Rabello-Soares: 1998. *A&A Sup. Series* **132**, 107.

Gelly, B., G. Grec, and E. Fossat: 1986. *A&A* **164**, 383–394.

Gelly, B., M. Lazrek, G. Grec, A. Ayad, F. X. Schmider, C. Renaud, D. Salabert, and E. Fossat: 2002. *A&A* **394**, 285–297.

Jiménez, A., T. Roca Cortés, and S. J. Jiménez-Reyes: 2002. *Solar Physics* **209**, 247–263.

Tassoul, M.: 1980. *ApJ Sup. Series* **43**, 469.

Toutain, T. and T. Appourchaux: 1994. *A&A* **289**, 649.

Toutain, T. and P. Gouttebroze: 1993. *A&A* **268**, 309.

# HD43318

# Characteristics of input model HD43318
## Structure and frequencies

G. Berthomieu

Global constraints on the input model

$$3.79 < log(T_{eff}) < 3.80 \quad \Longrightarrow \quad T_{eff} \sim 6280 \pm 100^0 K$$

$$2.75 < Mbol < 2.95$$

$$[Fe/H] = -0.18 \pm 0.1$$

With Mbol$_\odot$= 4.75 and $(Z/X)_\odot = 0.0245$

$$0.72 < log(L/L_\odot) < 0.8$$

$$0.01656 < Z/X < 0.02038$$

Rotation

$$V sini = 6 \pm 4km/s$$

If we take  $i = 45^0$  and a mean radius $2.210^{11}$ then

$$\nu_{rot} =\sim (1.825 \pm 0.3)\mu HZ$$

# Input model of HD43318

Properties of the input model:

M/Msol= 1.45

R/Rsol= 2.05

L/Lsol= 5.63

log(L/Lsol)= 0.7505

Age (My ) = 2275.6

Teff= 6212.09

$Z_s = 0.01493$
$X_s = 0.796$
$Y_s = 0.1886$
$Z_s/X_s = 0.01875$

$X_c = 0.109$

$T_c = 2.2375 10^7$

$x_{zcext} = 0.853$
$\tau_{zcext} = 3877.8$ s
$x_{zGamma} = 0.978$
$\tau_{zGamma} = 1614.7$ s
$x_{zccore} = 0.0514$

$\alpha = 1.6$
overshoot $\zeta = 0.05$

# Comparison of HD43318 frequencies

Frequencies extracted by P. Boumier and J. Lochard from temporal series computed by T. Appourchaux:

## P Modes (microHz) nu0 Err0 nu1 Err1 nu2 Err2 nu3 Err3

| nu0 | Err0 | nu1 | Err1 | nu2 | Err2 | nu3 | Err3 |
|---|---|---|---|---|---|---|---|
| 617.45 | 0.03 | 641.29 | 0.04 | 613.02 | 0.01 | 633.47 | 0.05 |
| 670.95 | 0.03 | 694.43 | 0.04 | 666.74 | 0.03 | 687.18 | 0.03 |
| 724.64 | 0.04 | 749.02 | 0.05 | 720.43 | 0.03 | 741.85 | 0.25 |
| 780.22 | 0.06 | 805.00 | 0.04 | 775.98 | 0.05 | 797.84 | 0.10 |
| 836.50 | 0.07 | 861.30 | 0.06 | 832.28 | 0.07 | 854.59 | 0.10 |
| 892.77 | 0.06 | 917.18 | 0.07 | 888.56 | 0.07 | 910.50 | 0.11 |
| 948.16 | 0.08 | 972.63 | 0.10 | 944.02 | 0.10 | 966.44 | 0.08 |
| 1004.13 | 0.10 | 1028.77 | 0.15 | 1000.10 | 0.10 | 1022.65 | 0.31 |
| 1060.95 | 0.11 | 1085.87 | 0.12 | 1056.48 | 0.12 | 1079.26 | 0.17 |
| 1118.09 | 0.13 | 1143.44 | 0.12 | 1114.05 | 0.15 | 1137.47 | 0.39 |
| 1175.62 | 0.20 | 1200.93 | 0.16 | 1171.55 | 0.16 | 1194.69 | 0.35 |
| 1233.74 | 0.54 | 1258.44 | 0.17 | 1229.08 | 0.30 | 1252.27 | 0.08 |
| 1290.62 | 0.74 | 1316.13 | 0.17 | 1287.03 | 0.45 | 1310.87 | 0.23 |
| 1346.87 | 0.45 | 1374.11 | 0.19 | 1343.53 | 0.32 | 1367.89 | 0.45 |
| 1405.45 | 1.17 | 1431.70 | 0.25 | 1402.03 | 1.22 | 1425.07 | 0.28 |
| 1464.04 | 0.39 | 1489.60 | 0.40 | 1460.18 | 0.72 | 1483.86 | 0.91 |
| 1522.87 | 0.97 | 1547.39 | 0.40 | 1518.76 | 0.82 | 1535.21 | 0.23 |

## Low Frequency modes (microHz)

| | | | | | | | |
|---|---|---|---|---|---|---|---|
| 474.77 | 478.86 | 501.16 | 506.94 | 514.66 | 521.68 | 522.53 | 531.56 |
| 558.26 | 562.89 | 563.97 | 586.96 | | | | |

with same error 0.08

# Comparison of HD43318 frequencies
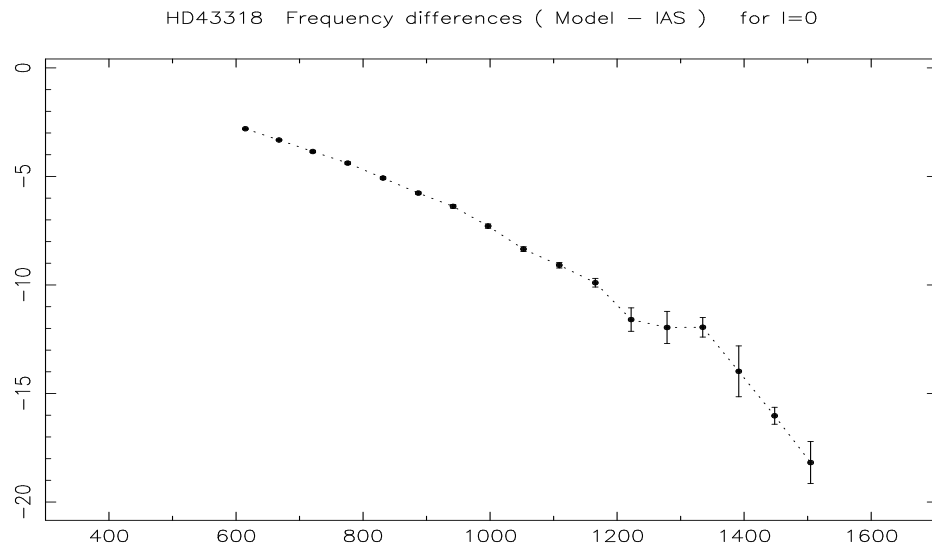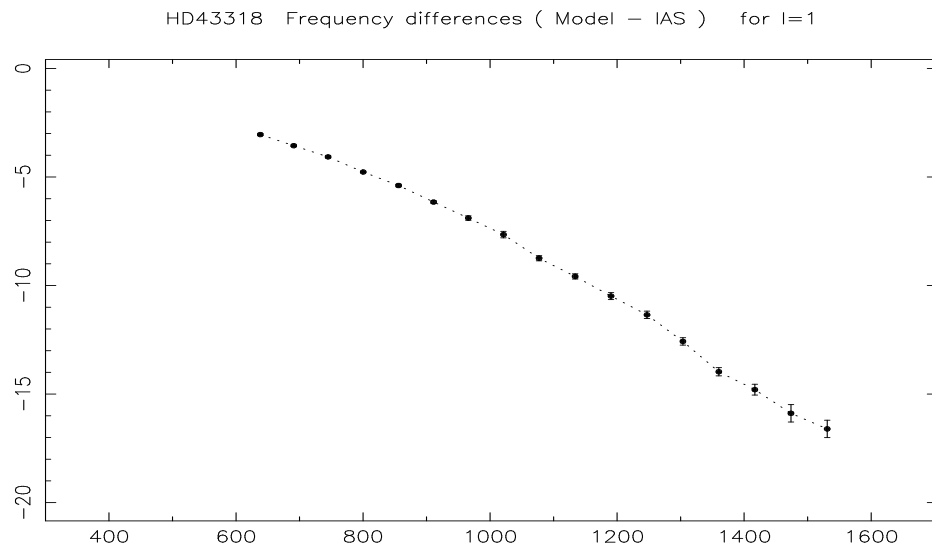
## Modes l=0

HD43318   Frequency differences ( Model − IAS )    for l=0



## Modes l=1

HD43318   Frequency differences ( Model − IAS )    for l=1

# Comparison of HD43318 frequencies

## Modes l=2

HD43318   Frequency differences ( Model − IAS )    for l=2



## Modes l=3

HD43318   Frequency differences ( Model − IAS )    for l=3

No overshooting

M=1.2,X=0.70,Z=0.011
M=1.2,X=0.70,Z=0.012
M=1.2,X=0.72,Z=0.011

overshooting = 0.2

M=1.2,X=0.70,Z=0.011
M=1.3,X=0.70,Z=0.011
M=1.3,X=0.70,Z=0.012
M=1.3,X=0.70,Z=0.013
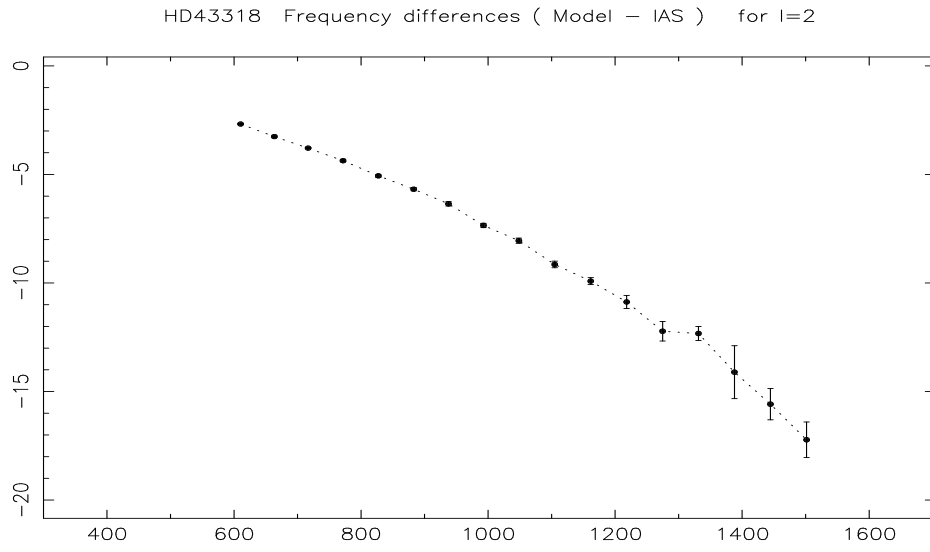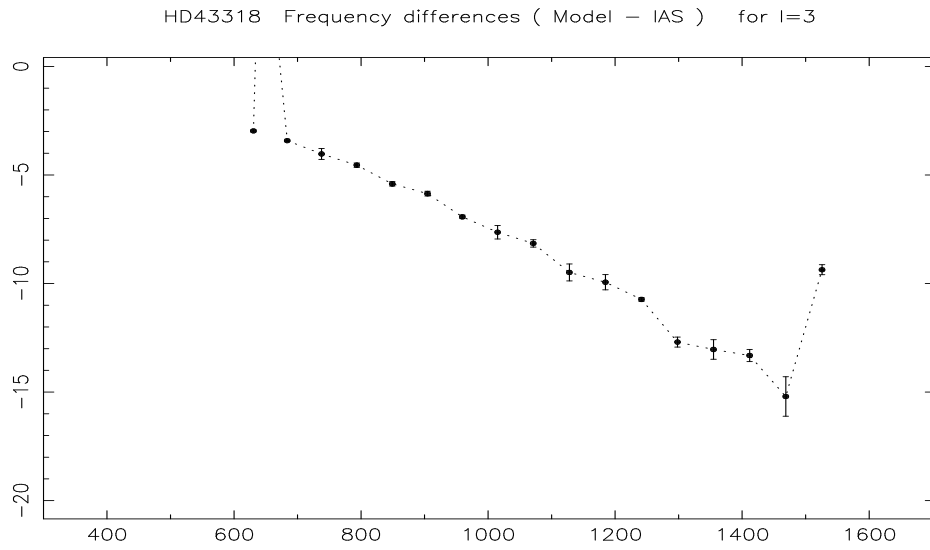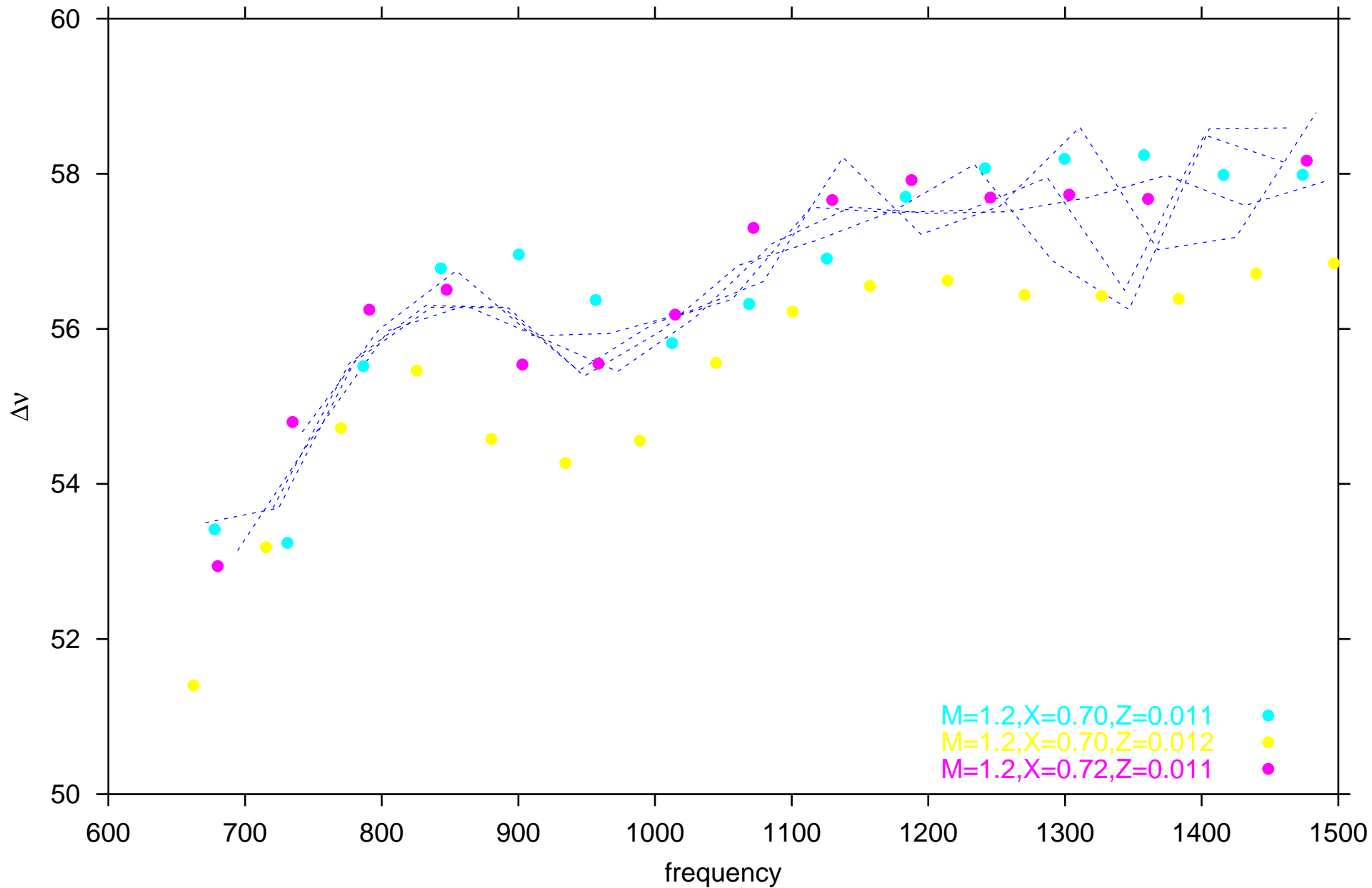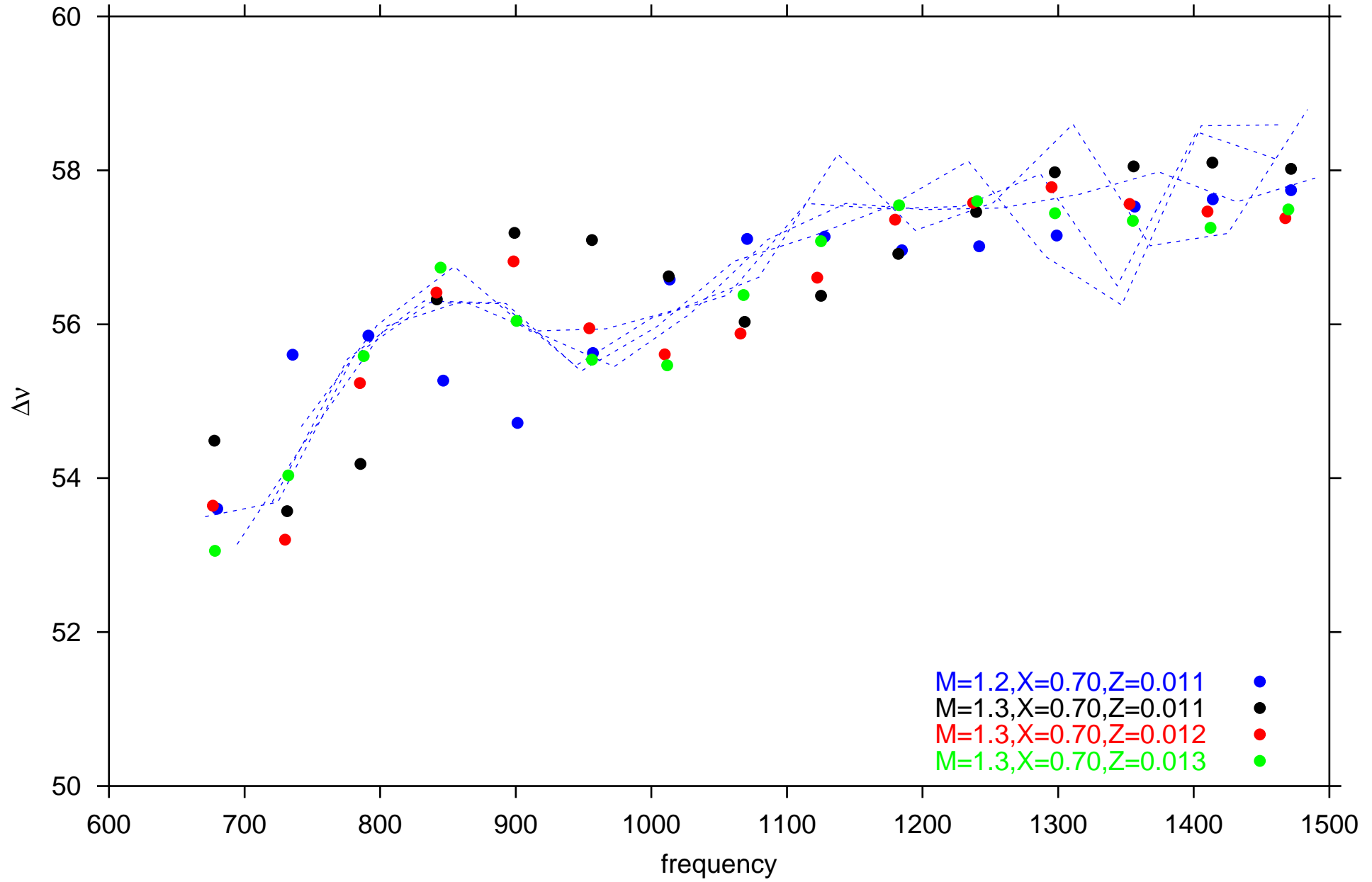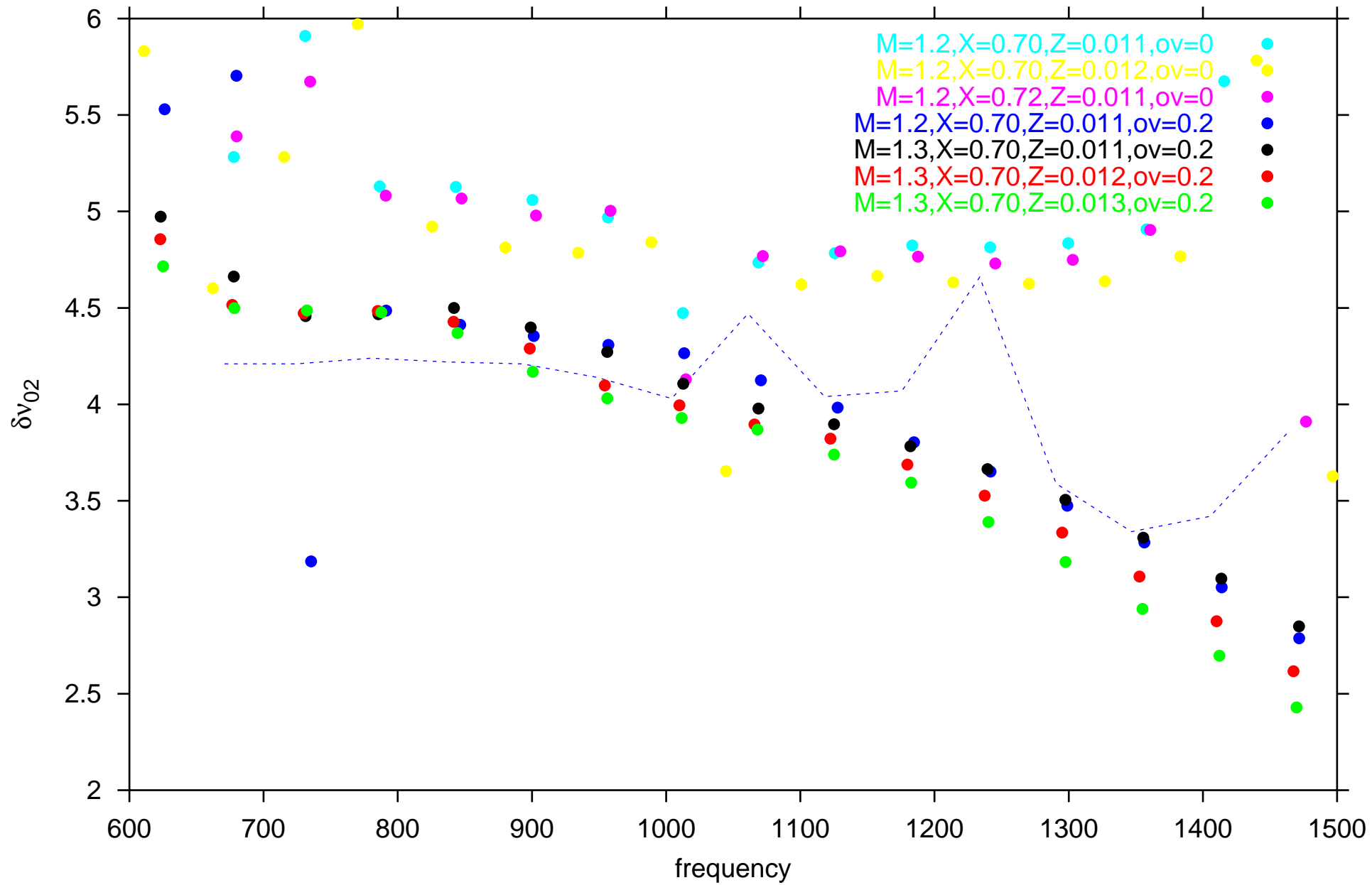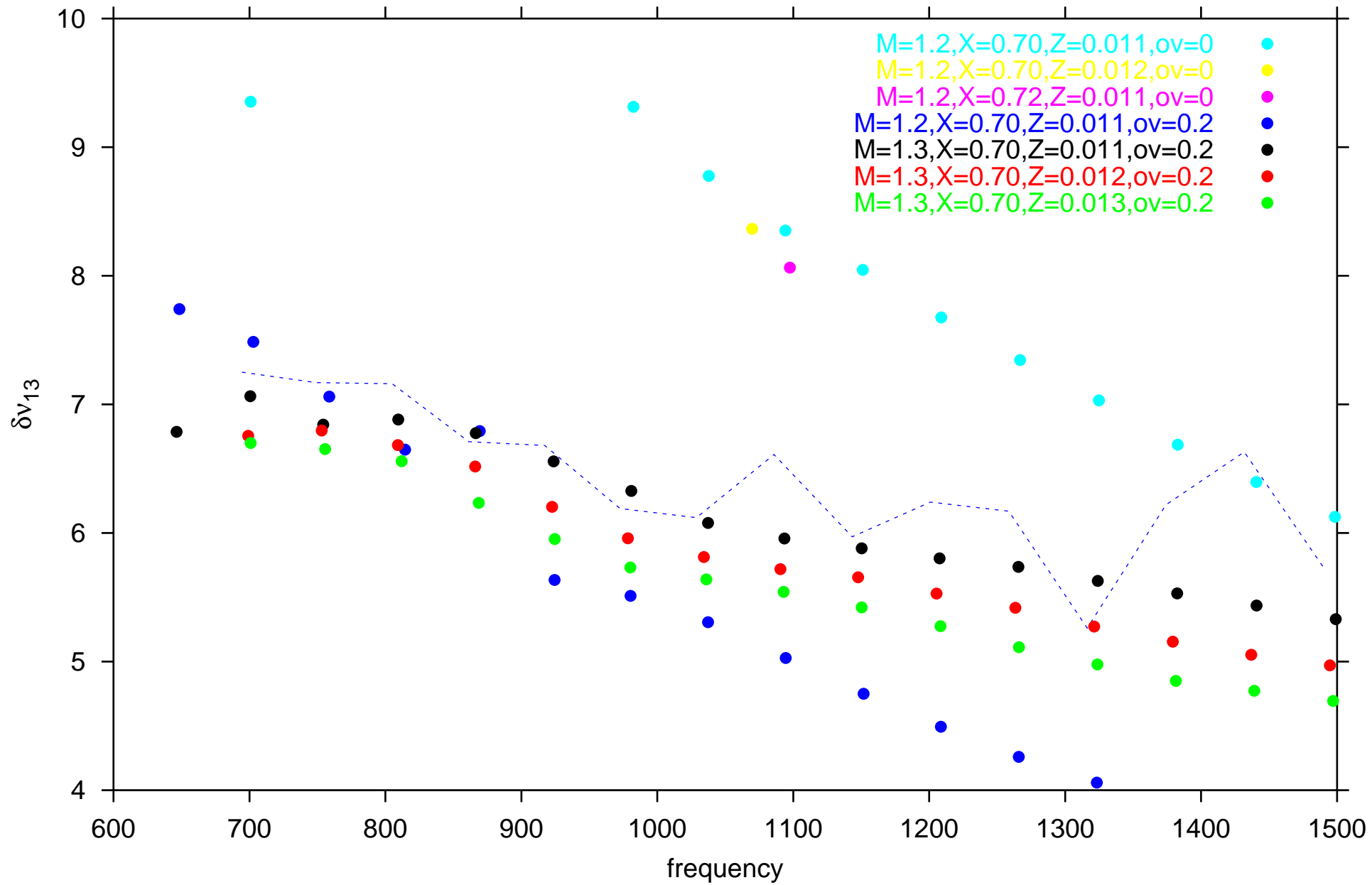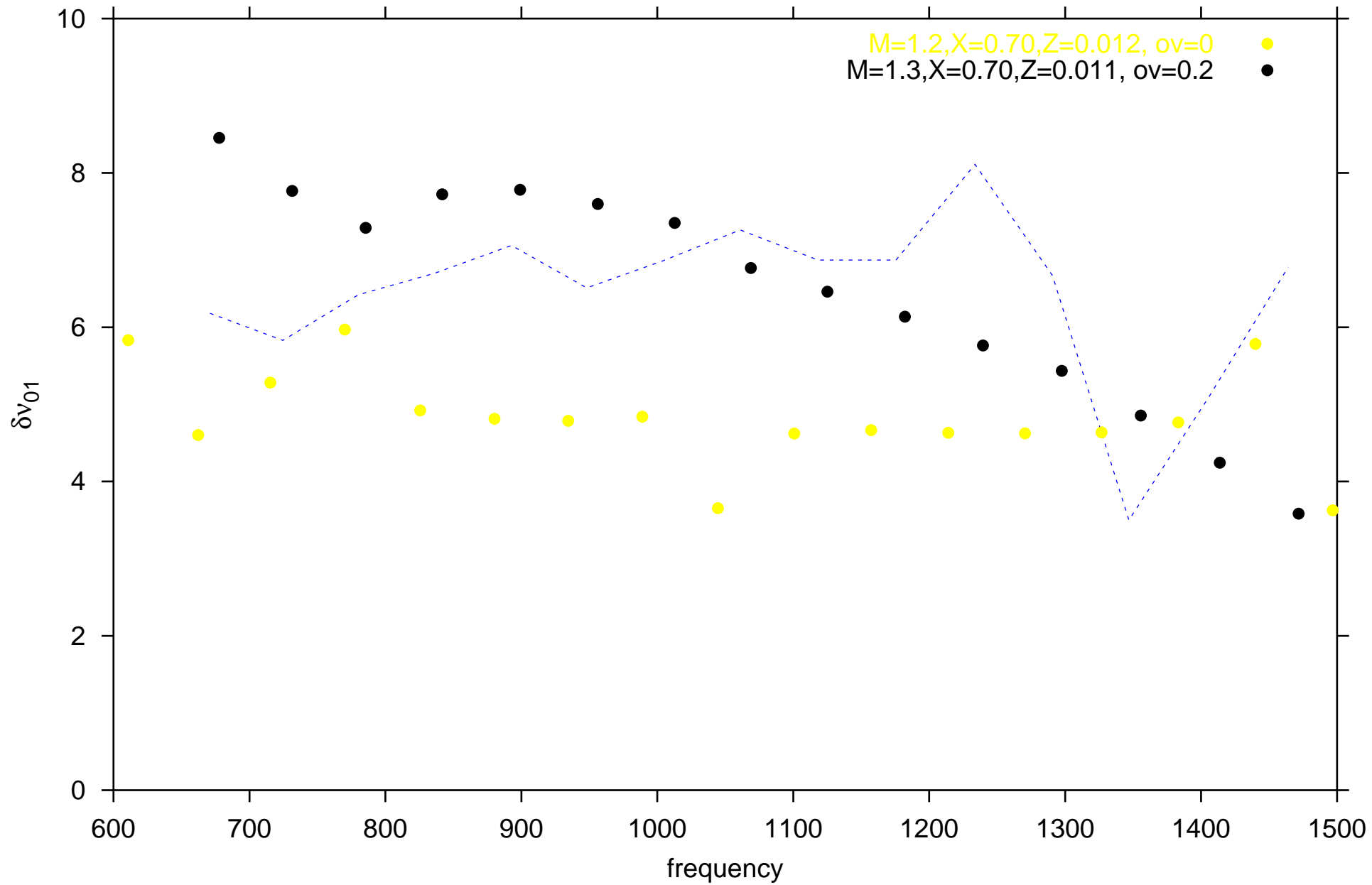
# STAR #4: HD 43318

$T_{eff} = 6280\pm 100$ K $\rightarrow logT_{eff}$=[3.791,3.805]
$M_{bol}$=[2.75,2.95] $\rightarrow \log L/L_\odot$=[0.72,0.80]
Convention: $M_{bol,\odot} = 4.75$
[Fe/H]=-0.18 $\pm$ 0.10 $\rightarrow$ Z/X=[0.0129,0.0204]
v sini= 6 $\pm$ 4 km/s
Frequency analysis $\rightarrow$ l=0,1,2,3

---

Models calculated:
M $\sim$ 1.2 to 1.4 $M_\odot$
X=0.70 to 0.72
Z=0.011 to 0.013
$\alpha_{ov} = 0$ or 0.2
No diffusion

---

CONCLUSION:
Cannot fit $\delta\nu_{02}$ and especially $\delta\nu_{13}$ without
overshooting.

Best model so far:
M=1.3 $M_\odot$
Z=0.013
X=0.70
$\alpha_{ov} = 0.2$

# HD 43318 — Seismic Interpretation

JEREMIE LOCHARD

*Observatoire de Paris-Meudon, France*

Collaborators: Anwesh Mazumdar, E. Michel and M-J. Goupil

We report on the seismic interpretation of the frequencies of the star HD 43318.

## Global Parameters of HD 43318

- $T_{eff} = 6280 \pm 100$ K

- $M_{bol} = 2.85 \pm 0.10$

- $[Fe/H] = -0.18 \pm 0.10$

- $vsini = 6 \pm 4$ km/s


- Original model produced by Gabrielle Berthomieu

- Time series produced by Thierry Appourchaux

- Frequencies extracted by Patrick Boumier & Jeremie Lochard

# Estimation of acoustic depths of base of CZ and HeII ionisation zone

Discontinuities in sound speed derivatives at the HeII ionisation zone and the base of the convective envelope give rise to oscillations in the frequencies.

We fit a function of the form

$$\delta^2\nu(n, \ell) = \left(a_0 + \frac{a_1}{\nu_{n,\ell}} + \frac{a_2}{\nu_{n,\ell}^2}\right)\sin(4\,\pi\nu_{n,\ell}\,\tau_{CZ} + \phi_{CZ})$$

$$+ \left(b_0 + \frac{b_1}{\nu_{n,\ell}} + \frac{b_2}{\nu_{n,\ell}^2}\right)\sin(4\,\pi\nu_{n,\ell}\,\tau_{HeII} + \phi_{HeII}).$$

to the second differences of the data, taking into account the errors.

# Estimation of acoustic depths of base of CZ and HeII ionisation zone
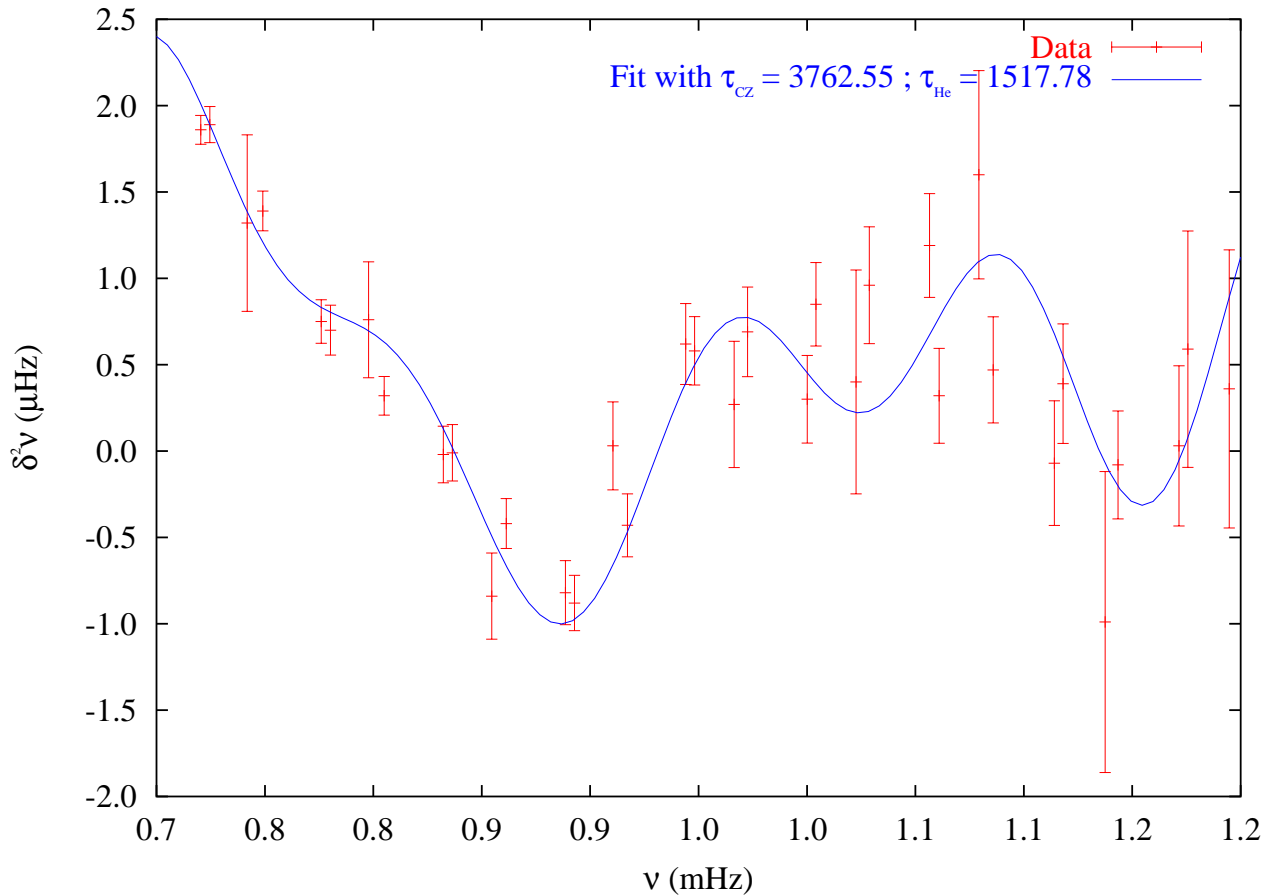


The fit provides us with values for the acoustic depths of

- the base of the convective envelope: $\tau_{CZ} = 3763 \pm 134$ s

- the HeII ionisation zone: $\tau_{HeII} = 1518 \pm 98$ s

These estimates help to search the closest model.

# Stellar Models

Evolutionary tracks were computed with CESAM using

- CEFF equation of state

- OPAL opacities

- NACRE nuclear reaction rates

- MLT convection

- Eddington atmosphere

- No diffusion

Frequencies were computed with ADIPLS.

# Variable parameters of models

- Core overshoot (in $H_P$)     :    $d_{ov}$   :    0    —    0.2

- Mixing length (in $H_P$)     :    $\alpha$   :    1.6   —   1.8

- Metallicity                 : $[Fe/H]$ :   $-0.28$  —  $-0.08$

- Initial Helium abundance   :    $Y_0$   :    0.25   —   0.28

All CESAM models are computed with a "high" precision parameter to avoid irregular features at convective zone boundaries
— more accurate models, but very time-consuming!!

Technique

- For a particular combination of these parameters we vary the mass of the model to check for overlap between main sequence tracks and the global parameters of HD 43318 on the HR diagram.

- Compare large and small separations of the "data" with the computed values to find the closest possible model.

# Some preliminary inferences from global parameters

Both MS and post-MS models are possible at the same point within the
HD 43318 box on the HR diagram.
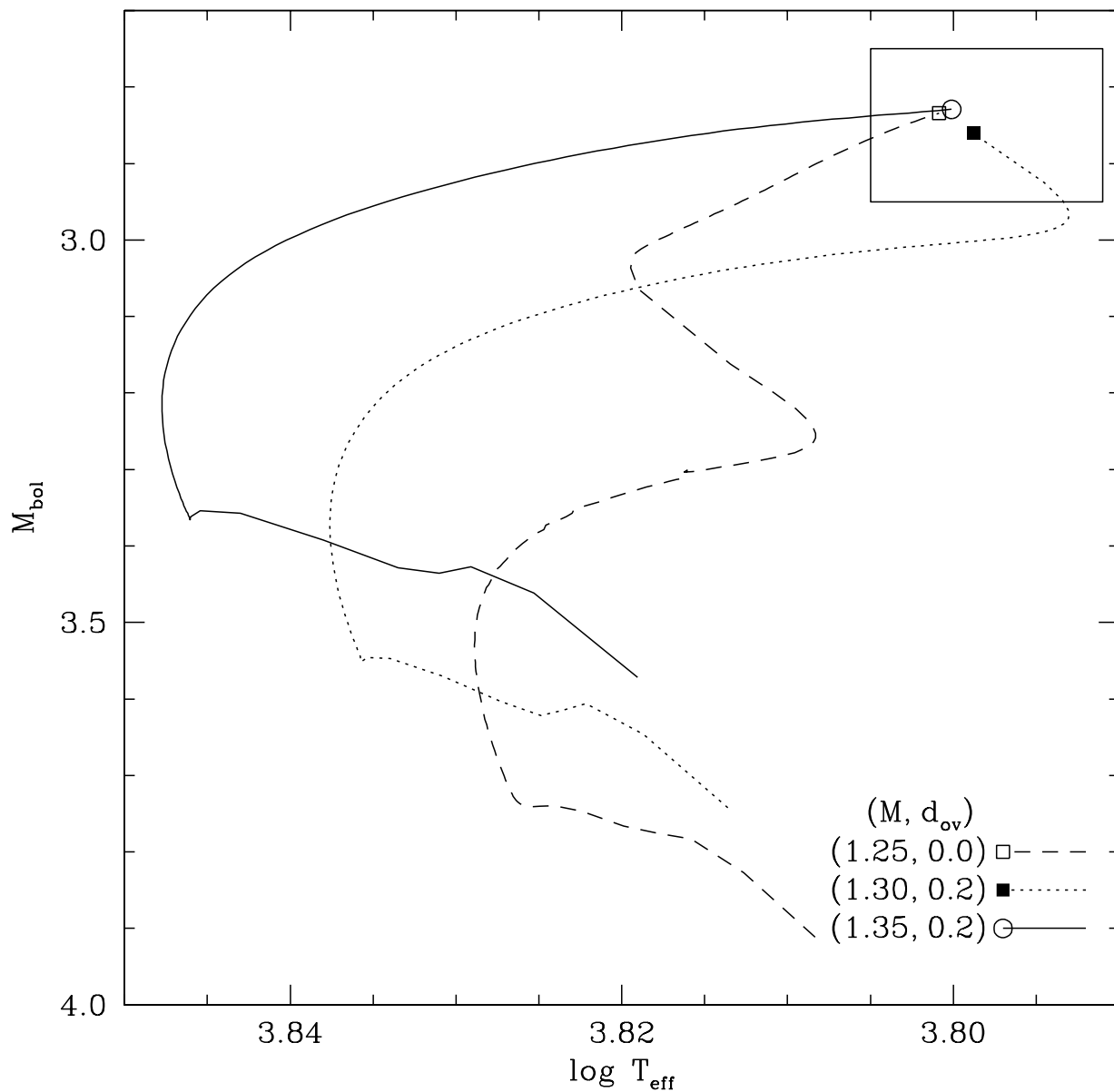
# Some preliminary inferences from global parameters

- Main sequence models are permissible only for

  - Moderate to high overshoot $(0.1\text{--}0.2\ H_P)$

  - Low value of $\alpha$

  - Higher metallicity $(\text{[Fe/H]} = -0.08 \text{ to } -0.23)$

- Near-end-MS models are possible for

  - Moderate overshoot

- Main sequence models are excluded for

  - Low or zero overshoot

  - Lower metallicity

# Table showing overlap of Main Sequence tracks and HD 43318 parameters

| Parameters | | $d_{ov}= 0.0$ | | $d_{ov}= 0.1$ | | $d_{ov}= 0.2$ | |
| --- | --- | --- | --- | --- | --- | --- | --- |
| [Fe/H] | $Y_0$ | $\alpha = 1.6$ | $\alpha = 1.8$ | $\alpha = 1.6$ | $\alpha = 1.8$ | $\alpha = 1.6$ | $\alpha = 1.8$ |
| $-0.08$ | 0.28 | (no MS) | (no MS) | 1.35 — 1.41 | 1.35 — 1.41 | 1.35 — 1.42 | 1.34 — 1.40 |
|  | 0.27 | (no MS) | (no MS) | 1.37 — 1.43 | 1.37 — 1.43 | 1.35 — 1.42 | 1.35 — 1.41 |
|  | 0.26 | (no MS) | (no MS) | 1.39 — 1.45 | 1.39 — 1.44 | 1.35 — 1.42 | 1.36 — 1.42 |
| $-0.18$ | 0.27 | (no MS) | (no MS) | 1.32 — 1.38 | (no MS) | 1.31 — 1.36 | 1.30 — 1.36 |
|  | 0.26 | (no MS) | (no MS) | 1.34 — 1.40 | (no MS) | 1.32 — 1.37 | 1.32 — 1.37 |
|  | 0.25 | (no MS) | (no MS) | 1.36 — 1.42 | (no MS) | 1.35 — 1.40 | 1.35 — 1.40 |
| $-0.28$ | 0.27 | (no MS) | (no MS) | (no MS) | (no MS) | 1.27 — 1.32 | 1.27 — 1.32 |
|  | 0.26 | (no MS) | (no MS) | (no MS) | (no MS) | 1.28 — 1.33 | 1.28 — 1.33 |
|  | 0.25 | (no MS) | (no MS) | (no MS) | (no MS) | 1.30 — 1.35 | 1.30 — 1.34 |

(red bar)    No Main Sequence stars within HD 43318 box

$M_1 - M_2$ (green background, green text)    Main Sequence stars of mass between $M_1$ and $M_2$ cover HD 43318 box partially

$M_1 - M_2$ (green background, red text)    Main Sequence stars of mass between $M_1$ and $M_2$ fully traverse HD 43318 box

# Large Separations

$$\Delta_{n\ell} = \nu_{n+1,\ell} - \nu_{n,\ell} \qquad \ell = 0, 1, 2, 3$$
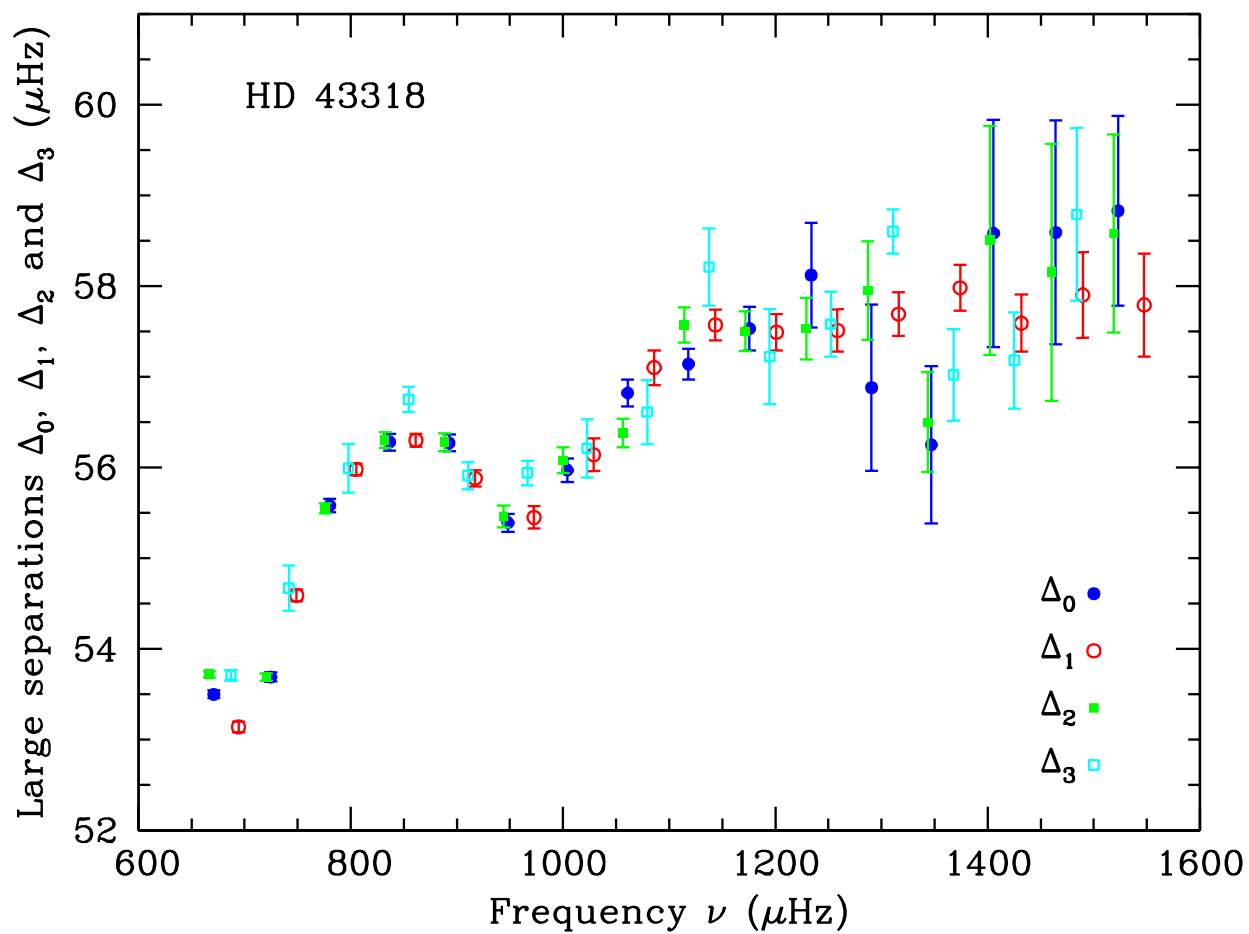
# Small Separations
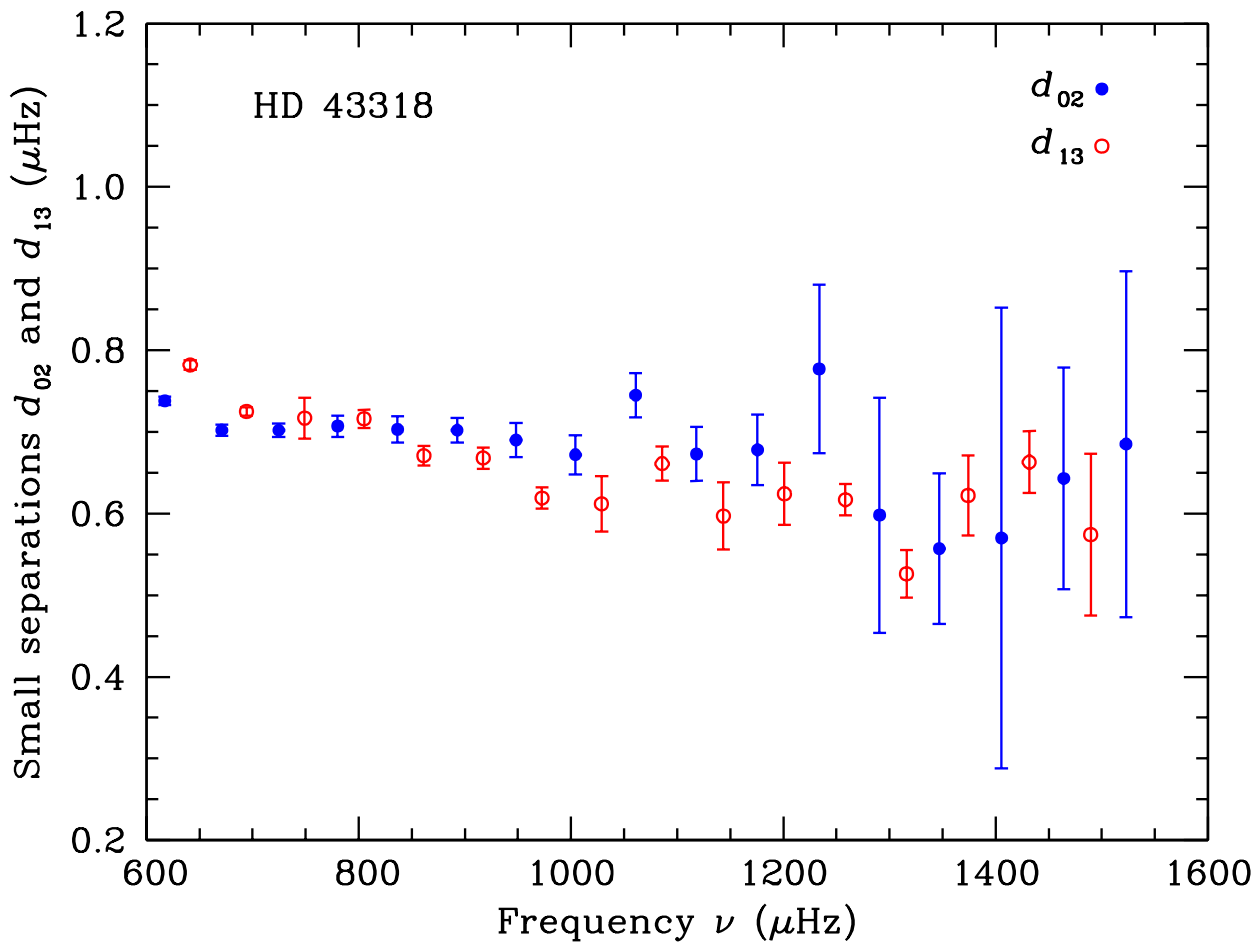
- Between $\ell = 0,\ 2$ modes and $\ell = 1,\ 3$ modes:

$$d_{02} = [\nu_{n,0} - \nu_{n-1,2}]/6$$

$$d_{13} = [\nu_{n,1} - \nu_{n-1,3}]/10$$

# Small Separations
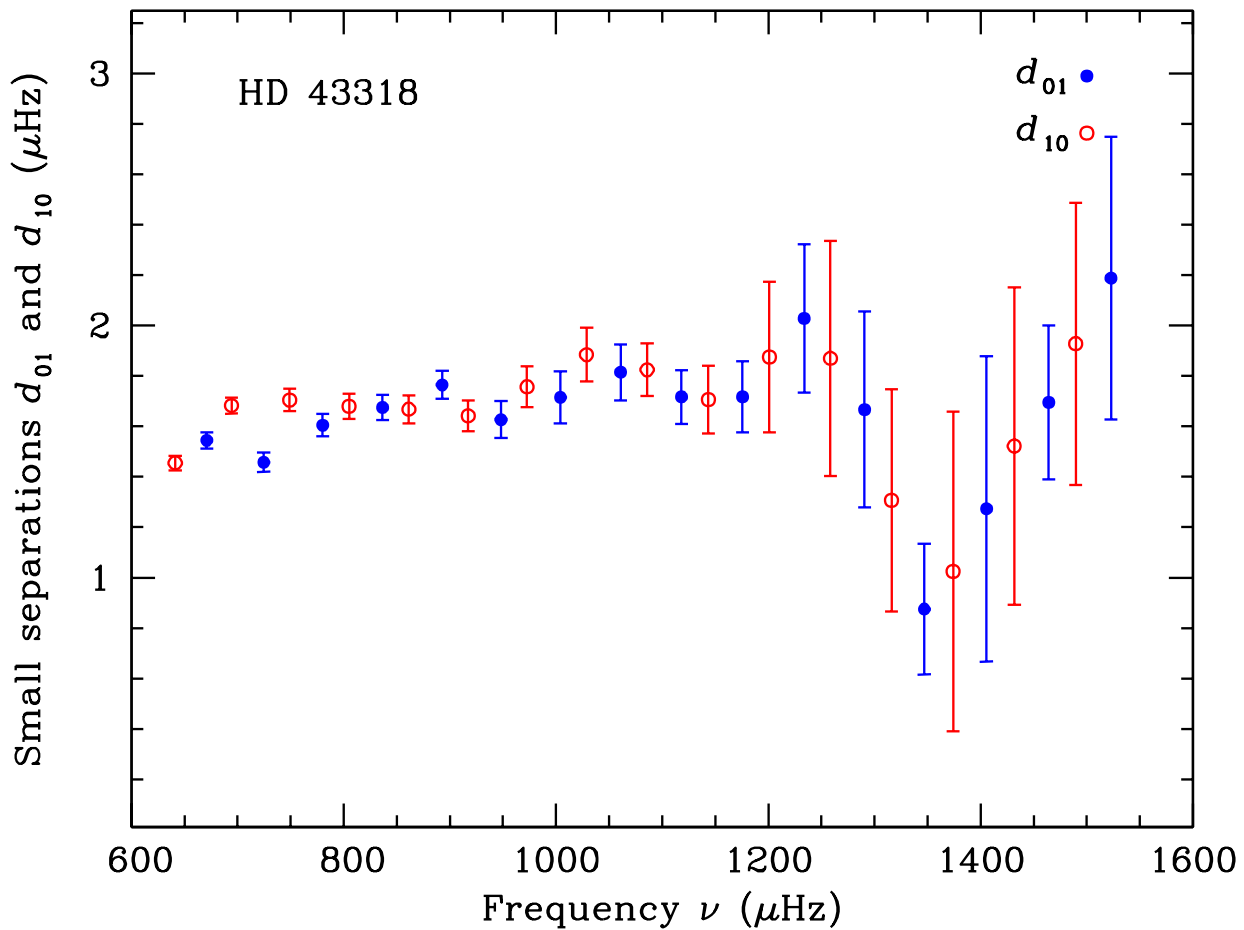
- Between $\ell = 0,\ 1$ modes:

$$d_{01} = \quad [\nu_{n,0} - (\nu_{n,1} + \nu_{n-1,1})/2]/2$$

$$d_{10} = -[\nu_{n,1} + (\nu_{n,0} + \nu_{n+1,0})/2]/2$$

# Approaching the closest model

- Average value of large separation provides initial estimate of the mean density of the model:

$$\bar{\rho}/\bar{\rho}_\odot = 0.17$$

- Explore the sensitivity of different features of the large and small separations to the six model parameters:

$$M, Age, Y, [Fe/H], d_{ov}, \alpha$$

- Simultaneous matching of large and small separations by tuning these parameters is desirable.

- Several "best case" scenarios are identified, and a comparison of the deviations of the large and small separations of the models from the data is made to select the closest model.

# Closest Model

Our closest model for HD 43318 corresponds to

- $M/M_\odot = 1.38$

- $X_c = 0.18$

- $[Fe/H] = -0.08$

- $Y = 0.26$

- $d_{ov} = 0.15$

- $\alpha = 1.6$

Values for

- $\bar{\rho}/\bar{\rho}_\odot = 0.1713$

- $\tau_{CZ} = 3763$ s

- $\tau_{HeII} = 1471$ s

# Closest Model
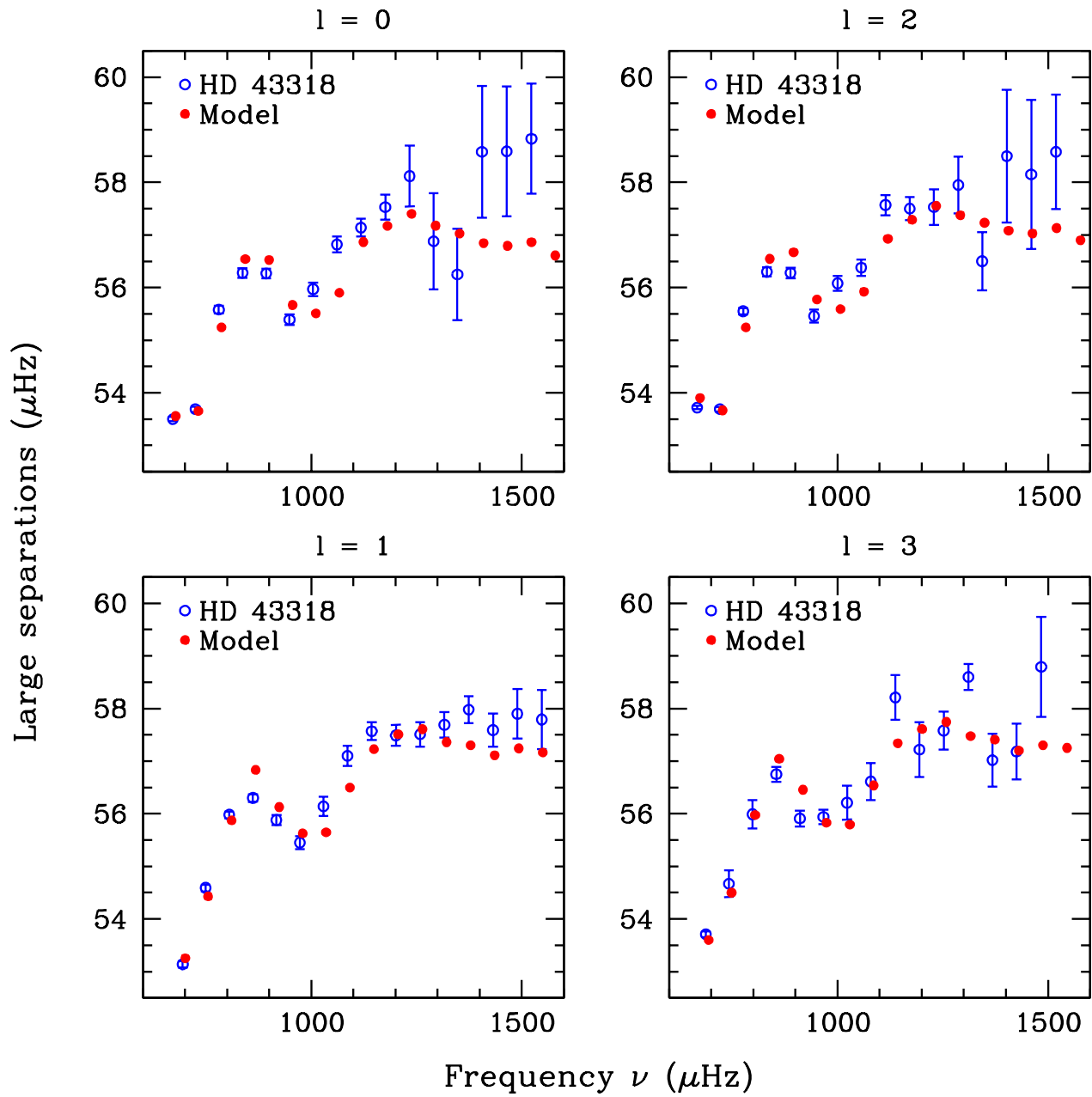
# Closest Model
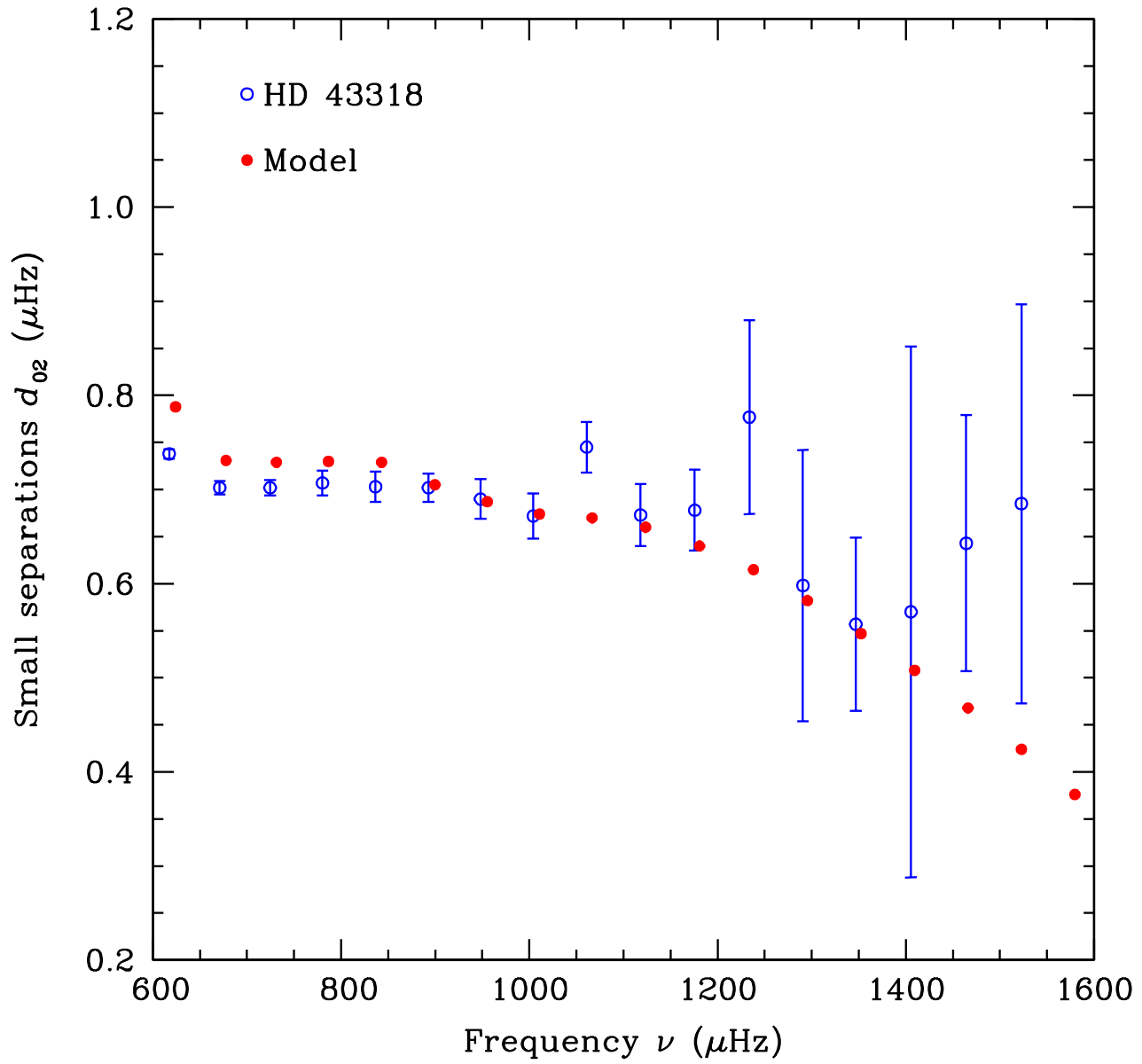
# Closest Model
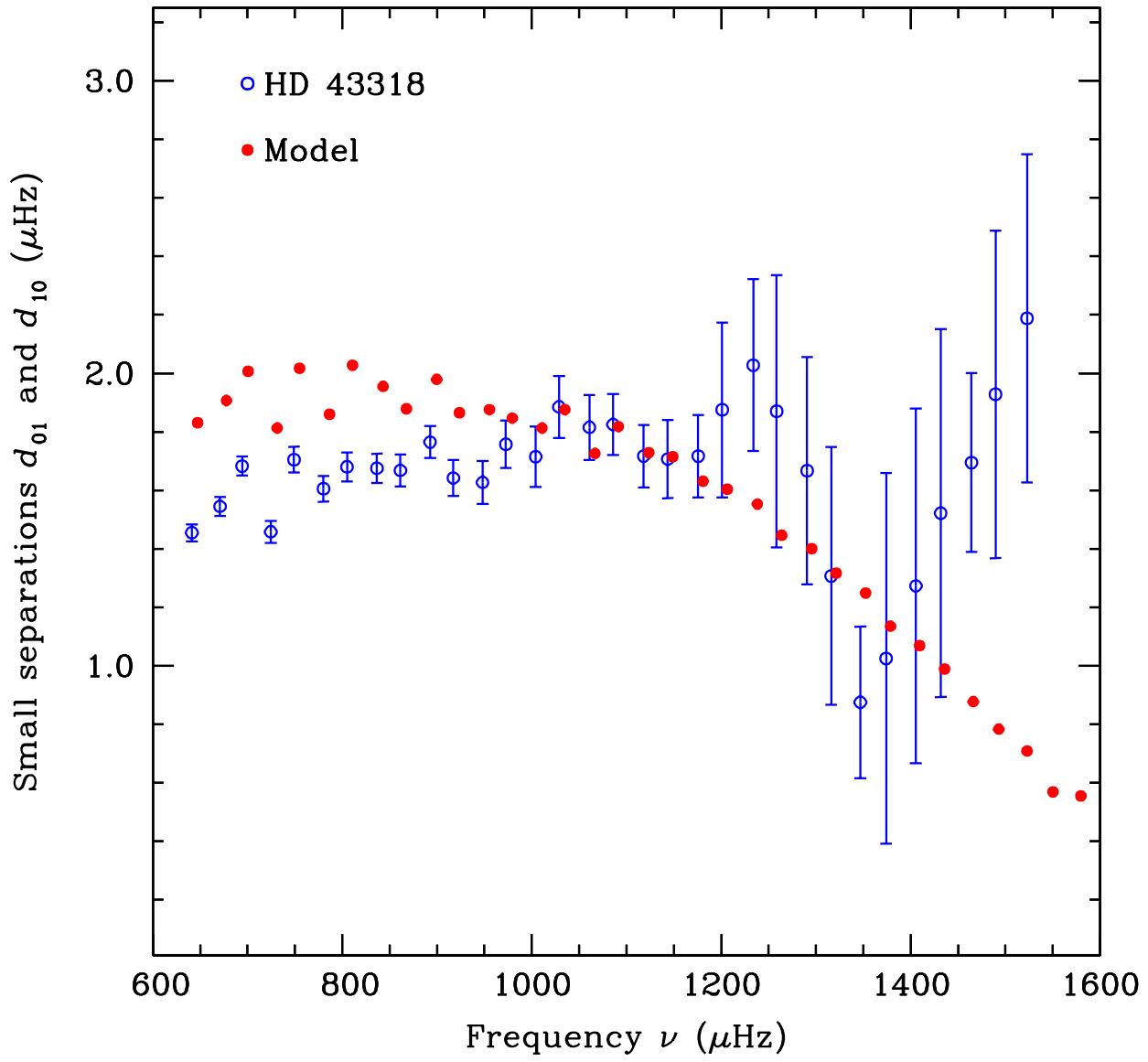
# Conclusion

We were able to:

- get an estimate of $\bar{\rho}$ through $\Delta_{n\ell}$

- tune $\mathrm{d_{ov}}$ and $[Fe/H]$ to approach $d_{02}$

We were not able to:

- reproduce the pattern of large and small separations at all frequencies

- retrieve the behaviour of $d_{01}$ and $d_{10}$

# HD45067

# BCZ extraction: used method

- Sound-speed sudden variation (located at an acoustic depth $\tau_d$) leads to oscillations in seismic observable parameters as

$$\propto \sin(2\tau_d\omega + \varphi)$$

- These oscillations can be found directly in the frequencies (Monteiro et al. 1994, 2000), large or second difference ($\Delta\nu$ & $\delta_2\nu$) (Gough 1990);

- The oscillation corresponding to the Base of the Convective Zone (BCZ) is found with a Fourier analysis (based on sine-wave fits) of the residue obtains by removing a smoothed curve to the choosen variable.

- $\delta_2\nu$ is noisier but the signal is larger too. In some cases (like the Sun) the expected signal-to-noise ratio in $\delta_2\nu$ is *not worse* than in the other magnitudes.

- Used $\delta_2\nu$ is robust, fast and easy to set up.

# The Sun Case

## GOLF data & Seismic$_1$ model
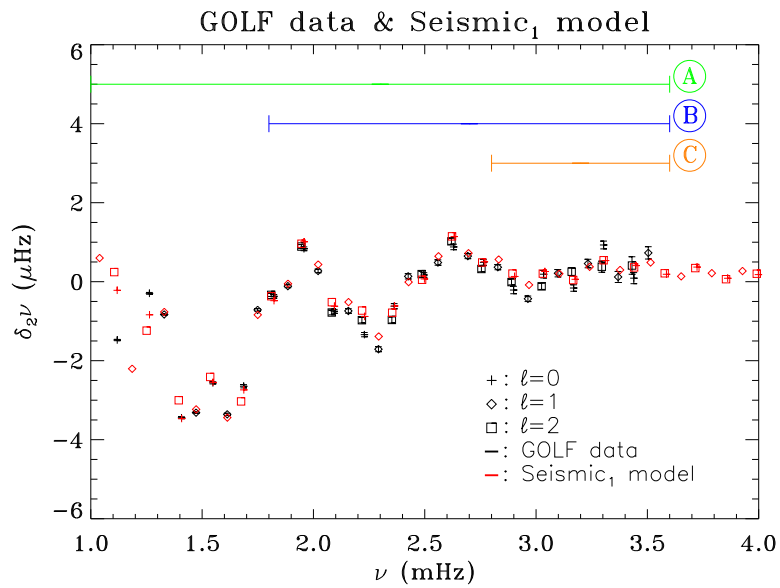


Second difference for 5yr of GOLF data ($\ell < 3$) and Fourier analyses:
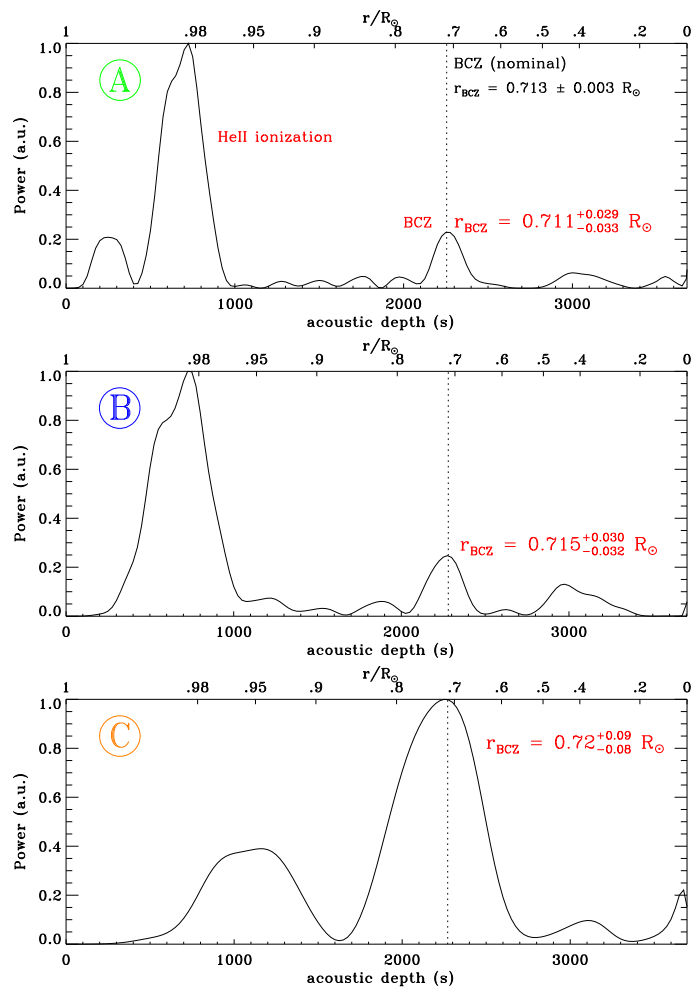
# Simulated observations
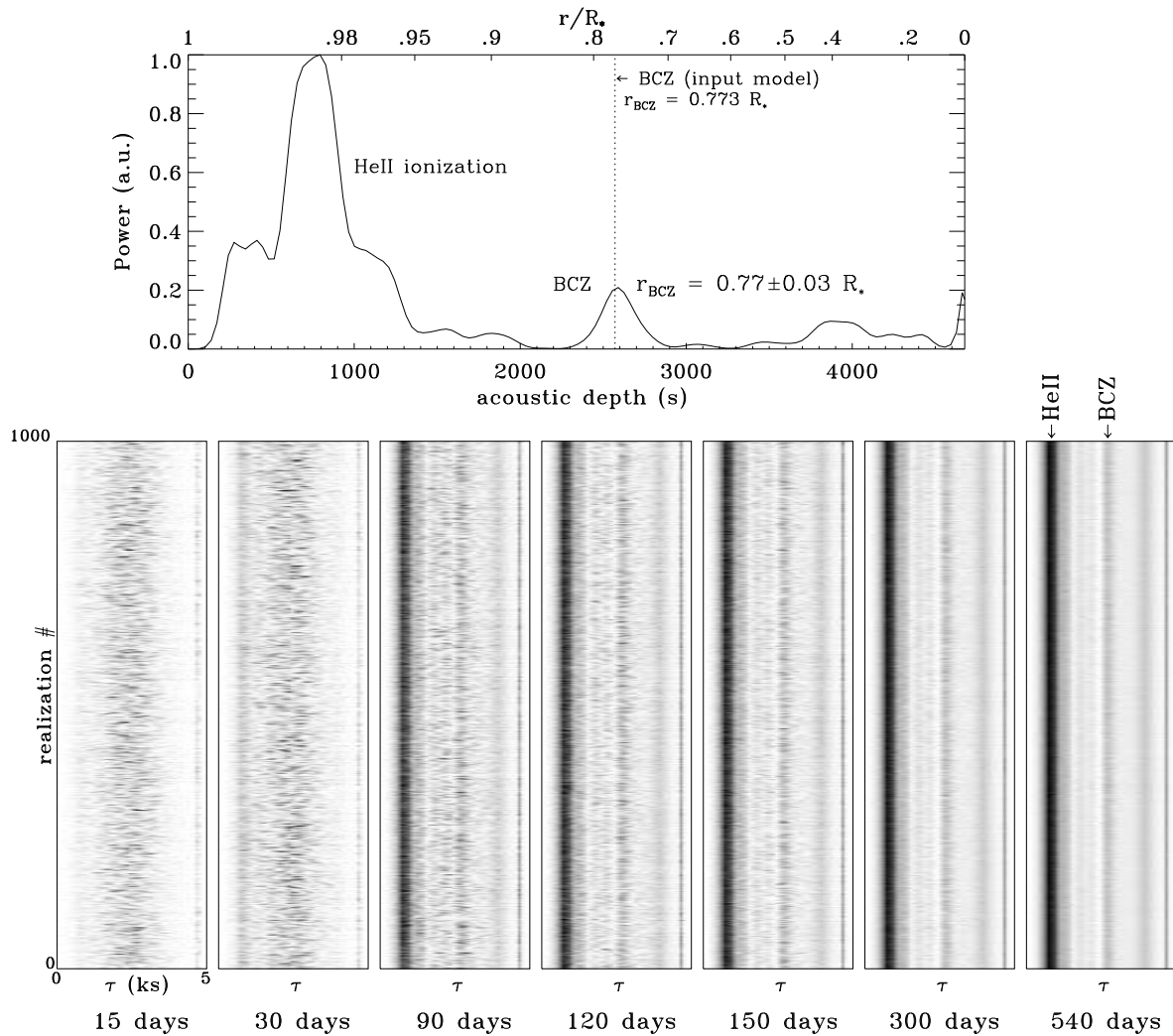


- Eigenfrequencies from a model of $\alpha$ Cen A

- Monte-Carlo simulations of different observation lengths

- Error bars: $1/T_{\mathrm{obs}}$

- 42 modes ($\ell = 0 - 2$) from 1.7 to 3.2 mHz

  – BCZ correctly derived:
    * 50% with 90 days
    * 75% with 120 days
    * 85% with 150 days

# VIRGO 150 days

- 12 sets of 3-months solar data

- BCZ extraction with this method ⇒ 8 cases out of 12 correctly derived

- Bad cases due to stochastic excitation



VIRGO 150 days
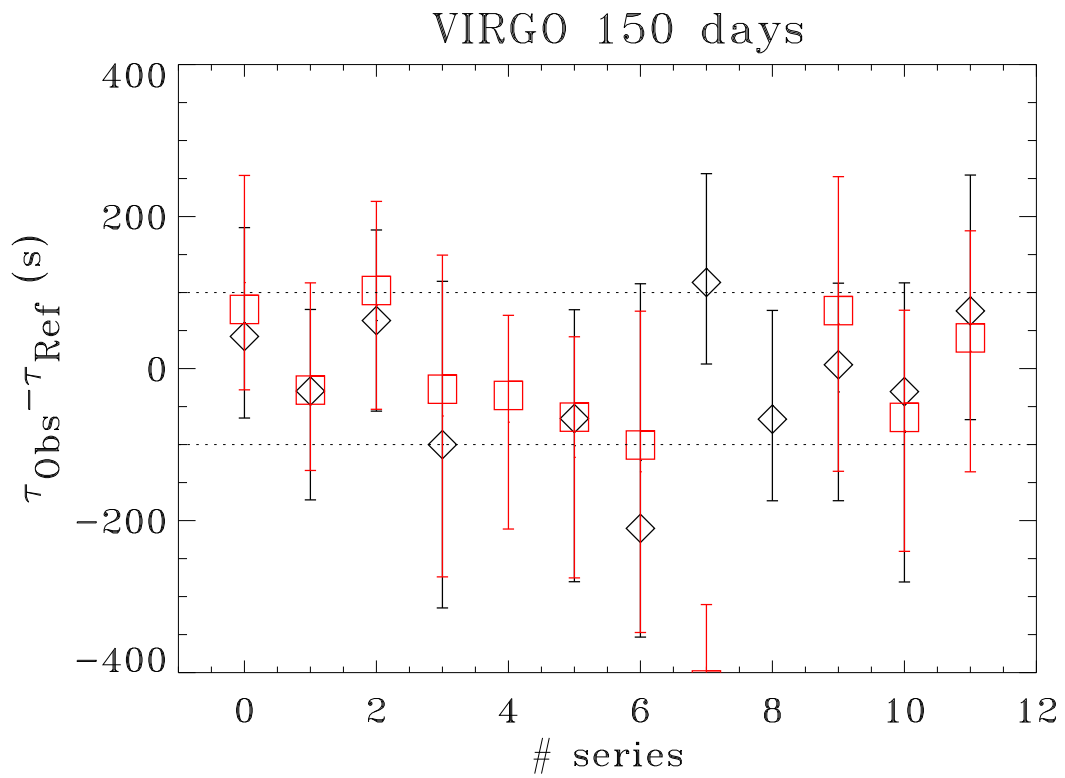
# HD 45067: $\delta_2\nu$ analysis

- A smooth component is removed

  → linear fit $a_0 + a_1\omega + \frac{a_2}{\omega^2}$ (Basu, 1997)

- Different Fourier analyses are done

  → using only $\ell = 0, 1$ or $\ell = 0, 1, 2$

  → and using different frequency ranges

---

$\nu \in [0.8; 1.3]$ mHz

$\ell = 0, 1, 2$: Black line; $\ell = 0, 1$: Red line

dotted line: $\frac{1}{<2\Delta\nu>}$
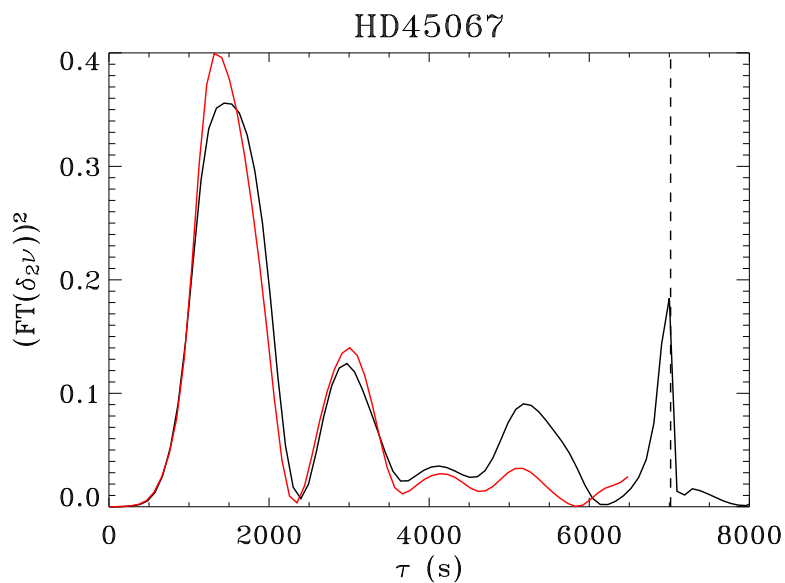


HD45067

- 1st peak ($\sim 1500$ s): HeII ionization

- 2nd peak ($\sim 3000$ s): BCZ (?)

- 3rd peak ($\sim 5500$ s): alias of the 1st one.

# HD 45067: $\delta_2\nu$ analysis (2)

- Found $\tau_{\mathrm{He}}$ and $\tau_{\mathrm{BCZ}}$ are used as guess to fit the *non-linear* expression: $(a_0 + \frac{a_1}{\omega^2})\sin(2\tau_{\mathrm{He}}\omega + \varphi_{\mathrm{He}}) + (b_0 + \frac{b_1}{\omega^2})\sin(2\tau_{\mathrm{BCZ}}\omega + \varphi_{\mathrm{BCZ}})$ (Basu, 1997)
  Note: Without good guess, no fit...

- acoustic depth: from where ?

- acoustic radius: $\sim \frac{1}{<2\Delta\nu>} - \tau$

## Results for different frequency ranges:

Red: $\ell = 0, 1$; Black: $\ell = 0, 2$
Diamonds: TF results; error bars: fit results
Range: $\nu \in [0.8; 1.2 + 0.1 \times i]$ mHz
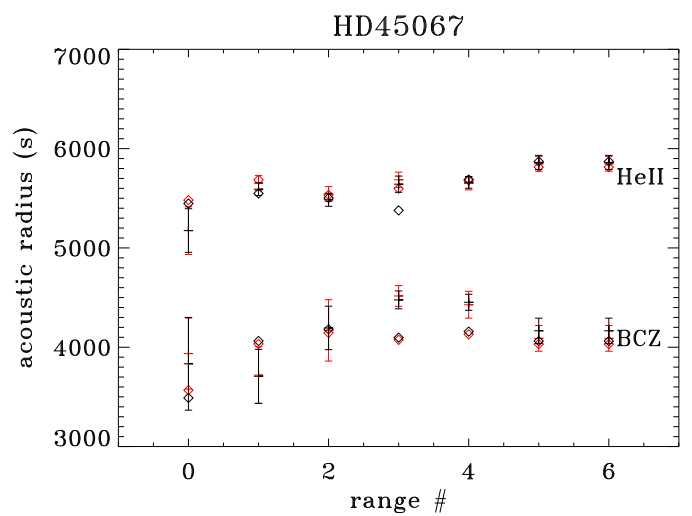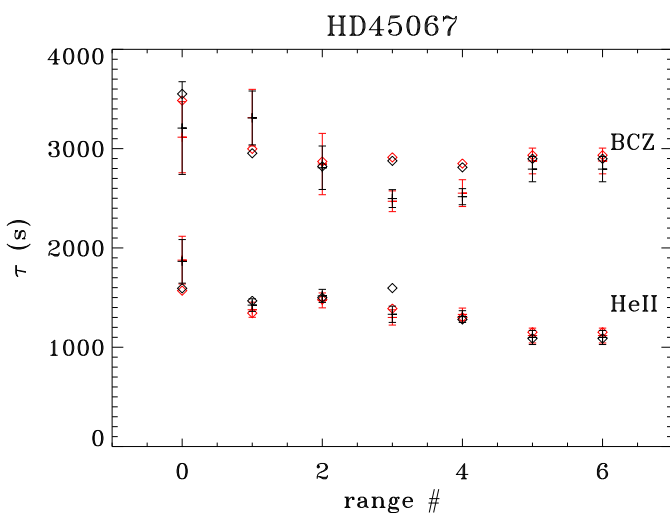


Extracted BCZ acoustic radius :$\sim$ 4060 s ($\pm$150 s)

# Conclusion

- This method is robust and easy to use

- We will be very happy to see the results obtained with more refined methods.

- Our frequency sets are available...
  Email: `jballot@cea.fr`

**Acknowledgments:** We would like to thank the VIRGO group for giving the data.

# Corot HH3, model star 1

HD 45067

$$T_{eff} = 6050 \pm 100 \text{ K} \qquad 3.15 \leq M_{bol} \leq 3.4$$
$$[\text{Fe/H}] = -0.17 \pm 0.1 \qquad V \sin i = 6 \pm 4 \text{ km/s}.$$

Conversion of $M_{bol}$ into physical units (erg s$^{-1}$)

$$M_{bol,\odot} = 4.75 \qquad L_\odot = 3.844 \times 10^{33}.$$

Conversion of [Fe/H] into Z/X

[Fe/H] $\simeq$ [Z/X] with unknown error $\qquad$ Z/X $= (\text{Z/X})_\odot \times 10^{[\text{Z/X}]}$
$(\text{Z/X})_\odot = 0.0245$ with at least a ten percent uncertainty.
$0.0146 \leq \text{Z/X} \leq 0.0186$

Input parameter ranges (E. Michel) $\longrightarrow$ Frequencies production (M.J. Goupil) $\longrightarrow$ Time series production (T. Appourchaux) $\longrightarrow$ Time series analysis (R.A. Garcia, C. Barban) $\longrightarrow$ seismic interpretation.

Evolutionary paths go through the box in the HR diagram at different stages of evolution.

|        | 010     | 020    | 024    | 027    |
|--------|---------|--------|--------|--------|
| M      | 1.080   | 1.230  | 1.150  | 1.090  |
| $X_0$  | 0.70    | 0.70   | 0.71   | 0.71   |
| $Z_0$  | 0.00115 | 0.015  | 0.0115 | 0.0115 |
| $\alpha$ | 1.8   | 1.7    | 1.8    | 1.8    |
| $\alpha_{ov}$ | 0  | 0.2    | 0.2    | 0.2    |
| diff   | no      | no     | no     | no     |
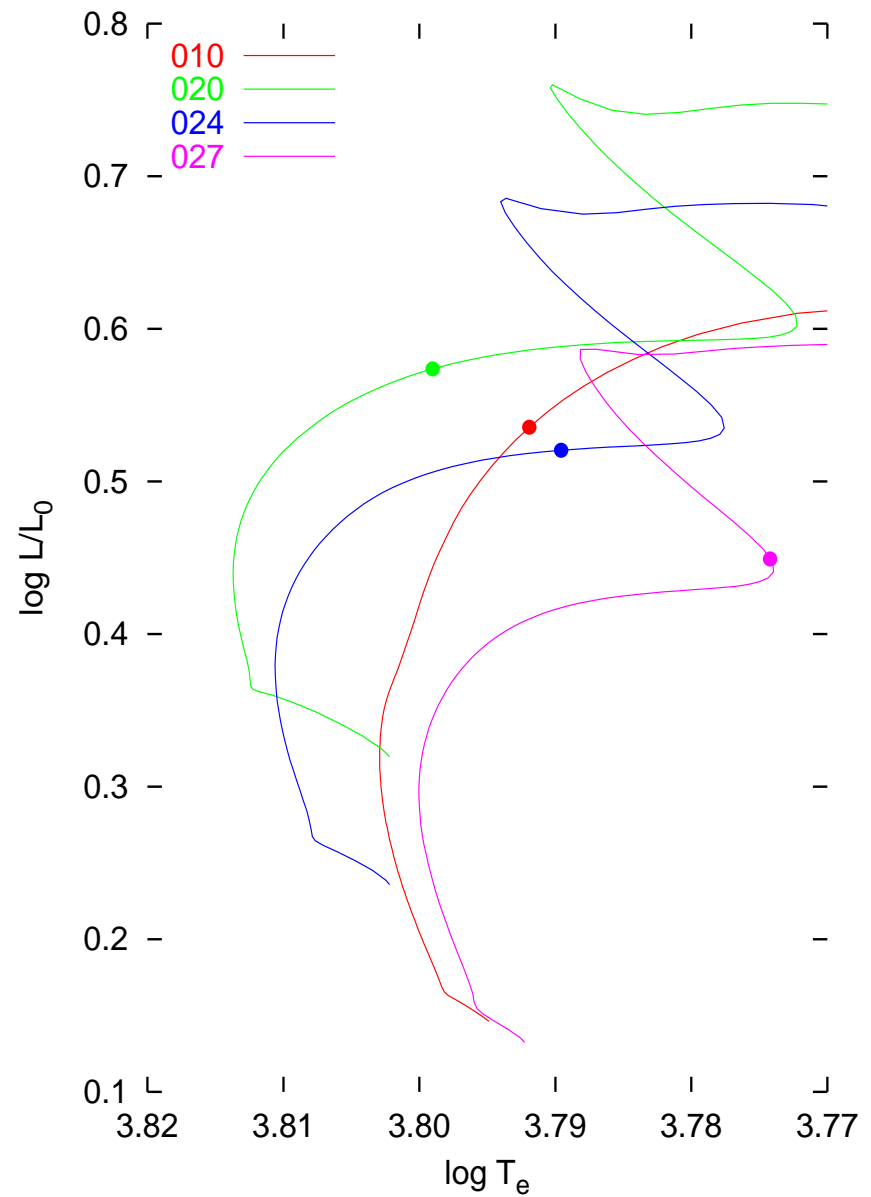
Seismic modelling: the method

- Compute sequences with different choices of $M$, $X_0$, $Z_0$, $\alpha$ (mixing-length parameter), $\alpha_{ov}$ (overshooting parameter), with/without diffusion ;

- on each sequence select the *best* model, which optimizes the fit in the $\Delta\nu$ and $\delta\nu$ space ;

$$\Delta\nu_{l,n} = \nu_{l,n} - \nu_{l,n-1}$$
$$\delta\nu_{l,n} = \nu_{l,n} - \nu_{l+2,n-1}$$
$$\delta'\nu_{l,n} = 2\nu_{l,n} - \nu_{l+1,n} - \nu_{l+1,n-1}$$

- accept or reject, try to improve.

The best fits were obtained for models on the end of the main sequence before or just at the beginning of the second gravitational contraction.

For models with overshooting, $\delta'\nu$ as function of $\nu$ shows a slope incompatible with the observations. The given model star has no overshooting or the overshooting parameter is clearly lower than generally admitted values.

Good fits can be obtained for parameters in the following ranges

$1.14 \leq M/M_\odot \leq 1.40$

$0.66 \leq X_0 \leq 0.72$

$0.0115 \leq Z_0 \leq 0.019$

$1.7 \leq \alpha \leq 1.8$

No overshooting or $\alpha_{ov} \ll 0.2$

with/without diffusion

We illustrate with two rather different models

| Best model of sequence 34 | Best model of sequence 42 |
| --- | --- |
| $M/M_\odot = 1.188$ | $M/M_\odot = 1.225$ |
| $X_0 = 0.72$ | $X_0 = 0.69$ |
| $Z_0 = 0.012$ | $Z_0 = 0.018$ |
| $\alpha = 1.7$ | $\alpha = 1.8$ |
| $\alpha_{ov} = 0.05$ | no overshooting |
| reduced diffusion (0.25) | with diffusion |
| age $= 4.37$ Gyr | age $= 3.77$ Gyr |
| $\log T_{eff} = 3.7873$ | $\log T_{eff} = 3.7853$ |
| $\log L/L_\odot = 0.5202$ | $\log L/L_\odot = 0.5225$ |
| $(Z/X)_{surf} = 0.0148$ | $(Z/X)_{surf} = 0.0174$ |
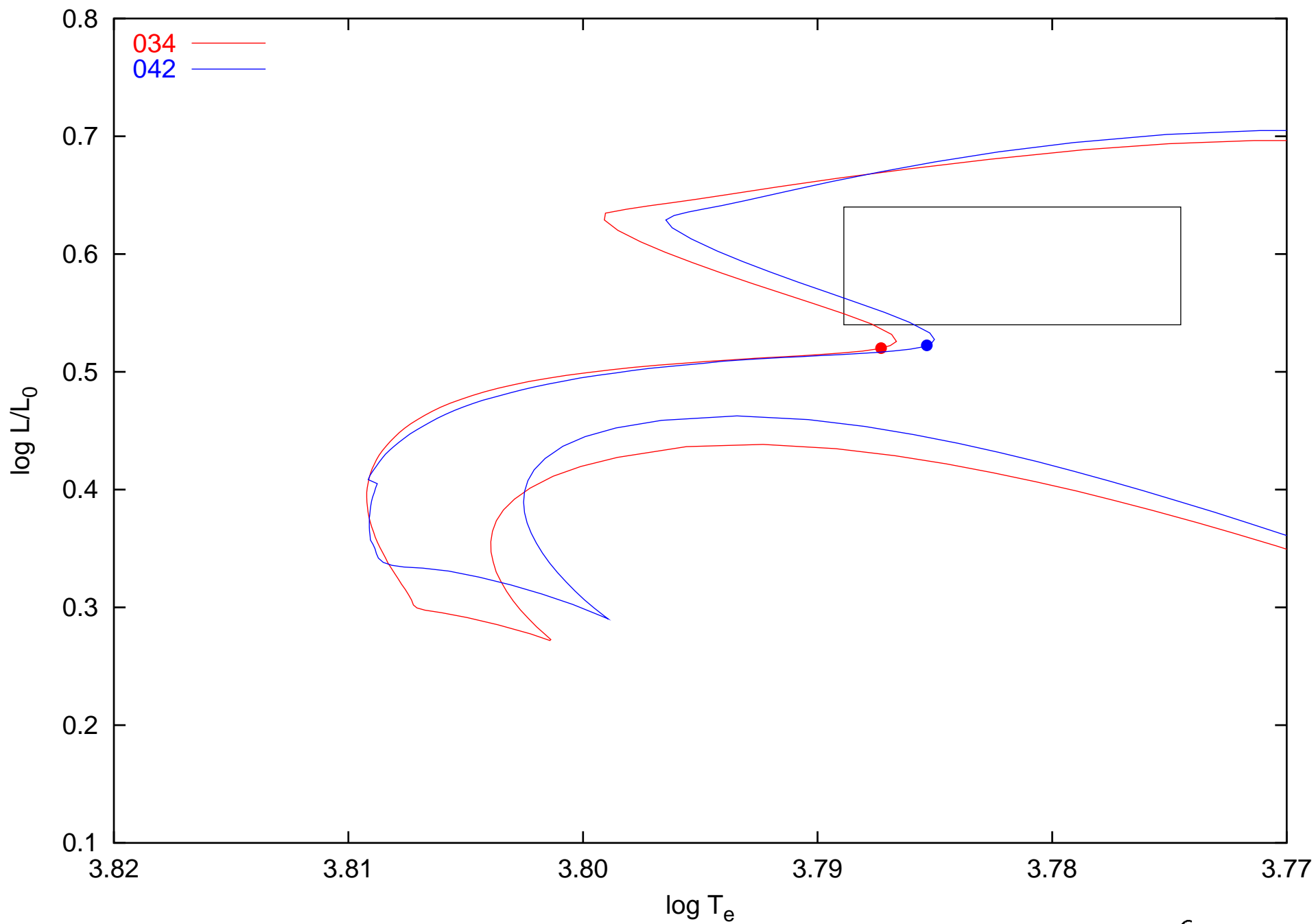
034
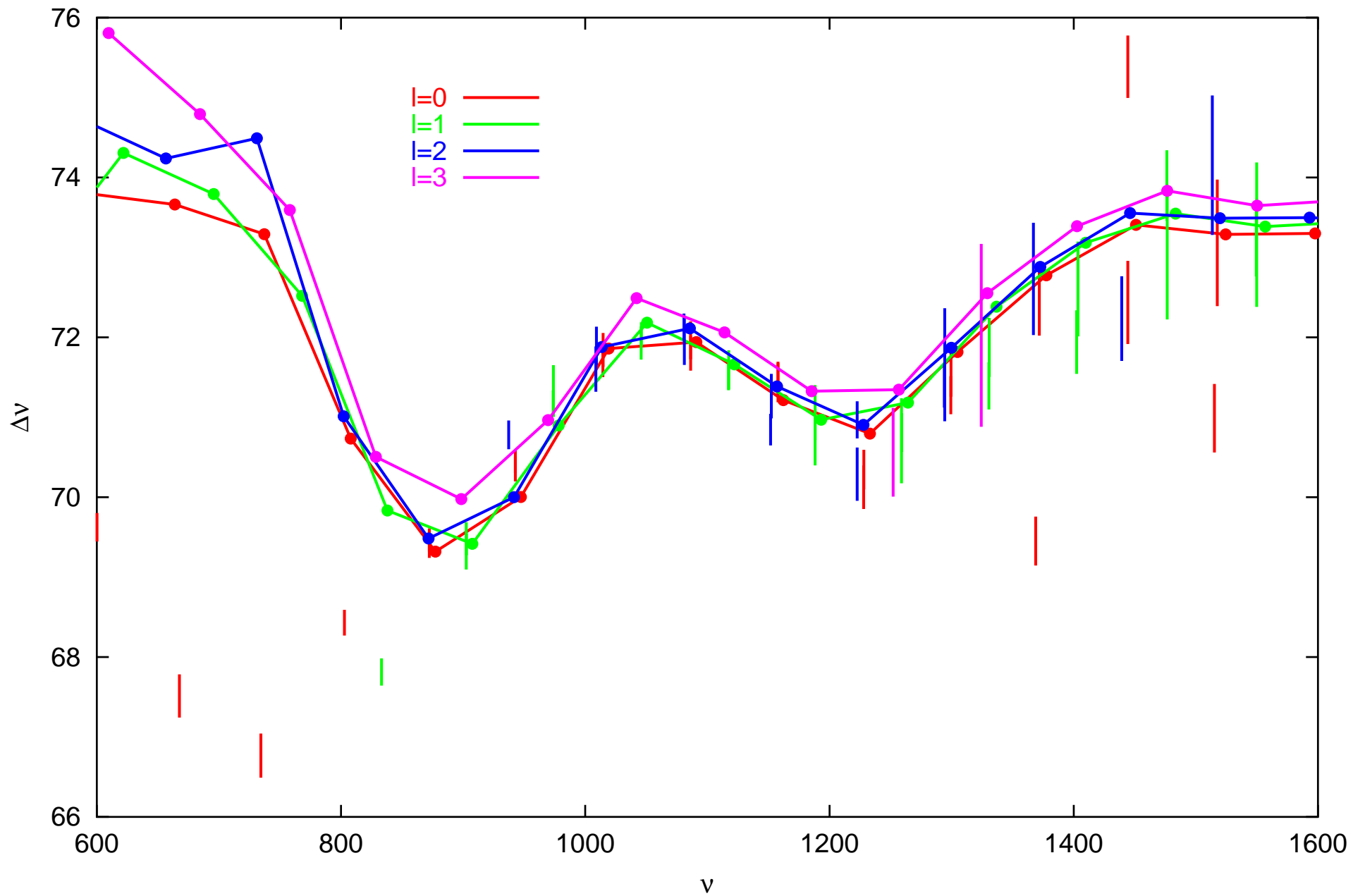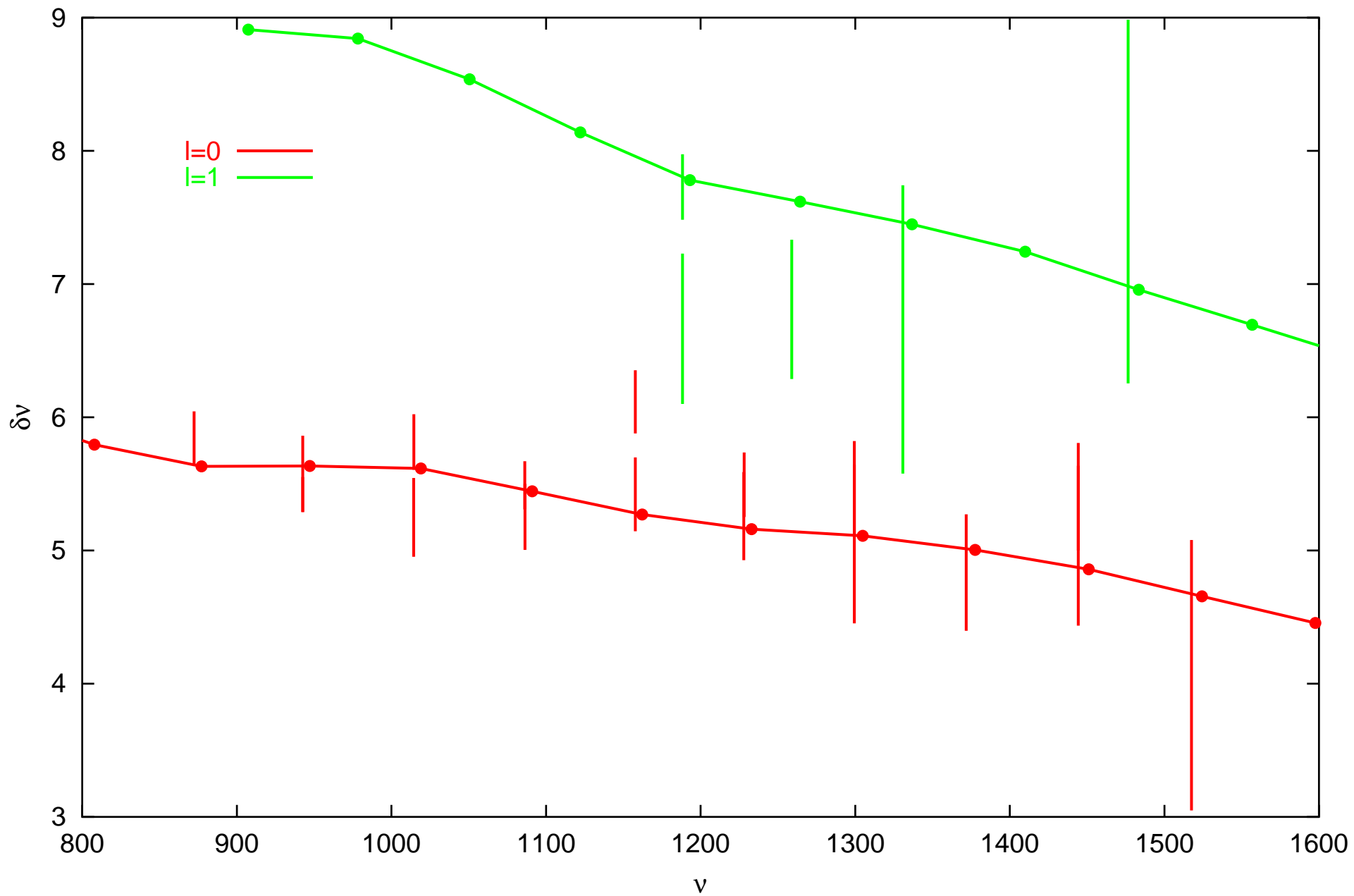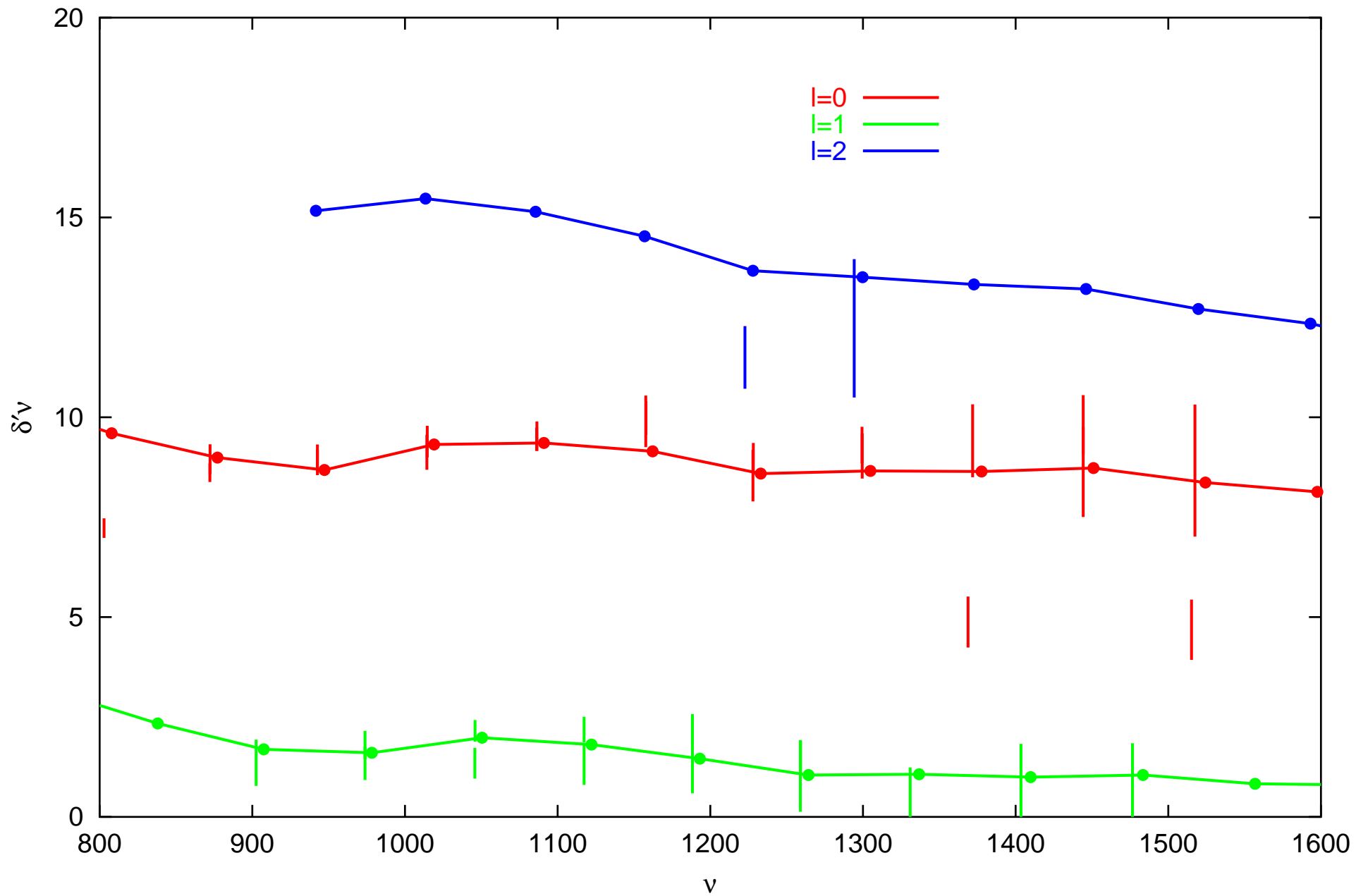
042

log L/L$_0$

log T$_e$

6

034/best        $\Delta\nu_{l,n}=\nu_{l,n}-\nu_{l,n-1}$

l=0
l=1
l=2
l=3

$\Delta\nu$

$\nu$

7

034/best    $\delta\nu_{l,n} = \nu_{l,n} - \nu_{l+2,n-1}$

l=0
l=1

$\delta\nu$

$\nu$

8

034/best    $\delta'\nu_{l,n}=2\nu_{l,n}-\nu_{l+1,n}-\nu_{l+1,n-1}$

l=0
l=1
l=2

$\delta'\nu$

9

042/best     $\Delta\nu_{l,n}=\nu_{l,n}-\nu_{l,n-1}$

l=0
l=1
l=2
l=3

$\Delta\nu$

$\nu$

10

042/best     $\delta\nu_{l,n}=\nu_{l,n}-\nu_{l+2,n-1}$

l=0
l=1

11

042/best    $\delta'\nu_{l,n}=2\nu_{l,n}-\nu_{l+1,n}-\nu_{l+1,n-1}$

l=0
l=1
l=2

$\delta'\nu$

$\nu$

12
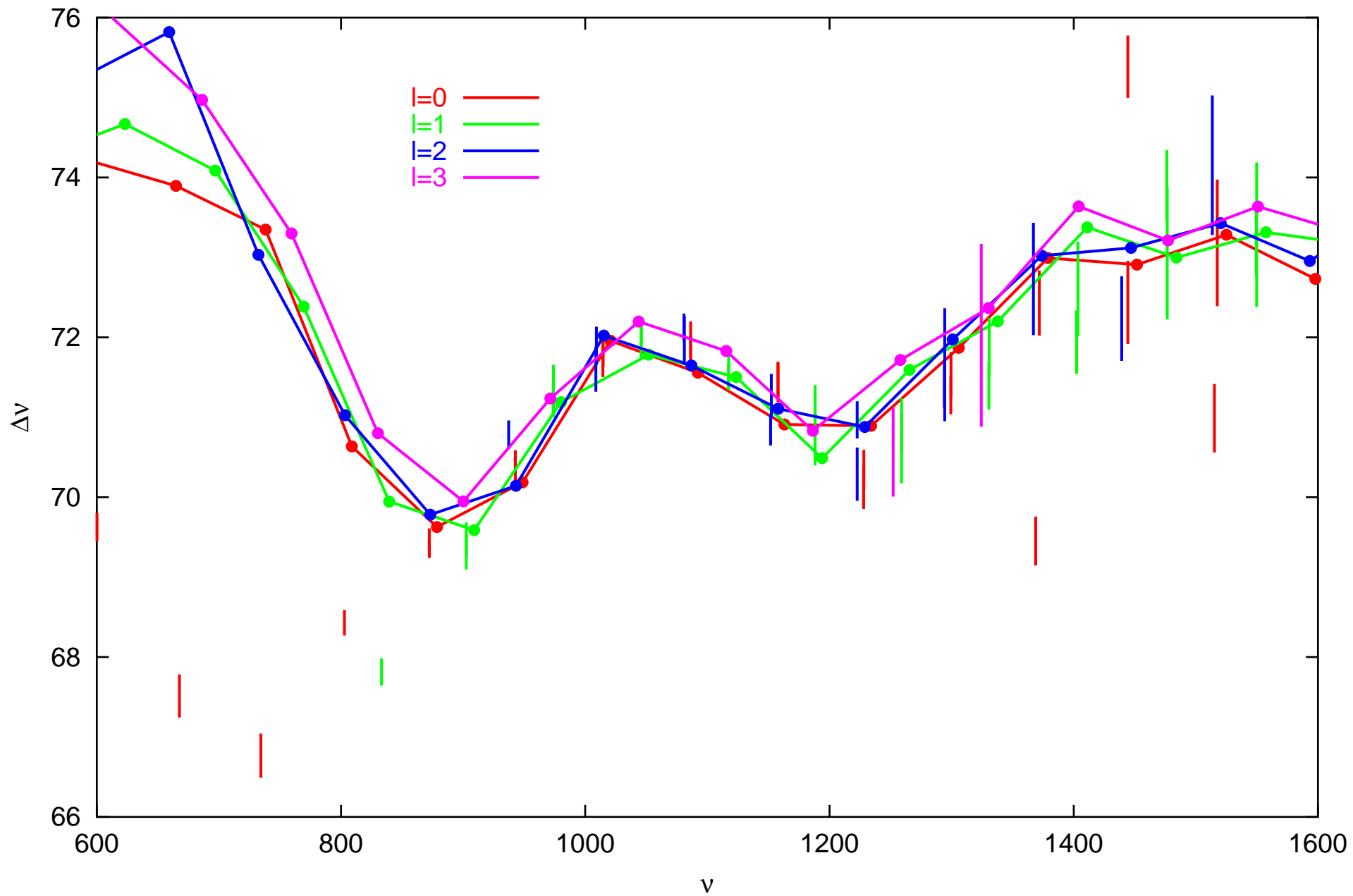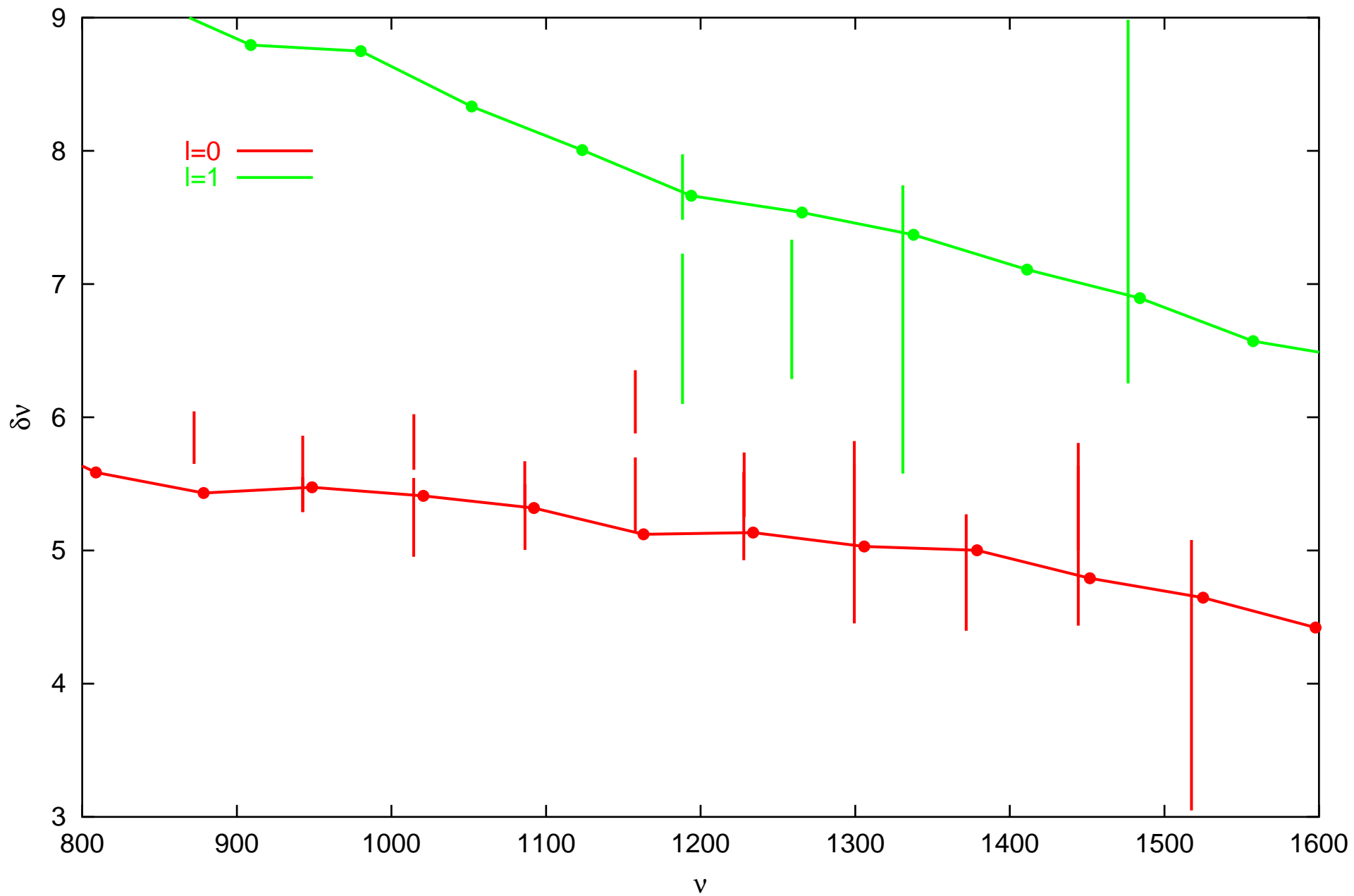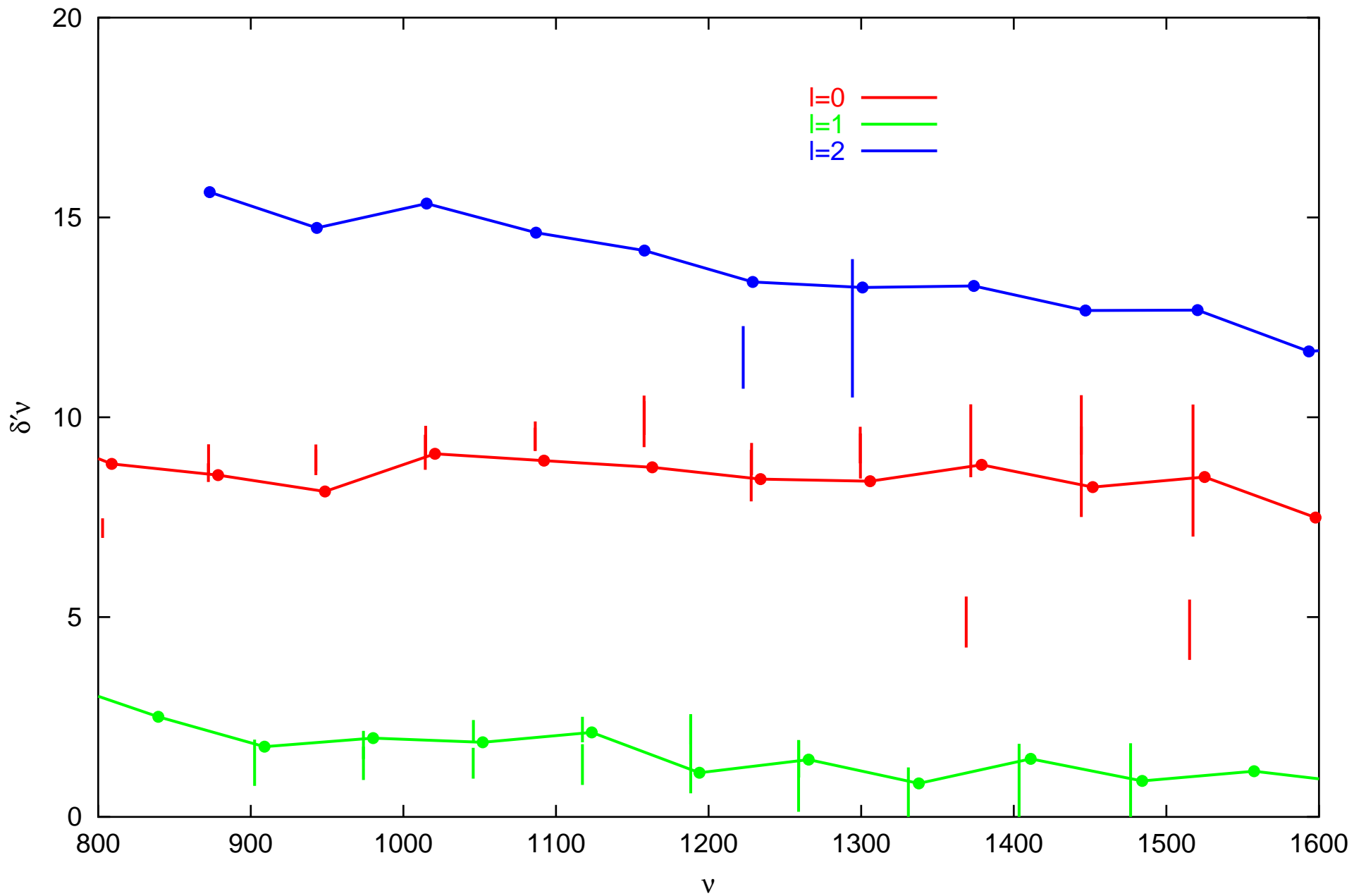
# Best model of sequence 034

$M/M_\odot = 1.188$
$X_0 = 0.72$
$Z_0 = 0.012$
$\alpha = 1.7$
$\alpha_{ov} = 0.05$
reduced diffusion (0.25)
age= 4.37 Gyr
$\log T_{eff} = 3.7873$
$\log L/L_\odot = 0.5200$
$X_c = 0.05886$
$(Z/X)_{surf} = 0.0148$
$R = 1.1258310 \times 10^{11}$ cm
convective core without overshooting extension: $r_c/R = 0.051619$, $m_c/M = 0.063324$
convective core with overshooting extension: $r_m/R = 0.053413$, $m_m/M = 0.068938$

Frequencies in $\mu$Hz

| mode | $\ell = 0$ | $\ell = 1$ | $\ell = 2$ | $\ell = 3$ |
|------|------------|------------|------------|------------|
| 3    |            |            | 4.33914112E+02 | 4.58793445E+02 |
| 4    |            | 4.10804803E+02 | 5.07650984E+02 | 5.33904814E+02 |
| 5    | 4.44251995E+02 | 4.74757867E+02 | 5.82425774E+02 | 6.09721557E+02 |
| 6    | 5.16457519E+02 | 5.47616157E+02 | 6.56676100E+02 | 6.84521244E+02 |
| 7    | 5.90273764E+02 | 6.21931711E+02 | 6.95765321E+02 | 7.58120403E+02 |
| 8    | 6.63941630E+02 | 6.95732673E+02 | 7.31143822E+02 | 8.28637740E+02 |
| 9    | 7.37240676E+02 | 7.68258899E+02 | 8.02180861E+02 | 8.52862299E+02 |
| 10   | 8.07975825E+02 | 8.38095896E+02 | 8.71672168E+02 | 8.98608474E+02 |
| 11   | 8.77304236E+02 | 9.07520376E+02 | 9.41678085E+02 | 9.69583104E+02 |
| 12   | 9.47312787E+02 | 9.78426242E+02 | 1.01356690E+03 | 1.04208026E+03 |
| 13   | 1.01918232E+03 | 1.05061635E+03 | 1.08568060E+03 | 1.11414288E+03 |
| 14   | 1.09112358E+03 | 1.12228162E+03 | 1.15707292E+03 | 1.18547493E+03 |
| 15   | 1.16234258E+03 | 1.19325398E+03 | 1.22797894E+03 | 1.25682379E+03 |
| 16   | 1.23313785E+03 | 1.26444212E+03 | 1.29985709E+03 | 1.32938460E+03 |
| 17   | 1.30496497E+03 | 1.33683142E+03 | 1.37273994E+03 | 1.40277876E+03 |
| 18   | 1.37774269E+03 | 1.41002185E+03 | 1.44630431E+03 | 1.47661810E+03 |
| 19   | 1.45115987E+03 | 1.48357316E+03 | 1.51979295E+03 | 1.55026921E+03 |
| 20   | 1.52444529E+03 | 1.55696361E+03 | 1.59330131E+03 | 1.62399047E+03 |
| 21   | 1.59775380E+03 | 1.63041468E+03 | 1.66672703E+03 | 1.69771647E+03 |
| 22   | 1.67095342E+03 | 1.70393021E+03 | 1.74051574E+03 |                |
| 23   | 1.74451607E+03 |            |            |            |

The following figure shows the ratios of $\delta\nu_{n,\ell} = \nu_{n,l} - \nu_{n-1,\ell+2}$ and $\Delta\nu_{n,l} = \nu_{n,\ell} - \nu_{n-1,\ell}$ for $\ell = 0$ and different $n$.
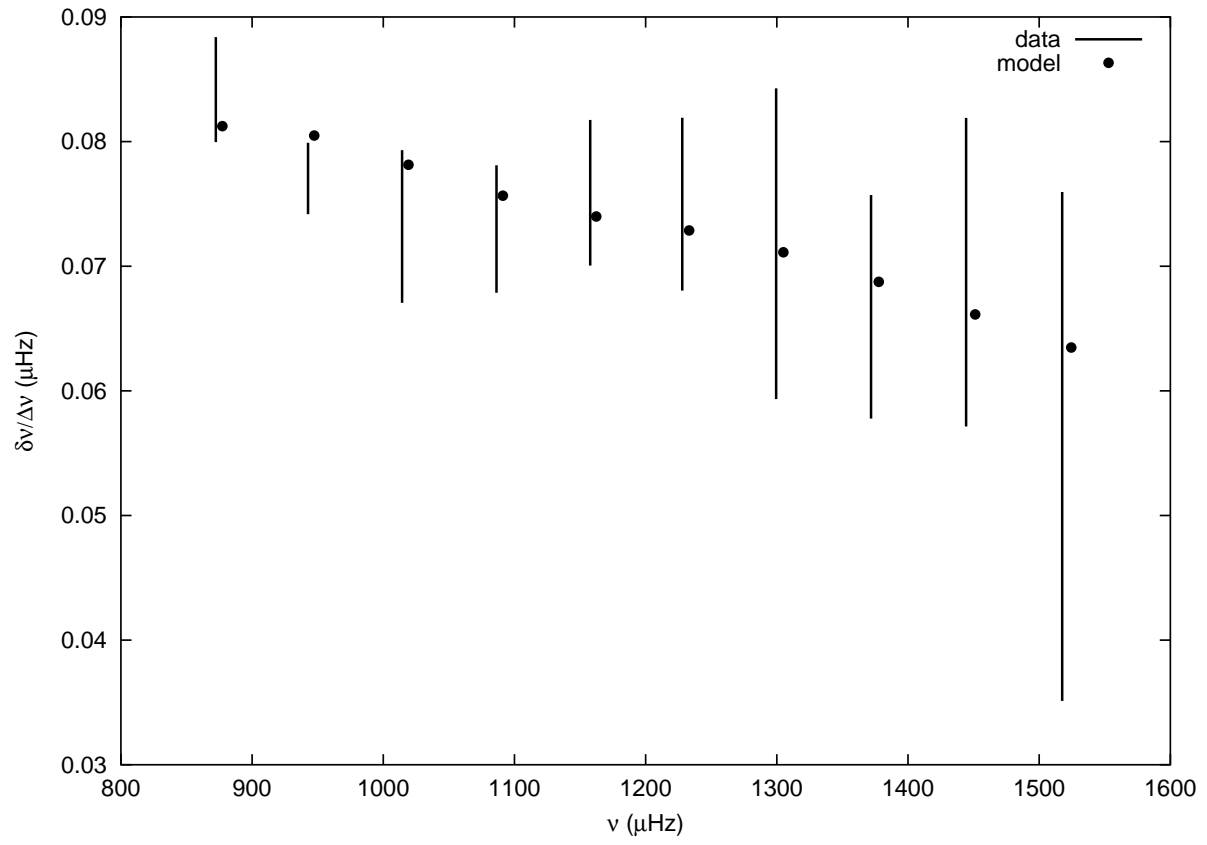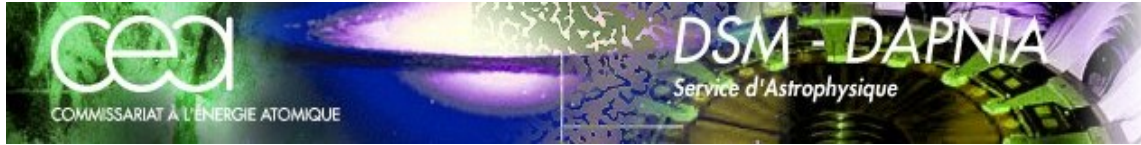
# HD-45067

## Hare & Hound # 3

by
R.A. García
Service d'Astrophysique CEA Saclay

**Saclay Team:**

**S. Turck-Chièze &  J. Ballot**
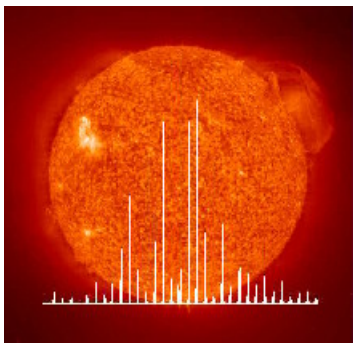
# PSD :

- 4 different estimators have been computed:

    – Periodogram (FFT)

    – Multitaper (4 Sine tapers)

    – Zero Padded Periodogram (4 times)

    – Averaged cross spectrum
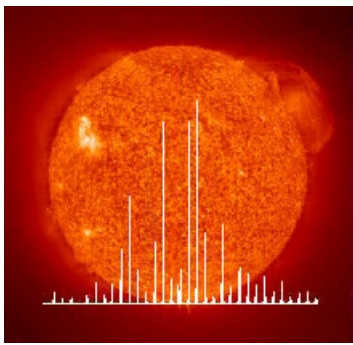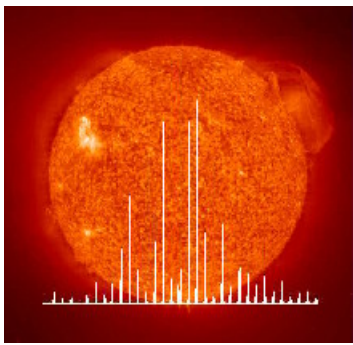
# Periodogram :
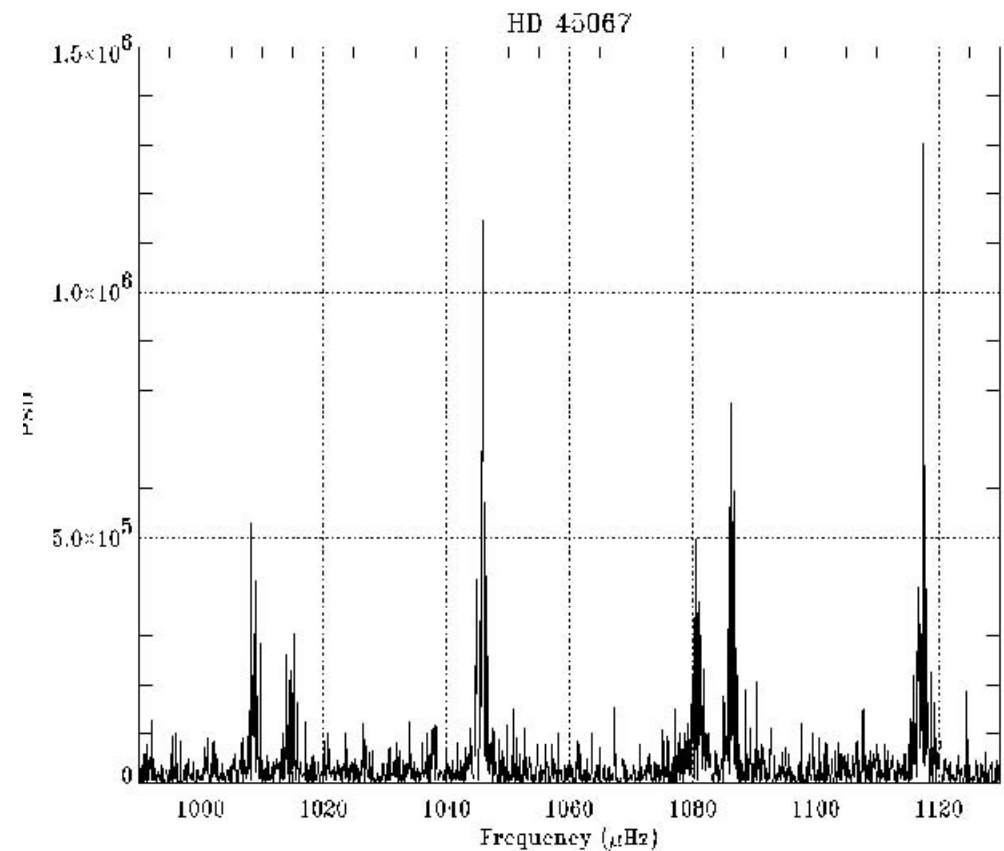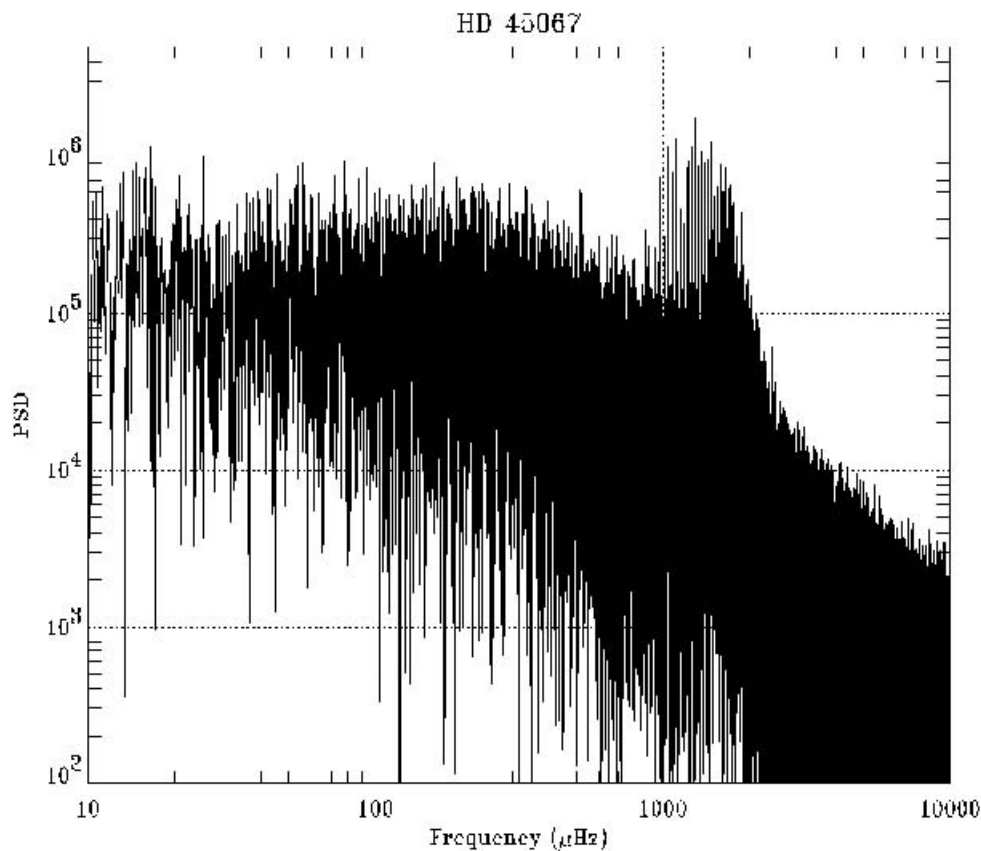
- Background fitted with a 2 elements Harvey model
- 2 groups of modes are clearly identified
- The individual multiplets are not directly recognized

Rafael A. García

# Identifying the modes :
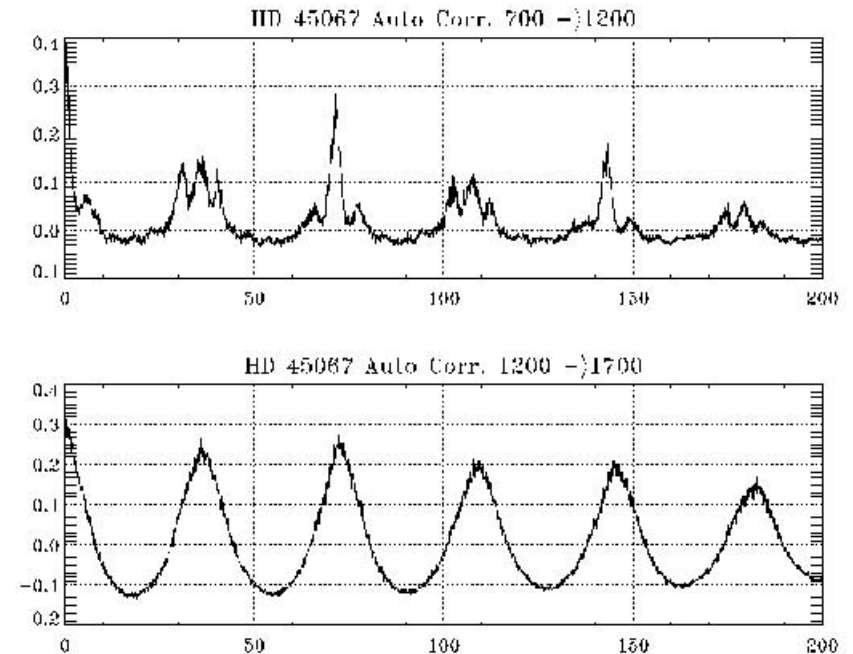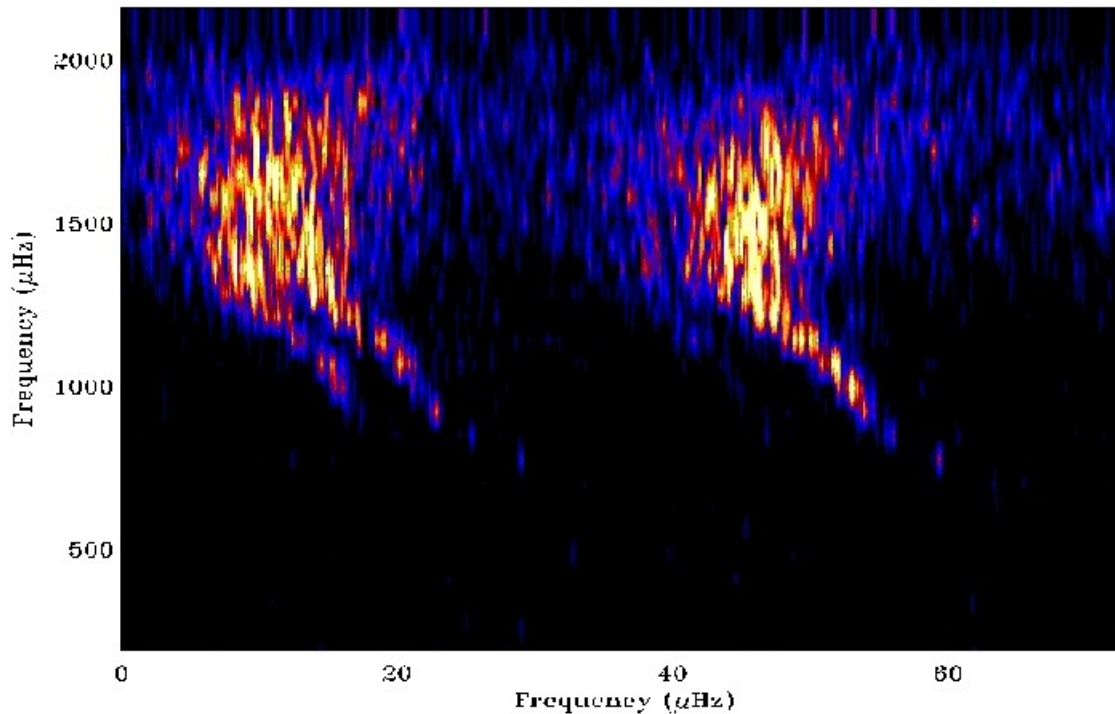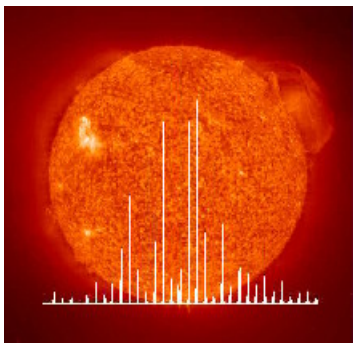


- Distance between the two left structures changing with frequency =>
  - Different modes not a "changing" splitting
- Amplitude ratio => doublet l=0-2 and l=1
- From the autocorrelation: Small and big differences
  - Constructing guessing frequencies for the fit
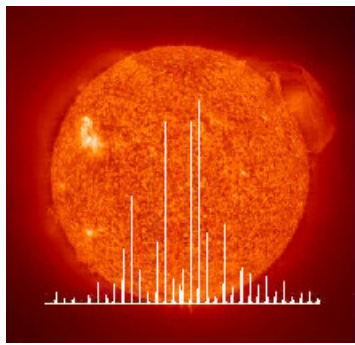
# Fitting model

- Symmetric and asymmetric profiles used
    - No systematic differences observed on the resultant frequencies
- Fitted parameters: Frequency, amplitude, Line-width
    - First step:
        - fitting only one lorentzian profile per mode
            - The asymmetry takes into account the asymmetry of the whole mode
            - Better determination of the central frequencies
    - Second step:
        - Using the new guessing table
            - free splitting and different fixed amplitude ratios of the components of the multiplets
            - Fixed splitting to the most common value found (~800 nHz)

- This process has been repeated for the 4 Fourier estimators

Rafael A. García

# Results :

| l=0 | l=1 | l=2 | l=3 |
|---|---|---|---|
| 530.5170  0.13 | | | |
| 600.1405  0.1227 | | | |
| 667.6530  0.2413 | | | |
| 734.4192  0.1332 | 765.3281  0.1320 | | |
| 802.8481  0.0893 | 833.1413  0.1070 | 866.4656  0.1602 | |
| 872.3123  0.1149 | 902.5326  0.2750 | 937.2448  0.0804 | |
| 942.6650  0.1042 | 973.8620  0.1706 | 1009.1386  0.2244 | |
| 1014.3876  0.1930 | 1045.7911  0.1186 | 1081.0989  0.2060 | |
| 1086.3512  0.1376 | 1117.3852  0.2129 | 1152.3626  0.1874 | 1181.6210 |
| 1157.7844  0.2039 | 1188.2857  0.4551 | 1222.6506  0.2759 | 1252.1820 |
| 1227.9085  0.1812 | 1258.9915  0.2774 | 1294.3077  0.6501 | 1324.2065 |
| 1299.4447  0.2135 | 1330.8657  0.2434 | 1367.0392  0.2661 | 0        0 |
| 1371.8733  0.3462 | 1403.4696  0.5409 | 1439.2745  0.4578 | 1468.8972 |
| 1444.3102  0.3877 | 1476.5164  0.6188 | 1513.4282  0.7430 | |
| 1517.4924  0.6915 | 1549.8008  0.6593 | | |
| 0        0 | 1622.9331  0.6533 | | |
| 0        0 | 1696.2605  0.6527 | | |
| 0        0 | 1769.5830  0.6735 | | |

\*



HD45067
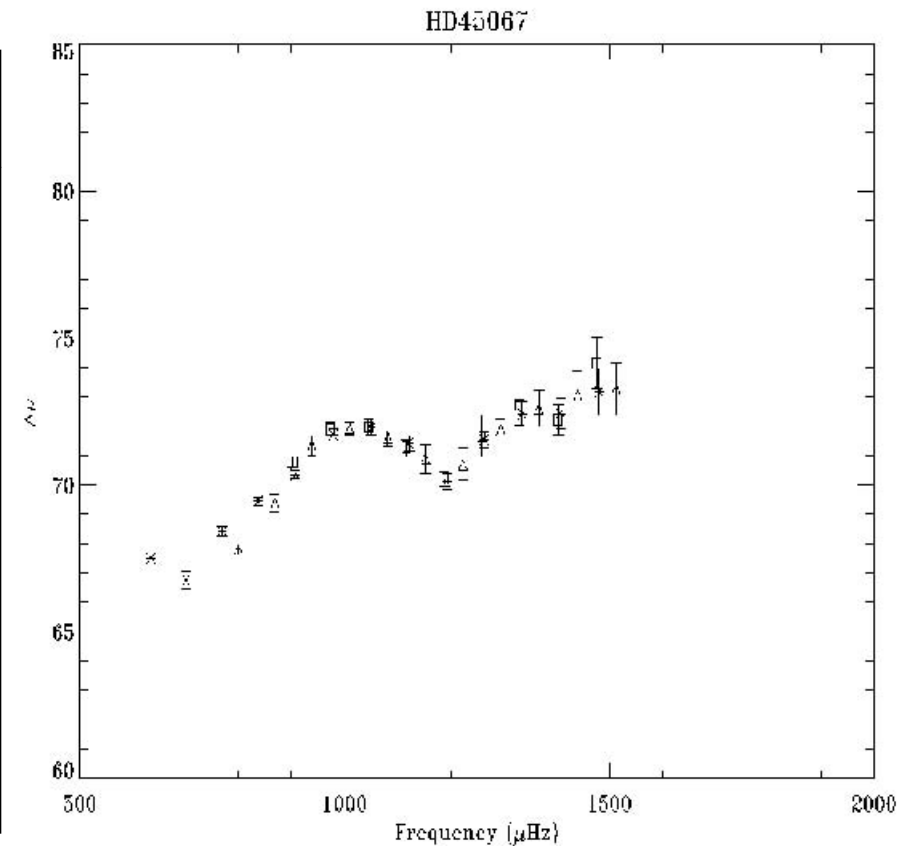
Resultant frequencies and Big difference
\* Candidate modes (not present in all the estimators)

Rafael A. García

# Periodogram (l=0):

Rafael A. García

# Multitaper (l=0):

Rafael A. García

# Periodogram (l=1)

Rafael A. García
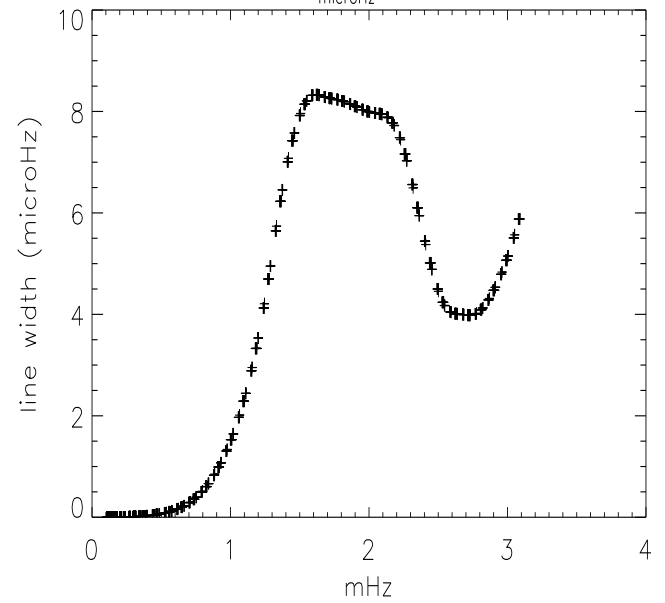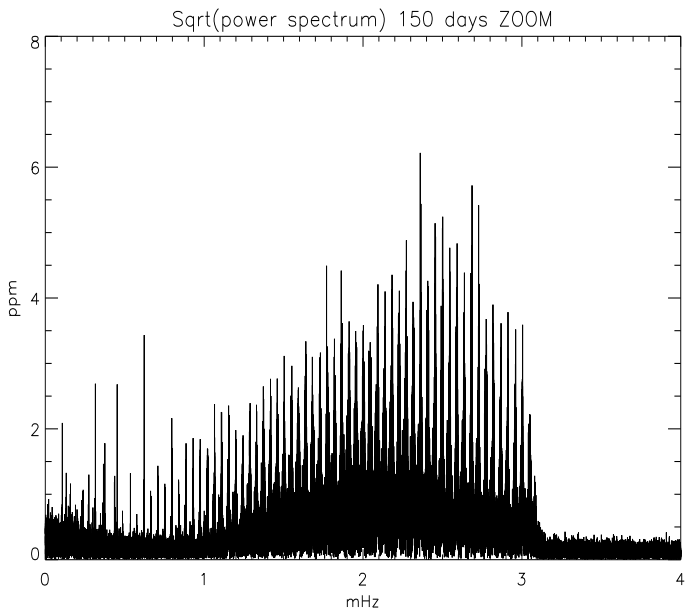
# Multitaper (l=1)

Rafael A. García
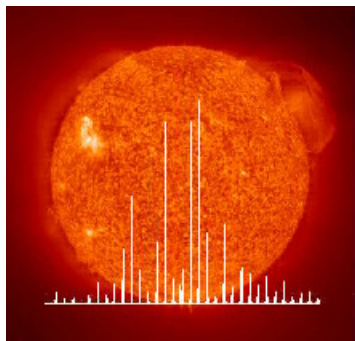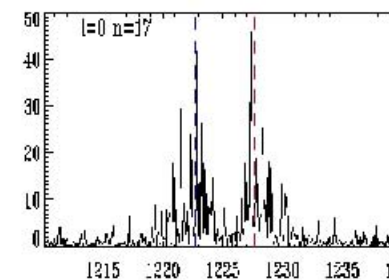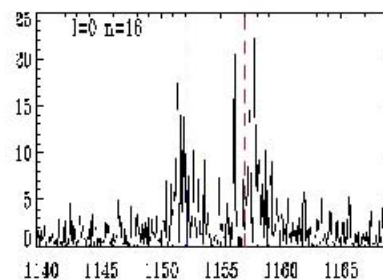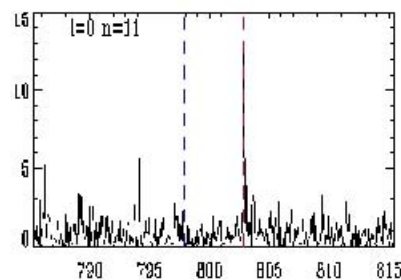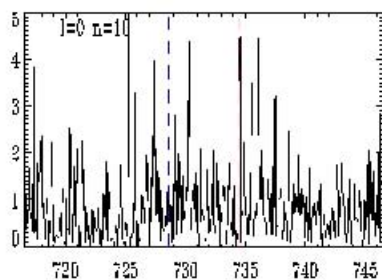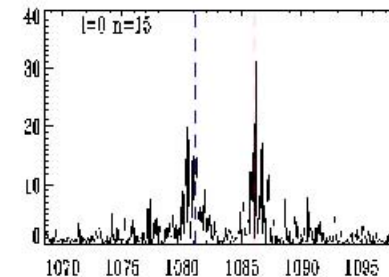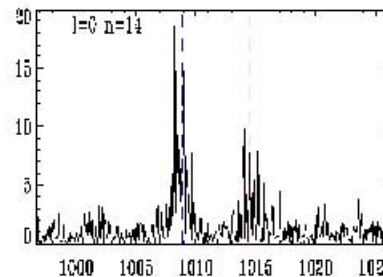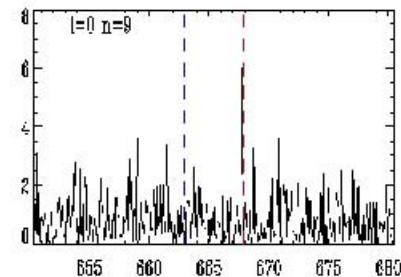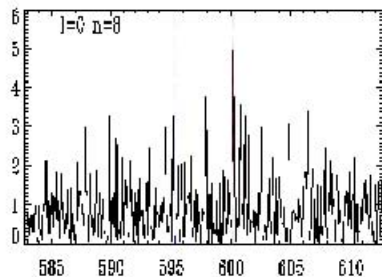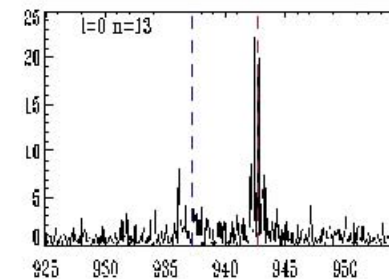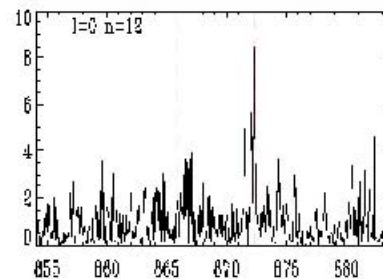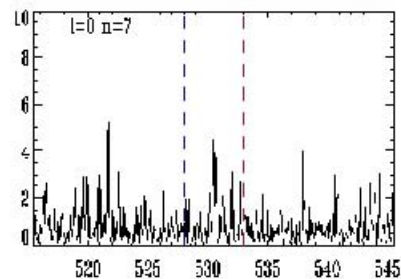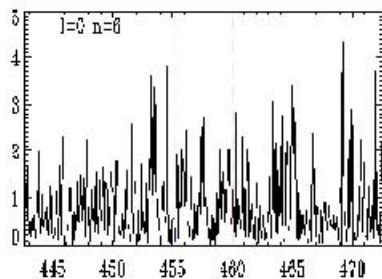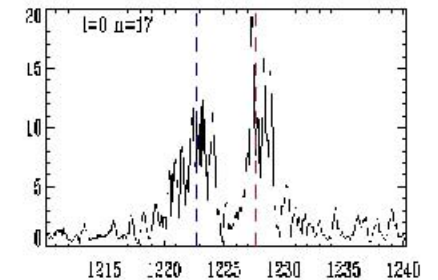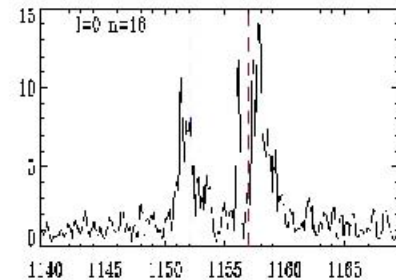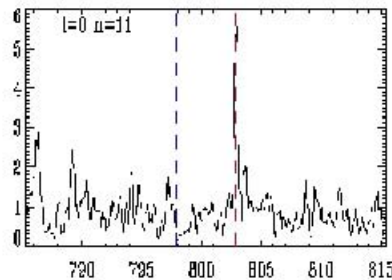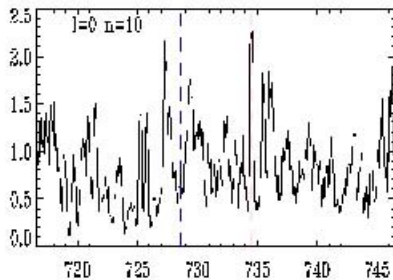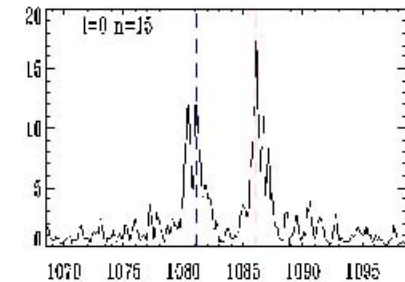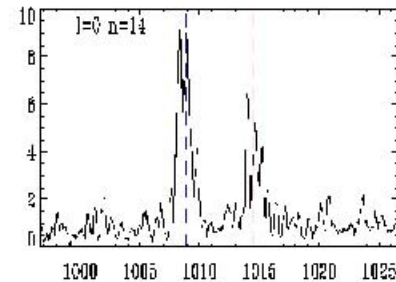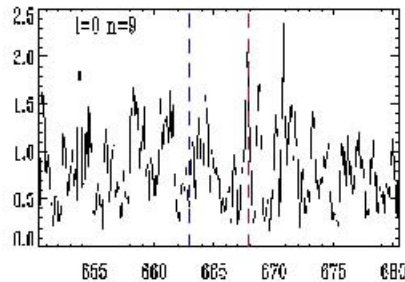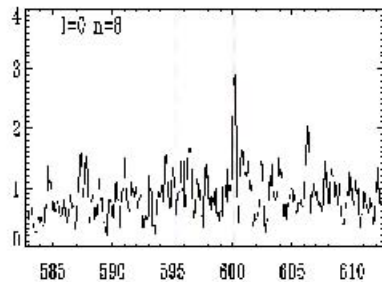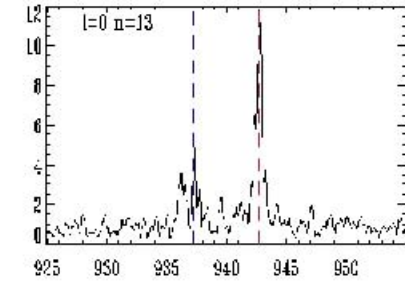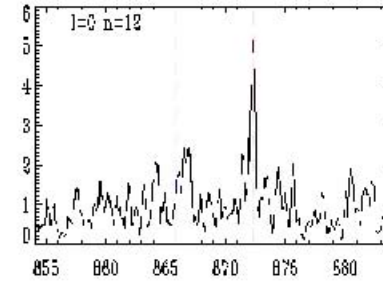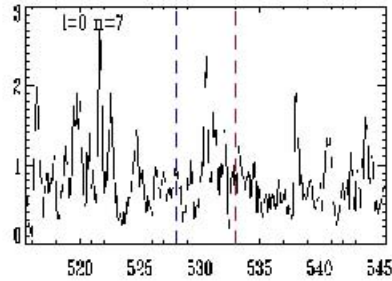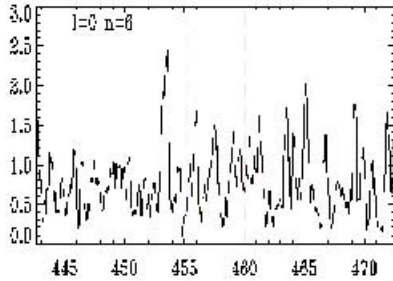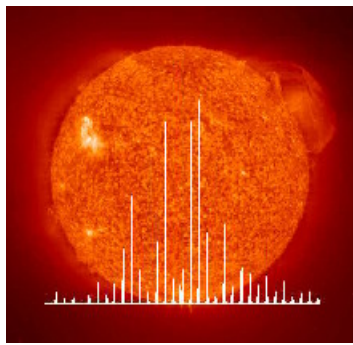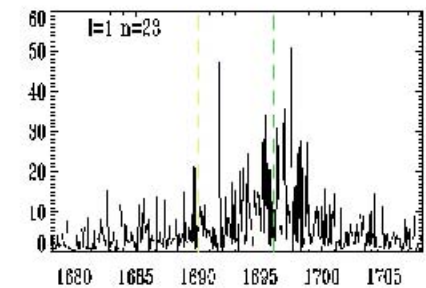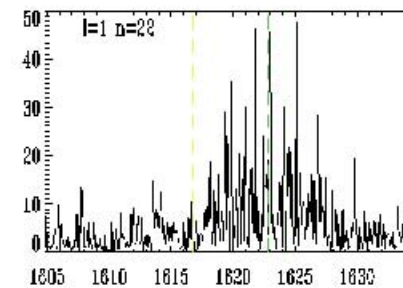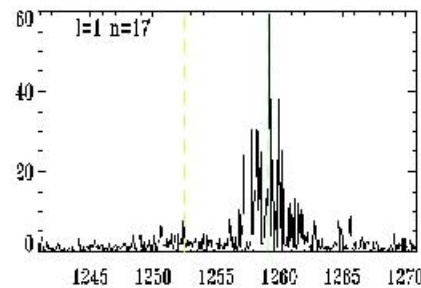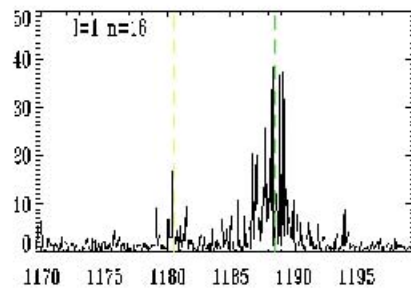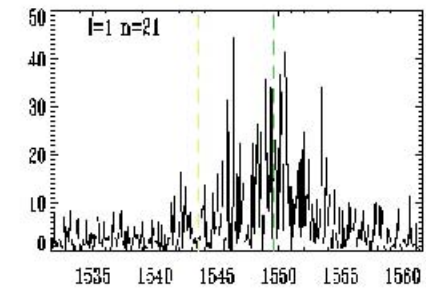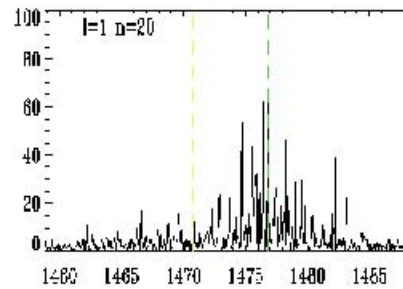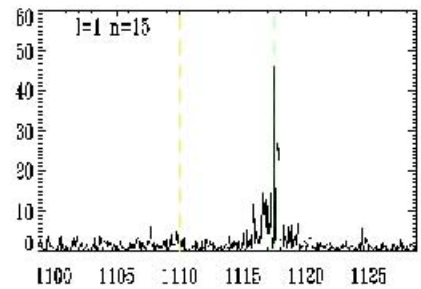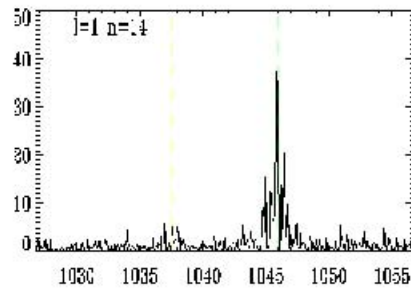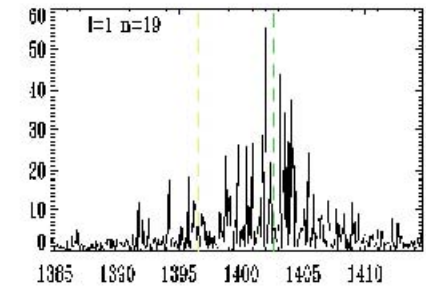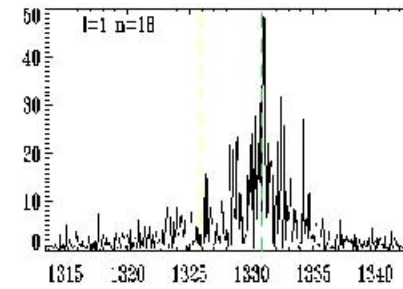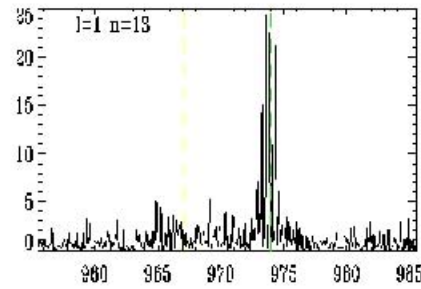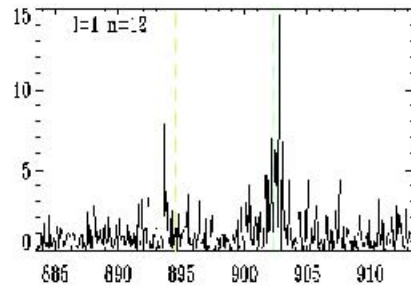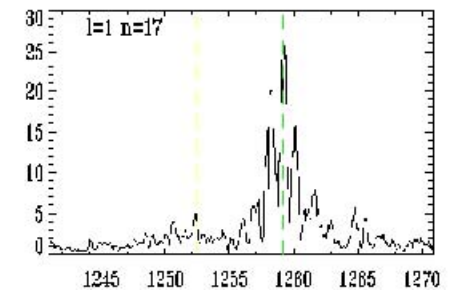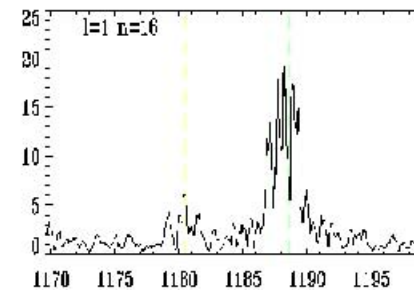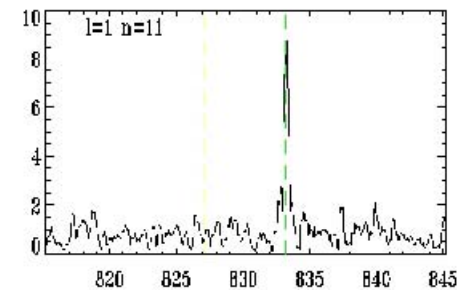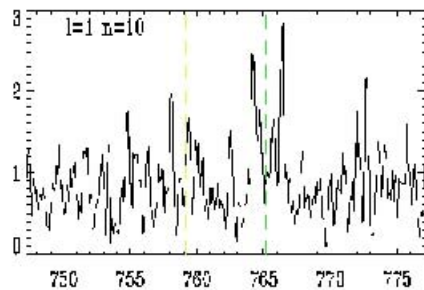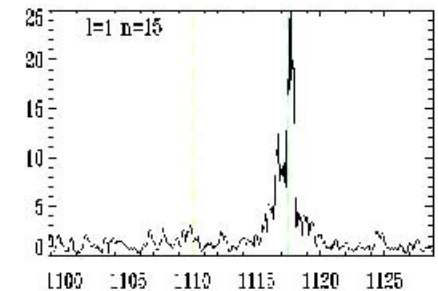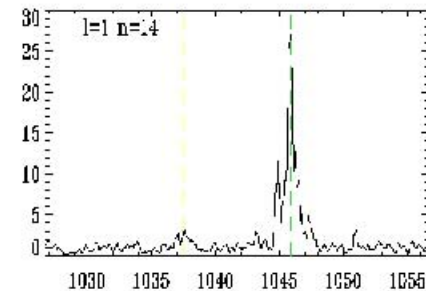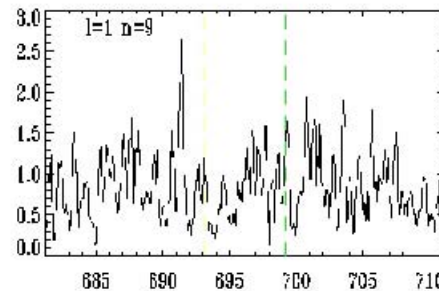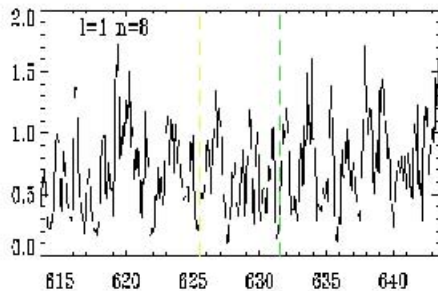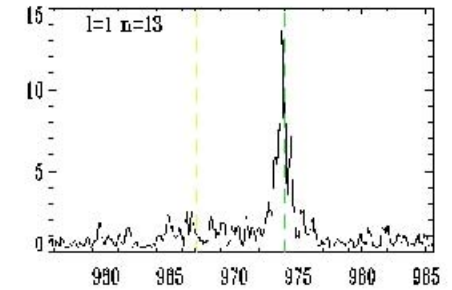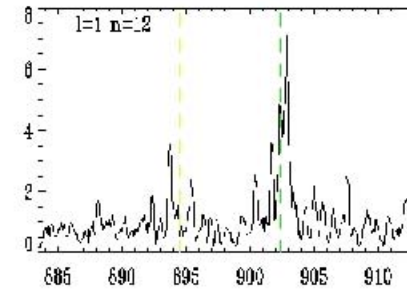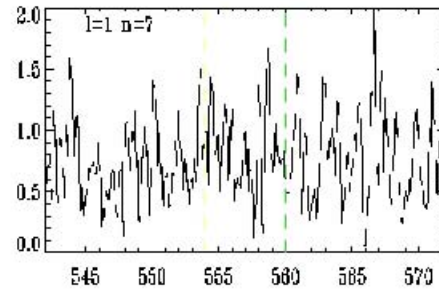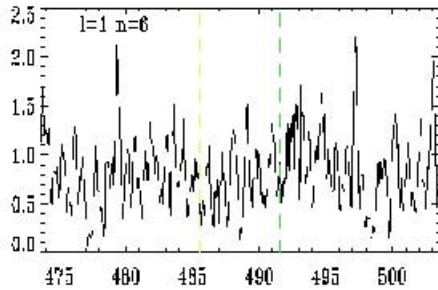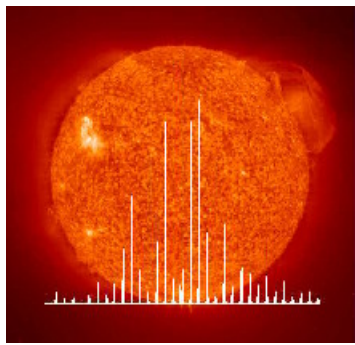
# CONCLUSIONS :
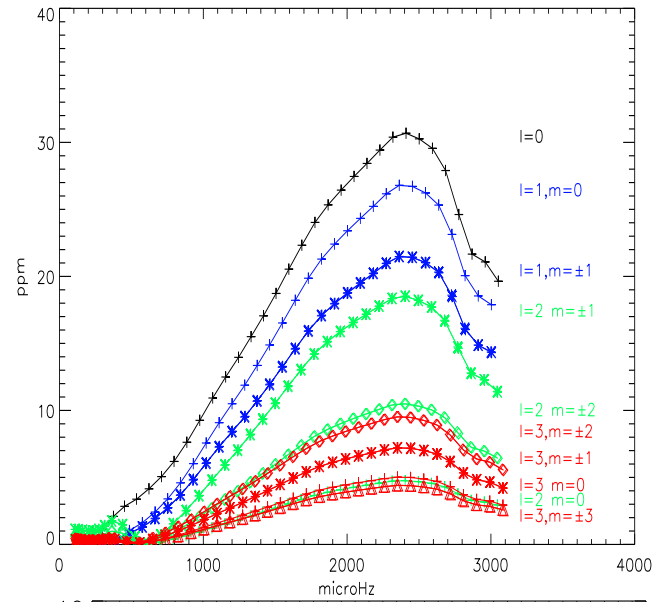
- **Improving the algorithm for :**
  - Fully automatic research
  - Find a criteria to select the modes form the different computed estimators
  - When a fit fails:
    - To reduce the number of free parameters
    - Using general trends for Amplitude & Line-width

- **How to determine the splitting????**
  - Is it a key parameter for the Stellar models????
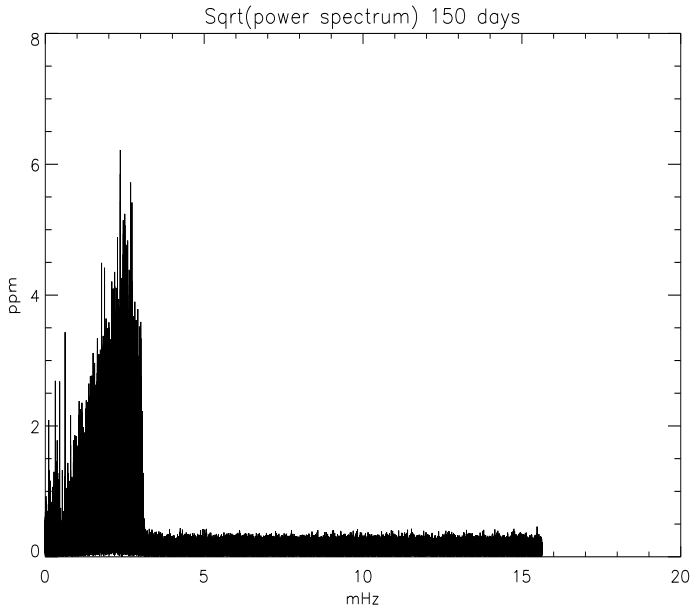
Rafael A. García

# HD49933

# HD 49933



Sqrt(power spectrum) 150 days





Sqrt(power spectrum) 150 days ZOOM

# HD 49933. $\ell = 0$, $\nu_{in} - \nu_{out}$



$\ell=0$, TA

$\ell=0$, TA

$\ell=0$, TT

# HD 49933. $\ell = 1, \nu_{in} - \nu_{out}$



$\ell=1$, TA

$\ell=1$, TA

$\ell=1$, TT

3

HD 49933. $\ell = 2$, $\nu_{in} - \nu_{out}$

# HD 49933. $\ell = 3$, $\nu_{in} - \nu_{out}$



$\ell=3$, TA

$\ell=3$, TA
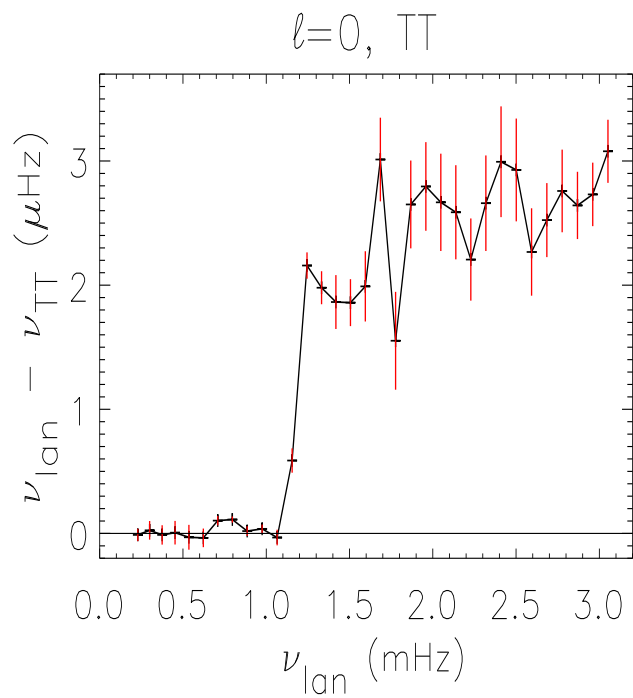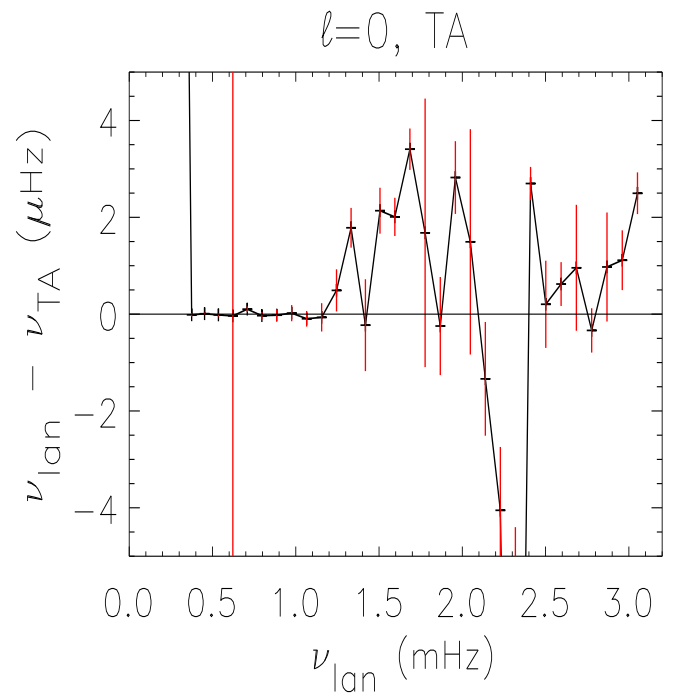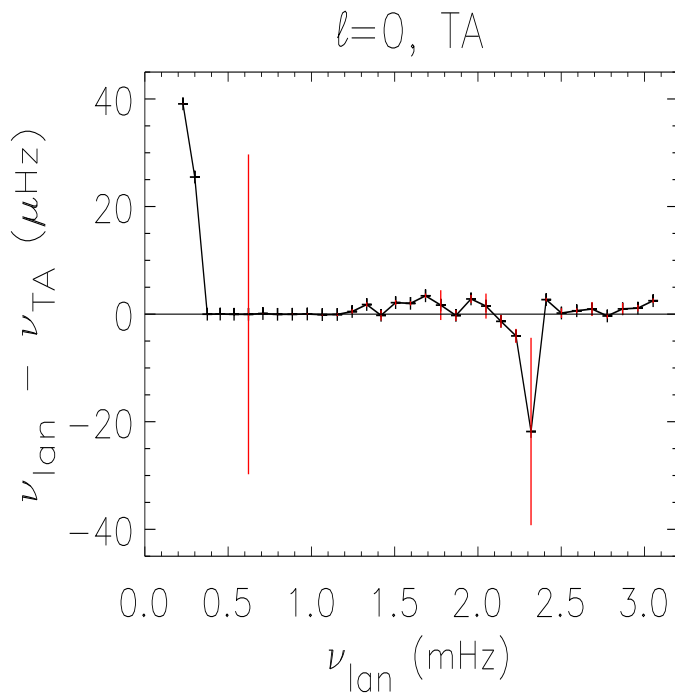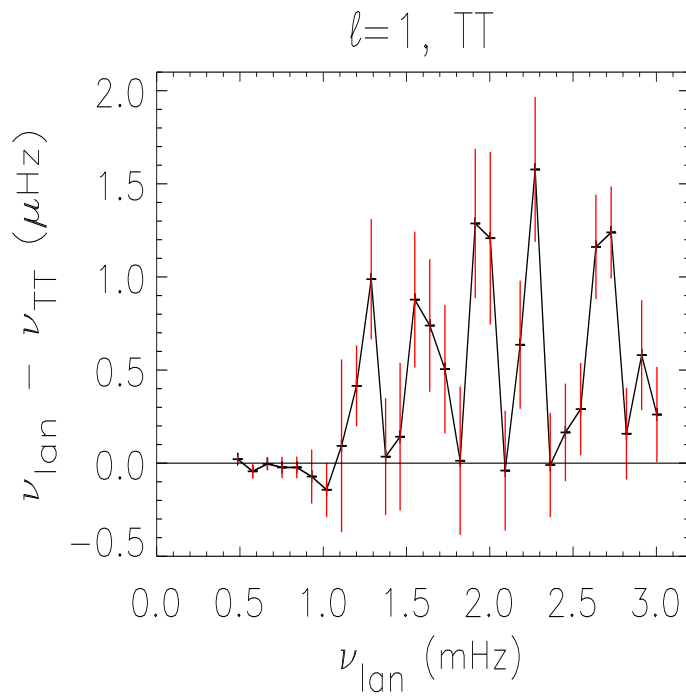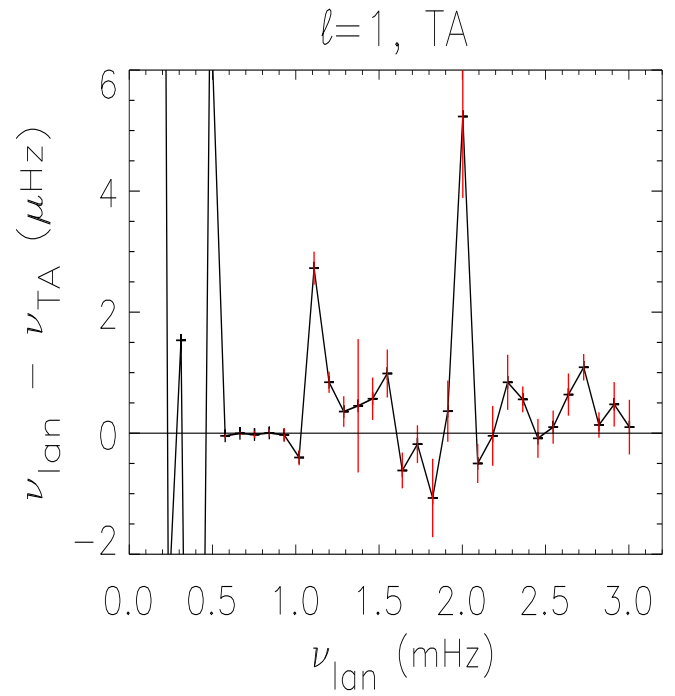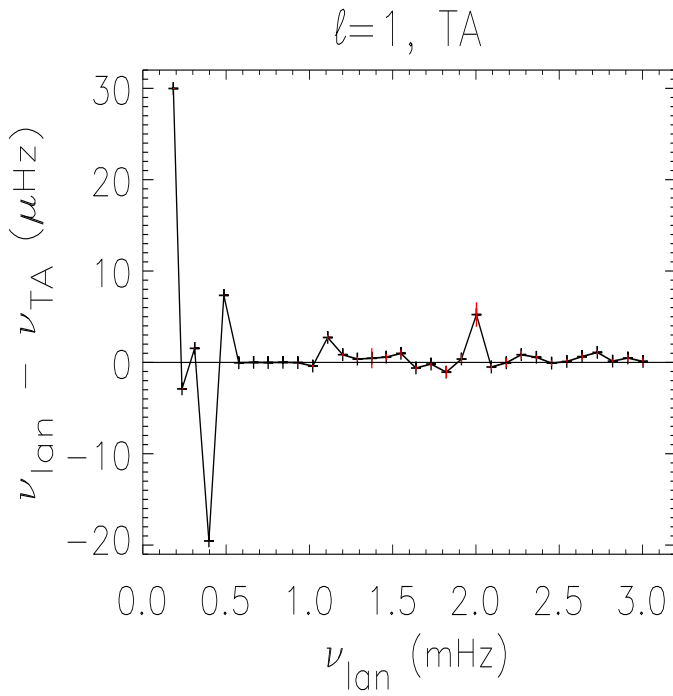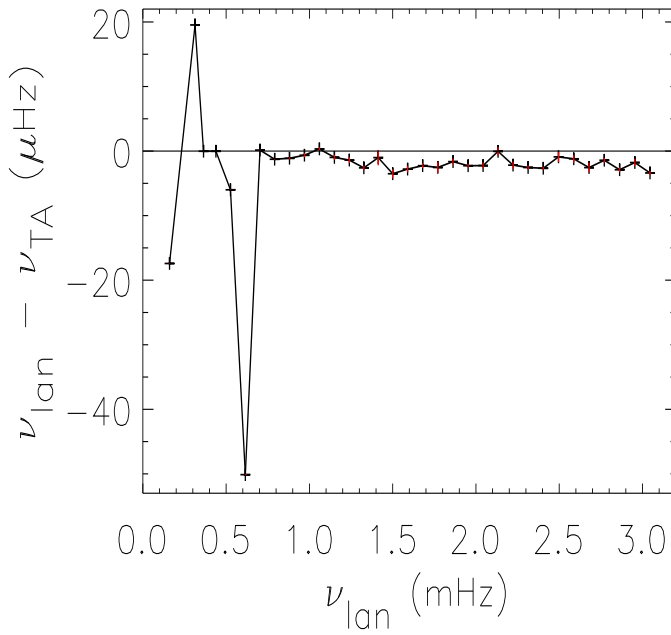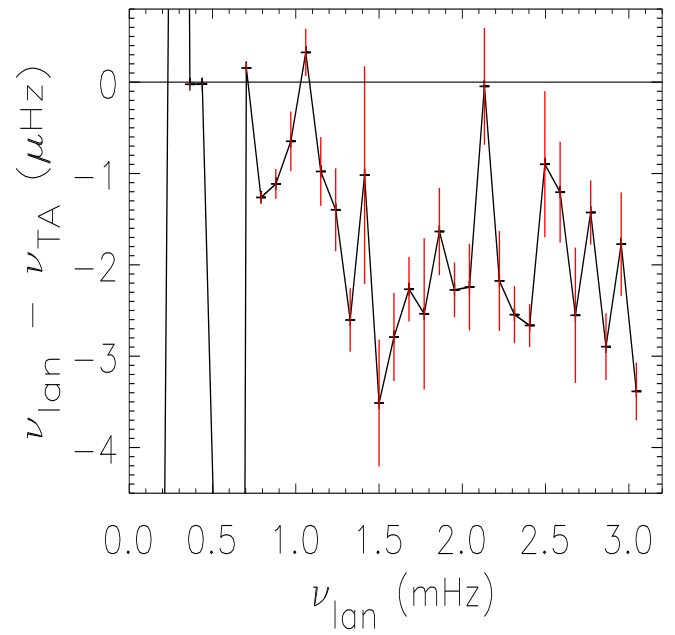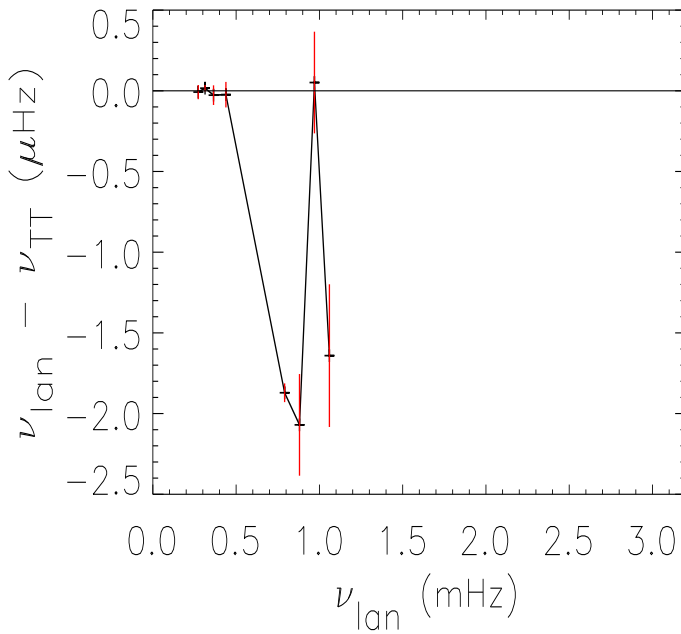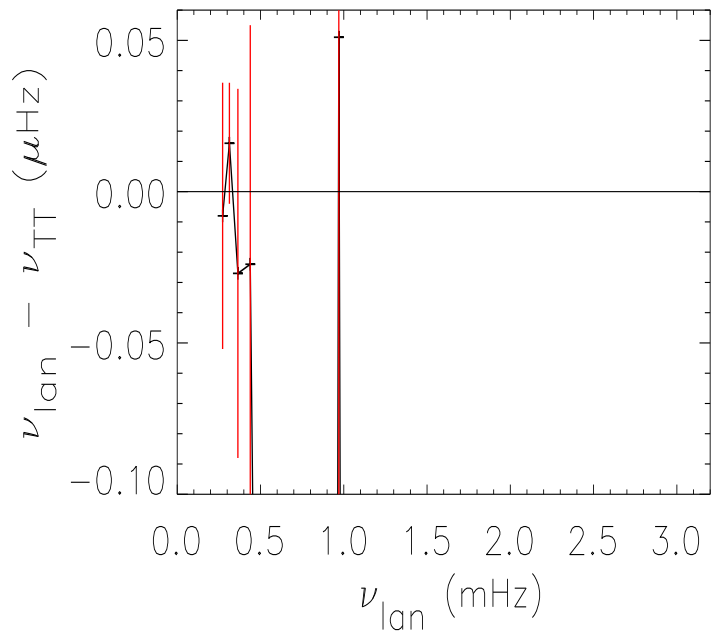
$\ell=3$, TT
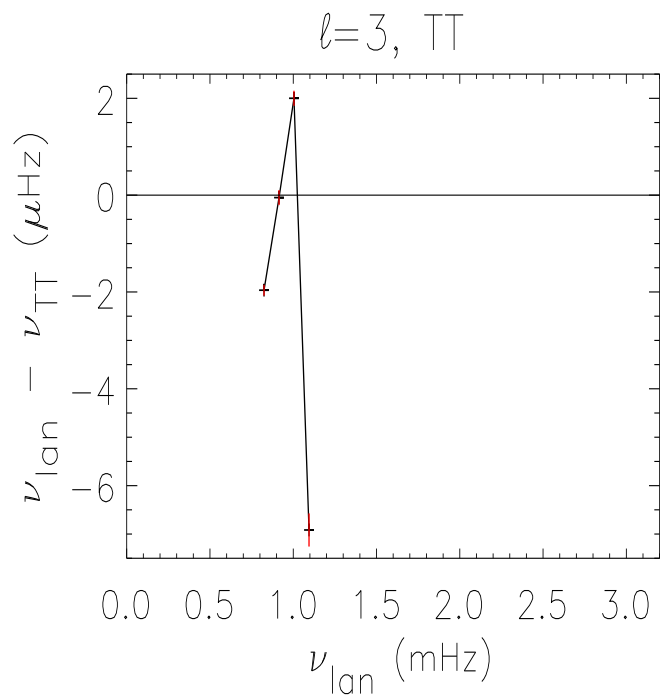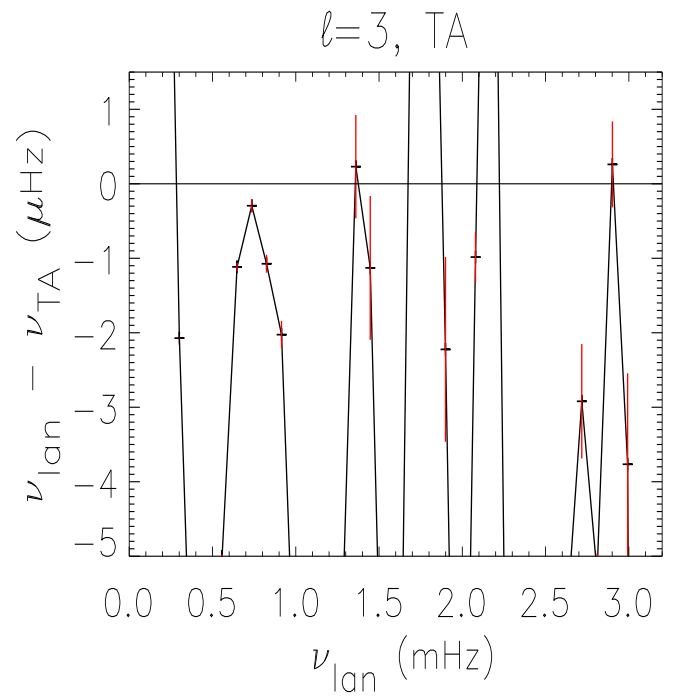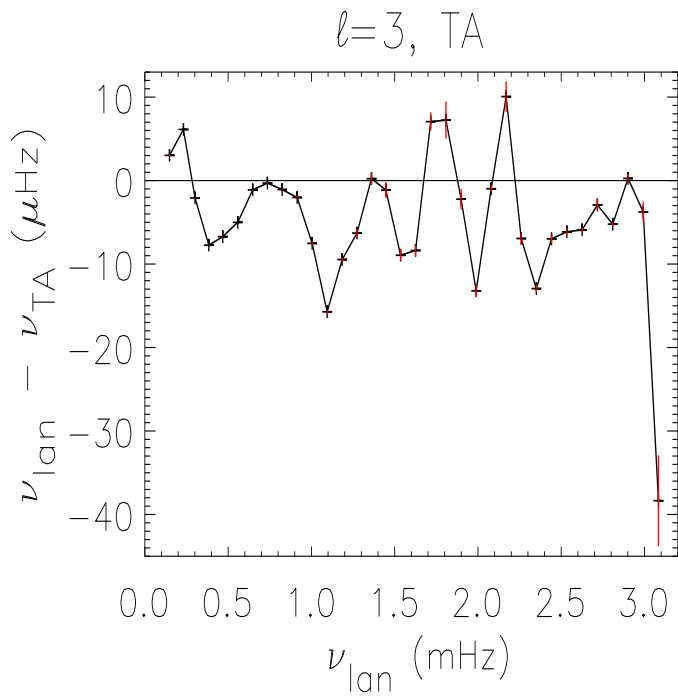
# HD 49933. $\ell = 1,\ \frac{dnu}{m}(in) - \frac{dnu}{m}(out)$



$\ell=1,\ TA$

$(dnu/m)_{lan} - (dnu/m)_{TA}$
$(\mu Hz)$

$\nu_{lan}\ (mHz)$



$\ell=1,\ TT$

$(dnu/m)_{lan} - (dnu/m)_{TT}$
$(\mu Hz)$

$\nu_{lan}\ (mHz)$
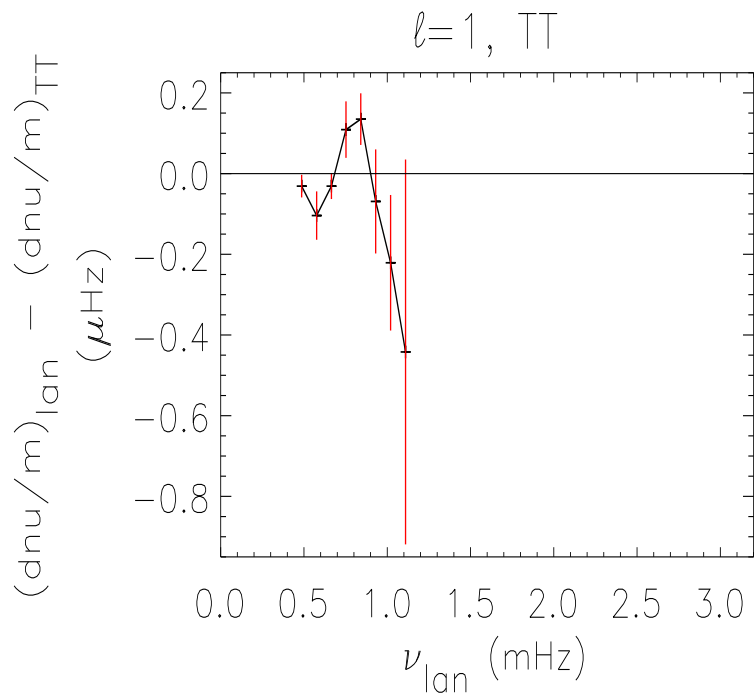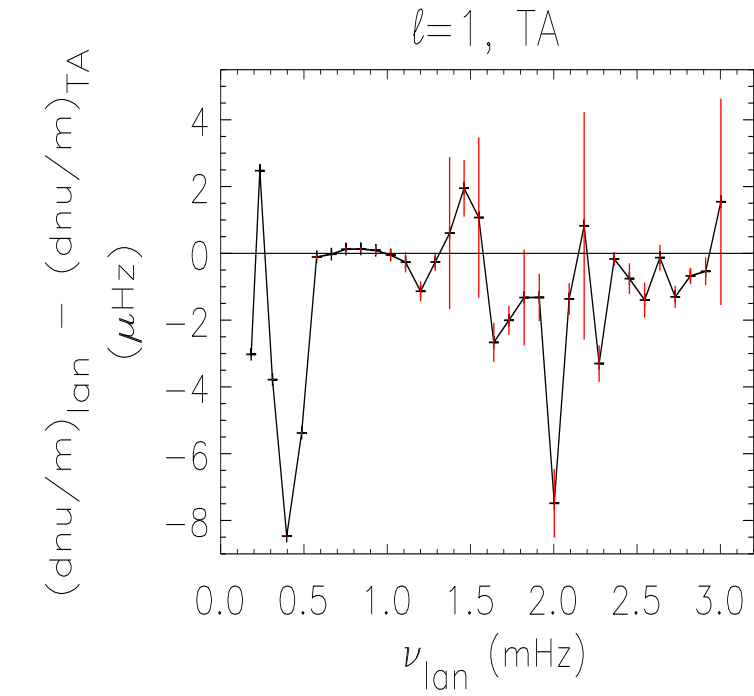
HD 49933. $\ell = 2, \frac{dnu}{m}(in) - \frac{dnu}{m}(out)$

$\ell=2$, TA

$\ell=2$, TA

$\ell=2$, TT
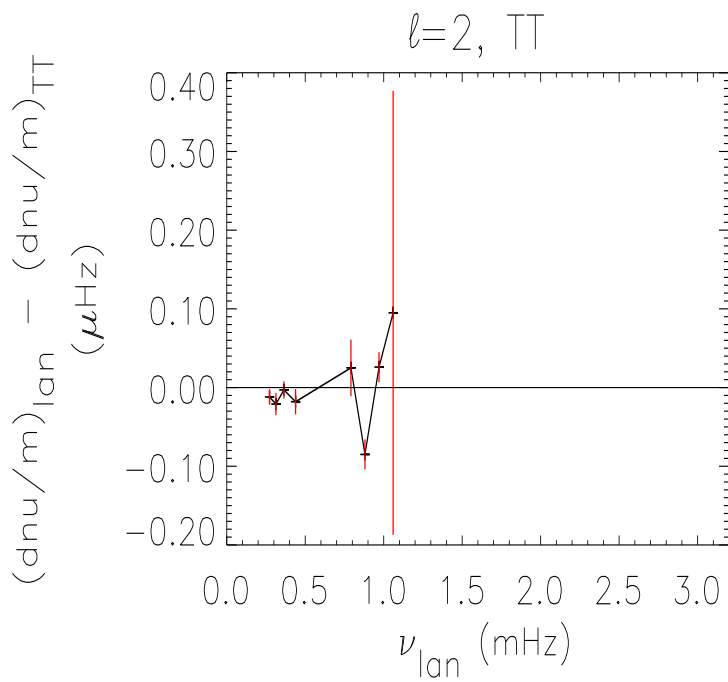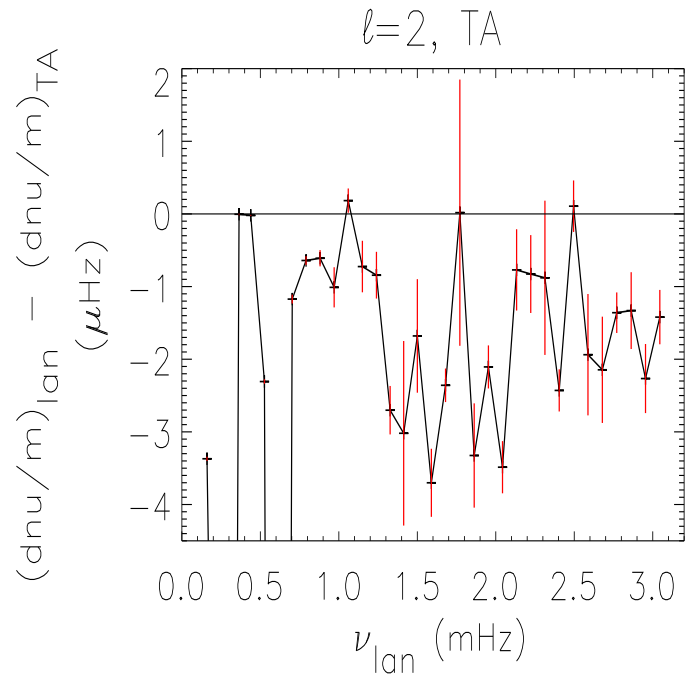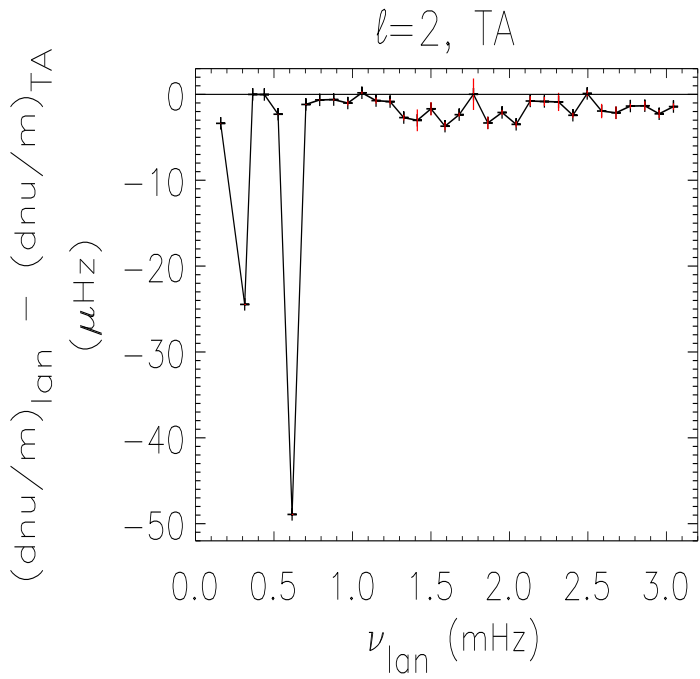
HD 49933. $\ell = 3$, $\frac{dnu}{m}(in) - \frac{dnu}{m}(out)$

HD 49933. i=58.6°

TA

I=1
I=2

Angle (degree)

$\nu_{TA}$ (mHz)
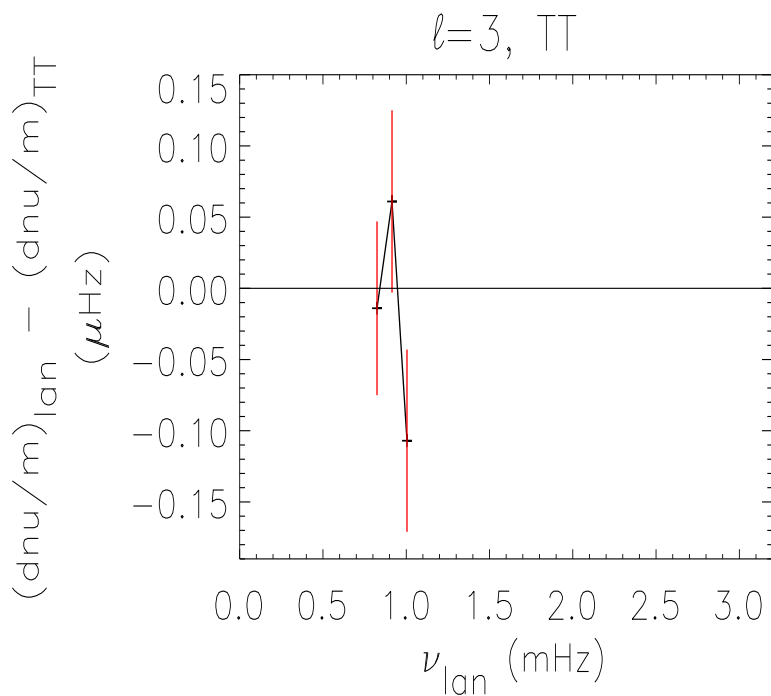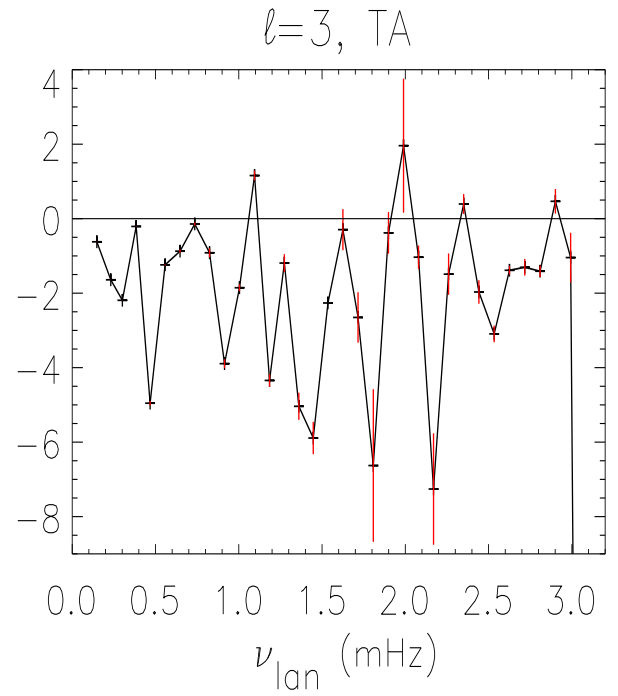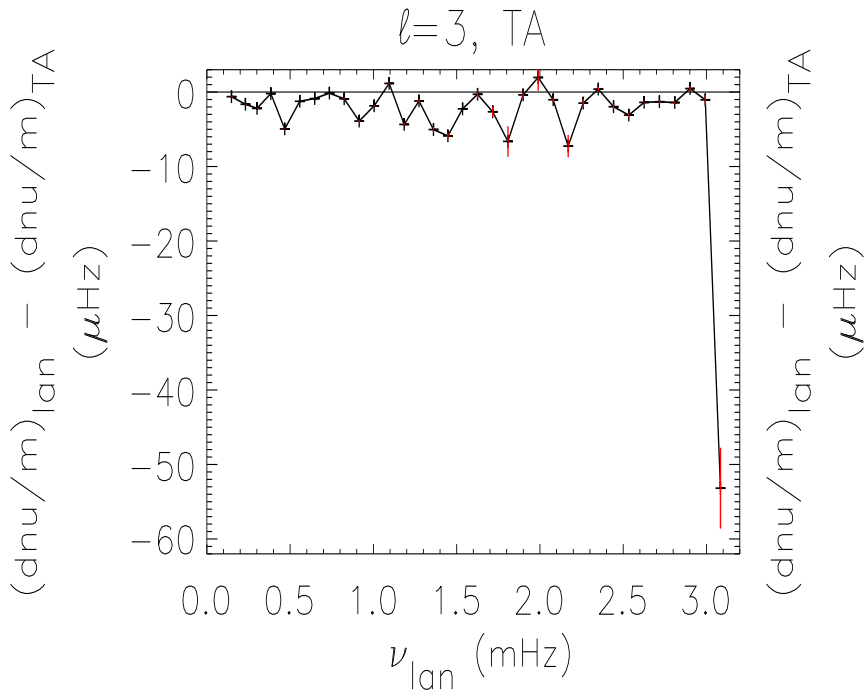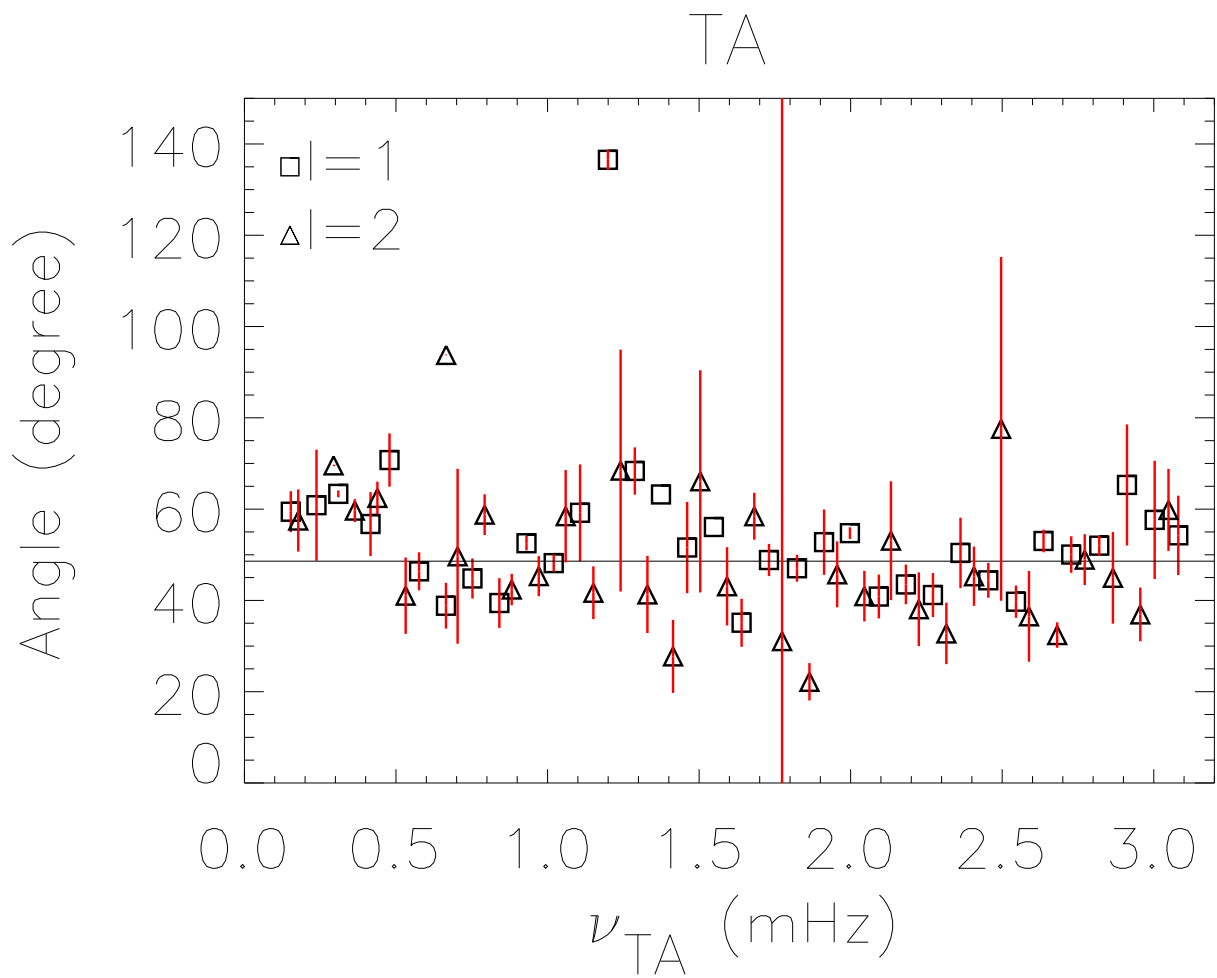
# HD 49933 — Seismic Interpretation

Anwesh Mazumdar

*Observatoire de Paris-Meudon, France*

Collaborators: Jeremie Lochard, E. Michel and M-J. Goupil

# Overview

We report on the seismic interpretation of the frequencies of the star HD 49933.

## Global Parameters of HD 49933

- $T_{eff} = 6700 \pm 100$ K

- $M_{bol} = 3.35 \pm 0.10$

- $[Fe/H] = -0.32 \pm 0.10$

- $vsini = 10 \pm 4$ km/s

- Original model produced by Ian Roxburgh

- Time series produced by Caroline Barban

- Frequencies extracted by Thierry Appourchaux

# Before the Models ....

## Estimation of acoustic depths of base of CZ and HeII ionisation zone
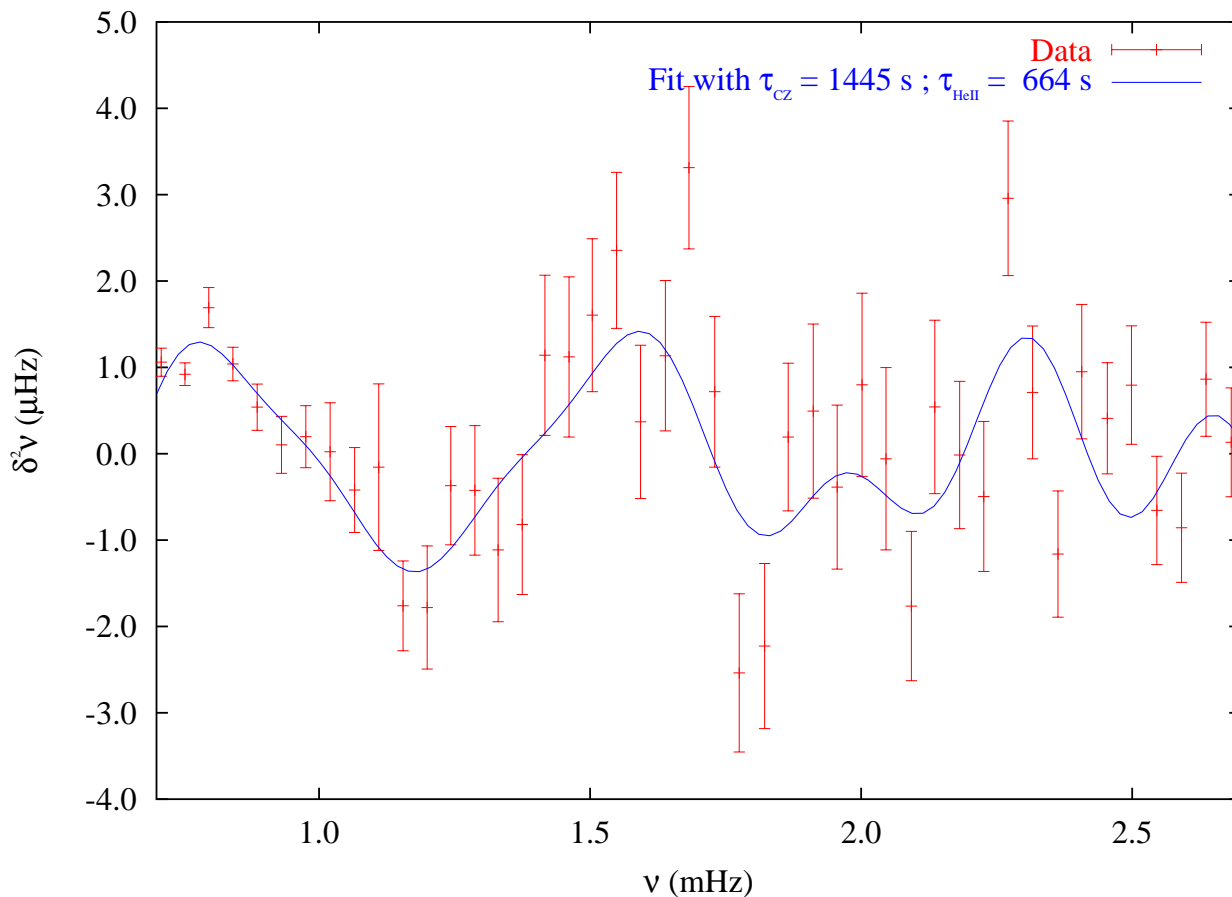
Discontinuities in sound speed derivatives at the HeII ionisation zone and the base of the convective envelope give rise to oscillations in the frequencies.

We fit a function of the form

$$\delta^2\nu(n, \ell) = \left(a_0 + \frac{a_1}{\nu_{n,\ell}} + \frac{a_2}{\nu_{n,\ell}^2}\right) \sin(4\,\pi\nu_{n,\ell}\,\tau_{CZ} + \phi_{CZ})$$

$$+ \left(b_0 + \frac{b_1}{\nu_{n,\ell}} + \frac{b_2}{\nu_{n,\ell}^2}\right) \sin(4\,\pi\nu_{n,\ell}\,\tau_{HeII} + \phi_{HeII})$$

to the second differences of the data, taking into account the errors (Mazumdar & Antia 2001).

## Estimation of acoustic depths of base of CZ and HeII ionisation zone



The fit provides us with values for the acoustic depths of

- the base of the convective envelope: $\tau_{CZ} = 1445 \pm 68$ s

- the HeII ionisation zone: $\tau_{HeII} = 663 \pm 49$ s

These estimates help to search the closest model.

# Stellar Models

Evolutionary tracks were computed with CESAM using

- CEFF and OPAL equation of state

- OPAL opacities

- NACRE nuclear reaction rates

- MLT convection

- Eddington atmosphere

- No diffusion

Frequencies were computed with ADIPLS.

# Stellar Models

## Variable parameters of models

- Core overshoot (in $H_P$)     :    $d_{ov}$   :    0   —   0.2

- Mixing length (in $H_P$)     :    $\alpha$   :    1.6   —   1.8

- Metallicity     :    $[\text{Fe/H}]$   :   $-0.42$  —  $-0.22$

- Initial Helium abundance   :    $Y_0$   :    0.25   —   0.27

All CESAM models are computed with a "high" precision parameter to avoid irregular features at convective zone boundaries
— more accurate models, but very time-consuming!!

- For a particular combination of these parameters we vary the mass of the model to check for overlap between main sequence tracks and the global parameters of HD 49933 on the HR diagram.

- Compare large and small separations of the "data" with the computed values to find the closest possible model.

# Nature of the Data

Total of $79$ frequencies : $(\ell = 0 : 37, \ell = 1 : 30, \ell = 2 : 8, \ell = 3 : 4)$

## Large Separations

$$\Delta_{n\ell} = \nu_{n+1,\ell} - \nu_{n,\ell} \qquad \ell = 0, 1, 2, 3$$

$$\Delta_{n\ell} = \nu_{n+1,\ell} - \nu_{n,\ell} \qquad \ell = 0, 1, 2, 3$$
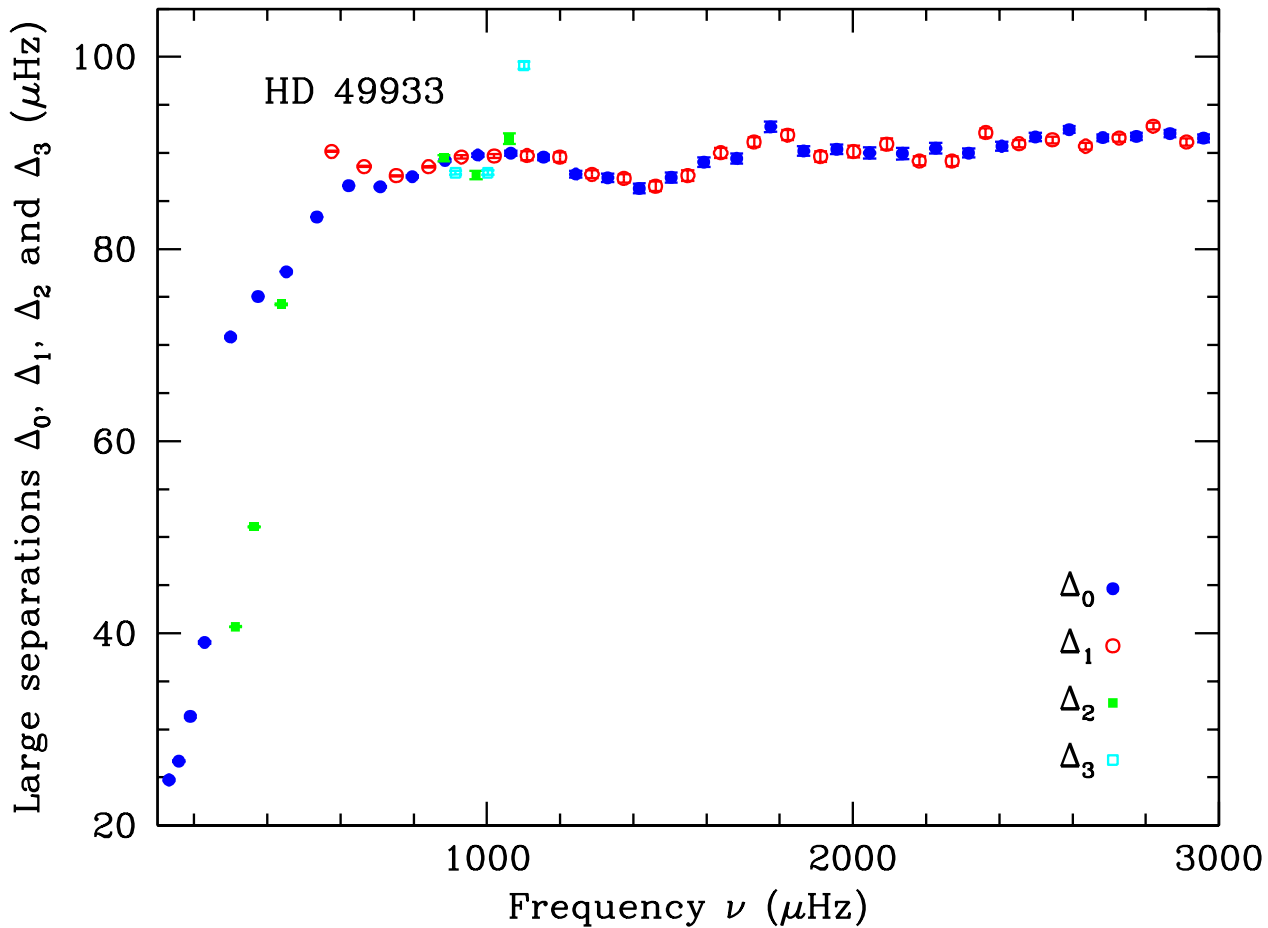
# Nature of the Data
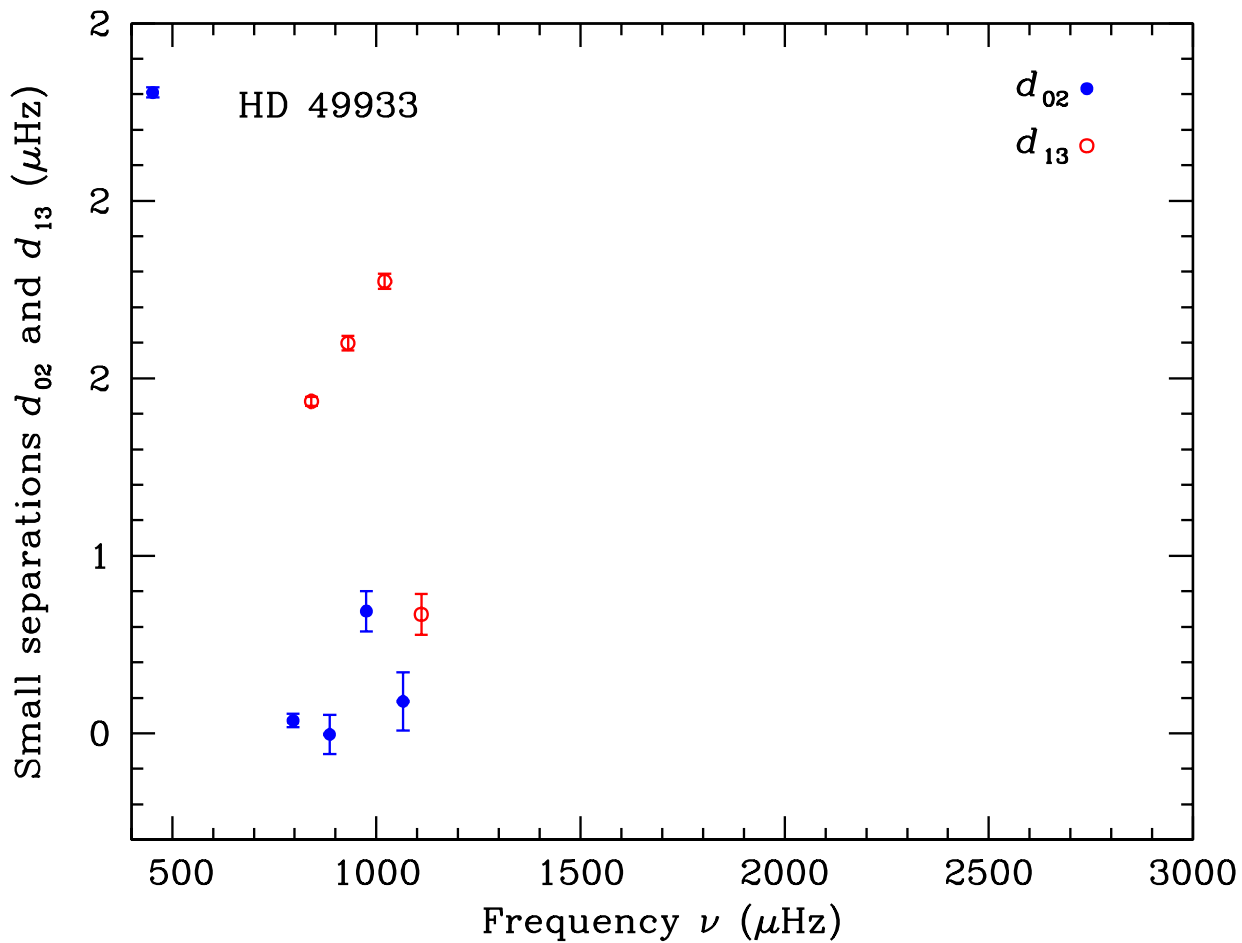
## Small Separations

- Between $\ell = 0,\ 2$ modes and $\ell = 1,\ 3$ modes:

$$d_{02} = [\nu_{n,0} - \nu_{n-1,2}]/6$$

$$d_{13} = [\nu_{n,1} - \nu_{n-1,3}]/10$$

# Nature of the Data
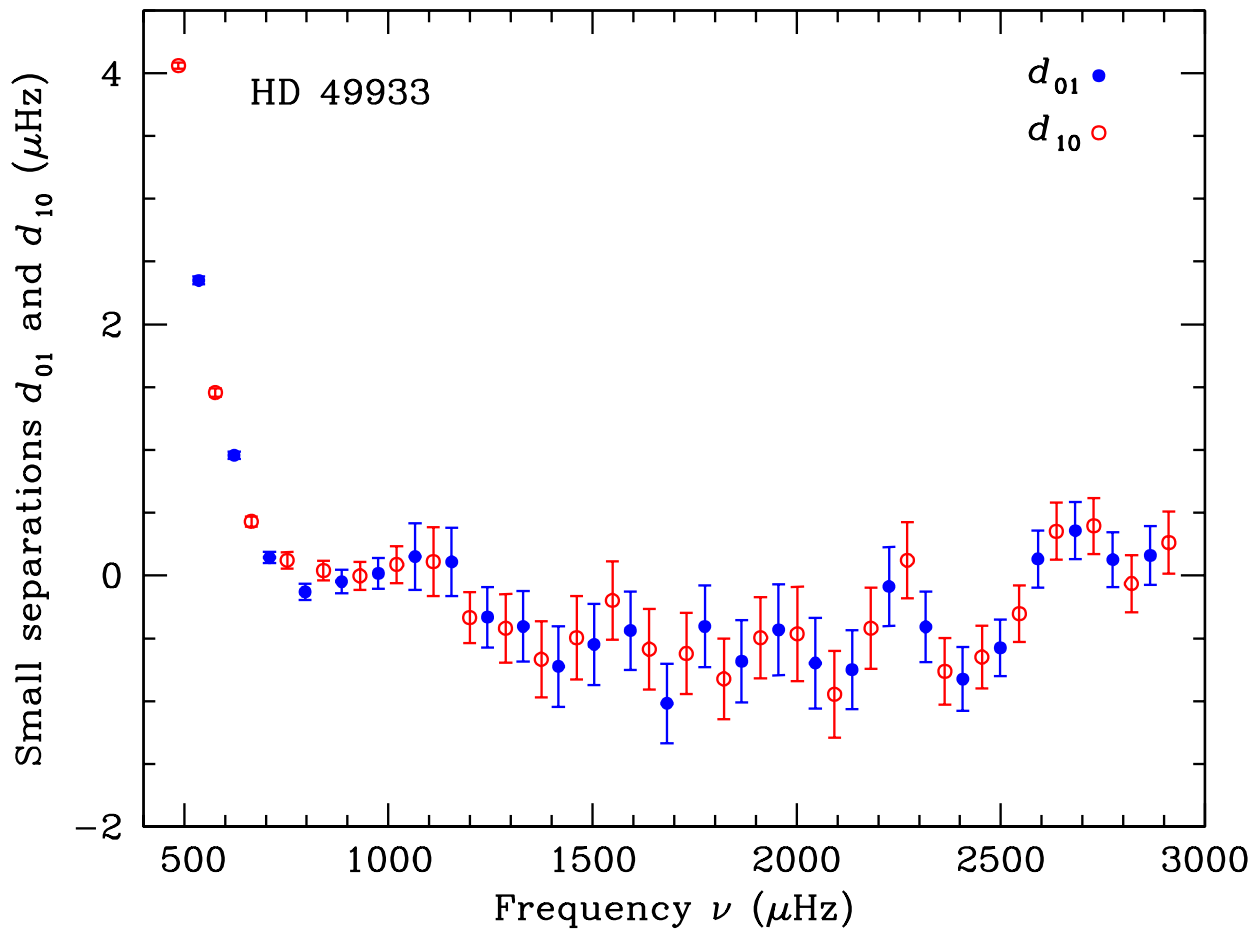
## Small Separations

- Between $\ell = 0,\ 1$ modes:

$$d_{01} = \quad [\nu_{n,0} - (\nu_{n,1} + \nu_{n-1,1})/2]/2$$

$$d_{10} = -[\nu_{n,1} + (\nu_{n,0} + \nu_{n+1,0})/2]/2$$

# Approaching the closest model

- Average value of large separation provides initial estimate of the mean density of the model:

$$\bar{\rho}/\bar{\rho}_\odot \sim 0.46$$

- Explore the sensitivity of different features of the large separations to the six model parameters:

$$M, Age, Y, [Fe/H], d_{ov}, \alpha$$

- Fitted values of the $\tau_{CZ}$ and $\tau_{HeII}$ provide strong indication.

**Approaching the closest model**
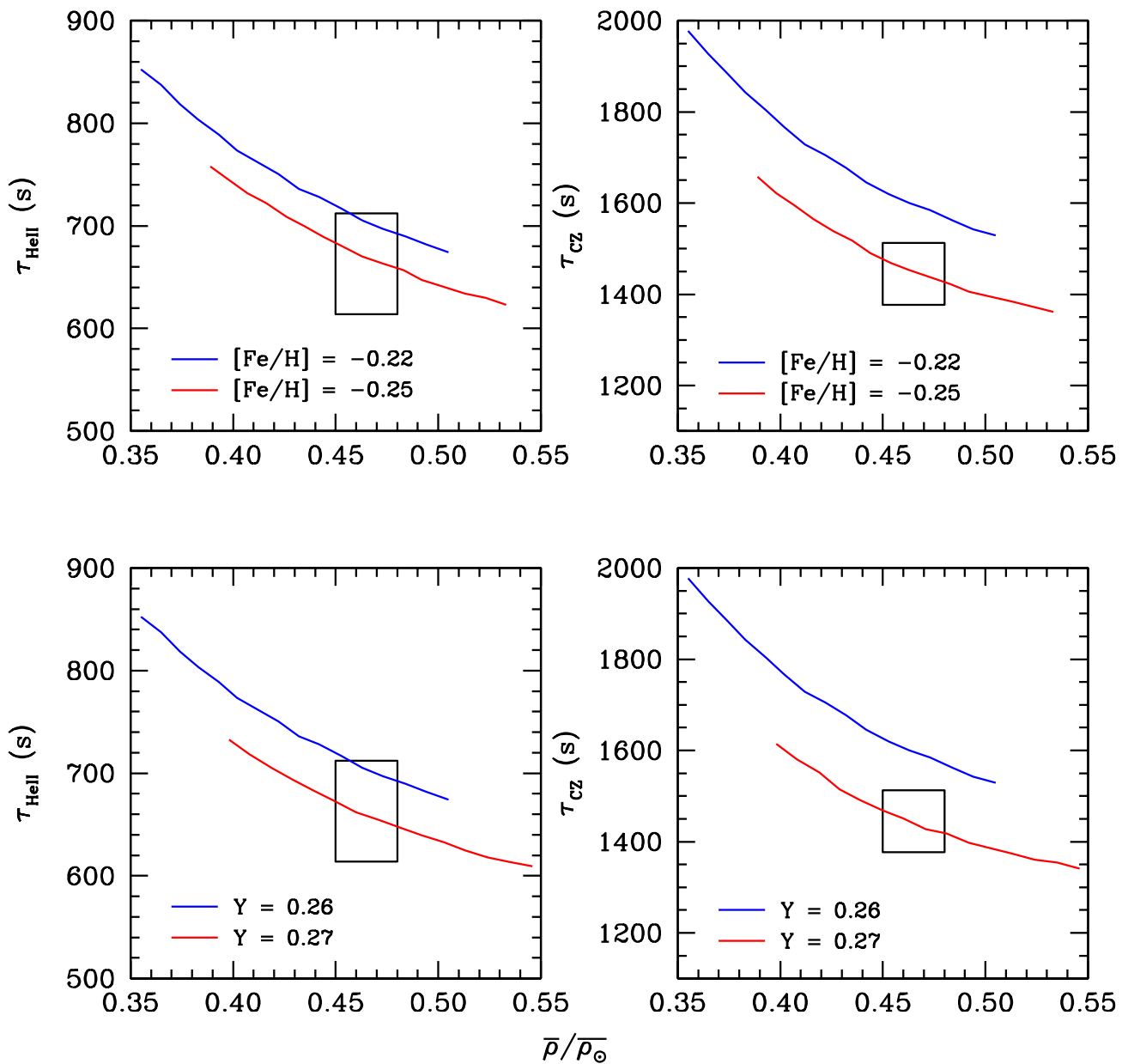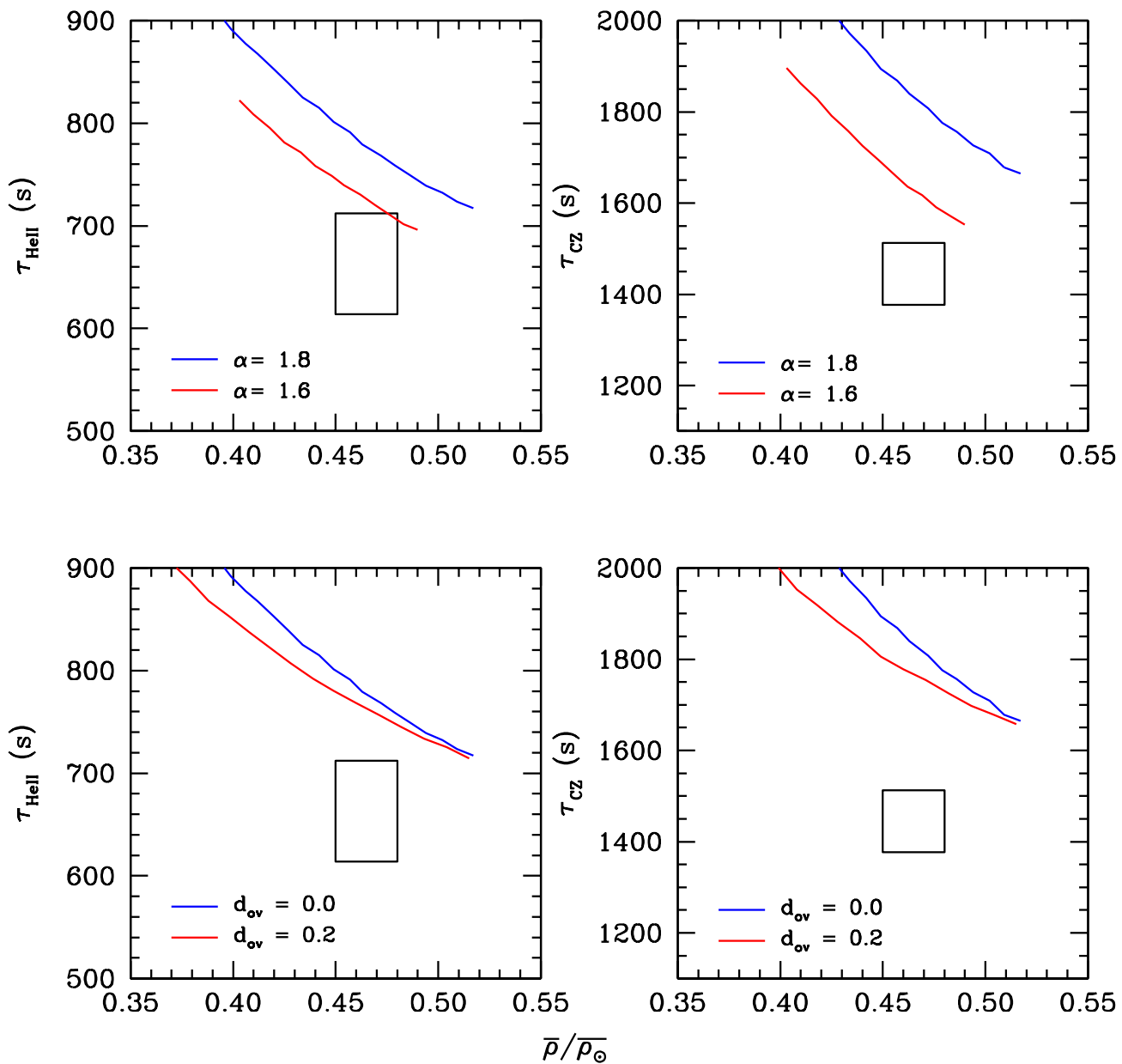
# Approaching the closest model
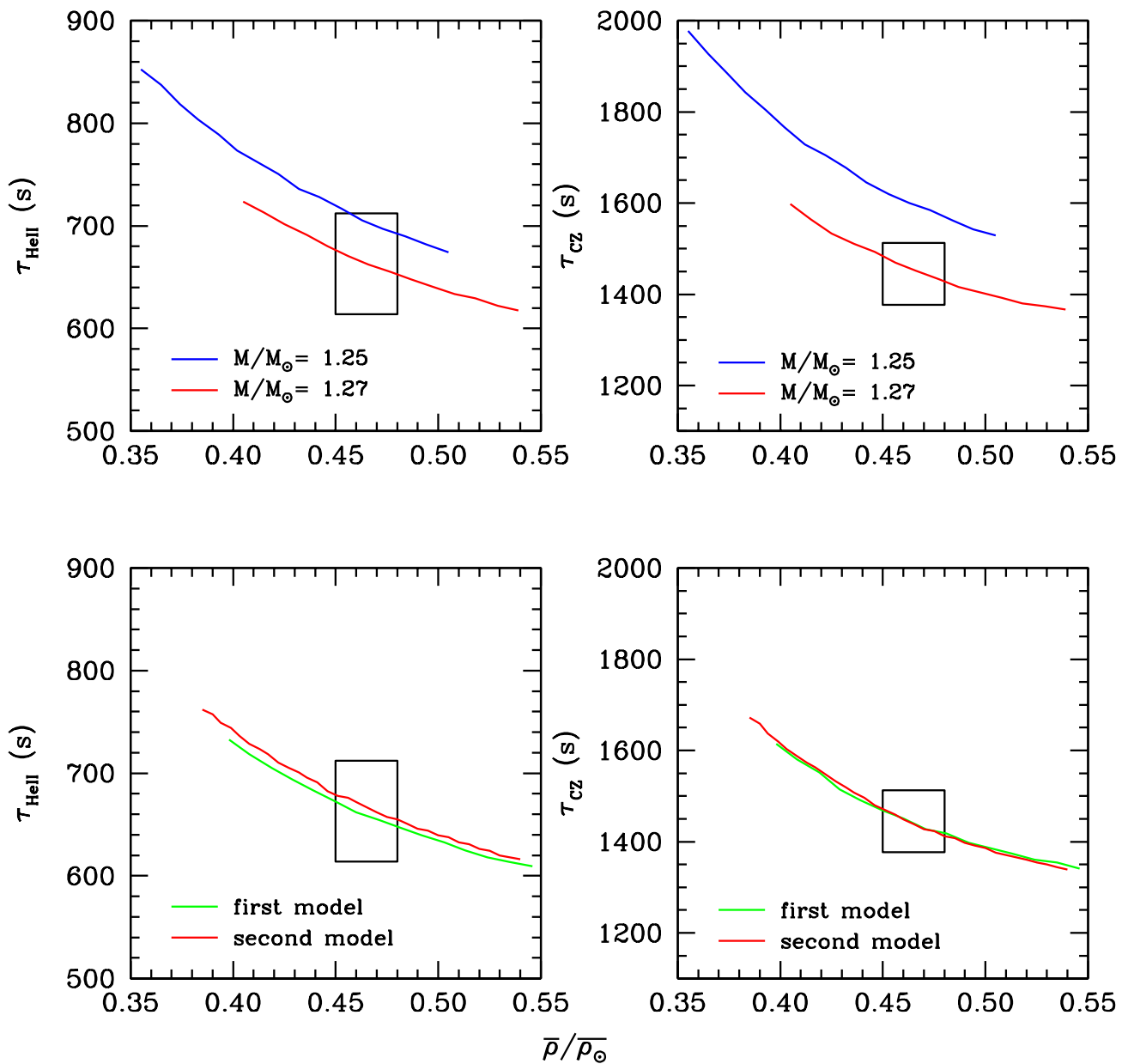
# Approaching the closest model

- Small separations between $\ell = 0, 1$ modes in the data have unusually small and even negative values!

- Small separations between $\ell = 0, 2$ modes are hardly available in the data.

- Inability to match the small separations between $\ell = 0, 1$ modes with any combination of parameters.

- Several "best case" scenarios are identified, based on the large separations alone and a comparison of the deviations of the models from the data is made to select the closest model.

# Closest Model

We have two close models for HD 49933.
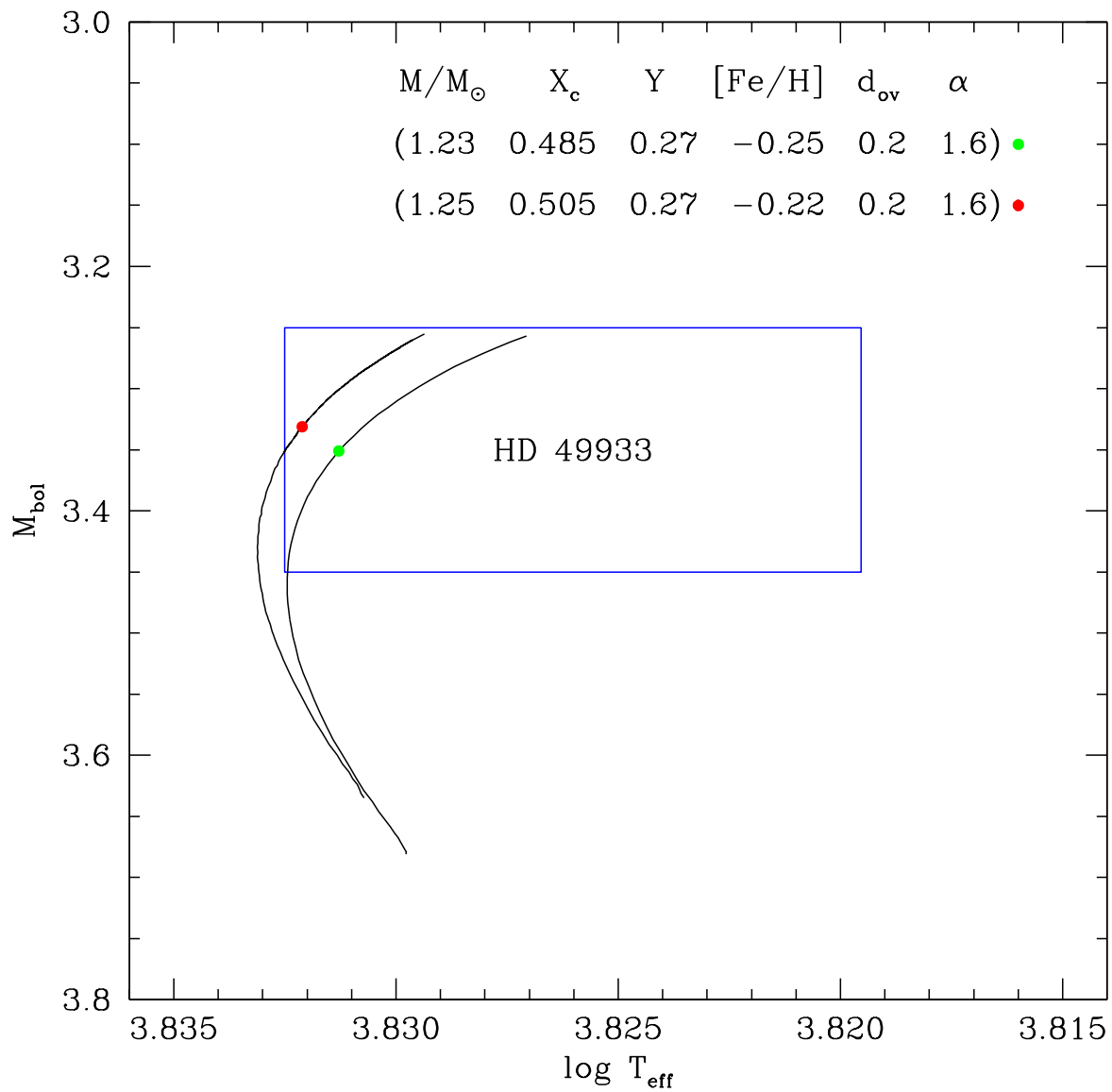
# Closest Model

Model Parameters:

- $M/M_\odot = 1.23$
- $X_c = 0.485$
- $R/R_\odot = 1.383$
- $Y = 0.27$
- [Fe/H] $= -0.25$
- $d_{ov} = 0.20$
- $\alpha = 1.6$

- $M/M_\odot = 1.25$
- $X_c = 0.505$
- $R/R_\odot = 1.390$
- $Y = 0.27$
- [Fe/H] $= -0.22$
- $d_{ov} = 0.20$
- $\alpha = 1.6$

Model values for

- $\bar{\rho}/\bar{\rho}_\odot = 0.465$
- $\tau_{CZ} = 1410$ s
- $\tau_{HeII} = 653$ s

- $\bar{\rho}/\bar{\rho}_\odot = 0.465$
- $\tau_{CZ} = 1438$ s
- $\tau_{HeII} = 667$ s

# Closest Model
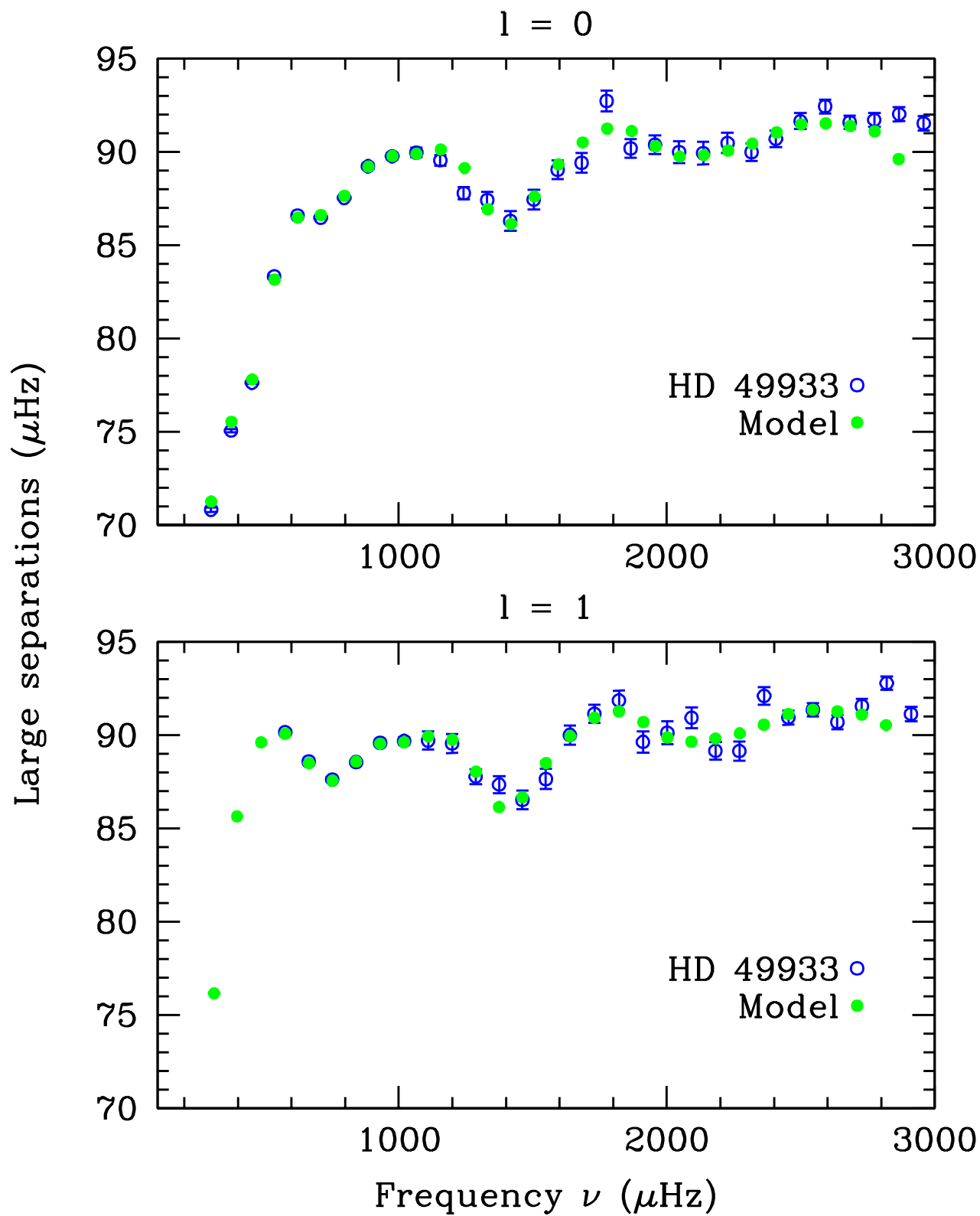
**Closest Model**
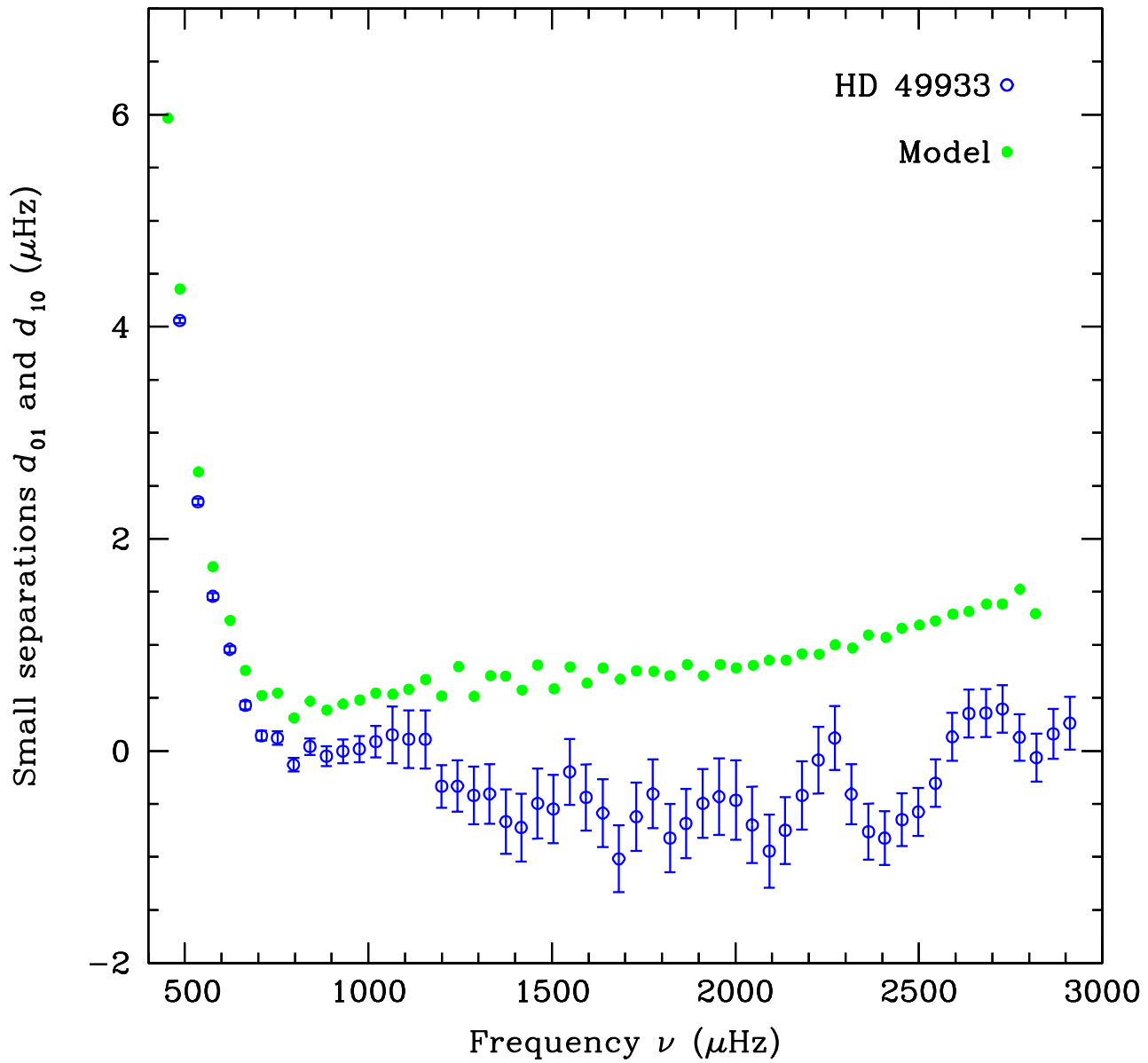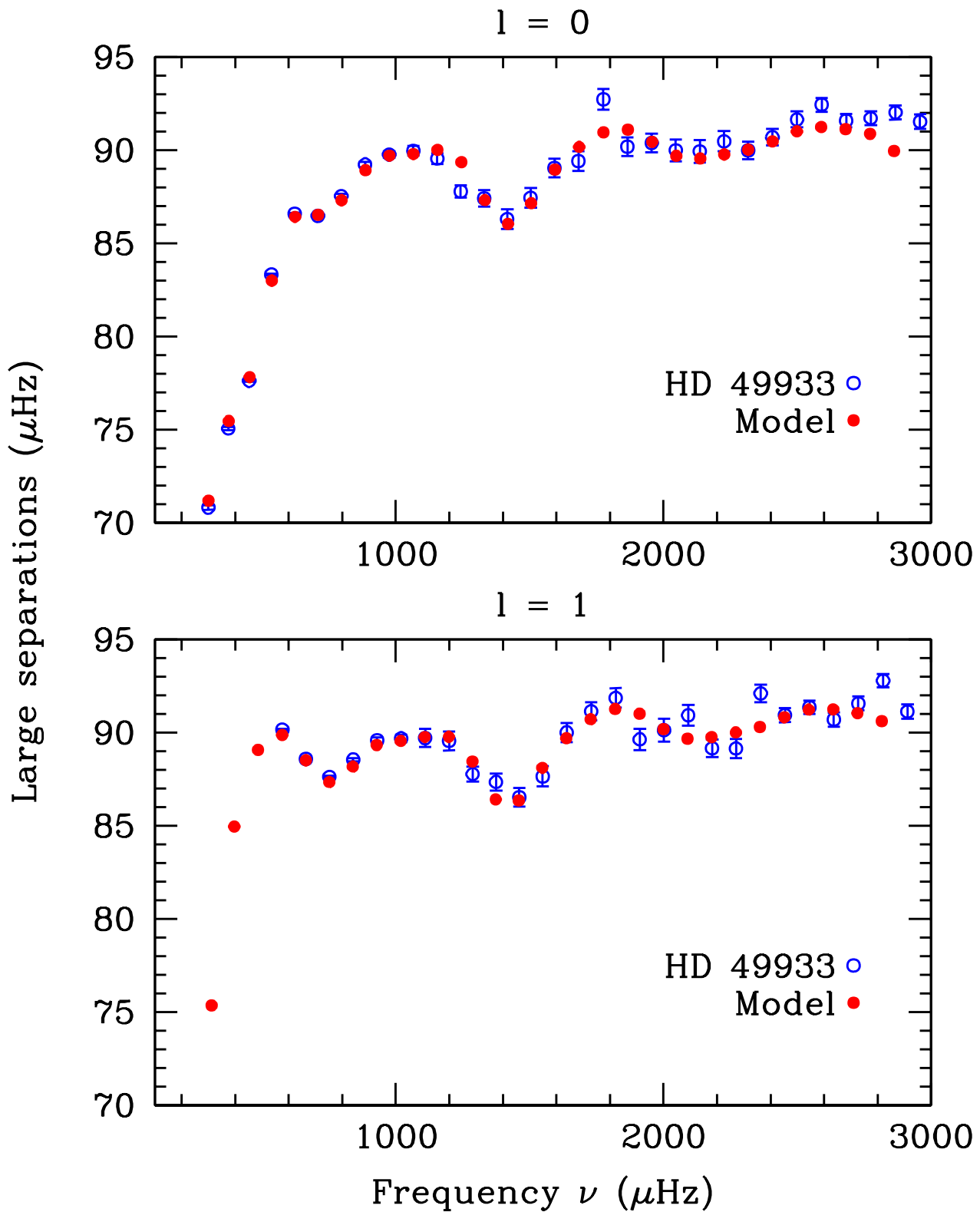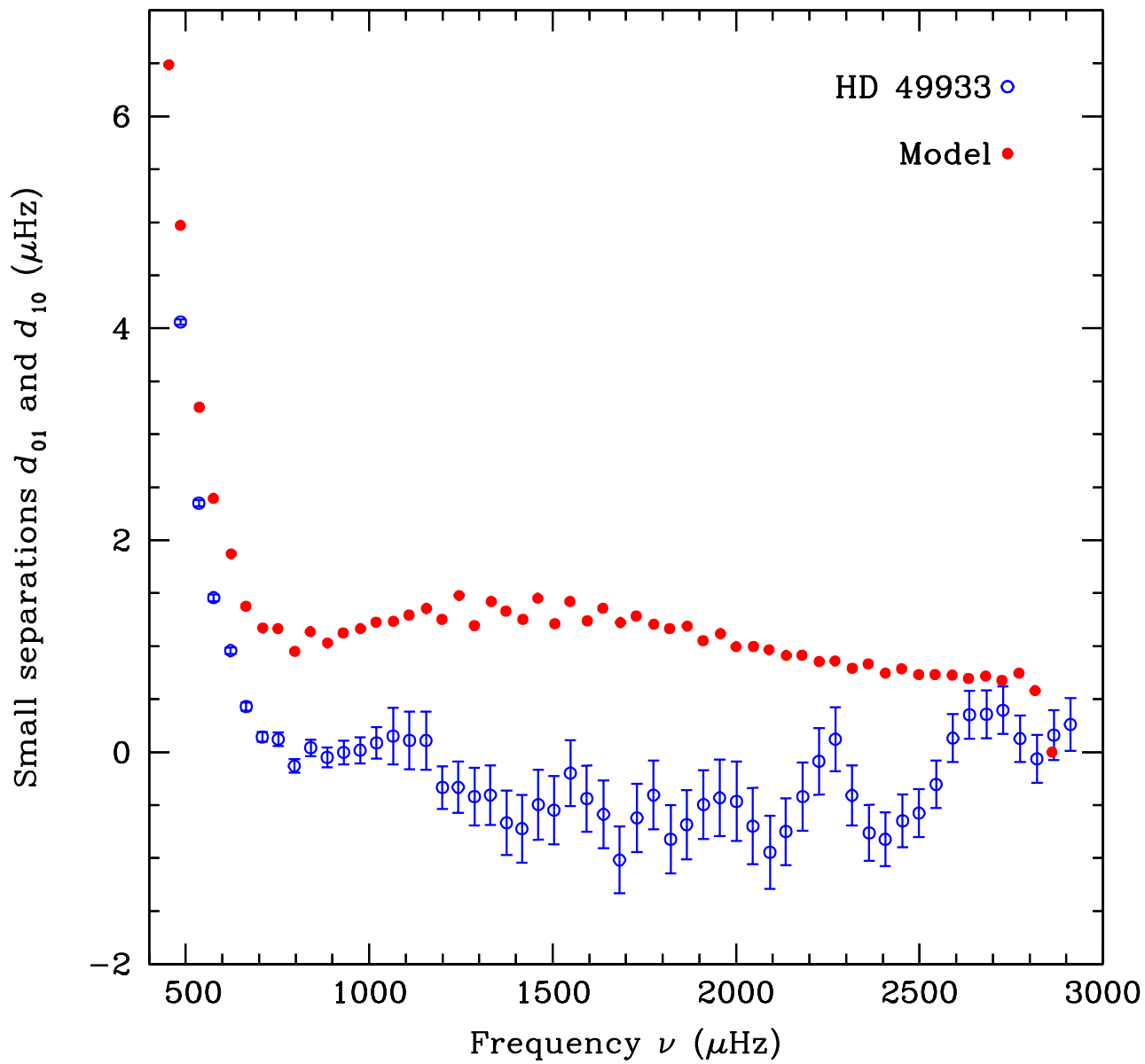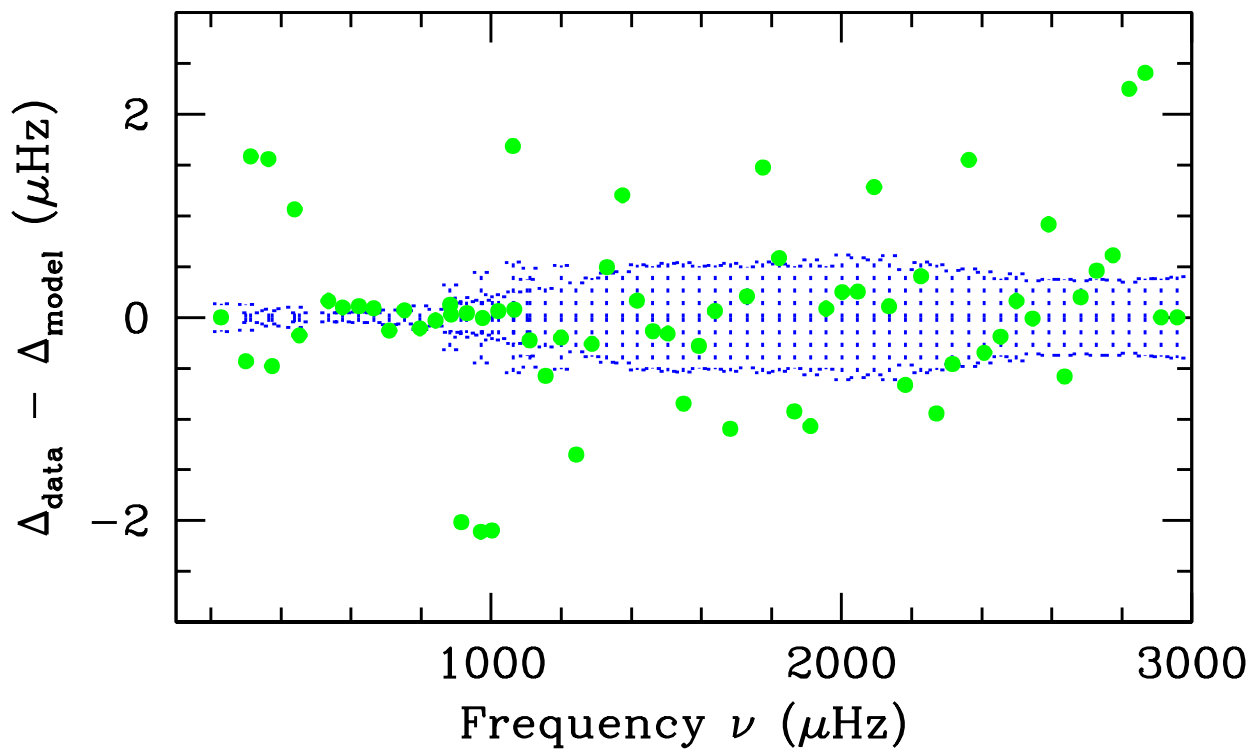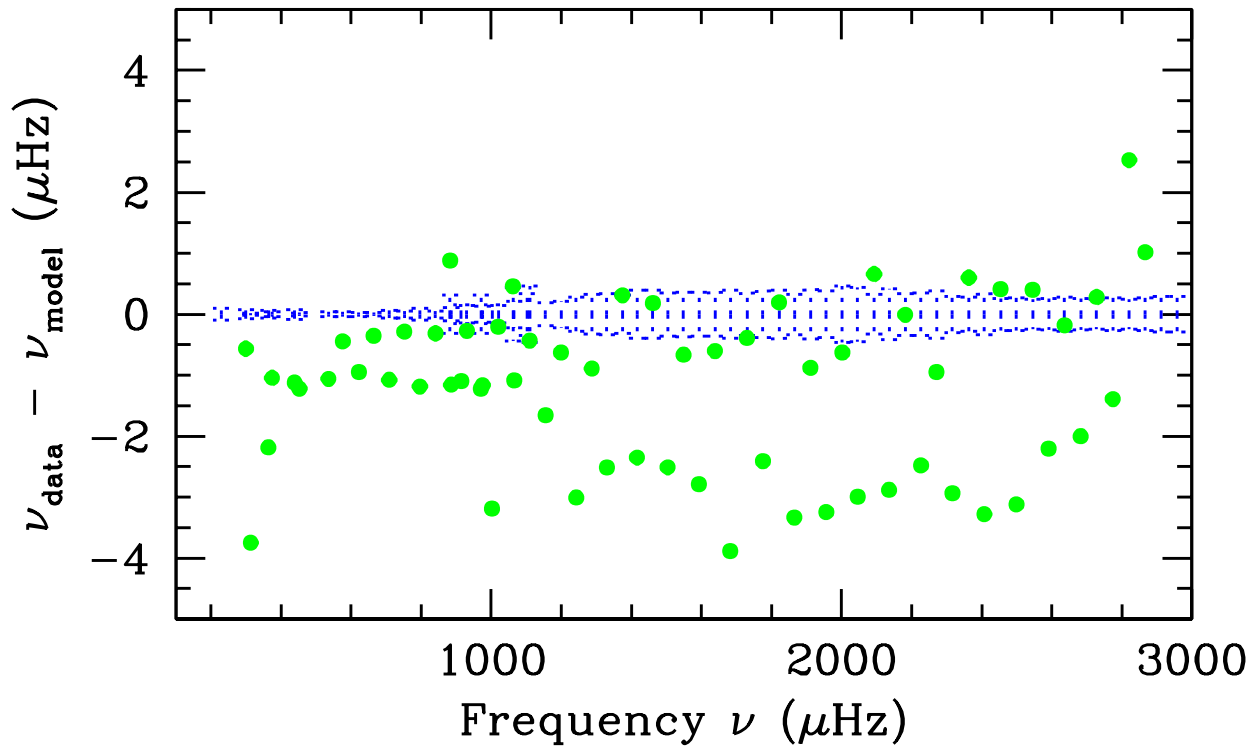
**Closest Model**

**Closest Model**
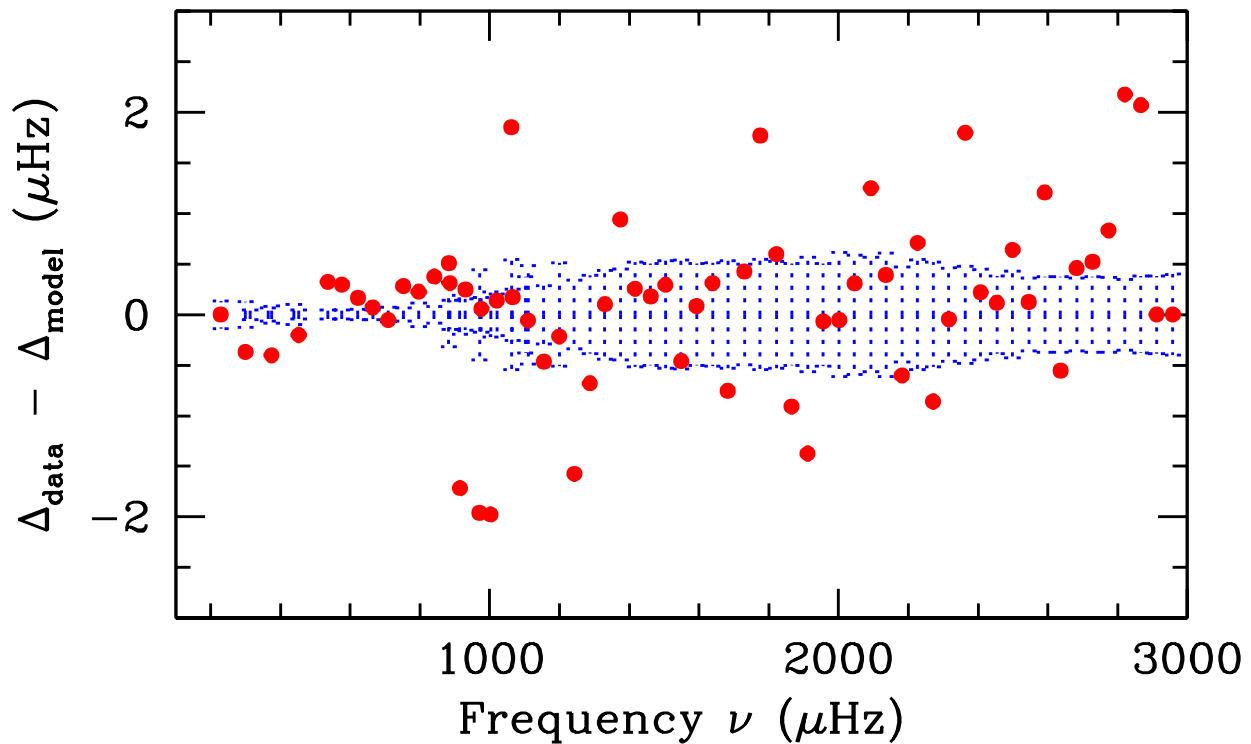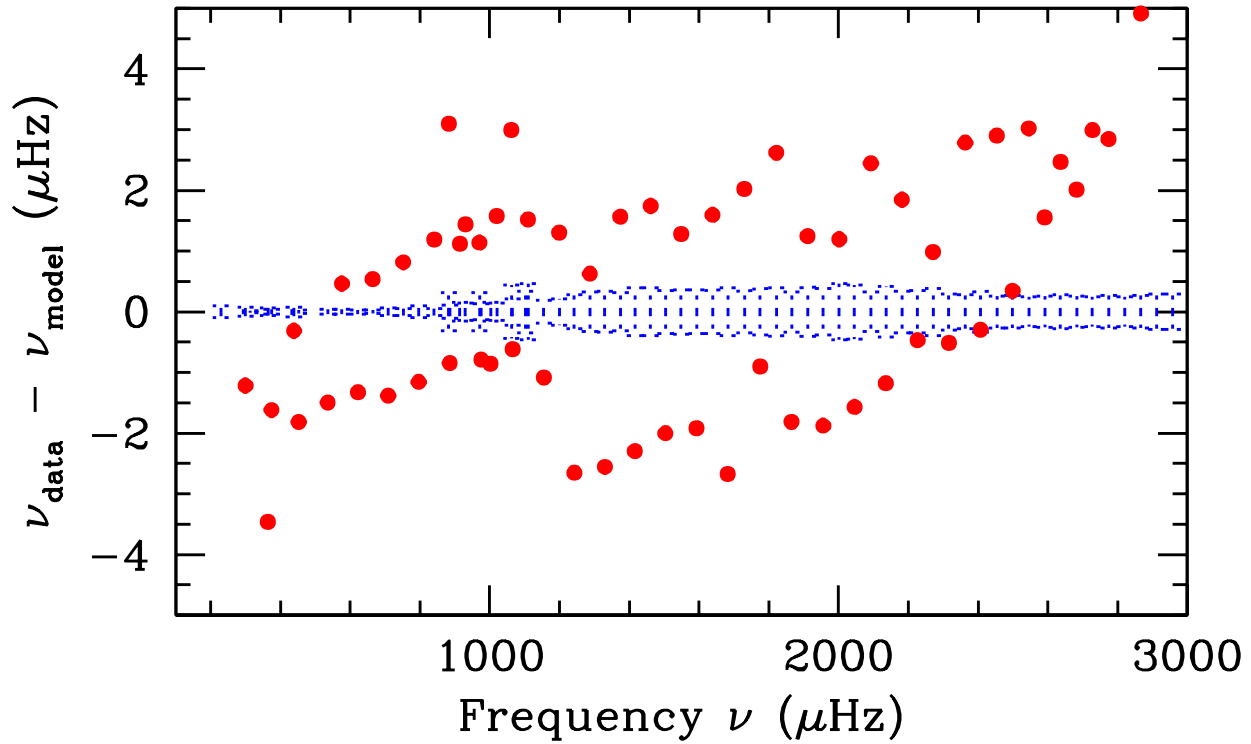
# Conclusions

- We could obtain close match between the large separations in the data and a model.

- The small separations of all models that we considered were much higher than the values obtained from the data.

- Our model is likely to be a good approximation of the original model in the outer layers, but lack of constraints from the small separations prevents gaining information about the inner layers.

- The sensitivity of the $\tau_{CZ}$ and $\tau_{HeII}$ on the model parameters provides good indication of what is to be changed from an initial trial model.

- The unusual values of the small separations might be indicative of misidentification of modes, or model inconsistencies in the inner layers. Or,...

it is a goldmine of information!

# Postscript

There might be misidentification of modes between $\ell = 0$ and $2$.

In that case, $d_{01} \to -d_{21}/2$ and $d_{10} \to -d_{12}/2$.
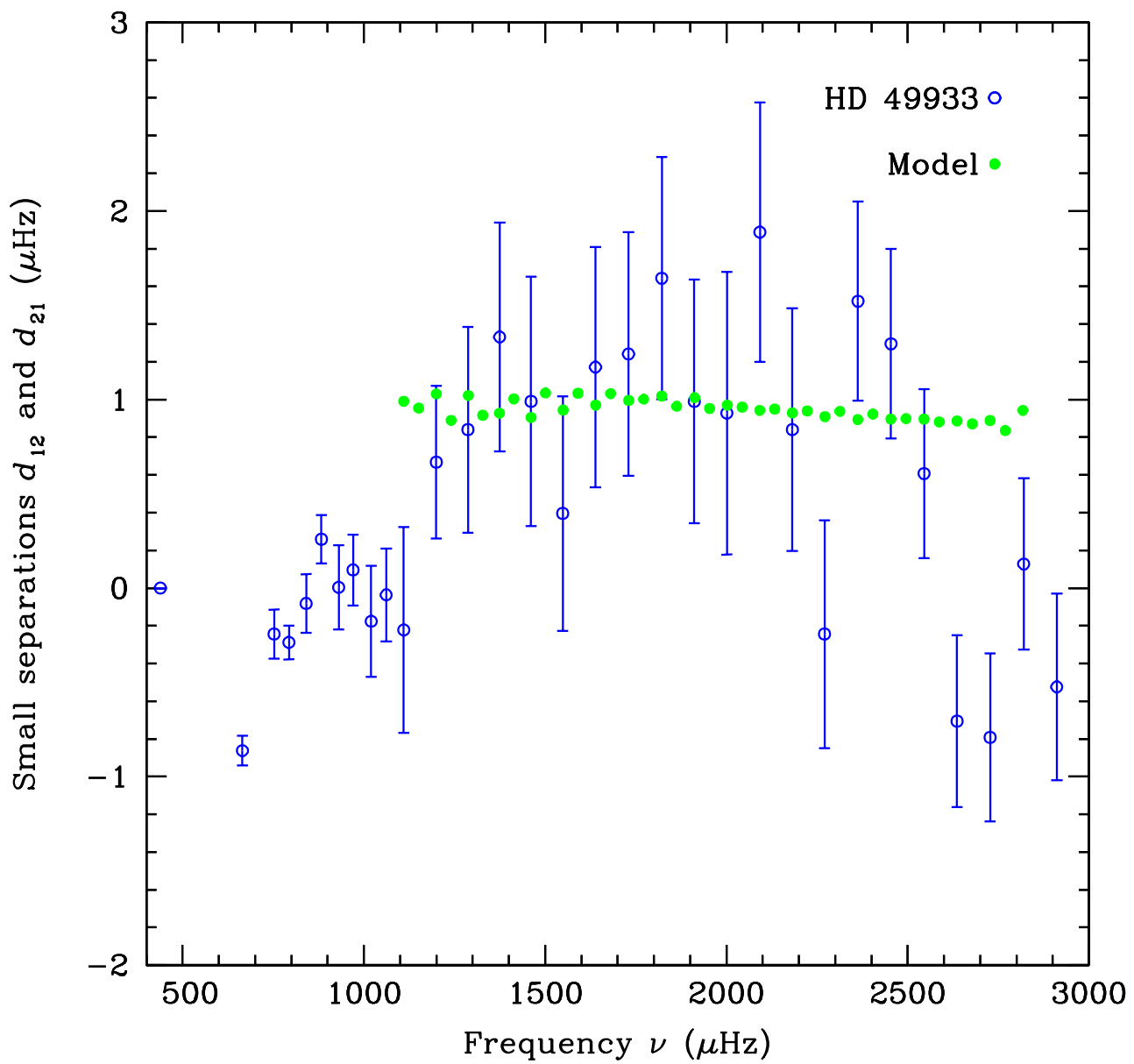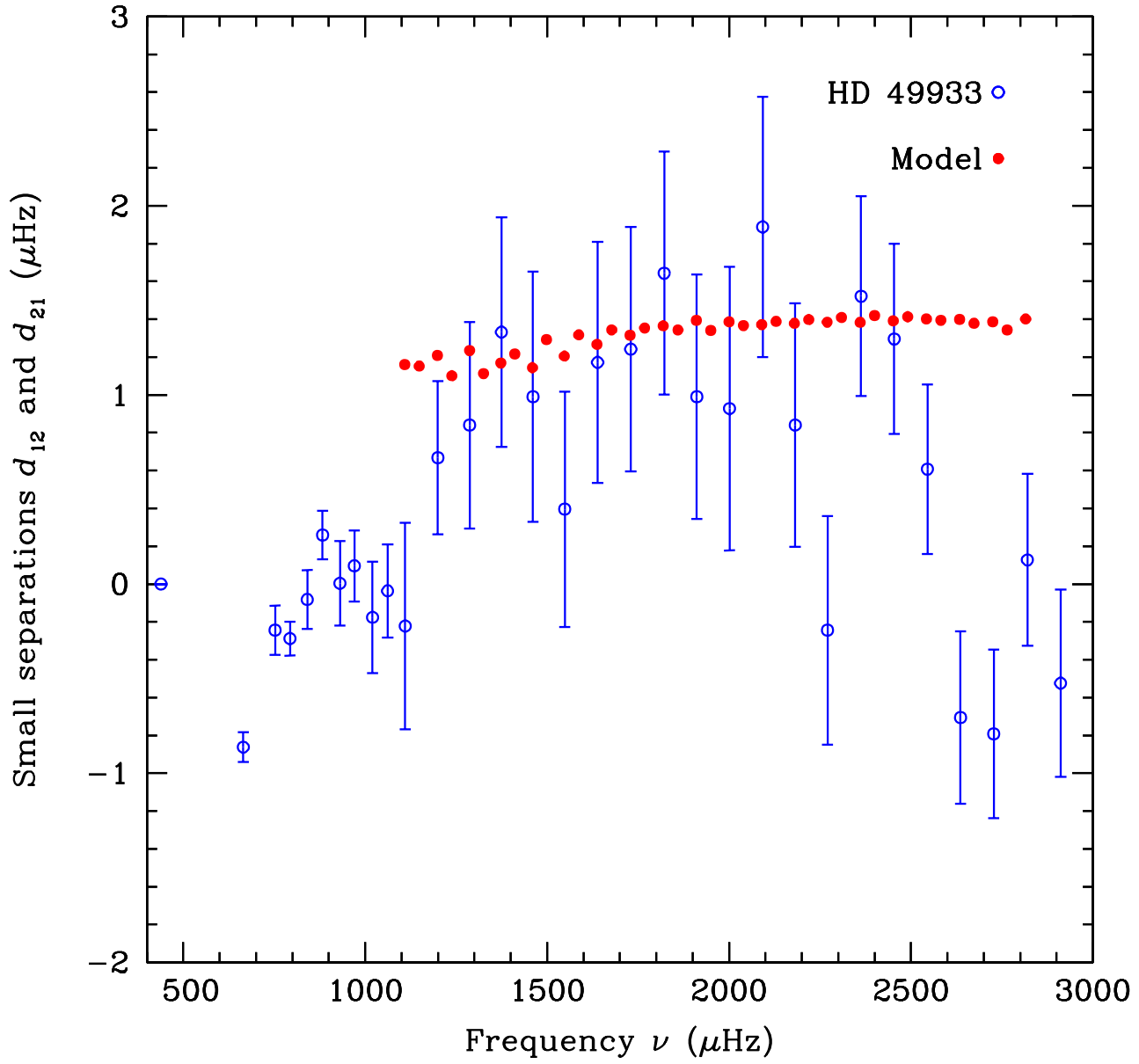
# HD49933

Teff = 6700 ± 100 K

Mbol = [3.25 ; 3.45]

[Fe/H] = -0.32 ±0.1

Vsin i = 10 ± 4 km/s

---

$3.8325 \leq \log T_{eff} \leq 3.8195$

$0.52 \leq \log L/L\_ \leq 0.6$ ( with $M_{bol,\_} = 4.75$)

$0.009315 \leq (Z/X) \leq 0.01476$ (with $(Z/X)\_ = 0.0245$)

$0.00652 \leq Z \leq 0.01033$ ( if X = 0.70)

---

$<\Delta\nu_{n,0}>_{n>10} = 90.1765$ (OM+TA)

$<\Delta\nu_{n,0}>_{n>10} = 90.1799$ (TT)

# **Models**

| M | X | Z | ov | α | diff |
|---|---|---|---|---|---|
| 1.05 - 1.15 | 0.70 | 0.00652 | 0.0 / 0.2 | 1.8 | N |
| 1.05 - 1.3 | 0.70 | 0.0082 | 0.0 / 0.2 | 1.8 | N |
| 1.1 - 1.25 | 0.70 | 0.01033 | 0.0 / 0.2 | 1.8 | N |
| 1.15 – 1.3 | 0.736 | 0.00857 | 0.0 / 0.2 | 1.8 | N |
| 1.35, 1.38 | 0.70 | 0.019 | 0.0 / 0.2 | 1.8 | Y |
| 1.5 | 0.70 | 0.03 | 0.0 / 0.2 | 1.8 | Y |

1. $\Delta\nu_{n,\ell} = \nu_{n,\ell} - \nu_{n-1,\ell}$
2. $\delta\nu_{0,2} = \nu_{n,0} - \nu_{n-1,2}$
3. $\delta\nu_{0,1} = 2\,\nu_{n,0} - (\nu_{n,1} + \nu_{n-1,1})$
4. $\delta\nu_{1,3} = \nu_{n,1} - \nu_{n-1,3}$

The best models fitting $\Delta\nu_{n,\ell}$ are

but they do not satisfy 2, 3, 4

M : 1.12 – 1.25 M_
Z : 0.00652 – 0.01033
X : 0.70 – 0.736
Age: 2 – 3 Gyr.
$\alpha_{ov}$: 0.0 – 0.2
No Diff

Introducing diffusion, the constraints on
the model parameter would be

$M > 1.35\ M\_$
$0.03 > Z_i > 0.019$
X : 0.70
Age < 1. Gyr.
$\alpha_{ov}$ : 0.0 – 0.2
Diff

It appears that $\delta\nu_{0,1}$ decreases at high frequencies
if overshooting is included, and $\delta\nu_{0,1}$ decreases
at low frequencies if microscopic diffusion is

Figure showing two panels. Top panel: $\Delta\nu$ versus $\nu$ with l=0 (TT) in red and l=1 (TT) in blue. Bottom panel: $\delta\nu_{01}$ versus $\nu$.

M = 1.35 $M_\odot$   DIFF
$\alpha$ = 1.8
$Xs_i$ = 0.7
$Zs_i$ = 0.019

● ov = 0.0
$\log T_{eff}$ = 3.8233
$\log L/L_\odot$ = 0.557
age = 1.00E+09
$Xc_f$ = 0.51992
$[Fe/H]_f$ = −0.51

○ ov = 0.2
$\log T_{eff}$ = 3.8228
$\log L/L_\odot$ = 0.562
age = 1.14E+09
$Xc_f$ = 0.57184
$[Fe/H]_f$ = −0.45
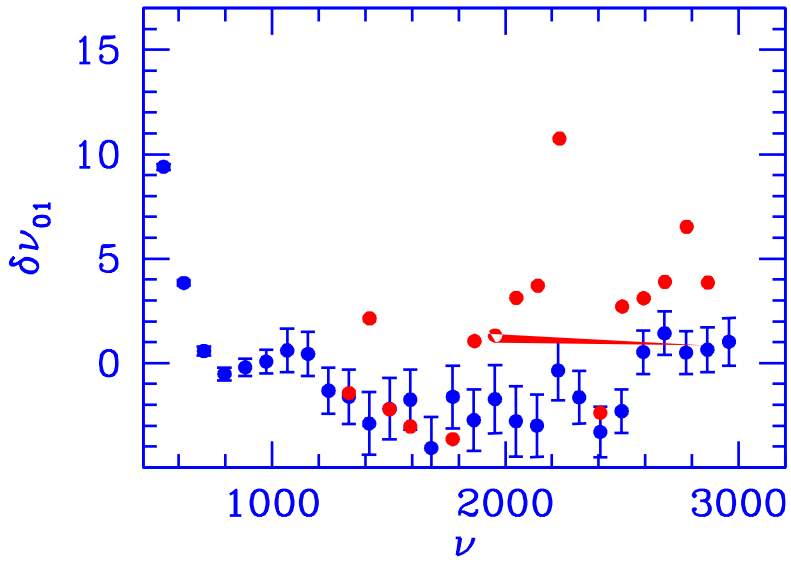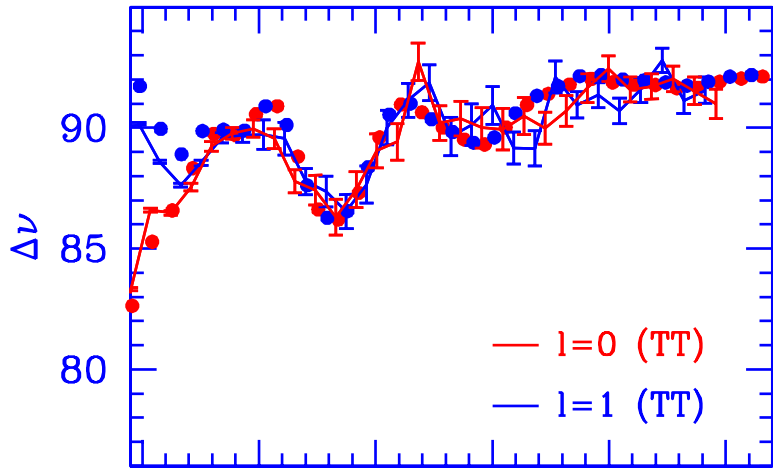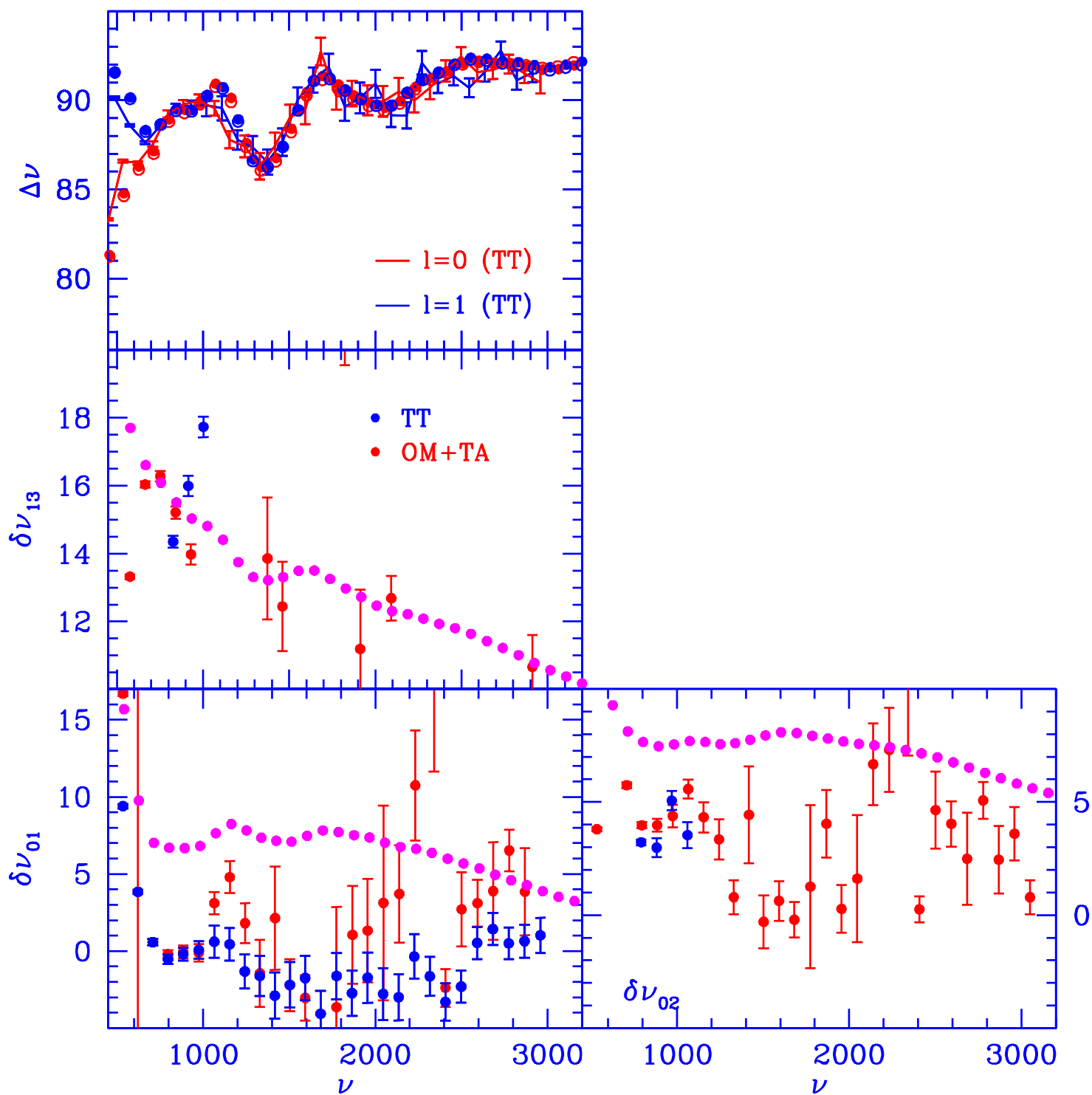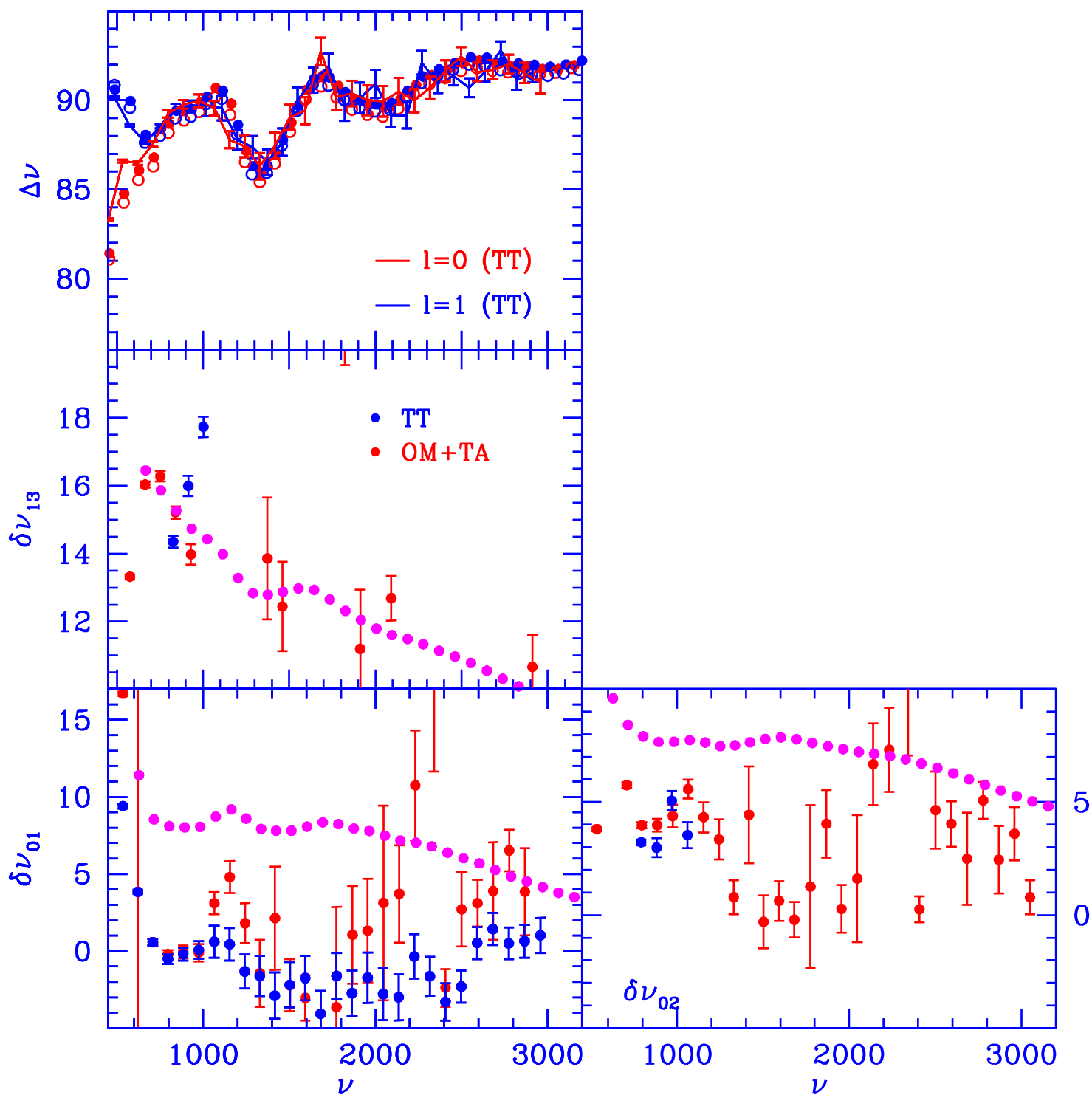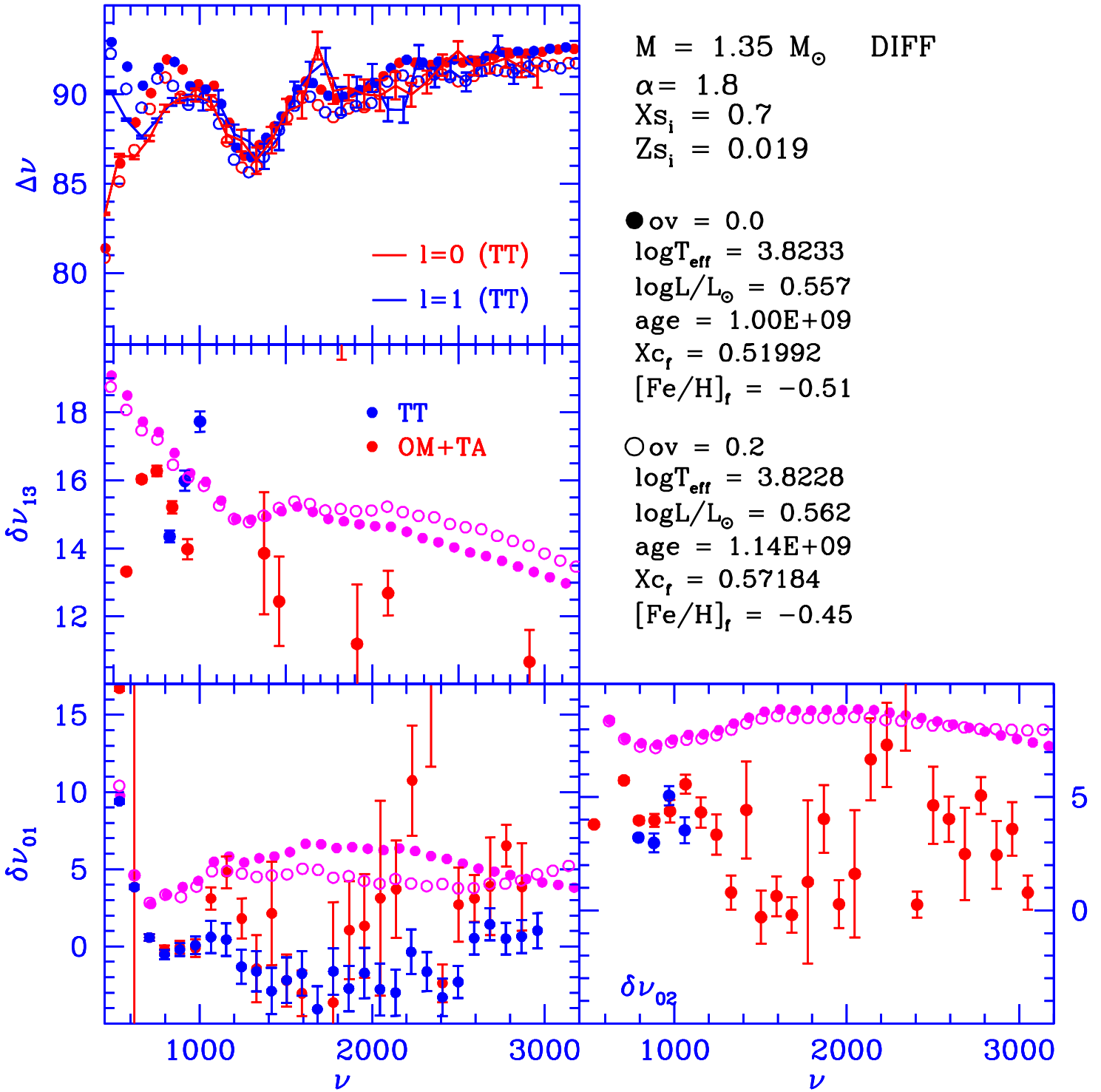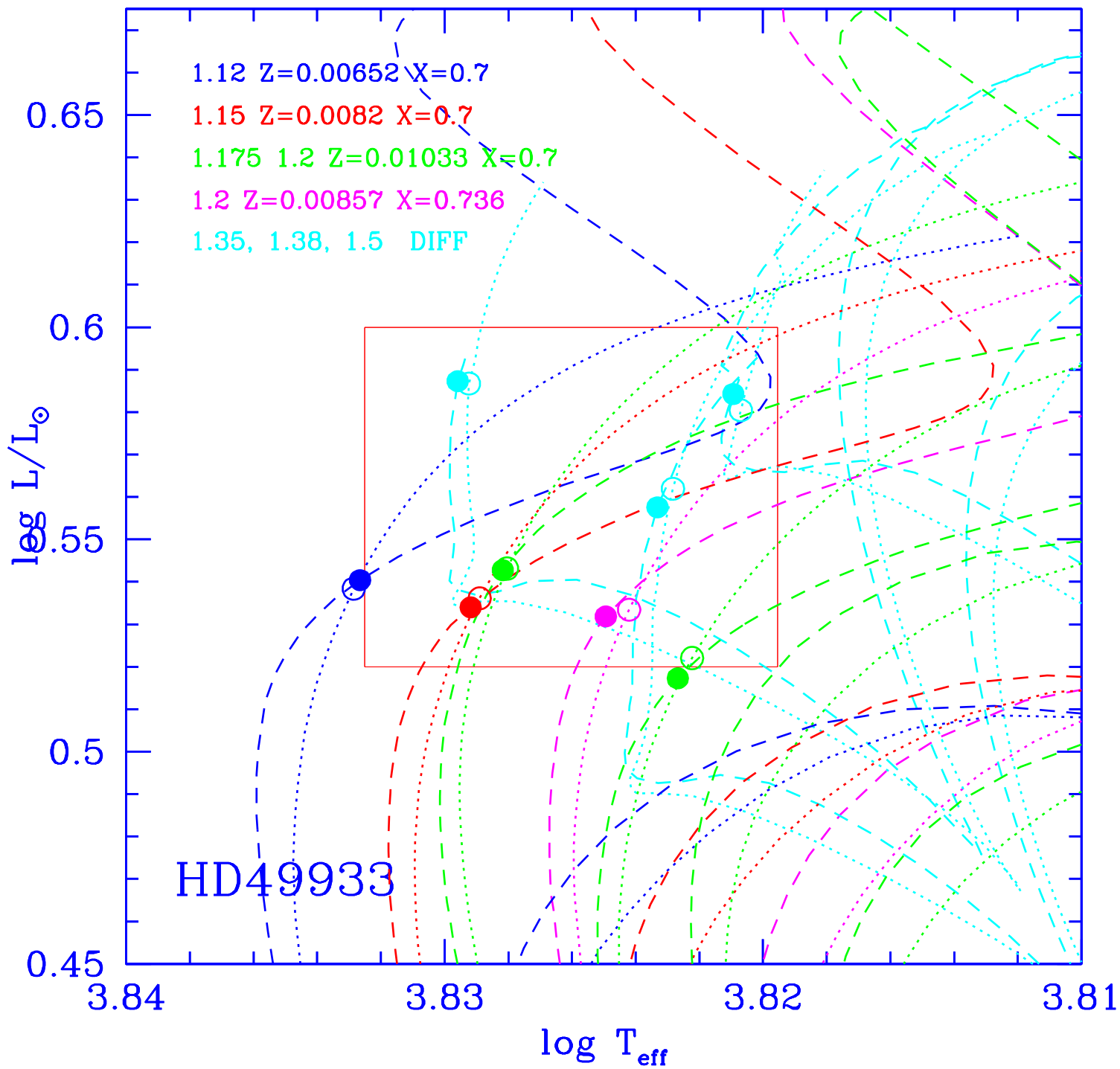
# HD57006

# Report of the Hare-and-Hound exercise #3 (HH3)
# The case of HD57006

May 13, 2003

**Abstract**

In this report we present the analysis done to the synthetic spectra of H57006. For this evolved star, we could not identify the modes and extract their frequencies and splittings with their formal errors in the same way as for a solar like star. For this reason, this star revealed to be very difficult from the data analysis point of view.

The Echelle diagram only permitted us to identify the $l = 0$ modes, but the fitting could reliably be made only below $500\mu$Hz. The understanding of the high-order-mode behaviour was rather impossible; we were restricted to the low order analysis.

For the study of long-lived modes, we had to devise a technique that could distinguish narrow peaks ('g-mode like') among the wider modes ('p-mode like').

## 1 Introduction

In the context of the Hare-and-Hound exercises, HD57006 is one of the targets chosen to be studied in terms of its seismology. It is a post main sequence star with about 1.6 M$_\odot$, an evolved star with a contracting core. Because of that, it is very complex in terms of its frequencies, and rise some doubts about our ability to identify the modes in such stars.

The oscillation frequencies are influenced by the sound speed, $c$, and the Brunt-Väisäla frequency, $N$ (Tassoul, 1980; Audard and Provost,1994). As both depend on the mean molecular weight, $\mu$, (hence on the central hydrogen abundance, $X_c$) they don't change very much during the main sequence. However, when the main sequence phase of stellar evolution ends, $X_c$ is exhausted and the star settles in a state in which the hydrogen burns in a shell surrounding a helium core. The mass of the helium core is increased by the hydrogen burning in the shell leading to an expansion of the envelope of the star. Such stellar interior transformation strongly affects $\mu$, consequently the oscillation frequencies.

The modes are trapped in propagation zones, whose extension and location depends on variation of $N$ and on the Lamb frequency $S_l = Lc/r$, with $L^2 = l(l + 1)$. The propagation of p modes happens when the mode frequency is greater than $N$ and $S_l$, while the propagation of g modes happens when the frequency of the mode is smaller than $N$ and $S_l$. At the beginning of the evolution $N$ is relatively small in stellar interior and varies smoothly with radius, therefore there is a well-defined separation between the modes whose eigenfunctions have nodes in acoustic propagation zone and those whose eigenfunctions have nodes in the gravity propagation zone. As the evolution proceeds a strong gradient of chemical composition develops at the convective core frontier, giving rise to a large peak in $N$ close to the frontier changing the structure of the mode propagation zones. As a result the eigenfunctions of g modes of low radial order develop nodes in the acoustic propagation zone, while eigenfunctions of the low order p modes develop nodes inside the zone of the peak of $N$. These modes have a mixed character, they behave as g modes close to the core frontier and as a p modes in outer regions of the star (Dziembowski and Pamyatnykh, 1991; Audard, Provost and Christensen-Dalsgaard, 1995).

In this report, we describe an attempt of identification of the modes and extraction of the frequencies of a star that has the terrifying scenario of such mixed modes.

1

# 2 Data Analysis

One fundamental quantity in seismology is the large separation, $\Delta\nu_0$. It represents nearly the uniform separation between the two modes of same degree and successive order ($\Delta\nu_0 \approx \nu_{n,l} - \nu_{n-1,l}$) for p modes of high radial order and low degree. The frequency of these modes can be described using an analytical asymptotic way (Tassoul, 1980). The $\Delta\nu_0$ is proportional to the characteristic frequency $\Omega_g = \sqrt{GM/R^3}$ therefore it can be a measure of the mean density of the star, and hence of its mass and radius if $g$ is known. The $\Delta\nu_0$ is also proportional to the inverse of the acoustic radius expressed in seconds.

Useful information can also be obtained from the small frequency separation that measures the departures from the uniformity. It corresponds to the difference between two modes with same $n + \frac{l}{2}$ and is defined as $d_{n,l} = \nu_{n,l} - \nu_{n-1,l}$. This quantity is sensitive to conditions in the structure of the core and to chemical composition and therefore can be an age indicator (Audard and Provost, 1994).

Another quantity that can be derived from the oscillation frequencies is the second frequency difference $\delta_2\nu = \nu_{n,l} + 2\nu_{n-1,l} + \nu_{n-2,l}$ that has an oscillatory behaviour. It is related with the rapid variation of the adiabatic exponent due to the HeII ionization, therefore this quantity may provide a diagnostic to determine the helium abundance (Audard and Provost, 1994).

## 2.1 Echelle Diagram

The method used to detect the large separation, $\Delta\nu_0$, is the Echelle diagram. The Echelle diagram consists in cutting the spectrum into pieces of width $\Delta\nu_0$ and pile them up atop of each other. If $\Delta\nu_0$ is the correct one, "vertical" ridges will appear clearly in the diagram.

In the case of HD57006 "clearly" is not the best word to describe it. The distribution of the modes in the Echelle diagram in the Figure 1 does not permit to take any conclusion about any $l$ but $l$=0, although for high orders it starts to be messy.
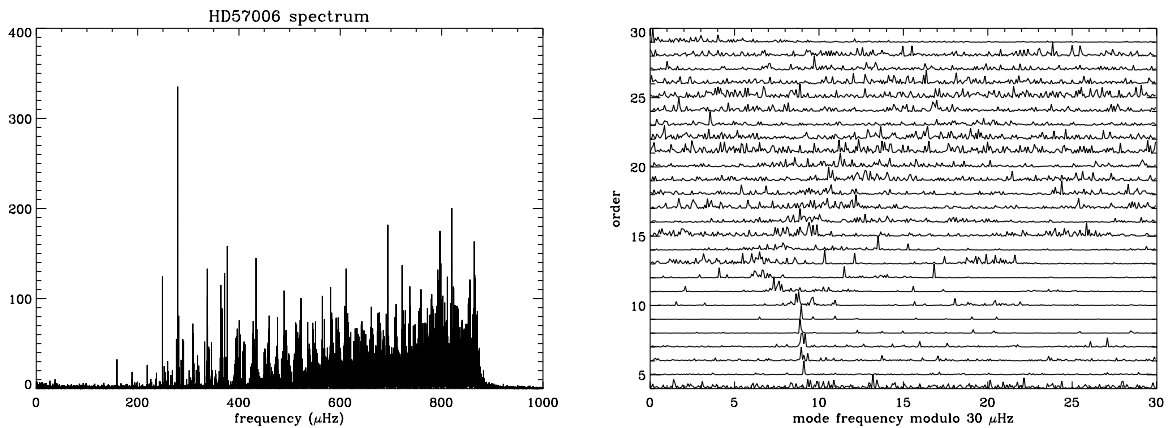


Figure 1: On the left hand side is the spectrum of the star HD57006, and on the right hand side the Echelle diagram with $\Delta\nu_0$=30$\mu$Hz.

Because of the oddness of the HD57006 Echelle diagram, additional theoretical information about this star was necessary. Two sets of frequencies were provided by Ian Roxburgh and by Mário Monteiro with the collaboration of João Marques.

As one can see on Figure 2, $l$=1 in both sets of frequencies behaves almost chaotic. After the $15^{th}$ order, $l = 2$ starts to have the familiar behaviour next to the $l = 0$ on the left hand side, as predicted by the asymptotic theory. However if one looks again at the Echelle diagram in Figure 1, it is very hard, if not impossible to recognize or to guess its location, therefore it wasn't possible to fit it. We only fitted $l = 0$, the results can be seen in Figure 3 and in Table 2.1.

Above $500\mu$Hz, since the $l = 0$ and $l = 2$ modes are very close to each other and apparently very wide, it is difficult to affirm that only $l = 0$ is fitted, because it is possible that some $l = 2$ were fitted with or
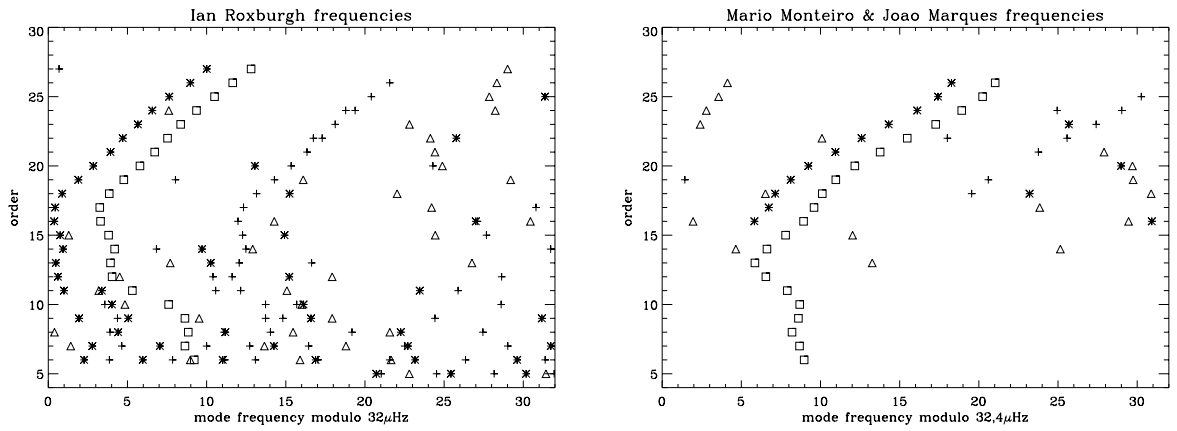
Figure 2: The Echelle diagram of the set of frequency given by the two stellar models of the star HD57006. $l=0$ is represented by a **square**, $l=1$ by a **triangle**, $l=2$ by an **asterisk** and $l=3$ by a **plus** sign.
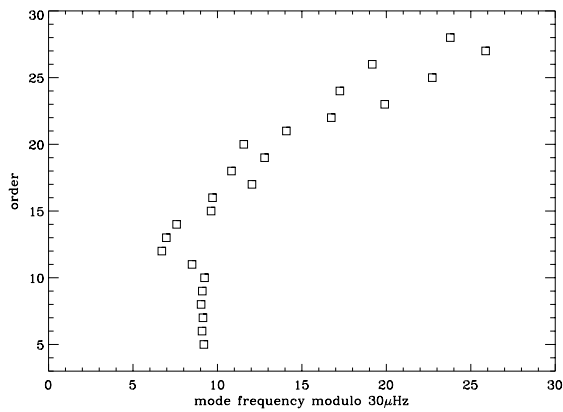


Figure 3: The result of the $l=0$ mode fitting. For high orders (n>15) the fit is rather erratic. Since the star spectrum is very messy, at least after n>15, the $l=2$ modes are sufficiently close to that of the $l=0$ modes (as it can be seen in the Echelle diagrams of the stellar models) for being mixed with the $l=0$ . It is possible that some $l = 2$ are among the fitted $l=0$.

3

instead of $l = 0$. Therefore we only present in Table 2.1 the frequencies fitted for $l = 0$ below 580 $\mu$Hz.

| $l = 0$ |
|---|
| 159.19391±0.038500000 |
| 189.08200±0.044807799 |
| 219.14301±0.036794599 |
| 249.03085±0.013279705 |
| 279.10117±0.038500000 |
| 309.23514±0.099702701 |
| 338.49667±0.14239374 |
| 366.45700±0.17383800 |
| 396.97388±0.40610036 |
| 427.58200±0.28380781 |
| 459.62387±0.15837938 |
| 490.79501±0.81077600 |
| 522.04315±0.44192797 |
| 550.83026±6.6242681 |
| 582.78986±6.8992927e-06 |

Table 1: $l = 0$ mode frequencies and their formal errors in $\mu$Hz as determined by maximum likelihood estimators. The errors determined for the frequency 582$\mu$Hz seems to be way too low to be reliable, this identified mode belongs to the high-order mess that can be observed in the echelle diagram. This is the reason why we concentrated our attention on frequencies below 500$\mu$Hz.

## 2.2   Mode identification challenge

The main goal in asteroseismology is to derive from the oscillation frequencies of the modes, the internal structure and rotation of the stars. With $l=0$ only we can measure $\Delta\nu_0$, the information that can be derived is the acoustic radius of the star. In order to know the internal structure and the rotational of HD57006 it is necessary to extract the frequencies of the other modes.

For the high orders, $n > 15$, the spectrum seems too messy to be able to understand it and extract useful information from it. The existence of large power narrow peaks spread along the lower part of the Echelle diagram $n < 15$ can be noticed. These peaks may lead us to additional information about the internal structure of the star. We believe that we may learn something from their frequency extraction. We concentrated our attention to the frequency range below the 500 $\mu$Hz.

Analyzing the power spectrum below 500 $\mu$Hz, one can notice two distinct features:

- the isolated narrow peaks and

- a bunch of peaks close to each other.

Two bunches of peaks can be well noticed on the left hand side of the Echelle diagram (Figure 1) within the 13$^{th}$ and 15$^{th}$ orders. These two kind of features can not correspond to the same physics, since that the isolated narrow peaks are probably modes which their energy fall only into one bin, therefore it can correspond to long-lived modes, while the bunches of peaks may correspond just to one broad mode, and it can correspond to short-lived modes.

To extract the frequencies of the isolated narrow peaks we need to assess whether they may be due to noise. In some cases they can be embedded in the bunches of peaks that are supposed to be short-lived modes. Therefore we also need to assess whether we can detect and distinguish them among the broad modes.

### 2.2.1 Long-lived modes detection

**Narrow peaks alone**

If one considered a pure noise signal with a $\chi^2$ statistical distribution, the probability that the power within one bin is greater than $m$ times the mean of the noise power, $\sigma$, is:

$$\mathcal{P}(m) = e^{-m} \tag{1}$$

For a frequency band containing $N$ independent bins, the probability that there aren't any bins with power greater than $m$ becomes:

$$\mathcal{P}_N(m) = (1 - e^{-m})^N \tag{2}$$

Therefore the probability that at least one bin has a power greater than $m$ becomes:

$$\mathcal{P}_N(m) = 1 - (1 - e^{-m})^N \tag{3}$$

then if $e^{-m} \ll 1$ the equation (3) can be approximated to:

$$\mathcal{P}_N(m) = N e^{-m} \tag{4}$$

Setting a given value for $\mathcal{P}_N(m)$, for instance 10% (which means 10% probability that one bin above $m$ is due to the noise), choosing a window range in our spectrum which contains N bins, and estimating $\sigma$, one can derive using the equation (4) the correct value for $m$. This way, we can create a statistical test that can detect the bins that can be considered as not being due to the noise (see also Appourchaux et al., 2000; Gabriel et al.,2002).

Below 300 $\mu$Hz there aren't any broad modes and we applied the test directly to $P(\nu)$ we filtered out the bins corresponding to the identified $l = 0$.

**Narrow peaks embedded in short-lived modes**

Above 300 $\mu$Hz the peaks that we wanted to analyze are among broad modes. Therefore, to apply the aforementionned test directly to the power spectrum is not very useful because it detects bins that are part of a single broad mode, in this case we can not assume that the detected bins are all individual modes. Furthermore in some cases the power peaks are very close to the broad modes, and is not possible to assume reliably if they are sharp modes or if they are just part of the broad mode. We need to find a test that can distinguish the broad modes from the sharp modes.

In order to solve this problem, we devised a technique that:

1. Fit the short-lived modes using MLE

2. Correct the spectrum for the fitted model

3. Apply the aforementionned test as if we had only narrow peaks

**Step 1**: Assuming that p modes are stochastically excited oscillator, one can derive that the power spectrum of p modes oscillator is distributed around a mean Lorentzian profiles with a $\chi^2$ probability distribution (Toutain and Fröhlich, 1992; Appourchaux et al., 1998), therefore it is possible to apply a statistical test. In our case we want to extract the frequency corresponding to the sharp peaks in the power spectrum, within the frequency range below 500 $\mu$HZ, that have high probability not to be due to noise. The power spectrum of the p modes can be described as:

$$P(\nu) = M(\nu)F(\nu) \tag{5}$$

Where $F(\nu)$ is a random function with a $\chi^2$ statistical distribution, and $M(\nu)$ is the model of the fitted mode made of a single Lorentzian profile plus noise.

**Step 2**: One can fit this model to the observed power spectra using the Maximum Likelihood Estimators technique (Toutain and Appourchaux, 1994). If one divide the power spectrum by the fitted profile, let's call it $M'(\nu)$, one obtain:

$$P'(\nu) = \frac{P(\nu)}{M'(\nu)} \sim F(\nu) \qquad (6)$$

In a first approximation $P'(\nu)$ has a $\chi^2$ statistical distribution. This is an approximation because $M'(\nu)$ is derived from data and has also a statistical distribution that should be taken into account[1]. In this way we solved the problem of the mixing between the the sharp modes and the broad modes.

**Step 3**: Applying the $\chi^2$ test to HD57006 spectrum, we set $\mathcal{P}_N(m) = 10\%$, $\sigma = 1$, and a window size of 30 $\mu$Hz (corresponding 389 bins). For each window we fitted the broad modes within using the MLE technique and after divided the power spectrum by the resulted fitting we applied the statistical test. The result can be seen in Figure 4.
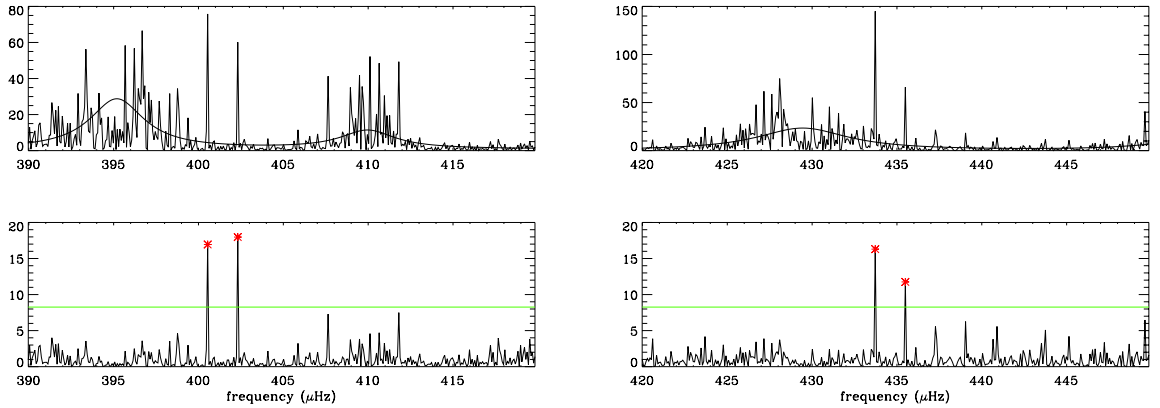


Figure 4: Result of the test for two different ranges of frequencies.The fitting is presented on the top of the figure, and the division of the power spectrum by the fitting, as well as the bins above the 10% probability level, are presented on the bottom of the figure.

The assumption that the g modes have long life-time implies that almost all of the energy from a single g mode will fall in one bin or, at most, in two neighbouring bins (Gabriel et al., 2002). Therefore we assumed that the sharp modes could be the g modes (and of course the broad modes are the p modes). The results are in Tables 2 and 3, and the distribution of the modes frequencies in the Echelle diagram can be seen in Figure 5.

| $\mathbf{non-\ell = 0}$ |
|---|
| 320.195±0.256729 |
| 353.860±0.246180 |
| 373.999±0.324451 |
| 409.970±0.225900 |
| 451.725±1.45902 |
| 474.797±0.512622 |

Table 2: Frequencies and their formal errors in $\mu$Hz of the non-$l = 0$ modes as determined by the MLE technique for the broad modes corresponding to the unidentified p modes below $500\mu$Hz.

---

[1] This shall be the subject of a Monte-Carlo analysis
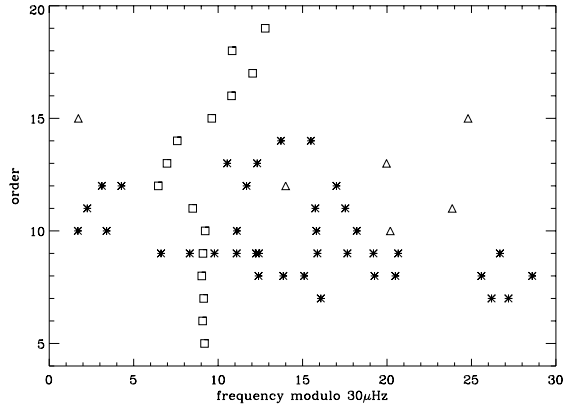
Figure 5: The distribution of the modes in the Echelle diagram. The $l = 0$ modes are presented as squares, the g modes as asterisks, and the non-$l = 0$ modes as triangles.

| g modes | | | | | | |
|---|---|---|---|---|---|---|
| 226.08025 | 236.18827 | 237.19136 | 252.39198 | 253.85802 | 255.09259 | 259.25926 |
| 260.49383 | 265.58642 | 268.59568 | 276.62037 | 278.31790 | 279.78395 | 281.09568 |
| 282.25309 | 282.40741 | 285.87963 | 287.65432 | 289.19753 | 290.66358 | 296.68210 |
| 301.69751 | 303.39504 | 311.11109 | 315.81788 | 318.20986 | 332.25308 | 345.75616 |
| 347.53085 | 363.11728 | 364.27469 | 371.68210 | 377.00617 | 400.54011 | 402.31481 |
| 433.71914 | 435.49383 | | | | | |

Table 3: Frequencies of the g modes extracted using the statistical test described in the subsection 2.2.1

7

### 2.2.2  Autocorrelation and correlation

The correlation determines the degree of similarity between two signals. If the signals are identical, then the correlation coefficient is 1 (or -1); if they are totally different, the correlation coefficient is small and close to 0.

The Autocorrelation is a method which is frequently used for the extraction of the fundamental frequency, in this context this is the $l = 0$ ridge. If a copy of the same signal is shifted, the distance between the central peak (corresponding to the non shifted) and the next correlation maximum is taken to be the fundamental frequency, in this case that this the large separation (Figure 6, left). Having this in mind, this can be applied to the extracted frequencies in order to check if there is some hidden pattern, or some kind of periodicity which is not very clearly to human eye.

We determined the autocorrelation of the extracted frequencies corresponding to the g modes plus those corresponding to the non$-l = 0$ p modes (Figure 6, right). We didn't find out a clear evidence for the existence of a correlation as we can find for the autocorrelation of the extracted frequencies of $l = 0$ modes alone.

Assuming that the shapes of $l = 0$ and $l = 1$ in Echelle diagram might be very similar, we correlated the $l = 0$ frequencies with the frequencies of g modes plus non-$l = 0$ p modes to check if one can find a repetition of the $l = 0$ ridge (Figure 7). However, once more we didn't clearly find any evidence for that.
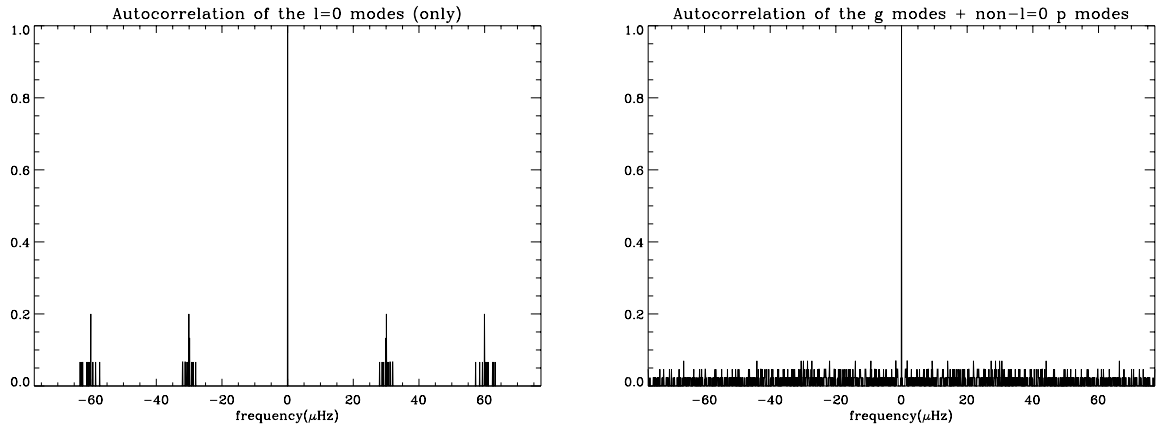


Figure 6: On the left hand side, we have the autocorrelation of the extracted frequencies corresponding the $l = 0$ modes; we can see a fundamental frequency corresponding to the large separation. On the right hand side, the correlation between the frequencies corresponding to the g modes plus the frequencies corresponding to the unidentified p modes; we can not see any fundamental frequency.

## 3   Conclusion

High-order low-degree p modes of the HD57006 do not behave in the same way as one could predict from the asymptotic theory for solar-like stars in the main sequence. Looking at the Echelle diagram, we cannot see the "vertical" ridges corresponding to $l = 0, 2$ and $l = 1, 3$, therefore it is not possible to determine the $d_{n,l}$ and $\delta_2\nu$, hence is not possible to deduce the internal structure of the star.

If one focus our attention to the low orders, the HD57006 power spectrum seems to be able to provide more information about the star; we can identify clearly the $l = 0$ modes that can be fitted without major difficulties. One can also notice the presence of sharp modes that can possibly correspond to g modes or p modes with mixed character, since in this phase of evolution both type of modes have a larger propagation zone close to the convective core frontier due to the Brunt-väisäla frequency peak.

For the extraction of the frequencies of the sharp modes we devised a technique that can distinguish them from the broad modes. This technique can also be applied to stars where the mixed modes character exists but not so strong as in HD57006.
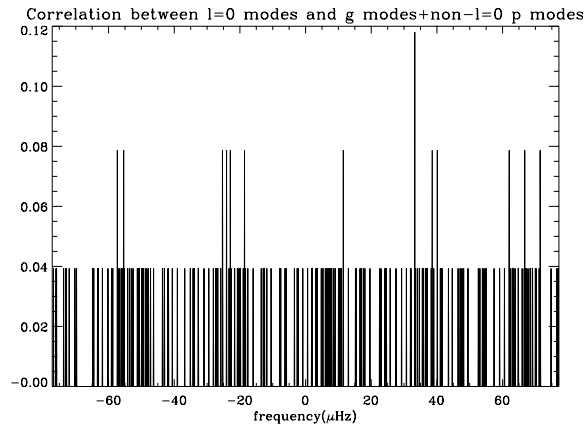
Figure 7: Correlation between the identified $l = 0$ p modes and the unidentified p modes plus the g modes. If one confine our attention to the interval $[-30\mu Hz, +30\mu Hz]$ we can see four maximums but they are not sufficient prominents to affirm that there is a clearly repetition of the $l = 0$ shape.

Last but not least, we were not able to identify any rotational splittings from the non-$l = 0$ modes.

# References

Appourchaux T., Fröhlich C., Andersen B. N., et al., 2000, Apj, 538, 401

Appourchaux T., Gizon L., Rabello-Soares M.-C., 1998, A&A,132,107

Audard N., Provost J., 1994, A&A, 282, 73

Audard N., Provost J., Chirstensen-Dalsgaard J., 1995, A&A, 297, 427

Dziembowski W. A., Pamyatnykh A. A., 1991, A&A, 248, L11

Gabriel A. H., Baudin F., Boumier P., García R. A., Truck-Chièze S., Appourchaux T., Bertello L., Berthomieu G., Charra J., Gough D. O., Pallé , Provost J., Renaud C., Robillot J.-M., Roca Cortés T., Thiery S., Ulrich R. K., 2002, A&A, 390, 1119

Tassoul M., 1980, ApJS 43, 469

Toutain T., Appourchaux T., 1994, A&A, 289, 649

Toutain T., Fröhich C., 1992, A&A, 257, 287

# Characteristics of input model HD57006
## Structure and frequencies

G. Berthomieu

Global constraints on the input model (E. Michel)

$$T_{eff} = 6150 \pm 100 \quad \Longrightarrow \quad 3.7817 < log(T_{eff}) < 3.7959$$

$$1.85 < Mbol < 2.2$$

$$[Fe/H] = -0.1 \pm 0.1$$

With $\mathrm{Mbol}_{\odot} = 4.75$ and $(Z/X)_{\odot} = 0.0245$

$$1.02 < log(L/L_{\odot}) < 1.16$$

$$0.01548 < Z/X < 0.0245$$

Rotation

$$V\,sini = 18 \pm 3km/s$$

If we take $i = 45^0$ and a mean radius $2.210^{11}$ then

$$\nu_{rot} =\sim (1.825 \pm 0.3)\mu HZ$$

# Input model of HD57006

Properties of the input model:

M/Msol= 1.65

R/Rsol= 3.19

L/Lsol= 13.10

log(L/Lsol)= 1.1174

Age (My ) = 1861.64

Teff= $6.15576 \ 10^3$

$Z_s = 0.016$
$X_s = 0.8004$
$Y_s = 0.184$
$Z_s/X_s = 0.01998$

$X_c = 0.000$

$T_c = 2.3940310^7$

$x_{zc} = 0.879$

$\alpha = 1.6$
overshoot $\zeta = 0.05$

# Comparison of HD57006 frequencies

Frequencies extracted by T. Appourchaux from temporal series computed by T. Toutain:

15 frequencies l=0 from 159 to 582 $\mu$Hz

6 frequencies "non l=0" from 320 to 475 $\mu$Hz

37 frequencies "gmodes" located to within 1 bin=0.077

| l=0 pmodes $(\nu \quad \sigma)$ | | non l=0 pmodes $(\nu \quad \sigma)$ | |
|---|---|---|---|
| 159.193 | 0.039 | 320.195 | 0.256 |
| 189.082 | 0.045 | 353.860 | 0.246 |
| 219.143 | 0.037 | 373.999 | 0.324 |
| 249.030 | 0.013 | 409.970 | 0.226 |
| 279.101 | 0.038 | 451.725 | 1.459 |
| 309.235 | 0.099 | 474.797 | 0.512 |
| 338.496 | 0.142 | | |
| 366.457 | 0.174 | | |
| 396.974 | 0.406 | | |
| 427.582 | 0.284 | | |
| 459.623 | 0.158 | | |
| 490.795 | 0.811 | | |
| 522.043 | 0.442 | | |
| 550.830 | 6.624 | | |
| 582.790 | 6.9e-06 | | |

## gmodes (located to within 1 bin=0.077)

| | | | | | | | |
|---|---|---|---|---|---|---|---|
| 226.080 | 236.188 | 237.191 | 252.391 | 253.858 | 255.092 | 259.259 | 260.493 |
| 265.586 | 268.595 | 276.620 | 278.318 | 279.783 | 281.095 | 282.253 | 282.407 |
| 285.879 | 287.654 | 289.197 | 290.663 | 296.682 | 301.697 | 303.395 | 311.111 |
| 315.817 | 318.209 | 332.253 | 345.756 | 347.530 | 363.117 | 364.274 | 371.682 |
| 377.006 | 400.540 | 402.315 | 433.719 | 435.494 | | | |

# Comparison of HD57006 frequencies

Modes l=0

HD57006  Frequency differences ( Model(l=0,1,2,3) − ThA (l=0) )

# Comparison of HD57006 frequencies
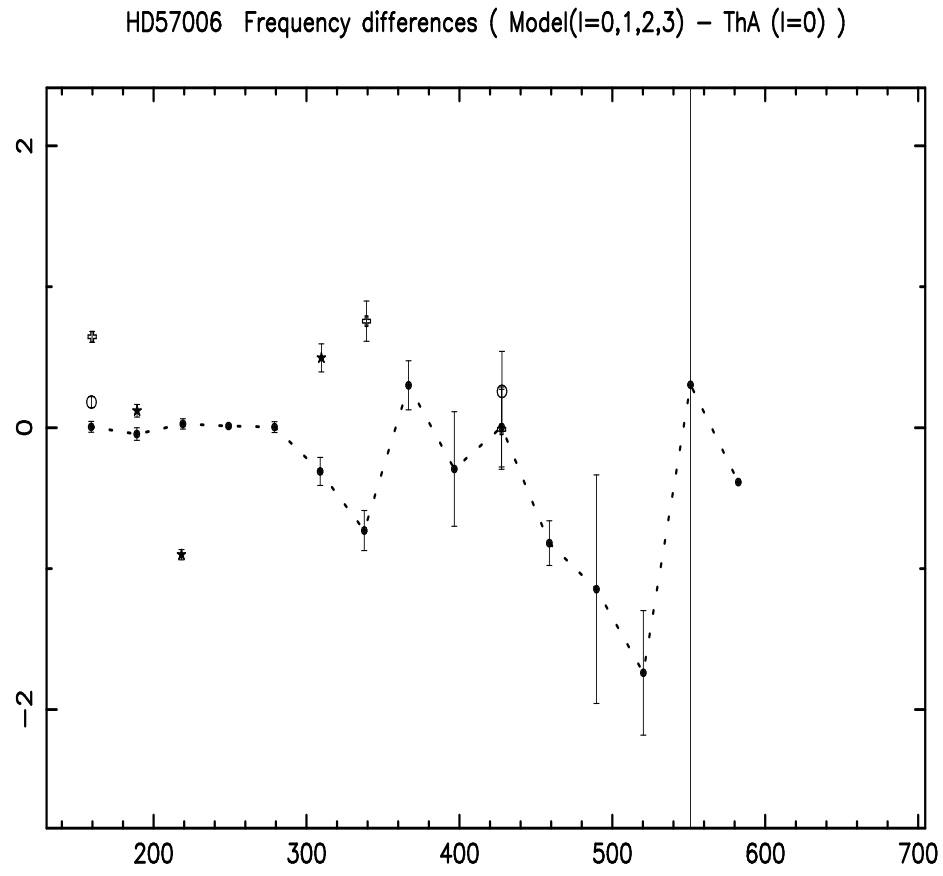
## Modes not l=0

HD57006  Frequency differences ( Model(l=0,1,2,3) – ThA (l=1) )
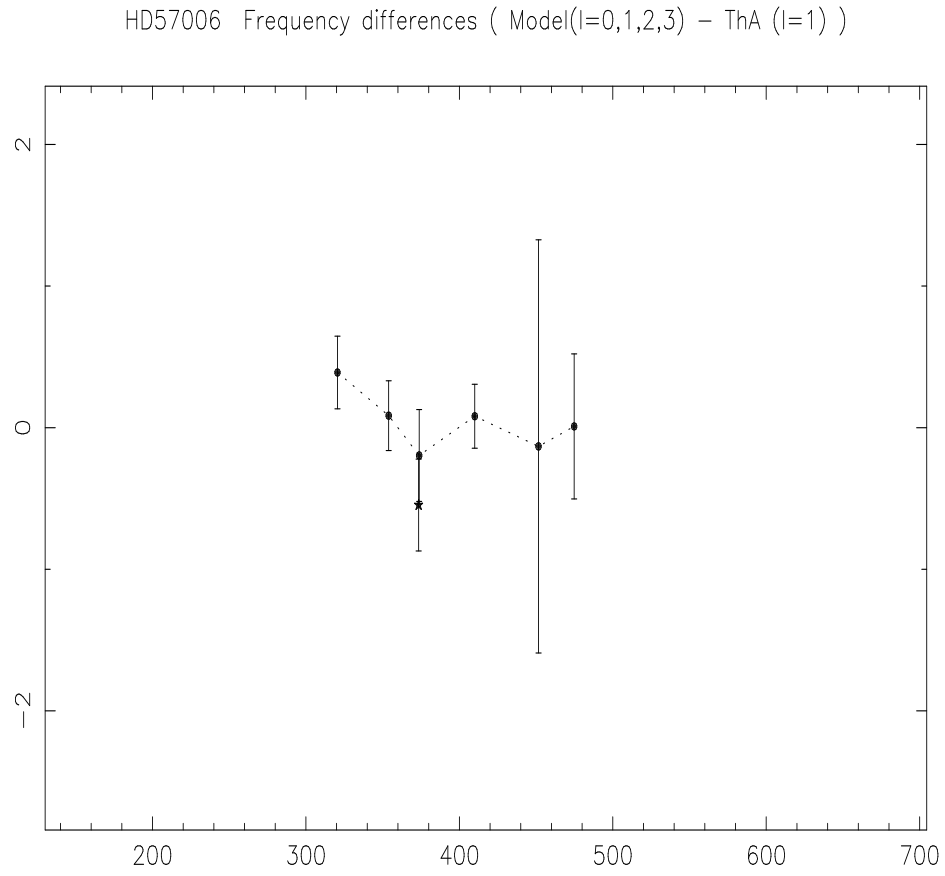
# Comparison of HD57006 frequencies

Modes "g"

HD57006  Smallest frequency differences ( Model(l=0,1,2,3) − ThA (modes "g") )
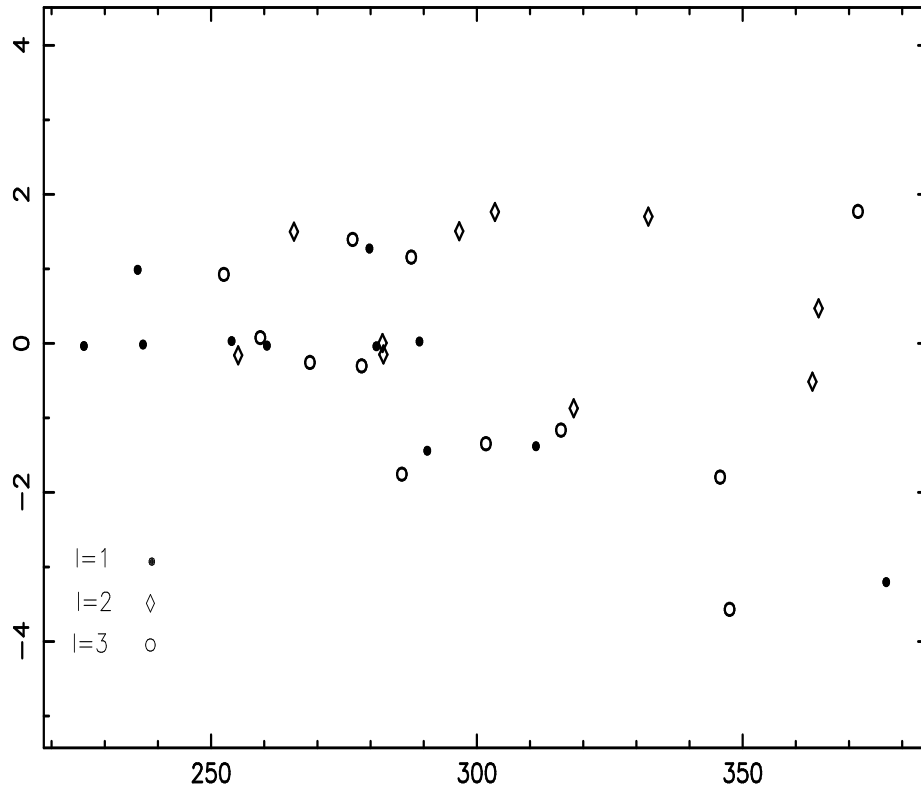
# On the detection of pure sine waves embedded in a spectrum of stochastically excited p modes

O.Moreira[1,2] and T.Appourchaux[1,3] and G.Berthomieu[4] and T.Toutain[4]

[1] *European Space Agency, P. O. Box 299, 2200AG Noordwijk, The Netherlands*
[2] *Institut d'Astrophysique et de Géophysique de l'Université de Liège, 17 Allée du 6 Août, 4000 Liège, Belgium*
[3] *Institut d'Astrophysique Spatiale, Bâtiment 121, 91405, Orsay Cedex, France*
[4] *Laboratoire Cassiopée, UMR CNRS 6202, Observatoire de la Côte d'Azur, BP 4229, 06304 Nice Cedex 4, France*

**ABSTRACT**

The mode identification and fitting of solar oscillations provide an observational tool to derive the physical properties of the Sun's interior. What has been devised for helioseismology can now be used for the future asteroseismology ground-based instruments and space missions such as HARPS or COROT. In the coming decade, numerous stars will be observed for which new tools will be needed. For instance, it is very likely that g modes and p modes will be detected rendering the identification difficult. In addition, modes having both characteristics, known as mixed modes, are also likely to be detected in evolved stars; these latter modes are crucial for the understanding of the internal structure of the stars as they propagate deeply inside the stars, unlike the p modes. Unfortunately, the mixing will not only occur physically but also in the frequency domain: mixed modes will appear very close to stochastically excited p modes. In this paper, we have devised a new technique for detecting long-lived modes (mixed or g modes) embedded in a common p-mode spectrum. The technique has been validated using Monte-Carlo simulations. In the framework of the hare-and-hound exercise of Corot, this technique has been applied to synthetic time series of the evolved solar-like star HD57006. The results showed that we can detect most of the mixed modes embedded by the hare. We also discuss the impact of how the long-lived modes are excited on the detection level. The technique described here can be applied to stars with a mass greater than 1.2 $M_\odot$ having evolved possibly beyond the Terminal Age Main Sequence (TAMS) such as Procyon.

**Key words:** Stars: oscillation – Methods: statistical

## 1 INTRODUCTION

P-mode spectra have been used for more than two decades to study the internal structure of the Sun in great details. However, because the major contribution to the p modes is in the outer layers of the Sun and only the $l = 0$ modes reach the core, the inversion techniques based on p-mode frequencies require great accuracy to determine the core structure. In contrast to the p modes, the g modes are confined in the radiative zone and have an energy maximum located near the center of the Sun. Therefore, the inversions of solar structure using g-mode frequencies do not require such a high frequency precision.

Seeking for g modes in solar data has always been the challenge of helioseismology. Statistical methods and pattern recognition techniques have been used aiming to detect g modes in the data collected by SOHO and ground-based instrument (Appourchaux et al., 2000; Gabriel et al., 2002;

Turck-Chièze et al., 2004). Although, the detection of the g modes has not been successful, space missions such as MOST and COROT will provide us, in the near future, with measurements of light fluctuations from other stars with enough precision to detect and identify modes of oscillation of any kind, p and g modes alike; similarly, the ground-based spectrometer HARPS will measure stellar radial velocities providing in the long term a larger asteroseismic database than the aforementioned exploratory space missions. Besides the g modes, there are other type of modes called *mixed* modes that may provide the information necessary to understand the structure of stellar cores. These modes occurring in evolved stars have the dual characteristics of a p mode in the convective part of the star, and of a g mode in the inside of the star. These modes may effectively be excited by convection to such level that they can be more easily detected at the surface of the star than any g mode would be. Given their mixed nature, they would per-

mit a much better understanding of the inside of the stars than with the p modes alone. The impressive spectrometer HARPS with its very low noise (Mayor et al., 2003) will undoubtedly be subject to the observation of such evolved stars. One or two detected mixed modes in well chosen stars by HARPS would be enough for providing important information on the internal structure of those stars.

The observation of such an evolved star as a principal target was envisaged for the COROT mission. Aiming to prepare for the future space mission COROT, the Data Analysis Team of the Seismology Working Group of COROT has been performing Hare-and-Hound (H&H) exercises for simulating the observation of those targets (Berthomieu and Appourchaux, 2002). These kinds of exercises have two steps. In the first step a team (the hares) generates theoretical mode frequencies and synthetic time series of the light curve. In the second step another team (the hounds) analyzes the time series, performs first, the mode identification, i.e. the tagging of each mode in term of the degree of the spherical harmonics; second, the determination of the oscillation mode parameters (such as frequency, amplitude, linewidth) and last the frequencies inversion. The work of the hounds is performed without having access to any other information but the known characteristics of the star. The knowledge achieved on the identification, tagging, peak fitting and inversions of the eigenmodes of the Sun is a great aid for performing the same tasks on solar-like stars.[1]

In the framework of the H&H exercise, a time series of the star HD57006 was generated by one of the authors (TT) with frequencies provided by another author (GB) and the modes identification and fitting by the other two authors (OM and TA). The star HD57006 has been presented (Appourchaux et al., 2003) as an evolved star with 1.6 $M_\odot$ which has mixed modes of oscillation. It is known that during its evolution from the Zero Age Main Sequence, the oscillation spectrum of HD57006 will become more and more different from a well-behaved solar-like star. For instance, the echelle diagram of the oscillation spectrum will be progressively scrambled until only the $l = 0$ ridge can be identified (Appourchaux et al., 2003). Besides the problems related to that complexity, this time series also had, below 500 $\mu$Hz, prominent peaks that correspond to long-lived modes amongst the short-lived p-mode spectrum.

In this paper, we will briefly recall the statistical tests used in the detection techniques of long-lived modes or g modes (Appourchaux et al. 2000, and Gabriel et al. 2002). Next we will introduce a technique for detecting these long-lived modes when they are embedded in short-lived modes. The validation of the new detection technique will be done through a Monte-Carlo analysis and through an evaluation of the result on the synthetic time series of HD57006 (COROT H&H).

## 2    LONG-LIVED MODES DETECTION

### 2.1    Detection of long-lived modes alone

A signal that has no detectable intrinsic width in the power spectrum (such as a pure sine wave or a mode with a lifetime

---

[1] type of stars as defined by Appourchaux (2003)

longer than the observation duration) can be detected in a white noise signal by testing the following hypotheses:

H0: A prominent observed peak within the power spectrum might be merely due to noise (pure noise observed)

H1: A sine wave signal embedded in white noise might be detectable above a given significance power level (pure noise observed with a deterministic signal)

The statistical test based on the H0 hypothesis consists in determining a significance level for which the peaks have a low probability of being due to noise. It is assumed that all bins in the power spectrum are independent and identically distributed (i.i.d) random variables. The H0 hypothesis does not check for the presence of signal, this is the 'rôle' of the H1 hypothesis. The test based on the H1 hypothesis gives the probability that a sine wave of a given deterministic amplitude can be detected reaching a pre-determined significance level in the power spectrum. It is applicable when the characteristics of the embedded sine wave are known. These two kinds of tests do not contradict each other but test two different assumptions.

### 2.1.1    *Statistics of pure noise*

The power spectrum of a pure noise signal made from full-disk integrated instrument has a $\chi^2$ statistical distribution with 2 d.o.f (Appourchaux et al., 1998). If $x_r(\nu)$ and $y_i(\nu)$ are normalized normal distributions, representing respectively the real and the imaginary part of the noise Fourier spectrum at frequency $\nu$, then the power spectrum can be described as:

$$P(\nu) = x_r^2(\nu) + y_i^2(\nu) \tag{1}$$

Which means if $z = x^2 + y^2$ is an observed value in the power spectrum then its probability distribution $G$ is given by:

$$G(z) = 1 - e^{-z/2} \tag{2}$$

If we normalize with respect to the mean value of $z$, that is 2, we have for the normalized power spectrum $\rho$:

$$G(\rho) = 1 - e^{-\rho} \tag{3}$$

Thus for a set of $N$ observed values of random variables having a distribution similar to $z$, the joint distribution is given by:

$$\mathcal{G}_N(\rho) = \left(1 - e^{-\rho}\right)^N \tag{4}$$

This leads to the following statement:

Statement 1. *For a frequency range containing $N$ power bins the probability that at least one bin has power greater than $\rho$ times the mean of the noise power is given by:*

$$\mathcal{P}_N(\text{power} > \rho) \approx N e^{-\rho}, \ when \ e^{-\rho} \ll 1 \tag{5}$$

Equation (5) allows us to determine a significance level (value of $\rho$) when $\mathcal{P}_N$ is small. The very same equation was used by Appourchaux et al (2000) to provide an upper limit to the amplitudes of solar g modes.

### 2.1.2 Statistics of a sine wave embedded in a noise

In this part, it is required to assume that the signal is present. Assumptions are made about how the signal interacts with the noise: either through additive noise or through multiplicative noise. Each assumption comes with a different probability that we will calculate.

**Case of additive noise**: The power spectrum of a pure sine wave embedded in noise is defined as the sum of the Fourier spectrum components of the noise and of the deterministic signal of amplitude $A$ and frequency $\nu_0$, The power spectrum is described as:

$$P(\nu) = \begin{cases} \left(x_r(\nu_0) + \frac{A}{2}\right)^2 + y_i^2(\nu_0) & , \nu = \nu_0 \\ \\ x_r^2(\nu) + y_i^2(\nu) & , \nu \neq \nu_0 \end{cases} \quad (6)$$

Here the detail of the phase of the sine wave has been discarded because we are only interested in the power spectrum. Would the phase of the signal be different from zero, it would still be possible by a linear transformation to have the case of Equation 6. At $\nu = \nu_0$ the power spectrum has no longer a $\chi^2$ statistics with 2 d.o.f. Instead it has a non-central $\chi^2$ statistical distribution. Thus, if $z = (x + \frac{A}{2})^2 + y^2$ is the observed value in power spectrum at $\nu = \nu_0$ then it can be derived that its probability distribution, as reported by Gabriel et al. (2002), is given by:

$$F(\rho, A) = \frac{e^{-\frac{A^2}{8}}}{2\pi} \int_0^\rho \int_0^{2\pi} e^{-\left(u - A\sqrt{\frac{u}{2}}\cos\theta\right)} d\theta du \quad (7)$$

where $\rho$ is the normalized power spectrum, $\theta$ and $u$ are dummy variables. From Eq. (6), it can be derived that the signal to noise ratio $r$ is given by:

$$r = \frac{1}{2}\frac{A^2}{4} = \frac{A^2}{8} \quad (8)$$

We can rewrite Eq. (7) as:

$$F(\rho, r) = \frac{e^{-r}}{2\pi} \int_0^\rho \int_0^{2\pi} e^{-\left(u - 2\sqrt{r}\sqrt{u}\cos\theta\right)} d\theta du \quad (9)$$

It is clear that when $A = 0$ the Eq. (9) is equal to Eq. (3).

Statement 2. *The probability that a sine wave with a deterministic amplitude A, having a signal-to-noise ratio r in the power spectrum ($r = A^2/8$), will have an observed power higher than a power level, $\rho$, is given by:*

$$\mathcal{P}_A(\text{power} > \rho) = 1 - F(\rho, r) \quad (10)$$

**Case of multiplicative noise**: In this case instead of adding the noise, the signal is not deterministic but its amplitude is defined by the local noise. The power spectrum is described as:

$$P(\nu) = \begin{cases} \left(1 + \frac{A^2}{4}\right) x_r(\nu_0)^2 + y_i^2(\nu_0) & , \nu = \nu_0 \\ \\ x_r^2(\nu) + y_i^2(\nu) & , \nu \neq \nu_0 \end{cases} \quad (11)$$

Since it is also a regular $\chi^2$ with 2 d.o.f, the probability distribution is then derived from Eq. 2, and given by:

$$H(\rho, A) = G(\rho/(r+1)) \quad (12)$$

where $\rho$ is the normalized power spectrum. From Eq. (11), it can be derived that the signal to noise ratio $r$ is given by:

$$r = \frac{A^2}{4} \quad (13)$$

The definition of the signal-to-noise ratio is different from that of the previous because the noise is multiplicative and not additive.

Statement 3. *The probability that a sine wave with a mean amplitude A, having a signal-to-noise ratio r in the power spectrum ($r = A^2/4$), will have an observed power higher than a power level, $\rho$, is given by:*

$$\mathcal{P}_A(\text{power} > \rho) = 1 - G(\rho/(r+1)) = e^{-\rho/(r+1)} \quad (14)$$

## 2.2 Detection of long-lived modes embedded in short-lived modes

The detection of pure sine waves embedded in a spectrum of stochastically excited p modes can be done by testing the same hypotheses. Using the following technique we can reduce this particular case to the case of a sine wave embedded in a noise with $\chi^2$ distribution:

(i) Fit the p modes spectrum
(ii) Divide the power spectrum by the fitted model
(iii) Apply the statistical tests described in section 2.1

### 2.2.1 Statistics of a p-mode spectrum

The power spectrum of a stochastically excited p mode can be described as:

$$P(\nu) = M(\nu)X(\nu) \quad (15)$$

Where $X(\nu)$ is a random function with a $\chi^2$ statistical distribution with 2 d.o.f, and $M(\nu)$ is the model of the fitted mode made of a single Lorentzian profile plus stellar and instrumental noise (Anderson et al., 1990). One can fit a Lorentz profile to the observed power spectrum using the Maximum Likelihood Estimators (MLE) technique (Toutain and Appourchaux, 1994). This is a classic and well-known approach used for the short-lived modes such as those observed on the Sun. After having done the fitting, one can divide the power spectrum by the fitted profile $\tilde{M}(\nu)$:

$$\tilde{X}(\nu) = \frac{P(\nu)}{\tilde{M}(\nu)} \approx X(\nu) \quad (16)$$

Here we would like to point out that we do not *remove* the mode by performing this ratio. Since we deal with random variable and with a finite amount of information, the fitted profile will never be identical to the true profile. Therefore, the so-called *removal* will be imperfect and subject to the realization noise itself. Knowing this limitation, in a first approximation $\tilde{X}(\nu)$ has also a $\chi^2$ statistical distribution with 2 d.o.f. Thus the *statement 1* is applicable to $\tilde{X}(\nu)$, it is possible to apply the H0 statistical test to the corrected $\tilde{X}$ spectrum.

### 2.2.2 Statistics of a sine wave embedded in a p-mode spectrum

As before two cases are studied here.

**Case of additive noise**: It can be derived that the power spectrum of a sine wave embedded in a p-mode spectrum can be described as:

$$P(\nu) = \begin{cases} M(\nu_0) \left( \left( x_r(\nu_0) + \frac{a}{2} \right)^2 + y_i^2(\nu_0) \right) & , \nu = \nu_0 \\[2ex] M(\nu) \left( x_r^2(\nu) + y_i^2(\nu) \right) & , \nu \neq \nu_0 \end{cases} \quad (17)$$

Where $a = \frac{A}{\sqrt{M(\nu_0)}}$

Dividing Eq. (17), when $\nu = \nu_0$, by $\tilde{M}(\nu_0)$ becomes:

$$\tilde{X}(\nu_0) = \frac{M(\nu_0)}{\tilde{M}(\nu_0)} \left( \left( x_r(\nu_0) + \frac{a}{2} \right)^2 + y_i^2(\nu_0) \right) \quad (18)$$

Thus $\tilde{X}(\nu_0)$ can also be approximated to a non-central $\chi^2$ statistical distribution. It is then possible to apply the H1 statistical test to the corrected power spectrum and to use the detection probability expression presented in the *Statement 2*.

**Case of multiplicative noise**: In this case, we have:

$$P(\nu) = \begin{cases} M(\nu_0) \left( 1 + \frac{a^2}{4} \right) \left( x_r(\nu_0)^2 + y_i^2(\nu_0) \right) & , \nu = \nu_0 \\[2ex] M(\nu) \left( x_r^2(\nu) + y_i^2(\nu) \right) & , \nu \neq \nu_0 \end{cases} \quad (19)$$

Where $a = \frac{A}{\sqrt{M(\nu_0)}}$

Dividing Eq. (19), when $\nu = \nu_0$, by $\tilde{M}(\nu_0)$ becomes:

$$\tilde{X}(\nu_0) = \frac{M(\nu_0)}{\tilde{M}(\nu_0)} \left( 1 + \frac{a^2}{4} \right) \left( x_r(\nu_0) + y_i^2(\nu_0) \right) \quad (20)$$

Thus $\tilde{X}(\nu_0)$ can also be approximated to a $\chi^2$ statistical distribution. It is then possible to apply the H1 statistical test to the corrected power spectrum and to use the detection probability expression presented in the *Statement 3*.

## 3  VALIDATION OF THE DETECTION TECHNIQUE

### 3.1  Monte-Carlo Analysis

As mentioned in the previous section, because of the realization noise, the fitted profile ($\tilde{X}(\nu)$) is derived from data and does not reflect the true profile. Therefore the fitted profile has also a statistical distribution that should be taken into account in the application of the H1 statistical test. Therefore we decided to use Monte-Carlo simulations for asserting the following:

1. The statistical distribution of the corrected power spectrum ($\tilde{X}(\nu)$) is close to a $\chi^2$ with 2 d.o.f distribution.

2. The statistical distribution of an embedded sine wave signal in the corrected power spectrum is close to a non-central $\chi^2$ statistical distribution with non-centrality parameter $\frac{a^2}{4}$ (*Statement 2* can be applied).

In order to test our approximations and the H1 hypothesis, we performed a Monte-Carlo analysis of the two
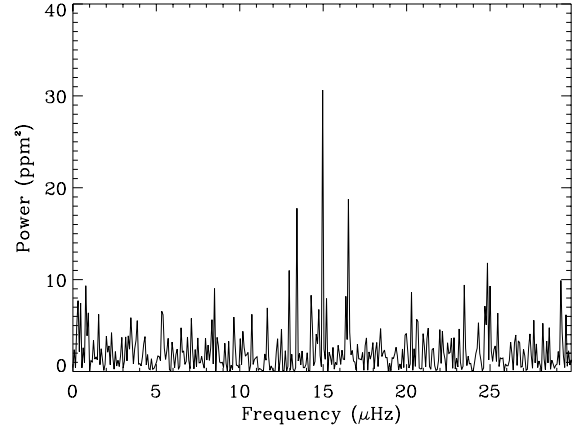


**Figure 1.** An example of a Monte-Carlo simulation of sine waves embedded in a white noise. The signal due to the embedded sine waves is present at $\nu = 13.5, 15, 16.5$ ($\mu$Hz). The input signal-to-noise ratios for the sine waves signal were 9, 10, 11, which correspond to a theoretical detection probability of 60%, 70%, 76%, respectively.

aforementioned cases. We generated synthetic power spectra with a frequency resolution of $0.077 \mu$Hz equivalent to an observation time length of 150 days. For both cases, we wanted to compare the analytical formula given by Eq. (10) with the detection levels as returned by the Monte-Carlo analysis.

The Monte-Carlo simulations were only performed for additive noise since multiplicative noise is always the underlying assumptions when fitting p-mode spectra. Equation 14 is implicitly assumed to be correct due our experience in helioseismology.

### 3.1.1  *Sine waves embedded in a noise signal*

We repeated for 1000 simulations the following steps for a 30-$\mu$Hz frequency range or window:

(i) Generate Fourier spectra for white noise

(ii) Add in the spectra three sine waves with different amplitudes as in Eq. (6)

(iii) Use MLE to estimate the mean value of the signal, $\sigma$

(iv) Determine the power level: 10% probability in a 30-$\mu$Hz gives $\rho = 8.26$ (Eq. 5)

(v) Frequency determination of the detected power bins

The power spectrum of one simulation is shown on Fig 1. After performing the simulations, we studied the distribution of the extracted frequencies. We counted the number of times that we detect each input sine waves signal and we compared the result with the predicted detection probability given by Eq. (9).

The significance level (Eq. 5) depends on a proper estimation of the mean value of the noise. The implicit hypotheses that the set of power bins to be tested should be i.i.d random variables (See Section 2.1.1) does not hold in the presence of sine waves signal (Eq. 6). The mean value of a non-central $\chi^2$ distribution with a non-centrality parameter $\lambda$ is given by $\lambda + \sigma$, where $\sigma$ is the mean value of the central $\chi^2$ distribution. In this context $\sigma$ corresponds to the

Flat noise, mean=1.000, sigma=1.080, chi 2 dof=2

Kol.=0.816
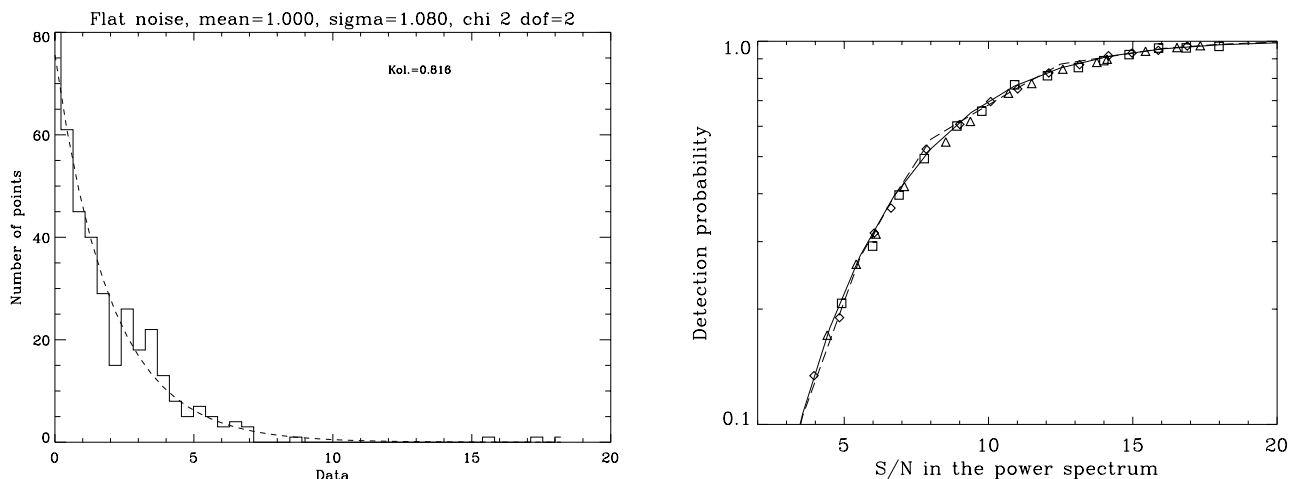
**Figure 2.** On the left hand side: statistical distribution of the simulation shown in Fig. 1. The statistical distribution of the power spectrum follows a $\chi^2$ with 2 d.o.f statistics. On the right hand side: the solid line represents the detection probability as a function of the signal-to-noise ratio given by Eq. (10); the detection likelihood as given by Monte-Carlo simulations are represented for one embedded sine wave (dashed lines), and for three embedded sine waves (squares, triangles and diamonds signs).

mean value of the noise signal, and $\lambda$ corresponds to the observed amplitude in the power spectrum that the sine wave would have had if not embedded in the noise, i.e. $\frac{A^2}{4}$. This means that the inclusion in the signal data set of power bins with such statistical distribution will produce an overestimation of the mean value of the noise (See Appendix A). To avoid this problem, we first applied the statistical test H0 (Step 4) for the detection of outliers in the data set and then we re-estimated the mean value of the signal excluding the detected outliers. The value estimated with this additional step provided a less biased estimate of the true mean than even using the median. As there are 3 embedded signals, if the outliers were not excluded from the noise estimation, the measured detection probability would be biased.

Figure 2 summarizes the statistical analysis of the power spectra simulation of sine waves embedded in a white noise showing the agreement between the Eq. (10) and the Monte-Carlo analysis. The similarity between statistical distributions can be measured by the Kolmogorov-Smirnov (K-S) test. It computes the significance level ($k$) of the maximum absolute difference between two cumulative distribution functions. The computed $k$ has values between 0 (the smallest value of agreement), and 1 (the largest value of agreement) (see Press et al. 1988). Figure 2 shows that $k$ is close to 1 implying that the statistical distribution of the power spectrum follows a $\chi^2$ with 2 d.o.f.

### 3.1.2 *Sine waves embedded in a p-mode spectrum*

Here we explicitly assumed that the noise was only additive as it was the main assumption for the H&H exercise. We repeated for 1000 simulations the following steps for a 30-$\mu$Hz frequency range or window:

(i) Generate Fourier spectra for white noise

(ii) Generate a model of two short-lived p modes (linewidth: 1 $\mu$Hz, 20 $\mu$Hz apart, signal-to-noise: 12)

(iii) Add in the spectra three sine waves with different amplitudes as in Eq. (17)

(iv) Use MLE for fitting the two p modes, and then divide the spectrum by the fit

(v) Determination for the power level: 10% probability in a 30-$\mu$Hz window gives $\rho = 8.26$ (Eq. (5))

(vi) Frequency extraction of the detected power bins

For each simulation we applied the technique described in Section 2.2 (Step 4) and then followed the same procedure as for the sine waves embedded in pure noise described in the previous section (3.1.1). One example of the generated power spectrum and the respective corrected power spectrum are showed in Fig. 3.

The agreement between the Eq.(9) and the detection ratios of the input embedded sine waves signal in the 1000 simulations proves the second approach (Fig.4).

### 3.2 Hare-and-Hound exercises of COROT: HD57006

#### 3.2.1 *The hares*

A model of the star HD57006 has been computed with the CESAM code. It is a 1.65 $M_\odot$ model with a surface metallicity and a position in the HR diagram in agreement with the observations. A set of adiabatic eigenfrequencies and their normalized inertia for degrees $l = 0$ to 3 have been computed by one of the author (GB). Since the star has evolved beyond the main sequence stage, the frequency spectrum includes both p, g and mixed modes in the same frequency domain (Appourchaux et al, 2003). The time series of HD57006 was then generated by another author (TT) using the model frequencies computed by GB. The length of the time series was 150 days with a 32-s sampling time. The background noise was derived from the solar noise as measured by the SPM instrument aboard the SOHO spacecraft (Fröhlich et al. 1997). The linewidth of the p modes was of the order of 1 $\mu$Hz, while that of the g modes was assumed to be much longer than the observation time. The g modes and mixed modes were introduced as sine waves being excited randomly
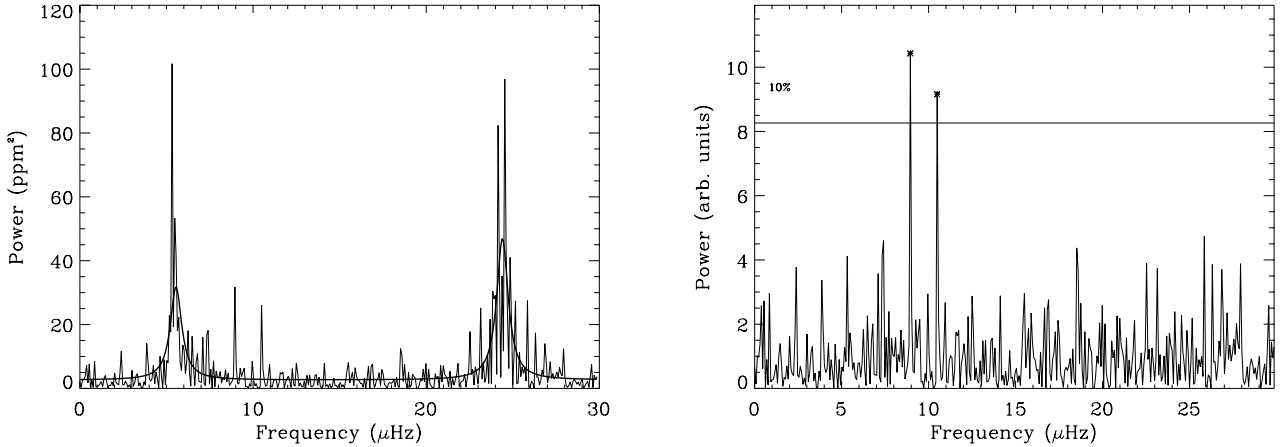
**Figure 3.** On the left hand side: one example of a Monte-Carlo simulation of a sine wave embedded in a p mode. The signal due to the embedded sine waves is present at $\nu = 7.5, 9, 10.5$ ($\mu$Hz). The solid line corresponds to the fitted model using the MLE. On the right hand side: The corrected power spectrum and the 10% detection threshold. Two modes are detected above the threshold indicated by star symbols. The signal-to-noise ratios of the sine waves signal in the corrected power spectrum were input to be 9, 10, 11, which correspond to a detection probability of 60%, 70%, 76%, respectively.
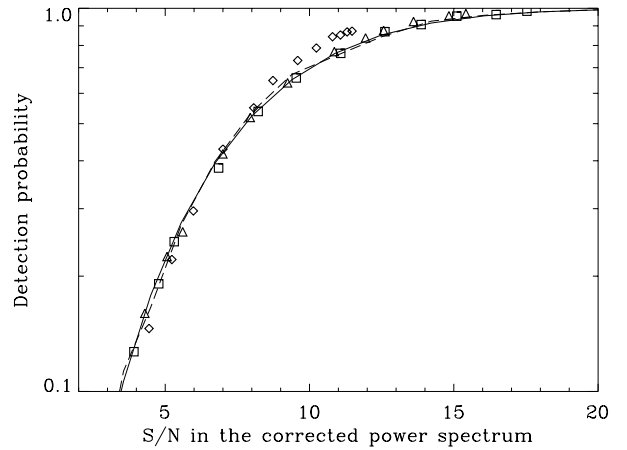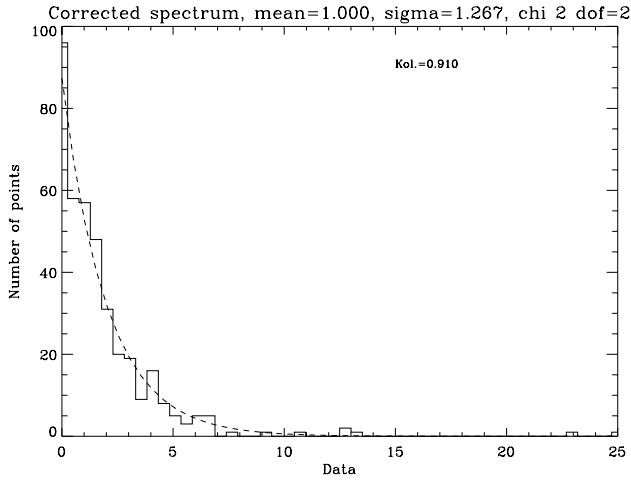


**Figure 4.** On the left hand side: Statistical distribution of the corrected power spectrum for the simulation showed in Fig.3. On the right hand side: the solid line represents the detection probability as a function of the signal-to-noise ratio given by Eq.10; the detection likelihood as given by Monte-Carlo simulations are represented for one embedded sine wave (dashed lines), and for three embedded sine waves (squares, triangles and diamonds signs).

at a given frequency (restricted to one frequency bin) and a given amplitude. This random excitation is believed to be at work in the Sun. For instance, it is well known that due to random excitation an $l = 1$ doublet may appear like a singlet as observed with SOI/MDI[2] for the $l = 1$ mode at 1329 $\mu$Hz. This *feature* is attributed to the stochastic excitation of that mode.

*3.2.2   The hounds*

The first step in the analysis of the time series is to compute a power spectrum (Fig 5, left hand side), and then to construct an echelle diagram (Fig 5, right hand side). Echelle diagrams are used for easing the mode identification as shown by Appourchaux (2003). One single ridge can clearly be identified as being that of the $l = 0$. The methodology described in section 3.1.2 was applied to 30-$\mu$Hz windows between 200 and 500 $\mu$Hz. Figure 6 shows two examples allowing to retrieve 4 long-lived modes.

[2] Solar Oscillations Investigation/Michelson Doppler Imager aboard SOHO
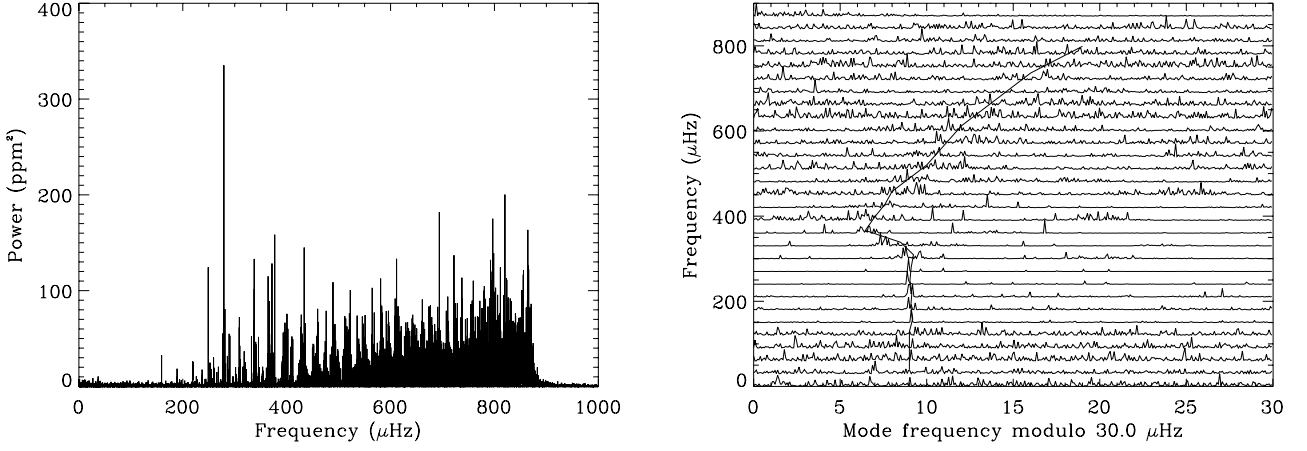
**Figure 5.** On the left hand side is the spectrum of the star HD57006, and on the right hand side the Echelle diagram with $\Delta\nu_0 = 30\mu$Hz.
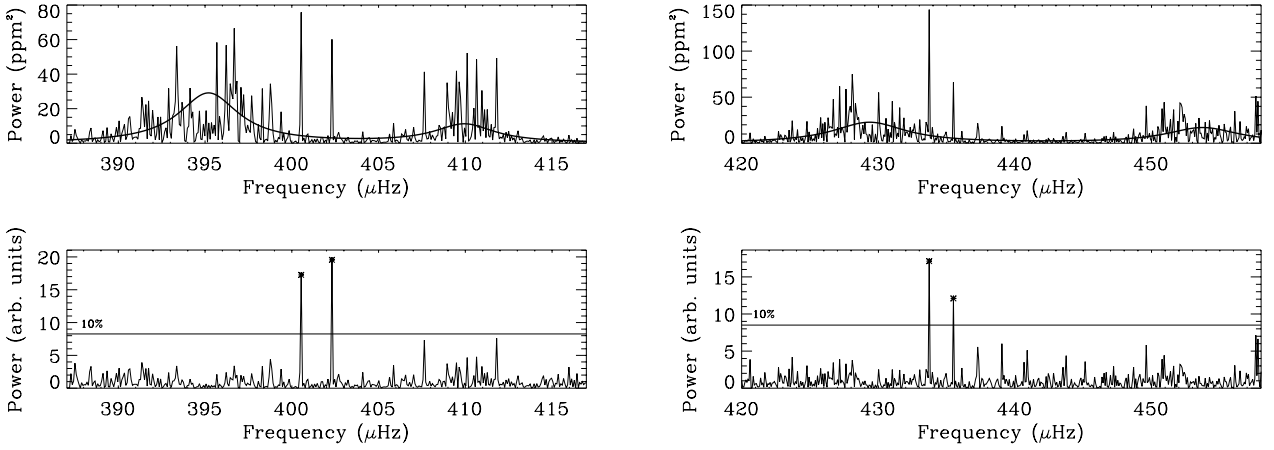


**Figure 6.** Result of the test for two different ranges of frequencies. The fitting is presented on the top of the figure, and the division of the power spectrum by the fitting, as well as the bins above the 10% probability level, are presented on the bottom of the figure.



**Figure 7.** Results of the COROT Hare-and-Hound exercise for the modes detected with the technique described in this paper. On the left hand side, frequency difference (measured-input) as a function of frequency; on the right hand side, amplitude ratio (measured divided by input) as a function of frequency.

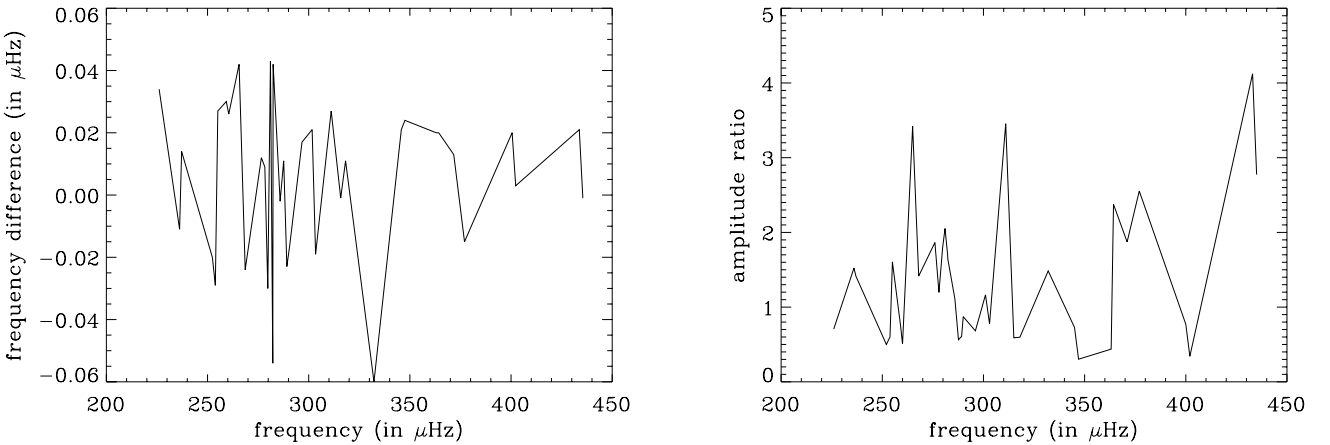| $\nu$ in $\mu$Hz | Degree $l$ | Azimuthal order $m$ | $n_p - n_g$ | Measured snr | Theoretical snr | Detection probability |
|---|---|---|---|---|---|---|
| 226.08 | 1 | 0 | -6 | 9.8 | 13.9 | 0.55 |
| 236.19 | 1 | -1 | -5 | 10.2 | 6.7 | 0.29 |
| 237.19 | 1 | 0 | -5 | 16.8 | 11.9 | 0.50 |
| 252.39 | 1 | -1 | 0 | 9.8 | 19.6 | 0.66 |
| 253.86 | 1 | 0 | 0 | 15.9 | 26.5 | 0.73 |
| 255.09 | 3 | +1 | -19 | 11.4 | 7.1 | 0.31 |
| 259.26 | 1 | -1 | -3 | 9.7 | 12.8 | 0.52 |
| 260.49 | 1 | 0 | -3 | 12.2 | 24.1 | 0.71 |
| 265.59 | 2 | -1 | -10 | 13.0 | 3.8 | 0.11 |
| 268.60 | 2 | +1 | -10 | 7.5 | 5.3 | 0.21 |
| 276.62 | 2 | +1 | -9 | 37.1 | 19.9 | 0.66 |
| 278.32 | 2 | +2 | -9 | 7.3 | 6.1 | 0.26 |
| 279.78 | 1 | -1 | +2 | 41.0 | 22.9 | 0.70 |
| 281.10 | 1 | 0 | +2 | 55.0 | 26.8 | 0.73 |
| 282.25 | 1 | +1 | +2 | 15.4 | 9.0 | 0.40 |
| 282.41 | 3 | -1 | -15 | 15.4 | 9.4 | 0.41 |
| 285.88 | 3 | +1 | -15 | 21.0 | 18.9 | 0.65 |
| 287.65 | 3 | +2 | -15 | 11.5 | 20.4 | 0.67 |
| 289.20 | 1 | 0 | -1 | 36.9 | 60.7 | 0.87 |
| 290.66 | 1 | +1 | -1 | 35.5 | 40.7 | 0.81 |
| 296.68 | 2 | -1 | -7 | 7.3 | 10.7 | 0.45 |
| 301.70 | 2 | -2 | -6 | 7.8 | 6.7 | 0.29 |
| 303.40 | 2 | -1 | -6 | 9.7 | 12.5 | 0.52 |
| 311.11 | 3 | -2 | -11 | 22.8 | 6.6 | 0.29 |
| 315.82 | 2 | -1 | -5 | 7.9 | 13.4 | 0.54 |
| 318.21 | 3 | +2 | -11 | 11.1 | 18.6 | 0.64 |
| 332.25 | 2 | -1 | -4 | 14.4 | 9.7 | 0.43 |
| 345.76 | 3 | +1 | -8 | 14.2 | 19.5 | 0.65 |
| 347.53 | 3 | +2 | -8 | 7.3 | 24.1 | 0.71 |
| 363.12 | 2 | -1 | -1 | 8.1 | 18.5 | 0.64 |
| 364.27 | 2 | +1 | -2 | 29.7 | 12.5 | 0.52 |
| 371.68 | 3 | -1 | -6 | 14.2 | 7.6 | 0.34 |
| 377.01 | 3 | +2 | -6 | 33.2 | 13.0 | 0.53 |
| 400.54 | 3 | -2 | -3 | 10.4 | 13.5 | 0.54 |
| 402.31 | 3 | -1 | -3 | 8.0 | 23.4 | 0.70 |
| 433.72 | 3 | -1 | -1 | 20.2 | 4.9 | 0.19 |
| 435.49 | 3 | 0 | -1 | 8.6 | 3.1 | 0.07 |

**Table 1.** Frequencies of the modes extracted using the statistical test described in the section 2.2. The identification in terms of $l, m$ and $n_p - n_g$ was performed *a posteriori*. The measured signal-to-noise ratio (snr) can be compared to that of the theoretical. The detection probability is computed after Eq. (20) using the theoretical snr.

### 3.2.3  *Post-exercise analysis*

The advantage of the H&H exercise is the possibility of understanding what was simulated and how it was simulated. This is clearly not possible with *real stars*. Figures 7 shows the difference of frequencies, and the ratio of the measured amplitudes to the theoretical ones. The measured mode frequencies are measured with an uncertainty commensurate with the frequency resolution. The distribution of the amplitude ratio are due to the stochastic nature of the excitation, as deduced *a posteriori*. Table 1 summarizes the narrow modes detected by our method together with the *a posteriori* mode identification, and the measured and theoretical signal-to-noise ratio. One of the author (TT) provided us (TA and OM) with the theoretical signal-to-noise ratio. The number of detectable modes is simply the sum of the probability of detecting the narrow peaks as computed according to Eq. (10) (See Appendix B). The total number of detectable modes was $77 \pm 9$. This is higher by $4\,\sigma$ than the 37 modes listed in Table 1. We would like to point out

that the sampling effect of the Fourier transform can reduce the amplitude of the mode by up to factor 2 (Gabriel et al. 2002). This additional fact will also reduce the number of detectable modes but is not sufficient to explain the discrepancy. This latter is related to the assumption made about the very nature of the excitation process of the g modes. We assumed that the modes have a long lifetime and behave like a pure sine wave of fixed amplitude. As a matter of fact, the hare (TT) generated a long-lived mode by stochastic excitation, i.e. using a multiplicative noise and not an additive noise (See Section 3.2.1). This has an impact on the detection probability that is indeed lower than for the case of additive noise (Eq. 10). In the case of multiplicative noise, Eq. (10) is then replaced by Eq. (14). For a signal-to-noise ratio greater than 10 the probability of detecting a mode is a factor two third lower for a multiplicative noise (Eq. 14) than for an additive noise (Eq. 10). Taking into account Eq. (14), the number of modes becomes then $48 \pm 7$. That is about $1.5\,\sigma$ away from the number of modes effectively detected, thereby confirming Eq. (14). The detection prob-

abilities derived from Eq. (14) are also included in Table 1. In summary, it is more difficult to detect a long-lived mode stochastically excited than to detect a pure sine wave. This finding is the result of the *a posteriori* analysis and is not strictly part of the hare-and-hound exercise.

## 4 DISCUSSION

This technique can be perceived as being applicable only to very peculiar stars. As a matter of fact, we did check that such mixed modes occur in stars of mass greater than 1.2 $M_\odot$ and being beyond the so-called Terminal Age Main Sequence (TAMS). These stars having exhausted the central hydrogen start to burn hydrogen in shells. The slight necessary contraction required to increase the temperature of the first shell produces a distinctive anti-$Z$ shape in the Hertzprung-Russell diagram. We have performed calculation up to 2 $M_\odot$ that do confirm the occurence of mixed modes after the TAMS evolution stage. Therefore, there are numerous stars for which that technique could be applied and useful. Procyon could be taken as an example of such a star. It could even be argued that the detection difficulties encountered might have been due to the presence of mixed modes (Martić et al, 2004; Eggenberger et al, 2004, and references therein).

## 5 CONCLUSION

We showed that we could detect long-lived modes embedded into short-lived p modes. This occurs for evolved solar-like stars having long-lived mixed modes. These modes appear due to the increase of the Brunt-Vaisäla frequency during the Helium core evolution phase. The detection of such mixed modes will provide a powerful tool for understanding the internal evolution of the stars. Here we introduce a new technique that allows, after having fitted the short-lived p modes, to detect these long-lived mixed modes. The steps of the detection technique are summarized in Section 3.1.2. The technique was first used in the frame work of the COROT hare-and-hound exercise. The reliability of this technique was then tested and validated by performing Monte-Carlo simulations. We showed during the hare-and-hound-exercise post analysis, that long-lived modes excited stochastically are more difficult to detect that deterministic sine waves. The technique can be applied to stars having evolved beyond the TAMS.

## ACKNOWLEDGEMENTS

## REFERENCES

Anderson, E. R., Duvall, T. L., Jr., Jefferies, S. M. 1990, ApJ, 364, 699

Appourchaux, T. 2003, Ap&SS, 284, 109
Appourchaux, T., Gizon, L., Rabello-Soares, M.-C., 1998, A&A Sup. Series, 132, 107
Appourchaux, T., Moreira, O., Berthomieu, G., & Toutain, T. 2003. In "Stellar structure and habitable planet finding", 2nd Eddington workshop, F. Favata, S.Aigrain eds., ESA-SP 538
Appourchaux, T., Fröhlich, C., Andersen, B., et al. 2000, ApJ, 538, 401
Berthomieu, G. and Appourchaux, T., 2002,in *Asteroseismology across the HR diagram*, Eds: Thompson M.J., Cunha M.S., Monteiro M.J.P.F.G., Kluwer Academic Publishers., 465
Brandt, S., 1970, Statistical and Computational Methods in Data Analysis, Amsterdam: North Holland
Eggenberger, P., Carrier, F., Bouchy, F., Blecha, A., 2004, A&A, 422, 247
Fröhlich, C., Andersen, B. N., Appourchaux, T. et al. 1997, Solar Physics, 170, 1
Gabriel, A.H., Baudin, P., Garcia, R.A., et al. 2002, A&A, 390, 1119
Mayor, M., Pepe, F., Queloz, D. et al. 2003, The Messenger, 114, 20
Martić, M., Lebrun, J.-C., Appourchaux, T., Korzennik, S. G., 2004, A&A, 418, 295
Press,W. H., Flannery, B. P. , S. A. Teukolsky, S. A., & Vetterling, W. T. 1988, Numerical recipes in C, Cambridge Univ. Press.
Toutain, T., & Appourchaux, T. 1994, A&A, 289, 649
Turck-Chièze, S., García, R., Couvidat, S. et al. 2004, ApJ, 604, 455

## APPENDIX A: MLE OF THE MEAN NOISE VALUE

Considering a random signal $z$ with a $\chi^2$ with 2 d.o.f statistics having a mean value of $\sigma$. From a set of $N$ observations, the mean value of $z$ (E[$z$]) can be estimated by using MLE (Brandt, 1970). The log likelihood $l$ of the observations is given by:

$$l = -\sum_{i=1}^{N} \left( \log \sigma + \frac{z_i}{\sigma} \right) \qquad (A1)$$

where $z_i$ is the i-th observation of $z$ (See Anderson et al, 1990 for a similar derivation). The minimization of $l$ requires to calculate:

$$\frac{dl}{d\sigma} = \frac{N}{\sigma^2} \left( \frac{1}{N} \sum_{i=1}^{N} z_i - \sigma \right) \qquad (A2)$$

therefore the minimum occurs when:

$$\sigma = \overline{z} = \frac{1}{N} \sum_{i=1}^{N} z_i \qquad (A3)$$

So $\tilde{\sigma} = \overline{z}$ is an unbiased estimator of $\sigma$ with a variance of $\frac{\sigma^2}{N}$.

With an embedded signal with different statistics not all $z_i$ are independent and identically distributed (i.i.d) random variables. In that case, $\overline{z}$ is no longer an unbiased estimator of $\sigma$. If $p$ signals ($x$) have a non-central $\chi^2$ statistics with non-centrality parameters $\lambda_i$ (representing the difference from the regular mean $\sigma$), while the other $N - p$ signals ($y$) have a $\chi^2$ with 2 d.o.f distribution with mean $\sigma$, then the mean of $z = x + y$, as derived from Eq. (A3) can be

written as:

$$E[z] \;=\; E\left[\frac{1}{N}\left(\sum_{i=1}^{N-p} x_i + \sum_{j=1}^{p} y_j\right)\right] \tag{A4}$$

$$=\; \frac{N-p}{N}E[x] + \frac{1}{N}\sum_{j=1}^{p} E[y_j] \tag{A5}$$

$$=\; \frac{N-p}{N}\sigma + \frac{1}{N}\sum_{j=1}^{p} (\lambda_i + \sigma) \tag{A6}$$

$$=\; \sigma + \frac{\sum_{j=1}^{p}\lambda_i}{N} \tag{A7}$$

Thus the bias, $b$, is given by:

$$b \;=\; E[z] - \sigma = \frac{\sum_{j=1}^{p}\lambda_i}{N} \tag{A8}$$

which means that $E[z] \approx \sigma$ when $\dfrac{\sum_{j=1}^{p}\lambda_i}{N} \ll 1$.

## APPENDIX B: AVERAGE NUMBER OF DETECTABLE PEAKS AMONGST $N$ PEAKS

A proper analysis of the number of detectable modes should take into account the probability of detecting each long-lived mode as generated by the hare. The mean number of detectable modes can be derived from the property of $N$ Bernouilli random variable $X_j$, each having a detection probability $p_j$ for which we have:

$$E[X_j] = p_j \tag{B1}$$

and the standard deviation is given by:

$$\sigma_{X_j} = p_j(1 - p_j) \tag{B2}$$

In our case, the observed random variable is the sum of the $N$ random variable $X_j$ written as:

$$X = \sum_{i=1}^{i=N} X_j \tag{B3}$$

Since the $N$ random variable are independent from each other, we have:

$$E[X] = \sum_{j=1}^{j=N} p_j \tag{B4}$$

The standard deviation is then given by:

$$\sigma_X = \sqrt{\sum_{j=1}^{j=N} p_j(1 - p_j)} \tag{B5}$$